New concept of completely sustainable biofuels and further applications of glycerol derivatives

Dissertation

zur Erlangung des Doktorgrades der Naturwissenschaften (Dr. rer. nat.)
der Fakultät für Chemie und Pharmazie
der Universität Regensburg

vorgelegt von

Damian Brock

aus Bogen

2019

Diese Doktorarbeit entstand im Zeitraum von Oktober 2015 bis Februar 2019 am Institut für Physikalische und Theoretische Chemie der Universität Regensburg unter der Betreuung von Prof. Dr. Werner Kunz.

Abgabe der Promotion: 21.02.2019

Datum des Promotionscolloquiums: 25.04.2019

Promotionskomitee:

1. Gutachter: Prof. Dr. Werner Kunz

2. Gutachter: Prof. Dr. Hans-Peter Rabl

3. Prüfer: Prof. Dr. Dominik Horinek

Vorsitzender: Prof. Dr. Henri Brunner

Acknowledgement

This PhD thesis was made at the Institute of Physical and Theoretical Chemistry, Faculty of Natural Science IV, of the University of Regensburg between October 2015 and January 2019 under the supervision of Prof. Dr. Werner Kunz.
This work would not have been possible without the support from many people. First of all, I want to thank Prof. Dr. Werner Kunz for giving me the opportunity to carry out my thesis at his institute, his trust in my capability, the numerous incentive discussions and the possibilities to present my work at national and international conferences.
I want to particularly express my special thanks to Dr. Didier Touraud for the nearly daily enriching and encouraging discussions. With his help, I was able to work on different research topics simultaneously, which all led to rewarding results eventually.
Further, I would like to thank Prof. Dr. Rainer Müller as well as Prof. Dr. Richard Buchner for supporting my thesis by providing their equipment.
I also have to thank all cooperation partners that I worked with during my thesis. Especially Prof. Dr. Hans-Peter Rabl and Dr. Alexander Koder from the Ostbayerische Technische Hochschule Regensburg significantly enriched the results of this thesis by providing their engine test bench. I would like to show my gratitude to Dr. Axel Ingendoh from inaCHEM GmbH, Walter Kanzler from GLACONCHEMIE GmbH, Dr. Oliver Kastner from Continental AG as well as Jürgen Runkel from Handelshaus Runkel for their generous biofuel gifts, productive discussions and collaborations with our research group. I additionally want to thank WIGO Chemie GmbH for their research contract and their invitation to their head office in Bad Kreuznach as well as the European patent attorneys Dr. Edith Kinder and Dr. Sarah Krüger of the Bayerische Patentallianz.
I would like to acknowledge and thank the bachelor students Leonie Koller, Evamaria Hofmann, Moritz Köglmaier and Stefanie Pongratz as well as the internship students Jutta Lehnfeld, Quentin Rossy, Martina Müller, Tomislav Krolo, Raj Maheshwari and Olivier Bruyen for their dedication and contributions to this work.
Admittedly, I am very proud to be part of this research group. I cannot imagine a better working atmosphere, including fun, motivation and progress and that is the reason why I want to show my gratitude to the whole institute and its members. In particular, I want to mention Dr. Roland Neueder, the secretaries Rosemarie Röhrl, Sonja Beutler and Bianca Frömel, Hellmuth Schönsteiner, Franziska Wolf and especially Dr. Stefan Wolfrum, as I was convinced and highly motivated to work at this institute after my internship as his assistant.
Finally, I want to thank my girlfriend Christina, my family, Gerrit, Rolf and especially my mother Marietta. Without her help and support until today, not only my dissertation, but also my whole scientific career would not have been possible.

Abstract

Within the scope of this thesis, a new concept of completely sustainable biofuels was developed and patented, which enables the usage of high amounts of vegetable oils and glycerol derivatives simultaneously in mixtures with biodiesel. This concept significantly enhances the profitability of biodiesel production and thus strongly contributes to the sustainability of future biofuels. Besides their successful implementation, the presence of these glycerol derivatives leads to further advantages due to their amphiphilic character. For the first time, natural, hydrophilic antioxidants, which are even more effective than the currently utilised, synthetic and highly toxic hydroquinones, can be solubilised in vegetable oil-containing biofuels without any additives. Further, water can be implemented into several biofuel formulations, so-called hydrofuels, without the necessity of surfactants, due to the presence of glycerol derivatives. During the investigations on ethanol as biofuel component, considerable contributions to ethanol-containing biofuels were achieved. The presence of nanostructures in these formulations could finally be indisputably verified and the term *ethanolotrope* was introduced to describe the decisive compound for this structuring. By precisely specifying the nanostructured areas of these mixtures, the influence of these structures on relevant physicochemical parameters of biofuels could be shown.
As a result of the versatile properties of the glycerol derivatives in biofuel formulations, their applicability in completely different, industrial processes was also investigated. After developing a simple extraction, detection and isolation method, it could be shown that some of these derivatives could be used as extracting agents for valuable antioxidants from vegetable oils. With regard to the biofuel concept, this extraction process could be realised before the biofuel formulation and within the same facilities, since the glycerol derivative is added to the vegetable oil anyway. Based on the research contract of WIGO Chemie GmbH, different alternatives to ethanol as freezing point depressants were also investigated. With one of the glycerol derivatives reducing the freezing point of water significantly, this request could be successfully fulfilled as well.
Besides several publications, these results led to many subsequent, industrial projects and collaborations, due to the direct applicability and versatility of the developed concept. While the Handelshaus Runkel will start selling its own biofuel in Austria this year, which will most likely make use of the biofuel concept, even more experiments are currently performed at the Volkswagen AG, the University of Applied Sciences Coburg and the GLACONCHEMIE GmbH.

Zusammenfassung

Im Rahmen dieser Doktorarbeit wurde ein neues Konzept bezüglich vollständig nachhaltiger Biotreibstoffe entwickelt und patentiert, das die gleichzeitige Verwendung von hohen Anteilen von Pflanzenölen sowie Glycerinderivaten in Mischungen mit Biodiesel ermöglicht. Dieses Konzept erhöht die Profitabilität der Biodieselproduktion deutlich und leistet somit einen wichtigen Beitrag zur Nachhaltigkeit von zukünftigen Biotreibstoffen. Zusätzlich zur erfolgreichen Implementierung führt die Anwesenheit dieser Glycerinderivate, aufgrund ihrer amphiphilen Eigenschaften, zu weiteren Vorteilen. Zum ersten Mal ist es möglich, natürliche, hydrophile Antioxidantien, die sogar noch effektiver als die momentan genutzten, synthetischen und hochgiftigen Hydrochinone sind, in Pflanzenöl enthaltenden Biotreibstoffen ohne Additive zu verwenden. Des Weiteren kann Wasser durch die Anwesenheit der Glycerinderivate in zahlreiche Biotreibstoffe, sogenannte Hydrofuels, ohne die Notwendigkeit von Tensiden implementiert werden. Während der Untersuchungen zu Ethanol als Biotreibstoffkomponente konnten weitere Erkenntnisse gewonnen werden. So wurde das Auftreten von Nanostrukturen in Ethanol enthaltenden Biotreibstoffen nachgewiesen und hierfür der Fachbegriff *Ethanolotrop* für die ausschlaggebende Komponente eingeführt. Da die vorliegenden Nanostrukturen präzise identifiziert wurden, konnte der Einfluss jener auf relevante, physikalisch-chemische Parameter gezeigt werden.
Aufgrund der vielseitigen Eigenschaften der Glycerinderivate in den Biotreibstoffen wurde zusätzlich deren Anwendbarkeit in weiteren, industriellen Prozessen untersucht. Nach der Entwicklung einer möglichst einfachen Extraktions-, Detektions- und Aufreinigungsmethode konnte nachgewiesen werden, dass manche dieser Derivate als Extraktionsmittel für wertvolle Antioxidantien in Pflanzenölen eingesetzt werden können. Im Hinblick auf das Biotreibstoffkonzept könnte dieser Extraktionsprozess vor der Biotreibstoffformulierung, bei der das Glycerinderivat ohnehin zum Pflanzenöl hinzugegeben wird, umgesetzt werden. Ausgehend von einem Forschungsauftrag der WIGO Chemie GmbH wurden außerdem verschiedene, alternative Substanzen zu Ethanol als Gefrierpunktserniedriger untersucht. Da ein Glycerinderivat den Gefrierpunkt von Wasser erheblich senken konnte, wurde diese Aufgabe ebenfalls erfolgreich erfüllt.
Neben mehreren Publikationen führten diese Ergebnisse, wegen der direkten Anwendbarkeit und Vielseitigkeit des entwickelten Konzepts, zu einer Reihe von weiteren Industrieprojekten und Kooperationen. Während das Handelshaus Runkel in diesem Jahr in Österreich damit beginnen wird, seinen Biotreibstoff, bei dem höchstwahrscheinlich das Biotreibstoffkonzept verwendet werden wird, zu verkaufen, werden aktuell noch weitere Experimente bei der Volkswagen AG, der Hochschule für Angewandte Wissenschaften Coburg und der GLACONCHEMIE GmbH durchgeführt.

Contents

1 Introduction

Unsustainable fuels like fossil oil are among the most widely consumed liquid mixtures all over the world. In the recent decades, their unstable and unpredictable prices, the uncertainties in their supply and the global warming problems caused by their continuous usage have raised interest in alternative energy sources. Since the worldwide energy demand is still growing and the fossil oil reserves are limited or rather difficult to exploit, the development of fuels based on sustainable resources becomes increasingly important [1, 2]. The urgency of new proceedings in this research topic was particularly influenced by latest scandals in the automotive sector, such as the "Dieselgate" scandal of Volkswagen. A very detailed and unbiased evaluation of this topic can be found in section 2.1.1.1. Thus, fuels in agreement with the principles of green chemistry, established by Paul Anastas in 1998, would have a significant, positive environmental impact [3, 4]. The strict application of these principles implies that all fuel components should be renewable instead of depleting [5]. Fuels, which fulfil this condition, are called biofuels and represent one of the biggest current research topics in sustainable and green chemistry [6, 7]. From an environmental point of view, biomass-derived fuels such as vegetable oils, biodiesel and bioethanol can help solving global warming and environmental pollution problems due to their renewability and negative CO_2 footprint as well as due to the absence of sulfur, aromatic hydrocarbons and metals [8, 9].

However, many companies and research groups mistakenly use the catchphrase “biofuel” as marketing strategy to promote mixtures of a green substance with fossil fuels. The fuel E10 is an example in Germany, which consists of common petrol and ten weight percent of bioethanol. Although the mixture is mostly composed of a fossil fuel, even the Federal Ministry for the Environment, Nature Conservation and Nuclear Safety of Germany frequently used terms including “biofuel”, “sustainability” and “green” to promote its implementation in 2010 [10]. But since environmentalists ambitiously informed the broad mass of citizens about this eyewash, the consumer acceptance was low from the very beginning [11, 12]. In fact, the main purpose of this new fuel mixture was to increase the amount of sustainable components in automotive fuels, but the promotion should have been more honest. Other currently promising fuel additives are, among others, furan derivatives and terpenes, which are more precisely described in section 2.1.5.1. While they could be potential substitutes for winter and aviation fuels, the main research is just focused on blends with either petrol or diesel [13, 14]. It is further remarkable that current literature almost exclusively reports on new or improved green chemical syntheses and reactions to obtain biofuels, but just a small part is devoted to the actual product formulation. Since this strategy just leads to slow environmental improvements, a new concept for the formulation of completely renewable biofuels seems desirable and even necessary.

As the demands for alternatives to fossil and biomass-derived fuels in general raised in the past years, the status quo of electrically produced fuels (E-fuels) and E-mobility is critically discussed in chapter 2.1.2. By pointing out the slow pace of the development of these alternatives, the motivation for the focus on biofuels in this work will become evident. Unfortunately, many known biofuels exhibit undesired physicochemical properties like high viscosities and freezing points. The consequences of these drawbacks for the formulation, combustion process and storage of the biofuel are precisely explained in chapter 2.1.3. Due to these problems, the usage of further components is usually necessary, which leads to another way of falsely advertising biofuels: Several enhanced biofuel formulations are already proposed, but most of the additives do not fulfil the guidelines of green chemistry, which makes the usage in biofuels inappropriate and pointless. Besides adding explosive organic peroxides as ignition promoters for biofuels or highly toxic hydroquinone as antioxidant, a current example is the usage of ethanol in blends of vegetable oils or diesel [15, 16]. Ethanol belongs to the oxygenated additives, which facilitate a complete combustion as well as the reduction of soot emissions and distinctly decrease the viscosity of the fuel [17]. While its advantages and disadvantages will be shown in detail in section 2.1.2.4, it is important to mention that ethanol is hardly miscible with vegetable oils and diesel. Therefore, further components, in particular emulsifiers, are necessary to prevent phase separation [18, 19]. Instead of using a surfactant, which is expensive and

unfavourable for the combustion process, other green substances with similar properties to hydrotropes are investigated to increase the solubility of rapeseed oil in ethanol. Analogous to a hydrotrope, the term *ethanolotrope* is introduced in this work to describe a substance, which is able to increase the solubility of organic compounds in ethanol without being a surfactant. These mixtures are further examined regarding the formation of nanostructures and its influence on important fuel parameters.
In the scope of my master thesis, completely green biofuels consisting of rapeseed oil, its biodiesel and either a furan derivative or a terpene were successfully formulated and characterised. Nevertheless, the amount of necessary furans or terpenes to fulfil the European and American viscosity and low-temperature standards for biodiesel was too high to commercialise these biofuels. This work, however, already showed that it is possible to implement high amounts of a vegetable oil in biofuels without using any unsustainable or highly toxic compounds, although the self-chosen conditions and standards that had to be fulfilled were very ambitious (see section 2.1.5.1). The direct usage of vegetable oils obviates their chemical transformation with methanol to biodiesel, which is coupled, among others, with the production of the by-product glycerol. Due to its strong hydrophilicity and high viscosity, there are just a few large-scale applications. Therefore, the new biofuel concept should implement high amounts of vegetable oils as well as glycerol without being noncommercial. Eventually, these conditions and approaches led to an European patent as part of this PhD thesis.
Additionally to some investigations on several other existing problems concerning the usage of biofuels, further applications of glycerol derivatives are examined. To this purpose, different industrial fields of application are chosen, in which hazardous substances, ranging from flammable to even highly toxic chemicals, are generally used. These substances have to be replaced due to either drastically increasing expenses for the usage of hazardous compounds or stricter guidelines. As a result of its flammability, alternatives to ethanol are sought in many formulations like freezing point depressants and window cleaners [20]. Alkanes are another group of chemical substances that require sustainable alternatives in their industrial applications. A typical example is the usage of toxic hexane as extracting agent for a variety of natural compounds [21]. For these completely different fields of application, formulations and methods could be developed, too, that enable a replacement of the harmful substances by glycerol derivatives on an industrial scale.

2 Fundamentals

2.1 Investigations on completely green biofuels

2.1.1 Fuels from biomass – biofuels

As it is the main topic of this thesis, this chapter deals with the current status of fuels derived from biomass. Thus, a closer look is given on the proceedings of the last decades. Especially incidents like the "Dieselgate" scandal and the upcoming driving bans for diesel cars in German cities are profoundly and objectively discussed. For that, headlines and reports of the media and their impact on political decisions in Germany and worldwide are analysed. Additionally, the current technical advances to improve the image of diesel engines are outlined and their influence on future biofuel formulations is explained. In the second part of this chapter, the status quo of liquid biofuels, in particular vegetable oils and their biodiesels, is shown in detail.

2.1.1.1 Increasing demand for sustainable energy

"A debacle for the whole automotive industry; [...] [German automotive industry] is in the deepest crisis of its history" [22]. Since September 2015, headlines like this could be read in the media all over the world and even in 2018, the "Dieselgate" scandal is still

one of the main political issues in Germany [23]. Since the automotive industry is the most influential and important employer in Germany, the media always have an eye on the original equipment manufacturers (OEM) like Volkswagen or Audi. According to the media, a software with a cut-off device was used in German diesel cars of Volkswagen, Audi, Porsche, Mercedes and Opel, which led to lower nitrogen oxide (NO_x) emissions in standardised test cycles, but not during common driving conditions. Thus, many German cars are allegedly dangerous for the environment and especially for humans [22]. Since negative news are, by far, more lucrative than positive ones nowadays, the population was exaggeratedly frightened of and incensed by this topic. Fig. 1 is exemplary for the overstated presentation of the "Dieselgate" scandal in the media.

Figure 1: Example of an exaggerated, but typical depiction of the "Dieselgate" scandal in German media [24]. Even though the caption *made in Germany* is true, the exhaust gas plume is drastically supersized compared to the car. Figures like this negatively influenced badly informed citizens about the scandal.

Due to the high pressure of the media, politics had to react immediately to calm down the population and to show their commitment. However, since the current German government is economically oriented and thus acting in the interest of industry and economic strength, the mood of the population was also incited by opposition parties. The party Bündnis 90/Die Grünen, for example, claim to know the cause for the crisis: organised government failure. Instead of referring to profound scientific research, which were published after a few months and precisely identified the real causes and environmental impacts of this scandal, they seized their moment. Their arguments and claims were based on the media's unscientific statements. This in turn unnecessarily pushed this topic into the foreground of governmental discussions, since complete investigations were already enacted, but have not been finished yet. Their most concise claim was the prohibition of combustion engines until 2030, justifiable and viable due to the economic power of the country, according to their opinion [25]. This example impressively shows the media's and politic's premature dealing with the scandal and proves the importance of scientific re-

search. To reduce the impact of road transportation on the air quality, emission standards for vehicles were introduced in 1991. Since their entry into force, the sales of light-duty diesel vehicles distinctly increased due to their lower CO_2 emissions, compared to petrol engines [26]. At that time, the reduction of CO_2 emissions was prioritised, because of international agreements on climate change, even though diesel engines emitted more NO_x emissions. As the environmental pollution caused by exhaust gas emissions did not decrease as considerably as expected, although newly registered vehicles passed the approval tests, authorities became suspicious [27]. Further, the European Environment Agency (EEA) complained about emissions of diesel engines being commonly higher during real-life driving conditions than during the type approval tests [28]. In May 2014, Thompson *et al.* measured excess emissions of light-duty diesel vehicles of Volkswagen, which led to allegations by the US Environmental Protection Agency (EPA) [29]. More than one year later, the Volkswagen Group admitted the usage of so-called "defeat devices". The software was designed to significantly reduce NO_x emissions during vehicle type approval tests to fulfil emission standards. These devices, however, are turned off during on-road driving conditions [30]. Globally, 11 million sold diesel cars of Volkswagen possess these devices, with 8.5 million being sold in Europe and 2.6 million particularly in Germany [26, 27]. In Europe, the first standard to limit the emissions of passenger cars, the Euro 1 standard, was introduced in 1992. With an interval of about five years, the limits were progressively tightened. Currently, the Euro 6 standards are in force, regulating the test methods and the most important emissions of diesel and petrol cars [31]. In 2017, this standard was extended by a new type approval for light-duty vehicles, in which real driving emissions are measured with portable emission measurement systems. The same applies for the USA, which introduced even stricter Low Emission Vehicle III / Tier 3 standards in 2017 [32]. Since the "Dieselgate" scandal, NO_x emissions gained most public attention. They consist of up to nine different gaseous nitrogen oxide compounds, with nitrogen monoxide (NO) being the most common one during engine combustion. It is produced at temperatures above 2000 K and low excess air. As it is thermodynamically unstable at ambient conditions, it reacts with atmospheric oxygen to nitrogen dioxide (NO_2). NO_2 emissions are perceptible and toxic for humans. Further, it can react with atmospheric water to form nitric acid, which led to acid rain due to too high concentrations in the 1980s. NO_2 is also responsible for the formation of ground-level ozone [31]. Even though the ozone layer in the stratosphere is inevitable for human viability, it is a toxic gas, which should not occur at ground-level [33]. Particulate matter emissions or soot emissions are defined as particles that pass through a size-selective air inlet of a monitoring device with a diameter of either 10 µm (PM_{10}) or 2.5 µm ($PM_{2.5}$). Soot is produced in the combustion chamber at oxygen deficiency, which leads to incomplete oxidation processes. Soot emissions are toxic for humans, as they can accumulate in the lungs due to their small sizes [31, 33].

Road traffic, industrial combustion processes, the energy sector, households and agriculture are the primary sources of air pollutants. The pollution level is also influenced by weather conditions, too. At low temperatures, emissions increase due to the usage of heating systems. High-pressure areas lead to a concentration of the ground-level pollutants because of low wind velocities. In the summer, this weather condition coupled with intense sunlight causes ozone formation [33]. The NO_x emissions produced by combustion engines account for about 70% of the total anthropogenic NO_x emissions in German cities like Stuttgart. With diesel engines emitting distinctly more NO_x than petrol engines, their share thereof prevails. The amount of soot emissions caused by diesel combustion engines in German cities, on the other hand, is about 8% of the anthropogenic overall exposure. Most of these 8% come from end-of-life vehicles, which possess no particle filter [31]. Due to the "defeat devices", affected diesel passenger cars emit 0.9 g NO_x per kilometre [29]. This is about 21 times the allowed amount in the USA and 5-11 times the permitted amount in the European Union [34]. Anenberg *et al.* could show that across eleven OEMs, which represent about 80% of the global diesel vehicle sales, more than half of the light-duty vehicles and approximately one third of the heavy-duty vehicles exceed the emission standards [32]. In another study, Oldenkamp *et al.* calculated the amount of additionally emitted NO_x by manipulated diesel cars from 2009 to 2015 with resulting 526 ktonnes [34]. It could even be shown that some Euro 5 light-duty diesel vehicles have higher emissions than previous Euro class vehicles at real driving conditions [35]. The excess emissions caused about 38 000 premature deaths globally in 2015, with heavy-duty diesel vehicles being the main contributor and $PM_{2.5}$ as well as ozone the most dangerous emissions for humans [27,32]. About half of these deaths would have been avoided if there were no difference between real driving and approval test emissions [26].
Due to these facts, the media attention and the demands for further restrictions or even driving bans are comprehensible. Nevertheless, it is necessary to evaluate from a scientific point of view, if these purposes are justified. The "dieselgate" scandal and the questionable reporting violated the public's trust in the automotive industry and the diesel technology. Even if driving bans for diesel vehicles are introduced in some city centres, the usage of diesel engines is crucial to fulfil international CO_2 emission goals. In its annual report on air quality, the German Federal Ministry of Environment shows the amount and geographic distribution of pollutants in Germany with respect to the past 17 years. They are determined several times a day at more than 650 measuring stations. Fig. 2 shows the evolution of the annual mean NO_2 values for the rural and urban background as well as urban traffic. The rural background relates to regions with an air quality uninfluenced by local emissions, whereas the urban background represents the typical air quality in German cities. The data for the urban traffic values is obtained from busy roads in cities. Thus, comparing the urban traffic results with the urban background, the direct road

traffic emissions can be obtained. From 2000 to 2017, the amount of NO_2 in the air of rural areas slightly decreased to about 10 µg/m^3. The same tendency applies to the air pollution of the urban background, which is about 20 µg/m^3.

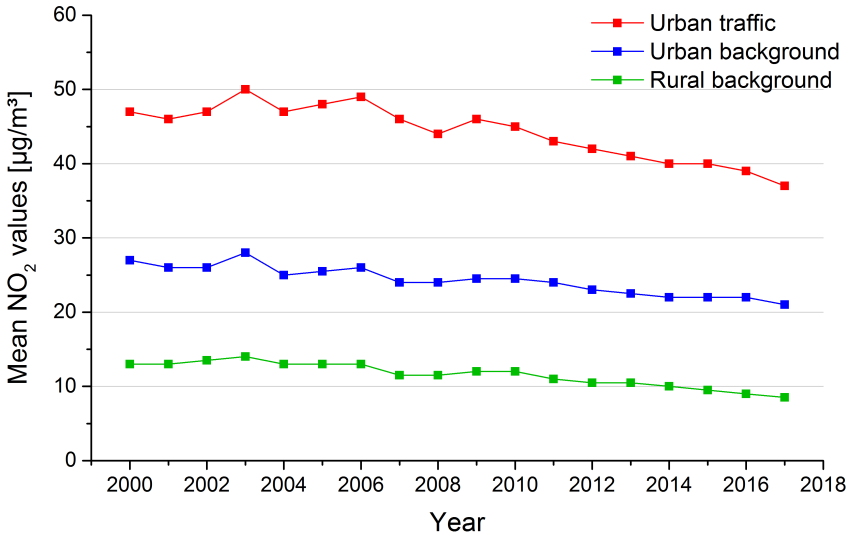

Figure 2: Comparison of the annual mean NO_2 values of the rural background, urban background and urban traffic in Germany, according to [33].

The European limit for the annual mean NO_2 exposure outdoors is 40 µg/m^3. Consequently, the results for the urban traffic are below the limit since 2016 (see Fig. 2). There are several reasons for the distinct decline of these emissions in the past ten years, which will be further discussed later in this chapter [33]. Nevertheless, there are still many German cities with exceeding NO_2 values, but, as confirmed by the executive director of the IVU Umwelt GmbH, Volker Diegmann, the measuring points are very selective. This means that already a few metres away from the measuring device, the obtained pollution value can be completely different [36]. Since the exceeding urban traffic values led to several controversial public discussions and headlines, it is indispensable to also mention mandatory NO_2 limits for other areas. While humans are allegedly acutely endangered by 40 µg/m^3 NO_2 outdoors, the maximum allowable concentration (MAC) at German workplaces is 60 µg/m^3 and at manufacturing facilities even 950 µg/m^3. With this data, the question arises, why there should be a driving ban for diesel vehicles [37]. Leading toxicologists like Helmut Greim of the Technical University of Munich and former chairman of the German MAC-commission even disputes the scientific basis of these limits. Since people are more than 70% of the day in interiors, he even says that limits are always political values [38]. As explained in the beginning of this chapter, politics could have possibly placated the public and the media with this unreasonable NO_2 limit for urban traffic.

Similar to the NO_2 emissions, Fig. 3 shows the annual mean PM_{10} emissions of the last 17 years measured for the rural and urban background as well as the urban traffic. With the European limit of 40 µg/m^3, identical to the NO_2 limit, it is evident that the emissions were already below this value 17 years ago. Compared to the NO_2 emissions, the share of the urban traffic on the total PM_{10} emissions is rather low, since the rural and thus also the urban background values are already high, comprising about 75% of the total PM_{10} pollution [33]. In this context, a closer look at the shipping industry is appropriate. Exhaust gases of ships consist of sulphur oxides (SO_x), NO_x, CO_2, soot, heavy metals, ash and sediments. Since generally heavy fuel oil is used in ships, they are responsible for about 15% of the global NO_x, 13% of the SO_x and 3% of the CO_2 emissions. Due to its high viscosity, the oil must be heated up to 130 °C for the injection into the combustion chamber. Surprisingly, there are no uniform regulations regarding the emissions of ships, which is the reason for the usage of the cheap, but highly toxic heavy fuel oil. The world fleet, which consists of about 90 000 ships, combusts 370 million tonnes fuel per year and emits 20 million tonnes of SO_x. Just the 15 biggest ships in the world already emit more pollutants per year than 750 million cars [39,40]. Not only these facts, but also the technical progresses of the last years concerning the optimisation of the diesel engine and its emissions shed another light on the whole discussion.

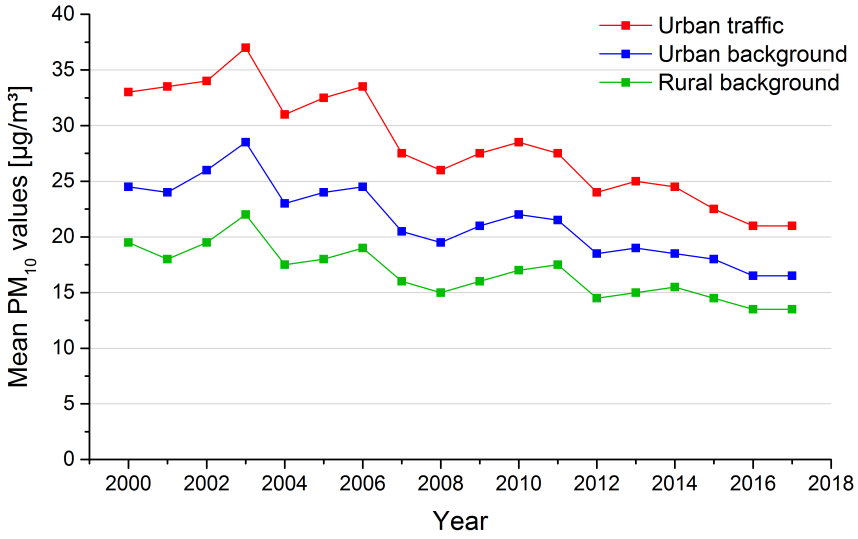

Figure 3: Comparison of the annual mean PM_{10} values of the rural background, urban background and urban traffic in Germany, according to [33].

Indicated by Fig. 2 and Fig. 3, many technical advances already show their effects concerning the reduction of emissions of diesel engines. There are two different approaches to reduce the emissions of a vehicle: engine internal measures and exhaust gas aftertreatment. Regarding the internal measures in diesel engines, there is a trade-off between

high NO_x and low soot emissions and vice versa. These measures act as basis for the subsequent exhaust gas after-treatments [31]. A very common measure is the exhaust gas recirculation method (EGR), which is explained in detail in section 2.1.3.5. For the exhaust gas after-treatment, it is state of the art to use a diesel oxidation catalyst (DOC), followed by a selective catalytic reduction (SCR) on a diesel particulate filter and an ammonia slip catalyst (ASC) [41]. The DOC oxidises unburnt hydrocarbons, CO and SO_x [31]. The SCR catalyst is used to reduce NO_x emissions. With ammonia (NH_3) being the selective reducing agent, a NH_3 precursor is necessary, since the on-board storage of gaseous NH_3 is too dangerous. An aqueous solution of 32.5 wt% urea, better known as AdBlue, is used as precursor and injected into the exhaust tract [41]. Due to thermal activation, urea is decomposed as follows:

$$(NH_2)_2CO \rightarrow HNCO + NH_3 \tag{1}$$

$$HNCO + H_2O \rightarrow CO_2 + NH_3 \tag{2}$$

After the evaporation of water, the thermolysis of urea leads to one equivalent of NH_3 and isocyanic acid. A second equivalent of NH_3 is obtained due to the hydrolysis of this acid, which also causes the formation of CO_2 (see Eq. 2). A TiO_2 supported $V_2O_5 - WO_3$ catalyst is commercially used to improve these two reaction steps [42]. The NH_3 molecules are stored on the surface of the SCR catalyst.

$$\text{Standard} - \text{SCR}: \quad 4\,NH_3 + 4\,NO + O_2 \rightarrow 4\,N_2 + 6\,H_2O \tag{3}$$

$$\text{Fast} - \text{SCR}: \quad 2\,NH_3 + NO + NO_2 \rightarrow 2\,N_2 + 3\,H_2O \tag{4}$$

$$NO_2 - \text{SCR}: \quad 8\,NH_3 + 6\,NO_2 \rightarrow 7\,N_2 + 12\,H_2O \tag{5}$$

Eq. 3-5 show the possible SCR reactions, depending on the NO/NO_2 ratio. As NO is the main NO_x emission with 85 to 95%, the standard-SCR describes the common reaction to reduce NO_x emissions. The fast-SCR reaction, which needs a NO/NO_2 ratio of 1:1, has high conversions at lower temperatures, which makes it the most favourable SCR reaction. The necessary NO_2 can be produced by the DOC. If the amount of NO_2 is too high, the NO_2-SCR reaction takes place, which leads to a higher AdBlue consumption, since more NH_3 is needed. To avoid NH_3 emissions, the ASC is used [41]. The drawback of this SCR catalyst is the necessary temperature of about 180 °C to decompose urea [31]. Thus, the SCR catalyst is deactivated at cold starts [43]. Due to the development of new vehicle architectures, the exhaust gas after-treatment can proceed close to the engine, where the temperature is increased [31]. Nevertheless, since future engine systems will have a higher thermal efficiency, which will lead to lower exhaust gas temperatures, this problem

will remain. There are two different approaches to solve this issue: the usage of another NH_3 precursor and SCR catalyst. Regarding the latter approach, iron and copper zeolites could replace the vanadia-based SCR systems. Many substances were already investigated as alternative NH_3 precursors like ammonium compounds and the commercially sold AdAmmine, which is a strontium complex. The alternatives are very similar, since ammonia is still the only known substance, which reduces NO_x in a stoichiometric ratio of 1:1. Nevertheless, most of them are hazardous or toxic and the handling of solid precursors is more complicated than of liquids [41].
There are further technologies to prevent NO_x emissions like a NO_x storage catalyst, a passive NO_x adsorber and a lean NO_x trap. The storage catalyst works at oxygen-rich gas compositions already at 120 °C, which is the reason for its combined usage with the SCR catalyst. It is regenerated during oxygen-poor conditions with CO and unburnt hydrocarbons [31]. With the passive adsorber, NO_x is stored at low temperatures. Since it gets released unconverted at higher temperatures, subsequent after-treatments are still necessary. The lean NO_x trap is an already common after-treatment method for passenger cars. At lean combustion conditions, NO_2 reacts with the storage compound like barium carbonate to form nitrates. During rich combustion conditions, NO_x is released again and reduced by the generated CO [41].
To reduce soot emissions, a diesel particulate filter (DPF) is commonly used. While filtering even small particles was already possible with this device, its regeneration was challenging. The particle loading leads to an exhaust gas counter pressure, which impedes exhaust emissions. Currently, the continuously regenerating trap method is used in passenger cars in combination with a DPF, which is also known as continuously regenerating diesel particulate filter (CRDPF). For that, the filter is coated with an oxidation catalyst. There are two different operating principles: the active and the passive regeneration. At low load conditions like the urban traffic, the active regeneration is performed by increasing the exhaust gas temperature to about 600 °C with a post-injection, which oxidises the soot to CO_2. To enable the usage of the passive regeneration method, the operating temperature as well as the NO_2 concentration must be high enough. With NO_2 being a stronger oxidant than O_2, soot is oxidised at temperatures between 200 and 500 °C [44,45]. Due to its high effectiveness, the DPF not only reduces the soot emissions of diesel engines, but also the soot of the sucked in ambient air [31].
From what is written before, it can be concluded that great technological progress was achieved in the last years concerning the reduction of emissions of diesel vehicle engines. In the past 20 years, the soot emissions produced by traffic were reduced by more than 50% and the NO_x emissions by even 64% without taking the Euro 6 standard into consideration [31]. Since it takes about 13 years to replace 90% of the passenger cars by modern ones, these reductions will even further increase in the years to come. It is also

mentionable that petrol engines like the GDI of Volkswagen or TFSI of Audi are currently sold, which inject the fuel directly into the cylinders. These vehicles produce emissions like old diesel cars without any filter systems, which are not necessary, since there are no comparable standards for petrol engines [46]. Thus, the diesel engine by itself is sufficiently developed to significantly contribute to the contemporary mobility. It is indisputable that the manipulations within the "Dieselgate" scandal must result in penalties for those responsible. The diesel technology, however, is still of great importance for the mobility sector due to its high efficiency. Therefore, this thesis deliberately focuses on new fuels for diesel engines. As the "Dieselgate" scandal also intensified the demand for a more sustainable energy production, the next section will explicitly describe the status quo of liquid biofuels.

2.1.1.2 Status quo of liquid biofuels

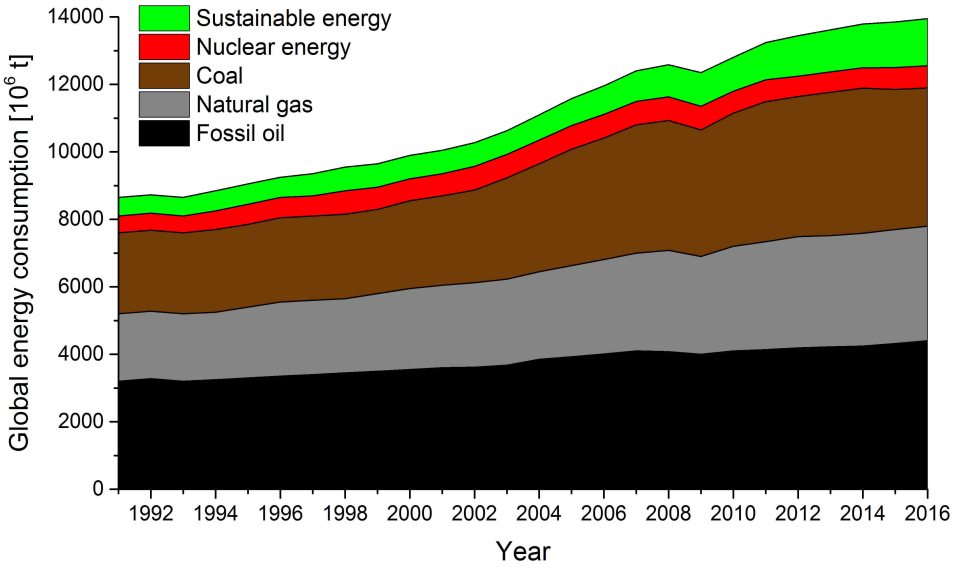

Figure 4: Global energy consumption of the last 26 years in million tonnes of oil equivalent, according to [47].

As already mentioned in the introduction of this thesis, sustainable energy production became one of the most urgent research topics of our time. Before going into detail concerning specific sources of bioenergy, an overview of the current global energy consumption is given. Fig. 4 outlines that less than 10% of the consumed energy is derived from sustainable resources. Even though the overall energy consumption increased during the last years, the main reason for that is not the growing demand for renewable energy, but the

increasing exploitation of coal deposits. Further, about 70% of the sustainable energy shown in this figure is obtained from hydroelectricity, which also entails several environmental and social drawbacks [47]. Since fossil fuels, which are still the most consumed energy source, have limited reserves and their production volume is already at its peak, alternatives are inevitably required [48].
With the industry being forced to develop either new exploitation methods for the remaining fossil fuels or fuels based on sustainable resources, this thesis deals with the latter possibility. To be able to compare the properties and the current state of biofuels with common diesel, a brief outline of fossil fuels, in particular diesel, is necessary. While petrol is spark-ignited, the heat of compression leads to the self-ignition of diesel in diesel engines. Therefore, a diesel engine is also called compression-ignition engine [49]. Diesel consists of about 75% aliphatic hydrocarbons, which are primarily paraffins, and 25% aromatic hydrocarbons. There is no precise composition of diesel, as it is a complex mixture obtained from distillation of crude oil. On average, the hydrocarbons of diesel range from C_{10} to C_{15}. Petrol, on the other hand, is mainly a mixture of small alkanes, aromatics, cycloalkanes and alkenes in the range of C_4 to C_{10} [50]. Assuming a fuel only consisting of alkanes, Eq. 6 shows the complete combustion, which leads to the products CO_2 and water [49].

$$C_nH_{2n+2} + (1.5n + 0.5)\,O_2 \rightarrow n\,CO_2 + (n + 1)\,H_2O \tag{6}$$

Certainly, not only hydrocarbons are combusted in diesel engines. About 10 to 50 ppm of sulphur components, for example, are present in diesel [51]. Further, since air is needed for the combustion process, nitrogen and oxygen are also inside the engine. This in turn leads to the common and in section 2.1.1.1 more thoroughly described emissions of fuel engines: CO_x, NO_x, SO_x, soot and water [52]. The most important advantage of diesel compared to petrol is its higher level of efficiency. As diesel is more than 20% more efficient than petrol, less diesel is consumed for the same distance. Additionally, diesel has a higher power output due to its higher torque to the drive shaft, compared to a petrol engine [31,53]. After introducing promising biofuels that could replace diesel in the future, the physicochemical properties of diesel will be explained within a comprehensive table (see Table 2).
The most utilised source for sustainable fuels is biomass, which commonly refers to plant-based materials. Before being used for power generation, it has to be converted into appropriate compounds [17]. Due to their global cultivation and thus large available quantity, vegetable oils are one of the most promising biofuel sources. Their use and applicability in diesel engines was already investigated by the inventor of the diesel engine, Rudolf Diesel, in 1900. He used peanut oil as fuel for his developed engine for demonstration purposes [54]. Because of the fuel and energy crisis of the late 1970s and early 1980s,

which led to concerns about the depletion of the fossil fuels for the first time, intensive research on alternative fuels started. Since then, hundreds of scientific articles, with many of them dealing with vegetable oil-based biofuels, were published every year [49]. Not only the increasing world population, but also this research distinctly increased the amount of produced vegetable oils in the past years.

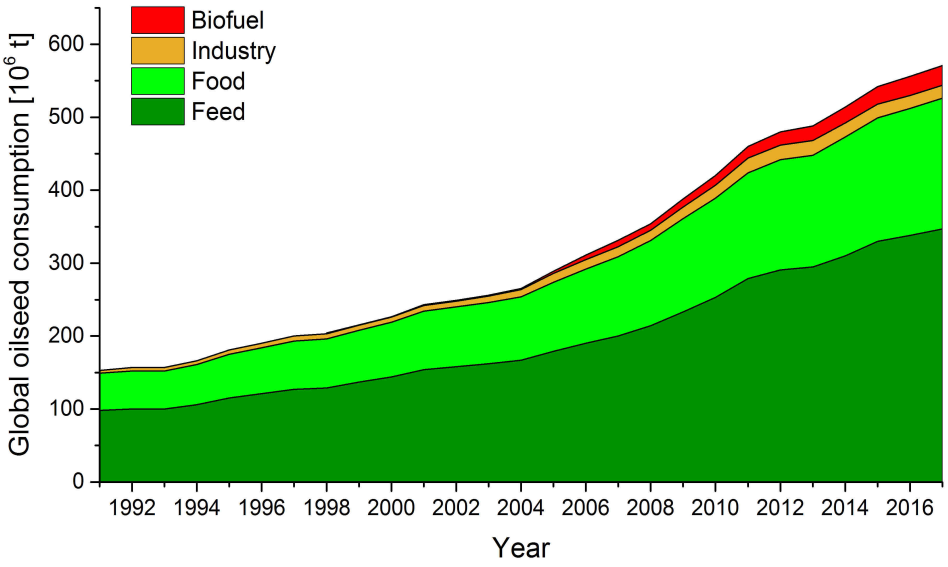

Figure 5: Global oilseed consumption of the last 27 years in million tonnes, according to [55,56].

Starting with the usage of vegetable oils as biofuels in 2000, its share compared to the global oilseed consumption was still very small even in 2017, since most of the oilseeds are used as animal feed (see Fig. 5). Considering the usage of just the oils, however, the share of biofuels increased from 1% in 2001 to 7% in 2008 and to 12% in 2017 [55,56]. A main reason for this fast increase are the simple agricultural and industrial processes like cold pressing and refining stages to obtain vegetable oils. Therefore, even small-scale production could be interesting for farmers, who could use vegetable oils for their on-farm energy generation [57,58]. To emphasise the global applicability of vegetable oil derived biofuels, De Almeida *et al.* examined the social and economic advantages of the Amazon region, exemplarily, resulting from the implementation of vegetable oils as fuel source. The population of this South American area is distributed to small villages in the margins of rivers. Since most of these people have a very low income, the costs of having access to conventional electricity are high. Thus, power is commonly generated by diesel combustion engines, which in turn enables the usage of vegetable oil-based biofuels as alternative. Especially these regions possess suitable soils and climatic conditions to cultivate their own biofuel source without the necessity of high investments. This implementation would considerably increase the

quality of life, rural employment and income opportunities, while simultaneously using sustainable energy [8, 59]. There are other examples pointing out the utilisation of arable wasteland by cultivating vegetable oils, which would scale up their production volume. This in turn could temporarily moderate the ubiquitous "Food vs. Fuel" problem and lead to decreasing costs due to improved mechanised farming and rising production yields. A study of Herres *et al.* concludes that only 2% of the arable land worldwide are necessary to produce enough vegetable oils for the global fuel consumption [60–62]. There are, however, still several problems: while most European, American and Asian countries focused on increasing their yields in the past decades, especially sub-Saharan countries just increased their cultivation areas. As the know-how is missing and high investments are necessary to cultivate crops efficiently in these regions, the "Food vs. Fuel" problem remains as major point for discussion [63, 64].

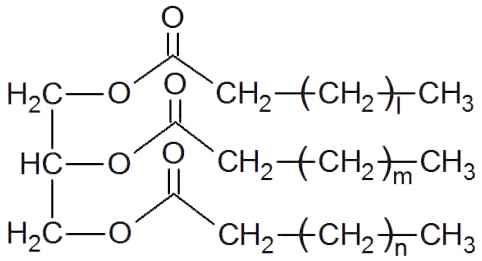

Figure 6: Chemical structure of vegetable oils with saturated fatty acid chains.

To understand the differences between vegetable oils regarding their physicochemical properties, a closer look has to be taken on their chemical structure (see Fig. 6). Primarily, they consist of triglycerides, which are characterised by a glycerol backbone and hydrocarbon chains. These chains belong to fatty acids, which are attached to the backbone by their carboxylic acid group forming ester bonds. The indices l, m and n indicate the variety of fatty acids that differ in the size of the carbon chain and the amount of carbon-carbon double bonds [7, 49]. Before explaining the influence of the fatty acid composition of the triglycerides on important biofuel properties, the global distribution of vegetable oils is outlined. More than 75% of the globally produced vegetable oils are palm oil, soybean oil and rapeseed oil [55]. Due to the necessity of tropical conditions, palm oil is mainly cultivated in Southeast Asia. With its low production costs and high yield, palm oil is not only used as feed and cooking oil, but also as base material for detergents, soaps and waxes [65]. Soybean oil, on the other hand, is grown all over the world, with the US being the main producer with a share of about 25% [66]. The third most cultivated vegetable oil is rapeseed oil, which is typically grown in Europe and especially in Germany. In general, the growing region of the respective vegetable oils is decisive for the research interest of the countries regarding the usage as biofuels. This means that soybean oil is of main interest

as biodiesel source in the US, whereas rapeseed oil is favoured in Europe [49]. This in turn is also the reason for the usage of rapeseed oil in this thesis.
As there are commonly three fatty acids attached to the glycerol backbone, there is a huge variety of possible vegetable oil compositions. In most cases, vegetable oils consist of about 95% triglycerides, 1–5% free fatty acids and a few sterols, phosphatides, phospholipids, carotenes and tocopherols [7, 67]. This already indicates a typical problem, when dealing with biomass-derived compounds: they are prone to impurities [59]. Compared to palm oil and soybean oil, rapeseed oil is mainly composed of unsaturated fatty acids, in particular oleic, linoleic and linolenic acid (see Table 1) [7, 49]. In general, vegetable oils do not contain any aromatic hydrocarbons, crude oil substances, metals and sulphur. Especially the absence of the latter is important, since SO_x emissions are a considerable problem of fossil fuels [8,67]. While the meaning and determination of the physicochemical properties shown in Table 2 are explained in detail in chapter 2.1.3, a correlation between the fatty acid composition of rapeseed oil and its properties can already be established.

Table 1: Fatty acid composition of palm oil, soybean oil and rapeseed oil [7, 49]. The fatty acids are described by their carbon chain length and the amount of carbon-carbon double bonds. Therefore, *18:1*, for example, represents a C_{18}-chain with one double bond.

Vegetable oil	$\omega_{\textbf{fatty acid}}$**[wt%]**					
	14:0	16:0	18:0	18:1	18:2	18:3
Palm	0.5–2	32–46	4–6	37–53	6–12	–
Soybean	–	2–11	2–6	22–31	49–55	2–11
Rapeseed	–	1–5	1–4	53–70	15–30	5–10

Considering the usage of a vegetable oil as biofuel, the most demanding challenge for formulators as well as engineers is its high viscosity. The kinematic viscosity η_{kin} of a vegetable oil is typically in the range of 30 to 40 mm^2/s at 40 °C. As depicted in Table 2, η_{kin} of the used rapeseed oil is nearly ten times higher than that of the used diesel. Since the viscosity of a vegetable oil increases with the chain lengths of the fatty acids and their degree of saturation, Table 1 explains the particularly high viscosity of rapeseed oil. Palm and soybean oil do not only consist of distinctly more short-chain, but also less unsaturated fatty acids. Additionally, the high molar mass of vegetable oils facilitates the polymerisation induced by the unsaturation of the fatty acids, leading to agglomerations and subsequent gumming. This low degree of saturation also causes a low stability of rapeseed oil towards oxidation and thus storage problems [59, 67, 68]. Another problem regarding the usage of vegetable oils are their high cloud and freezing points. Although the used rapeseed oil possesses an unusually low cloud point, which is explained in chapter

2.1.3, this parameter restricts its implementation as biofuel in cold regions and in the aviation sector [69]. The worse ignition quality of a vegetable oil compared to a fossil fuel like diesel is depicted by the lower cetane number (CN) of rapeseed oil in Table 2 [60]. Since diesel must have a CN of at least 51, this value can be used as reference to estimate the ignition quality of other fuel components investigated in this thesis (see Table 2). The literature values of the combustion enthalpies $\Delta_C H_{298}$ of rapeseed oil and diesel indicate that vegetable oils possess nearly the same energy content as diesel [7]. During short-term engine tests, their power outputs are the same and the thermal efficiency of vegetable oils is even higher than that of diesel [70]. On the one hand, the chemically bound oxygen of the ester bonds facilitates the combustion process, but on the other hand, the presence of oxygen atoms in the molecule reduces the heating values. Due to its high flash point compared to most of the oxygenates like ethanol, rapeseed oil can be stored at high temperatures without any fire hazard. This high flash point, however, is coupled with a low volatility, which increases engine problems like deposit formation, lubricating oil dilution, carbonisation of injector tips and ring sticking [7, 67].

Table 2: Measured densities ρ, kinematic viscosities η_{kin}, cloud points T_{Cloud}, cetane numbers (CN) and combustion enthalpies $\Delta_C H_{298}$ of most of the investigated, single components of the biofuel formulations compared to literature values. The densities and kinematic viscosities were determined at 40 °C according to current fuel standards, except for the literature values marked by *, which were measured at 25 °C. The difference between the measured viscosities as well as cloud points and the literature values of rapeseed oil and FAME result from their diversity, depending on their origin and producer. As the glycerol derivatives, methyl decanoate (MeC_{10}), 2-methylfuran (2-MF) and ethanol are pure components, their freezing points are given and marked by * instead of the cloud points [1, 49, 59, 71–87].

Compound	**ρ[kg/m^3]**		**η_{kin}[mm^2/s]**		**T_{Cloud}[°C]**		**CN**	**$\Delta_C H_{298}$[MJ/kg]**	
	Used	Lit.	Used	Lit.	Used	Lit.	Lit.	Used	Lit.
Diesel	840	820–860	3.8	2.0–4.5	−10	−10	≥51	–	−44.8
Rapeseed oil	903	912	33	35–37	−14	−3.9	41	−38.5	−39.7
FAME	862	860–900	4.3	3.5–5.0	2.5	−2.0	54	−35.4	−40.4
MeC_{10}	856	870	1.8	1.7	<−20*	−10*	52	−32.3	−36.7
Glycerol	–	1262*	–	749*	–	18*	0	–	−19.0
Solketal	1049	1066*	5.1	5.4	–	−26*	<10	−24.9	−25.9
Triacetin	1141	1160*	4.6	7.8*	–	4.0*	<5	–	−4.21
Tributyrin	1014	1028*	5.4	9.7*	–	−75*	7	−9.2	−8.12
2-MF	915	916	0.39	0.37	–	−89*	8	−24.6	−27.6
Ethanol	–	790	–	1.0	–	−114*	8	–	−29.8

Despite these drawbacks, there are many proposals to optimise the implementation of vegetable oils as biofuels. Besides mechanical adaptions of the injecting system, for example, most suggestions are focused on changing the combustion conditions like increasing

the injection pressure or adding a turbo-charger to increase the pressure and temperature inside the cylinders [8]. Mainly the emission characteristics of vegetable oils justify these implementation efforts. They drastically reduce NO_x emissions by up to 70% compared to diesel and produce less PM emissions, while the CO_x and total hydrocarbon (THC) emissions are just slightly increased [60, 67, 69]. Since vegetable oils require CO_2 from the atmosphere during their growth period, they consume more CO_2 than is produced during their combustion, leading to a negative CO_2 balance [7, 67].

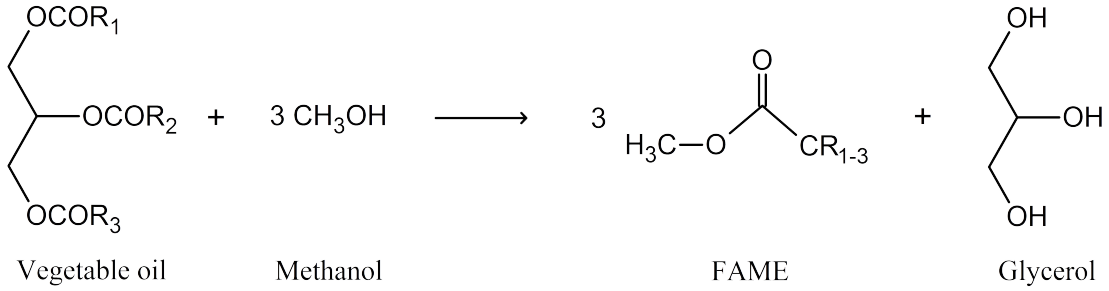

Figure 7: Transesterification reaction of a generalised triglyceride with three different fatty acid residues R_{1-3} with methanol, leading to different fatty acid methyl esters (FAME), also known as biodiesel, and glycerol [1].

A commercially implemented method to solve most of the abovementioned issues, when using vegetable oils as biofuels, is the biodiesel production. Biodiesel is defined as the fatty acid mono-alkyl esters derived from sustainable lipid feedstock like vegetable oils or animal fats that are used in diesel engines [49]. It is obtained by a transesterification reaction of a triglyceride with a mono-alkyl alcohol (see Fig. 7). As methanol is the least expensive and most available alcohol, fatty acid methyl esters (FAME) are the most widely produced biodiesel [1, 7]. On an industrial scale, the reaction is performed with a molar ratio between methanol and the vegetable oil of 6 to 1 for one hour at 60 °C with either 0.5 mol% sodium methoxide or 1 mol% sodium hydroxide as catalyst [88]. Thus, besides the byproduct glycerol, further components like methanol, waste water and the catalyst have to be removed after the transesterification [89]. There are new reactor designs that improve the contact between oil and methanol. A particularly promising method is the usage of ultrasound that induces the formation of cavitational microbubbles in the reactor, whose collapse causes better convection and mixing [90, 91]. Another obstacle are mass transfer limitations, which can be negotiated by supercritical conditions, in particular 300 – 400 °C and 15 – 45 MPa. With this method, the reaction mixture is monophasic, the reaction rate and its yield is increased, no catalyst is necessary and the reaction is insensitive to water and free fatty acids [92]. Another possibility to obtain a monophasic mixture is the usage of co-solvents like tetrahydrofuran [93].

Coming back to the already mentioned "Food vs. Fuel" issue, which refers to the usage of vegetable oils as biofuels and thus also affects the utilisation of FAME, there are not enough vegetable oils cultivated to completely replace diesel. Further, the production costs of FAME are mostly determined by the price of the feedstock. Therefore, less expensive feedstocks like waste oils, greases and animal fats have been investigated for decades. Since they usually contain free fatty acids, water and further impurities, their quality needs to be improved before producing FAME [1]. In recent years, jatropha oil was a very promising example of an alternative feedstock. After cultivating more than 12 million hectares of *Jatropha curcas* in Asia and Africa, farmers had to deal with much less seed production and slower growth of the plants as expected. Especially in India, this cultivation became famous for being a well-intentioned climate mitigation approach without adequate preparation and ignoring conflicts of interest, driving thousands of farmers into bankruptcy [94]. This in turn drew most of the researchers' attention towards photosynthetic microalgae. They can also be cultivated on non-arable land and the photosynthetic efficiency of microalgae is even higher than of plants [95]. Nevertheless, their oils can contain high amounts of polyunsaturated fatty acids, depending on the climatic conditions, making them prone to oxidation [96]. Additionally, they require more fertilisers and energy for cultivation, harvest and post-harvest treatment than vegetable oils, demanding further technological breakthroughs, before implementing the production of microalgae oils on an industrial scale [97].

FAME is a technically competitive and sustainable alternative to conventional diesel due to its physicochemical properties. It is obvious that FAME possesses the same advantages as vegetable oils concerning sustainability, non-toxicity and biodegradability [71]. The latter is improved by its high oxygen content, which lets FAME degrade about four times faster than diesel [98]. It also contains no sulphur as well as aromatics and is completely miscible with diesel [1, 99]. As shown in Fig. 7, the transesterification leads to a distinctly reduced molecular weight of FAME, which in turn decreases the viscosity by about an order of magnitude compared to the vegetable oil. In the scope of this thesis, FAME derived from rapeseed oil is used, whose kinematic viscosity is very close to diesel (see Table 2). This makes FAME compatible with the existing fuel distribution infrastructure and diesel engines without further modifications, increasing its economic applicability [1]. Table 2 also shows that the CN of FAME is usually even higher than that of diesel, which can be explained by its higher oxygen content [7]. There are further advantages of FAME like its high flash point and inherent lubricity, which are not further described, since these properties were not considered in this thesis.

Despite its high CN, FAME usually leads to slightly more NO_x emissions than diesel [100]. Its most important drawbacks, however, are the flow properties and the phase behaviour at low temperatures. They affect the usage of pure FAME and of blends with diesel [1].

As it is a mixture of various esters, which differ in the degree of saturation of the fatty acid chains, its cloud and pour point are distinctly higher than that of vegetable oils or diesel (see Table 2) [49,101]. In general, the higher the degree of saturation, the higher the melting point of the compound [1]. There are several approaches to improve the properties of FAME at low temperatures. Many additives, usually polymers, are known to reduce the cloud and pour point of FAME. Further, the usage of branched alcohols like *iso*-propanol instead of methanol, leading to branched esters, also decreases these points [102, 103]. A very similar and promising approach is the utilisation of branched fatty acid chains, since branching the ester moiety negligibly influences the viscosity [1]. Within the winterisation method, the esters are cooled down and solid components, mainly saturated esters, are removed. As these esters have higher CNs than unsaturated esters, this method improves the low-temperature properties of FAME, but simultaneously deteriorates its ignition quality [104, 105]. Besides saturated esters, there are more compounds that affect the cold flow properties. Especially monoacylglycerols, which are intermediates of the transesterification reaction, and steryl glucosides are problematic. Already the presence of 0.01 wt% increase the cloud point of a FAME/diesel blend by 4 °C [106]. Another important drawback of FAME is its low oxidative stability. As already mentioned for vegetable oils, unsaturated fatty acid residues are prone to oxidation and thus lead to loss of quality during long-term storage, which is explained in more details in section 2.1.3.3 [1]. The combustion enthalpies of Table 2 indicate that FAME has a lower energy content than diesel. Again due to its unsaturation, the heating values are reduced by about 12%, which causes higher fuel consumption [98]. This drawback is at least partially compensated by the higher density of FAME compared to diesel [1].

Since the properties of FAME depend on the source and growing conditions of the vegetable oils, the search for the best suitable source for FAME production bothered many research groups in the past decades. Especially Knothe *et al.* achieved success by screening and comparing a variety of vegetable oils as well as their respective biodiesels. Their most promising source is the cuphea plant, which is native to North and South America. With most of its species containing oils with high amounts of saturated fatty acid residues with chain lengths between C_8 and C_{16}, the auspicious properties can be attributed to its chemical composition. It is well known that saturated medium-chain fatty acids are most qualified for FAME processing [71]. Thus, especially the species *Cuphea lanceolate* and *Cuphea Viscosissima* are suitable, as they contain about 84% and 62% of decanoic acid, respectively [107]. Therefore, the methyl ester of decanoic acid, methyl decanoate (MeC_{10}), is investigated as alternative to common FAME within the scope of this thesis and its properties are also outlined in Table 2.

Due to standards like the ASTM D6751 in the US and the EN 14214 in Europe, which promote the usage of FAME, it became the prevailing biofuel [74, 108]. In 2005, all Euro-

pean Member States had to blend diesel with 2 vol% of FAME for vehicles because of the 2003/30/EU guideline [109]. Simultaneously, Minnesota was the first U.S. state to introduce the same amount of FAME to diesel [110]. According to the standard EN 14214, the amount of FAME added to diesel should increase to 10 vol% until 2020, with 7 vol% being currently used in Germany [111]. As shown in Fig. 8, global FAME production increased to more than 30 million tonnes in 2016. Further, it is produced all over the world, with Europe, USA and Brazil being the main contributors [112]. In 2017, Germany produced about 3.1 million tonnes of FAME, mostly derived from rapeseed oil [113]. Many investigations are currently carried out leading to so-called "designer" biodiesel. On the one hand, there are common approaches like the usage of additives or changing the feedstock to optimise its properties. But on the other hand, highly complex processes like genetic modifications are developed to change, for example, the fatty acid profile of a vegetable oil specifically [1].

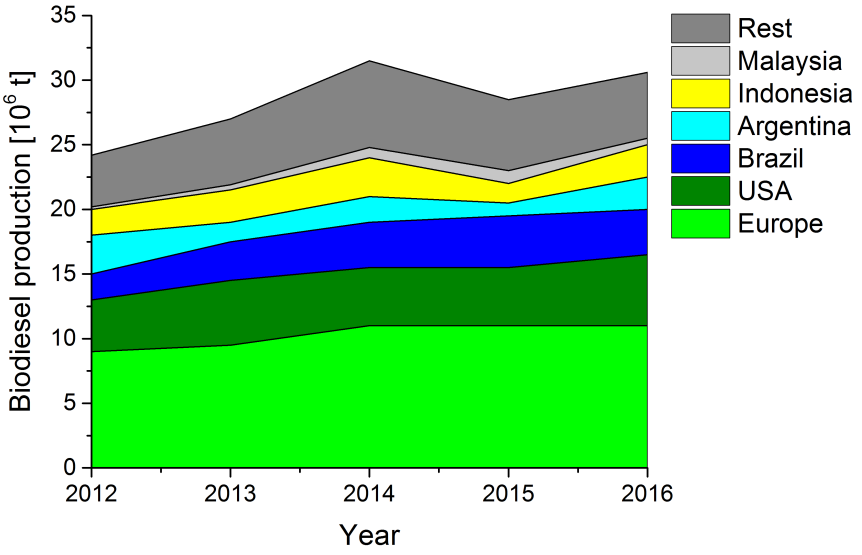

Figure 8: Global biodiesel production of the past years in million tonnes, according to [112].

In general, biodiesels and especially FAME are currently crucial to fulfil international climate objectives, dealing with the implementation of sustainable energy. Since vegetable oils are more expensive than fossil resources and the transesterification to FAME is coupled with the production of the by-product glycerol, the production profitability of FAME is about half compared to diesel. This implies that the industrial applicability of glycerol has a huge impact on FAME's profitability. Already decades ago, bio-derived glycerol was used in pharmaceutical, cosmetic and food industry, sufficiently satisfying the demand for 100 kilotonnes in 1995 [114]. Since glycerol arises in a weight ratio of 1:10 compared to

FAME, the amount of produced glycerol sharply increased to about 3.5 million tonnes per year in 2015, which led to an oversupply and low prices [115,116]. With the crude glycerol price currently being 20 ct/kg, just the large scale producers refine the waste stream for industrial applications. The small scale producers, however, are unable to justify the refining costs. Therefore, they pay a fee for the glycerol removal, causing huge environmental problems regarding waste disposal [114,117].

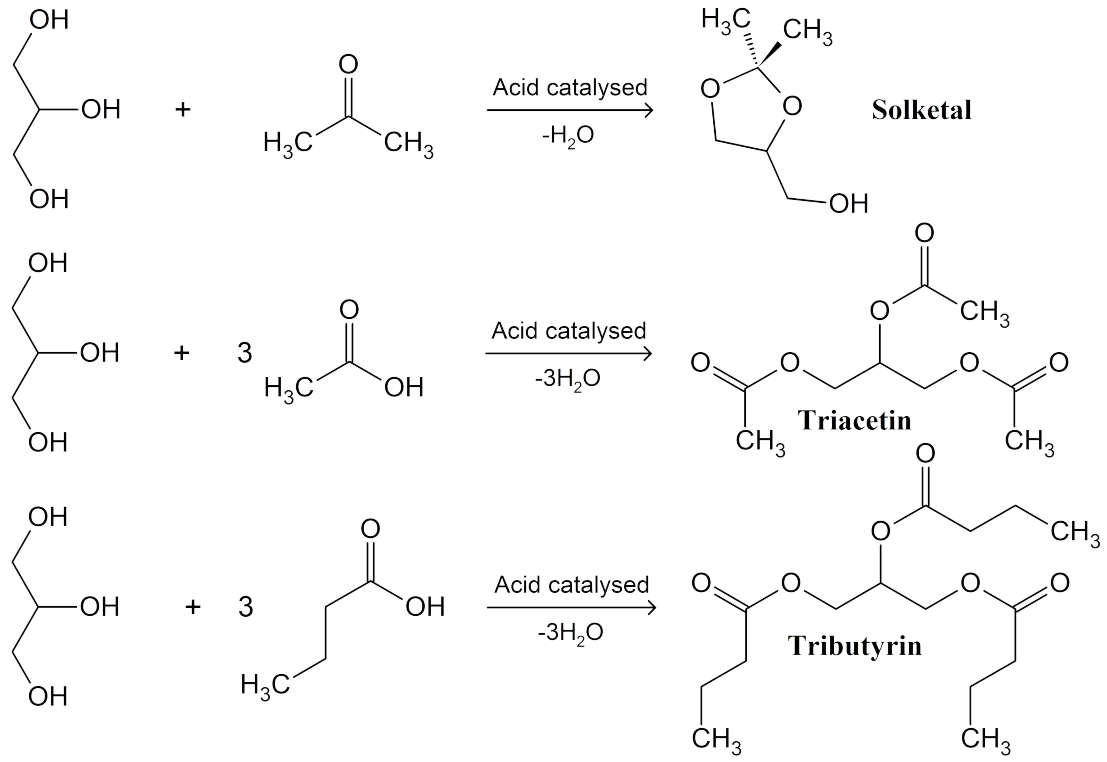

Figure 9: Glycerol derivatives obtained by addition reactions of glycerol with either short-chain carboxylic acids or building block chemicals. This work explicitly focuses on the products of the reactions with acetone, acetic and butyric acid, leading to solketal, triacetin and tributyrin, respectively.

The demand for glycerol is mainly limited due to several drawbacks. Its strong hydrophilicity makes it completely immiscible with many organic compounds, vegetable oils and common fuels. This already excludes the implementation of glycerol into fuels, which would obviously be the best-case scenario. Further, it possesses a very high viscosity and freezing point [117, 118]. Therefore, the usage of glycerol as feedstock for the preparation of more valuable products is still of considerable interest for companies and research groups. Besides the utilisation of glycerol as reaction medium, there are many patents and publications dealing with the syntheses of important building block chemicals like propanediol, glycerol carbonate, lactic and acrylic acid [114, 119]. Lari *et al.* showed that the implementation of biorefineries based on glycerol combined with the FAME pro-

duction process would increase the FAME profitability from the current value of about 0.01–0.1 $/kg(vegetable oil) to 0.07–0.18 $/kg(vegetable oil). This in turn is comparable with the current profit of fossil fuels [114].
Regarding the scope of this thesis, especially simple and cheap derivatisation reactions of glycerol to more hydrophobic compounds like glycerol ethers, esters and acetals are relevant (see Fig. 9). After easy and industrially already price-competitive addition reactions with short-chain carboxylic acids or building block chemicals like acetone, glycerol derivatives with low viscosities and freezing points are obtained (see Table 2) [116, 120]. During this thesis, investigations dealing with the usage of glycerol derivatives as possible fuel components explicitly focused on the products of the reactions with acetone, acetic and butyric acid, referred to as solketal, triacetin and tributyrin, respectively [116, 118]. The comparison of the properties of these three glycerol derivatives with fuels like diesel or FAME in Table 2 shows that their kinematic viscosity is nearly as low as the value of FAME. Regarding their freezing points, just solketal and tributyrin possess sufficiently low values. Besides their very low CNs, the combustion enthalpies especially of triacetin and tributyrin are reduced due to the presence of ester bonds [82, 83, 85].
Another promising solution of the "Food vs. Fuel" debate could be the hydrotreating of vegetable oils or animal fats. Hydrotreated vegetable oils (HVOs) can be either produced from common vegetable oils, similar to FAME, or from waste cooking oils or non-agricultural feedstocks. HVOs, which are nowadays also referred to as "renewable diesel fuels", exclusively consist of paraffinic hydrocarbons [121, 122]. Therefore, in contrast to FAME, they have no increased gaseous emissions as well as no deposit formation, no stability problems during storage and they do not depend on the feedstock. Since HVOs are similar to diesel regarding their chemical composition, they possess high CNs and fulfil conventional diesel standards [121]. This in turn enables the utilisation as drop-in fuel, which indicates that HVOs can be used in high blends [122]. Due to the absence of aromatic compounds and their low emissions in general, HVOs could significantly contribute to a cold start phase with less unburnt raw emissions, as current diesel engines have low exhaust gas temperatures, leading to issues at cold starts [123]. Although there is just one considerable drawback, it is severe enough to distinctly retard the implementation of HVOs into the fuel market: the production expenses of the hydrotreatment. The process consists of two steps. Firstly, paraffins are produced during a catalytic hydrotreatment at pressures of about 4 – 6 MPa and 300 – 350 °C. During this process, triglycerides, fatty acids and FAME are hydrogenated and converted by decarboxylation, decarbonylation and hydrodeoxygenation reactions in the presence of silica- and alumina-supported catalysts containing nickel or molybdenum. Secondly, these paraffins are catalytically isomerised to a mixture of *n*- and *iso*-paraffins. A few years ago, a new method, the catalytic cracking process, was developed to produce HVOs with lower expenses. After decarbonisation, the

hydrogenation takes place at 1 MPa and 150 °C, consuming only a tenth of the amount of hydrogen used during direct hydrogenation [122, 124]. Although being costly processed, HVOs are currently promoted by several countries and companies. The Neste Oyj company is the most important manufacturer of HVOs with a total capacisty of 2.6 million tonnes per year, mainly produced in Finland and the Netherlands [125].

2.1.2 Alternatives to biofuels – E-fuels and E-mobility

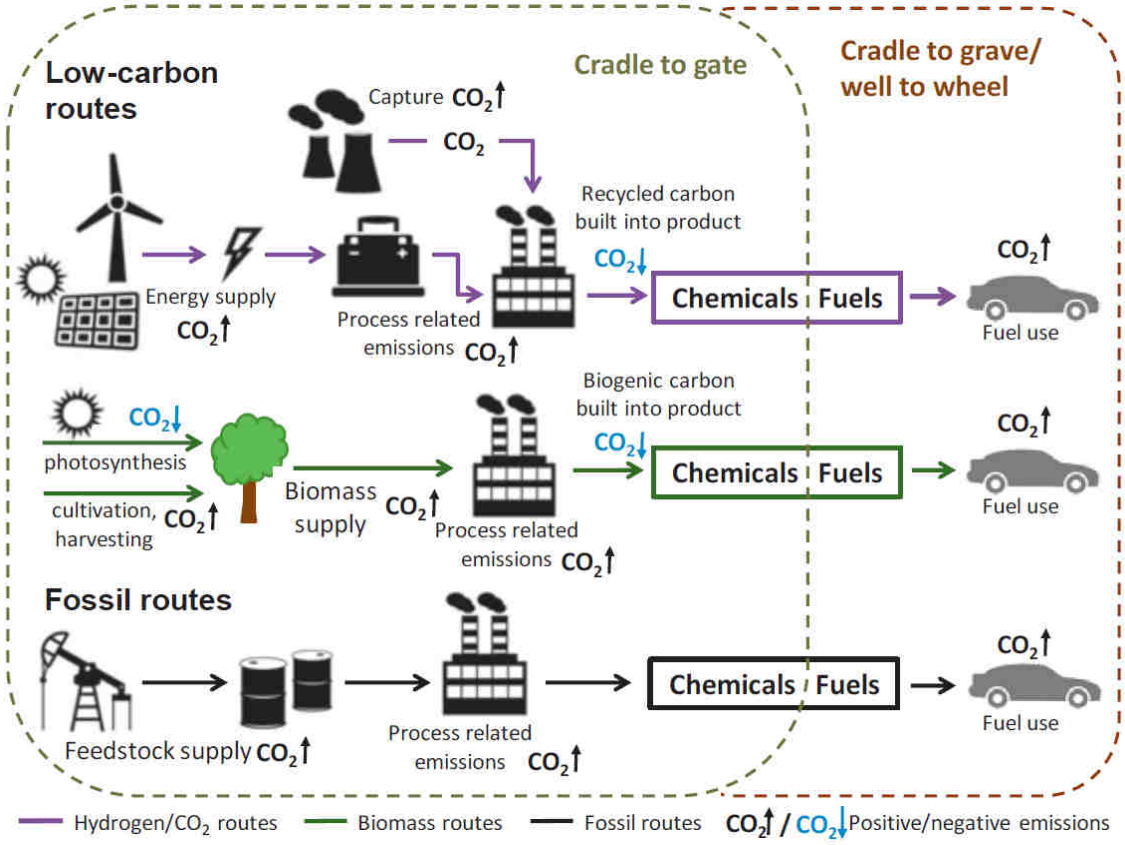

Figure 10: Different fuel production routes displaying their CO_2 footprints. In particular, the production of fossil fuels, biofuels and E-fuels is shown [126].

With the current fuel situation and the proceedings in developing sustainable biofuels being described in detail in the previous chapter, alternatives to these biofuels need to be mentioned as well. To keep track of the different fuel production routes, Fig. 10 outlines the three main fuel types of our time: fossil fuels, biofuels and E-fuels [126]. The latter comprises synthetic fuels, also known as tailor-made fuels, produced with electricity from sustainable energy sources [127]. Fig. 10 also indicates the CO_2 footprint of these processes. It is obvious that the usage of fossil fuels does not contribute to the reduction of CO_2 emissions, whereas the production of biofuels and E-fuels gives the opportunity to achieve neutral or even negative CO_2 emissions [126]. This chapter will give an insight into the currently most promoted E-fuels, in particular the base materials hydrogen, methane and methanol as well as Fischer-Tropsch hydrocarbons and oxymethylenethers (OMEs). In this context, the usage of ethanol as fuel is also explained, although it belongs to the biomass-derived fuels. Since most of these compounds possess properties that impede their industrial application as competitive alternative to fossil fuels, ethanol takes an

exceptional position in this chapter. Further, the present stage of development regarding the establishment of pure electric mobility is described, before summarising and evaluating E-fuels with respect to their impact on international climate objectives.

2.1.2.1 Electrolytic production of hydrogen and fuel cells

Hydrogen is one of the most important starting materials of the chemical industry. As it is part of the synthesis gas, it is essential for the production of many platform chemicals. H_2 is also necessary to obtain most of the already mentioned E-fuels, which will be further described in the subsequent sections. Nevertheless, H_2 itself can also be used as fuel in a combustion engine or in fuel cells [126]. Since about 96% of H_2 is obtained from fossil resources like coal gasification, alternative H_2 production routes are required to use it as E-fuel [128]. The usual sustainable source for H_2 is water, which is split to O_2 and H_2 during water electrolysis according to following net reaction [126]:

$$2\,H_2O \rightarrow 2\,H_2 + O_2 \qquad \Delta H^0 = 571.8\,\mathrm{kJ/mol} \tag{7}$$

The high reaction enthalpy displays the main problem of H_2 obtained from sustainable sources. H_2 production is typically the most energy demanding step of chemical syntheses. Thus, water electrolysis is currently just used to produce H_2 with high purity [129]. As the reduction of the energy consumption during electrolysis is a main research topic, there are already different industrial approaches to solve this problem. Alkaline electrolysis is the state-of-the-art industrial process, which uses an aqueous solution of 20–40 wt% potassium hydroxide. Commonly, the electrodes are coated with nickel as catalyst and both half cells are separated by a diaphragm. In the past 20 years, the proton-exchange membrane (PEM) electrolysis has been developed, which uses pure water and enables a compact setup. Nevertheless, this technology leads to high investment costs due to the utilisation of platinum and iridium as catalysts [126]. In the scope of the e-gas project of Audi, the PEM technology is essential. In a unique facility in Werlte, Germany, wind turbines provide the necessary electricity to produce H_2 with PEM electrolysers. H_2 is then further processed to methane, with the required CO_2 coming from the exhaust stream of an adjacent biogas plant. After that, methane is fed into the natural gas grid [130]. A promising method to distinctly reduce the energy consumption of water electrolysis is the addition of activating compounds into the electrolyte. These ionic activators commonly consist of ethylenediamine metal chloride complexes ($[\mathrm{M(en)_3}]\mathrm{Cl_x}, \mathrm{M} = \mathrm{Co}, \mathrm{Ni}$) or sodium molybdate and tungstate. During electrolysis, these compounds are electrodeposited in situ on the cathode surface and increase the catalytic activity for hydrogen generation even more than an ex-situ electrodeposition. With this method, the energy consumption decreases by about 15% [131–133].

In general, the amount of electricity necessary to split water can be reduced by higher temperatures. Compared to water electrolysis at 25 °C, energy consumption decreases by 23%, when performed at 900 °C. This effect is utilised in a solid oxide electrolysis cell. Within this approach, the cathode and anode are isolated by a solid electrolyte. At temperatures between 600 and 1000 °C, water is decomposed to H_2 and O^{2-}, with the anions being transported through the electrolyte and oxidised to O_2 at the anode. Although this method possesses the highest energy efficiency of the currently investigated electrolysis approaches, it is still not suitable for industrial application. With zirconium dioxide, doped with yttrium oxide, and lanthanides being used as solid electrolyte and electrode materials, respectively, more development time is required to establish H_2 as E-fuel [129].
Since the solid oxide electrolysis method can be also described as reverse fuel cell process, a brief comparison with this power generation approach can be drawn. In a typical hydrogen-oxygen fuel cell, H_2 is catalytically oxidised to protons, which move through a polymer membrane that is only permeable for protons. The electrons are first redirected to an electrical load and then to the cathode, where O_2 is reduced to O^{2-}, which in turn reacts with the protons to water [129]. Considering the overall system, dealing with the high costs, low energy density of H_2 and its storage problems, the fuel cell technology will not be able to replace fossil fuels for passenger cars. One possible application of fuel cells in the driving sector could be their implementation into heavy-duty vehicles. In the case of trucks, for example, there could be enough space for H_2 storage, although the permission for this modification still needs to be granted [134].

2.1.2.2 Methane and methanol-to-gasoline hydrocarbons

Other very important starting materials for chemical syntheses are currently promoted as alternative E-fuel sources: methane and methanol. Apart from methane (CH_4) being obtained from fossil resources, it can also be produced according to the Sabatier process (see Eq. 8). After generating H_2 from water electrolysis powered by sustainable energy, it can react with CO_2 from either the ambient air or exhaust streams [135].

$$CO_2 + 4\,H_2 \rightarrow CH_4 + 2\,H_2O \qquad \Delta H^0 = -165\,\mathrm{kJ/mol} \tag{8}$$

As already mentioned in the section before, this concept is tested by Audi regarding its industrial applicability. The main advantages of using methane as fuel in Germany are the accessibility and compatibility of the natural gas grid. Thus, the infrastructure to implement methane into the fuel market already exists. As in the case of Audi's pilot plant, the produced methane is fed into the grid, reducing the amount of natural

gas required by the transportation sector [127]. Thus, the production of methane is a promising energy storage option for intermittent power from sustainable sources. During this process, however, large amounts of water are produced, which indicates that half of the costly generated H_2 is used to form water [126].
Similar to methane, methanol (CH_3OH) is commonly obtained from synthesis gas with a production volume of several million tonnes per year. The alternative approach to produce methanol is again based on the hydrogenation of CO_2 by H_2 generated by water electrolysis (see Eq. 9).

$$CO_2 + 3\,H_2 \rightarrow CH_3OH + H_2O \qquad \Delta H_{298\,\mathrm{K},\,50\,\mathrm{bar}} = -40.9\,\mathrm{kJ/mol} \tag{9}$$

The *George Olah Renewable Methanol Plant* in Iceland is the most prominent pilot project to produce methanol from sustainable resources. Starting in 2011 and being further optimised, it currently synthesises 4000 tonnes of methanol per year. The CO_2 comes from a geothermal power plant, which is used for H_2 production by water electrolysis. With a continuous operation and the methanol being added to gasoline, this sustainable pilot plant substitutes about 2.5% of Iceland's fuel consumption [136]. In general, a maximum of 3% of methanol can be added to fuels without subsequent drawbacks, classifying it as possible drop-in fuel. For blends with higher amounts of methanol, the respective fuel standards and the engine setup need to be adjusted. As for nearly every alternative to fossil fuels, the infrastructure must be extended and further developed to be able to refuel vehicles with methanol. Further, even if common fuels are considered as harmful for human health, the implementation of a sustainable, but very toxic compound could fail because of lacking acceptance [127]. The main obstacle, however, is once again the production of H_2 by water electrolysis. This process prevails regarding capital costs, with the electrolysers representing 75% of the total installation costs. It can be assumed that upscaling will not significantly reduce these costs, since the capacity of electrolysers is mainly increased by a higher amount of stacks [126].
As methanol also serves as chemical base material, it is used to produce further fuels and fuel additives. In this so-called methanol-to-gasoline or methanol-to-olefins process, olefins like ethylene or propylene are produced from methanol with zeolite catalysts [126]. Within this context, the Fischer-Tropsch process should be mentioned, which describes several reactions of gaseous compounds to liquid hydrocarbons (see Eq. 10 and 11).

$$n\,CO + (2n+1)\,H_2 \rightarrow C_nH_{2n+2} + n\,H_2O \tag{10}$$

$$n\,CO + 2n\,H_2 \rightarrow C_nH_{2n} + n\,H_2O \tag{11}$$

Similar to the methane and methanol syntheses, the hydrocarbons are generated from synthesis gas with high amounts of water as by-product [137]. There are several approaches to remove the produced water and to obtain purified hydrocarbons. Besides uneconomic drying steps, the water-gas shift reaction is utilised to convert the by-product into hydrogen again (see Eq. 12). In the presence of iron catalysts, the overall yield of the Fischer-Tropsch process is distinctly increased. In contrast to E-fuels like methanol, these synthetic fuels can not only be used as drop-in fuels, but also completely replace fossil hydrocarbons [126, 137].

$$CO + H_2O \rightarrow CO_2 + H_2 \qquad \Delta H^0 = -41.2\,\mathrm{kJ/mol} \tag{12}$$

The German start-up company *sunfire* operates the first power-to-liquid pilot plant in Dresden. Combining a steam electrolysis, Fischer-Tropsch synthesis and water-gas shift reaction, fuels like synthetic diesel are produced from renewable energy, water and CO_2. Nevertheless, while the company claims to save about three tonnes of CO_2 for each tonne of fuel they produce, the production volume of the plant is one barrel per day [126].

2.1.2.3 Oxymethylenether

As already explained in section 2.1.1.1, the upcoming legislations for real driving emissions will demand complex exhaust gas after-treatment systems. Simultaneously, the carbon footprint of the fuels as well as the soot formation during combustion have to be reduced. Especially oxygenated fuels are considered as promising option to solve these problems. Among the synthetic fuels, in particular oxymethylenether (OME) gets a lot of attention in Europe and Asia nowadays [138]. Although just 10 000 tonnes per year are currently produced from coal in China, there is a sustainable synthesis route based on methanol [127, 138]. To produce OME from methanol on a large scale, its monomer, formaldehyde, is required. There are several approaches to obtain formaldehyde from methanol, with the silver catalysed process being the most economic one (see Eq. 13). During this reaction, methanol is partially oxidised and dehydrogenated. In the next step, formaldehyde is converted into trioxane in the presence of sulfuric acid as catalyst (see Eq. 14). To isolate trioxane, several distillations are required, increasing the production costs of OME. Methylal is another necessary compound of the OME synthesis, which is obtained from methanol and formaldehyde according to Eq. 15. Similar to the trioxane production, an acidic catalyst is used and methylal is subsequently distilled to remove the by-product water. As shown in Eq. 16, the acid catalysed reaction of trioxane and methylal finally leads to the formation of OMEs [139].

$$CH_3OH \rightarrow CH_2O + H_2 \tag{13}$$

$$3\,CH_2O \rightleftharpoons (CH_2O)_3 \tag{14}$$

$$2\,CH_3OH + CH_2O \rightleftharpoons CH_3O - CH_2O - CH_3 + H_2O \tag{15}$$

$$CH_3O - CH_2O - CH_3 + (n-1)\,CH_2O \rightleftharpoons H_3C - O - (CH_2O)_n - CH_3 \tag{16}$$

By using OME as fuel, NO_x as well as soot emissions can be simultaneously reduced due to the elimination of the trade-off between these emissions, mentioned in section 2.1.1.1. In particular, the exceedingly high amount of oxygen bound in the molecule, the lack of carbon-carbon bonds, high volatility and low reactivity enable this favourable property [127, 138]. Härtl *et al.* compared many oxygenated fuels concerning their soot reduction potential, with OME leading to the lowest emissions. Therefore, they propose implementing OME as non-toxic blending component into diesel fuel to reduce its emissions [140]. Its production process already indicates OME's high costs and energy consumption. Further, its high vapor pressure causes fugitive emissions and a flammability hazard, when the tank is open. Together with its incompatibility with common sealing materials, several engine and tank modifications are necessary, before implementing OME into fuel industry. The unalterable handicap of OME, however, is its low heating value, which is with about 23 MJ/kg far below the typical values of fuels and biofuels shown in Table 2 [127, 138]. The usage of OME as blending compound could thus be a compromise to still benefit from its considerable advantages, but without being too affected by its drawbacks [2].

2.1.2.4 Exceptional position of ethanol

Bioethanol is currently the most widely used biofuel in the world [87]. Already in 1894, bioethanol was utilised in internal combustion engines [141]. The main reason for its worldwide application in blends with petrol, like the fuel E10 in Germany, is its high octane number and thus high performance in petrol engines [87]. In general, bioethanol is obtained by the fermentation of sugar-rich biomass and subsequent distillation steps. After extracting the sugar from the plant material or enzymatically dissolving the sugar of starch, it is fermented by common yeasts. Eq. 17 shows the common fermentation reaction of glucose to ethanol [126].

$$C_6H_{12}O_6 \rightarrow 2\,C_2H_5OH + 2\,CO_2 \tag{17}$$

The fermentation process leads to an aqueous ethanol solution with an alcohol content of about 12 vol%, as the toxic effect of ethanol on the yeast inhibits its further production. For the usage as biofuel, the ethanol content must be increased to 98.7 wt% by several distillation and dehydration steps. In total, about 2.1 tonnes of glucose are necessary to obtain 1 tonne of ethanol. This high overall biomass utilisation efficiency is one of the main advantages of bioethanol compared to other substances derived from biomass [126, 142]. Initially, oxygenated compounds like ethanol were added to diesel to reduce particulate emissions by lowering the ignition temperature due to their high oxygen content [15, 86]. This effect also leads to a significant reduction of NO_x emissions in the presence of about 10 wt% of ethanol without affecting the energy output [84]. Further, the addition of ethanol improves the cold flow properties of diesel, in particular its cloud and pour point as well as viscosity [143].
Nevertheless, the usage of ethanol in mixtures with diesel entails serious drawbacks, which also question its promotion as sustainable biofuel compound. The most important disadvantage is the immiscibility of ethanol with diesel. Since 10–25 wt% of ethanol are necessary to utilise its abovementioned properties, high amounts of surfactants or co-solvents must be added [18, 69]. Without using these additives, phase separation will occur if the temperature is below 10 °C or if the fuel mixture is exposed to water due to high humidity in the fuel delivery tank [18, 144]. Suitable surfactants, however, are too expensive for this application and their presence considerably affects engine and combustion properties, which is further explained in section 2.1.4.1. Since the octane number of a substance describes its potential to prevent early ignition, it is obvious that ethanol reduces the CN of diesel (see Table 2). Therefore, harmful cetane improvers, usually isoamyl nitrite or 2-ethylhexyl nitrate, have to be used to compensate the presence of ethanol. With its low viscosity, ethanol also affects the lubrication of the injection pumps, when used in high amounts [145, 146]. Considering these issues, the still challenging implementation of bioethanol as fuel in diesel engines justifies its appearance in this section, although it is not an E-fuel.

2.1.2.5 Electric mobility

With the European Commission setting the target of emission-free urban freight transportation until 2030 and urban passenger transportation until 2050, completely different alternatives to combustion engines are necessary [147]. Not only these targets prohibit the use of conventionally fuelled cars in European cities in the future, but also the increasing fossil fuel dependence. The key technology to achieve these goals can be summarised as electric mobility (E-mobility) and, concerning the transportation as well as automotive

sector in particular, the introduction of electric vehicles (EV). An EV is either fully or partially electrically powered and its usage does not lead to any driving emissions. Besides the reduced air pollution and thus improved human health, there are also economic reasons like low operational costs due to their high efficiency, which favour EVs [148]. Especially the freight transportation sector is supposed to be an early adopter of E-mobility, as the concerned companies have high purchasing rates and use their vehicles intensively. Regarding the lifetime vehicle costs, E-mobility becomes attractive to these companies, since the high vehicle purchase price is compensated by its low operational costs [149,150]. There are several types of EVs, which differ considerably in their technology and sustainability. A battery electric vehicle (BEV), for example, runs solely on electricity due to on-board batteries, which are charged by using power outlets or charging stations. Thus, BEVs contain no combustion engines and do not cause any tailpipe emissions. A hybrid electric vehicle (HEV), on the other hand, possesses an internal combustion engine, which utilises common fuels or biofuels, and an additional electric motor, which uses energy from batteries. These are charged during regenerative braking and by the combustion engine, which obviates their manual recharging. To reduce the fuel consumption even further, plug-in hybrids were developed, whose batteries can be recharged by both the combustion engine and power outlets [148, 151].
Indicated by the detailed description of the most important E-fuels in this chapter, the implementation of E-mobility into the transportation and automotive sector makes currently just slow progress due to several significant obstacles. This statement is supported by the market share of EVs in Europe, which was above 2% for just very few countries like Sweden and Belgium in 2017. Apart from the necessity of sustainable electricity to recharge EVs, there are some severe environmental issues concerning the batteries of EVs. Lithium ion batteries are currently the most used and further investigated batteries for EVs, because of their high energy density and cycling stability. With the Chinese government promoting their EV industry, research is primarily focused on optimising the performance of the batteries without considering the environmental impact [152]. While layered oxides like $LiNiCoMnO_2$ and $LiNiCoAlO_2$ are typically used as cathode material, graphite with intercalated lithium is utilised as anode material. In presence of a lithium ions containing salt as electrolyte, following reactions occur during discharging the battery [153, 154]:

$$\text{Anode :} \qquad Li_xC_n \rightarrow C_n + x\,Li^+ + x\,e^- \tag{18}$$

$$\text{Cathode :} \qquad Li_{1-x}NiCoMnO_2 + x\,Li^+ + x\,e^- \rightarrow LiNiCoMnO_2 \tag{19}$$

$$\text{Total :} \qquad Li_{1-x}NiCoMnO_2 + Li_xC_n \rightarrow LiNiCoMnO_2 + C_n \tag{20}$$

As the anode material is rather cheap, most of the expenses arise from the cathode preparation. Besides the production of highly purified lithium, which consists of several extraction and electrolysis steps, nickel, cobalt and manganese, the synthesis of the cathode material $LiNiCoMnO_2$ is based on heat treatment processes and is thus also very energy consuming [155]. In order to assess the environmental impact of the battery production of EVs, Martin Wietschel, deputy head of the competence centre for energy technology and energy systems of the Fraunhofer Institute in Karlsruhe, made following comparison: A passenger car with an old internal combustion engine, which means that it does not fulfil the Euro 6 standard, must drive 60 – 80 000 km to emit the same amount of CO_2 as during the current battery production for EVs, depending on the production process [134]. From a political point of view, the insufficient infrastructure for EVs is the most urgent obstacle. With the unavailable charging station network being a key barrier for market diffusion and consumer acceptance, the public as well as private sector are required to shoulder the large-scale implementation of this expensive infrastructure [148]. At this point, it is once again important to emphasise that current public and political discussions about E-mobility rarely take into account the necessity of a sustainable electricity source. Without further breakthroughs concerning the production, accessibility and distribution of renewable energy, most of the latest arrangements and guidelines become irrelevant. There are even much more unsolved economic, logistic and social problems that impede the implementation of E-mobility, but their evaluation exceeds the scope of this thesis.

2.1.2.6 Evaluation and forecast for the future of E-fuels and E-mobility

Since many alternatives to fossil fuels are already developed, including biofuels, E-fuels and E-mobility, an impartial evaluation is necessary to make a reliable forecast for the future of the transportation and energy sector. Currently, biofuels like bioethanol and biodiesel are just used in blends with petrol and diesel fuels. Further, in only a few cases worldwide, E-fuels are produced on an industrial scale, but still from fossil resources. In China and South Africa, for example, Fischer-Tropsch hydrocarbons and methanol are obtained from coal, whereas Malaysia and Qatar use natural gas to produce these E-fuels. With international climate objectives prescribing the reduction of CO_2 emissions until 2050 by 80% compared to 1990, fundamental technological changes are still necessary in the transportation sector. Within the Effort Sharing Decision, Germany committed itself to increase the ratio of renewable energy used in the transportation sector to 10% until 2020. To curtail the expectations and to accurately reflect the preliminary up-to-date status in Europe, the emissions caused by traffic increased by 20% compared to 1990. Solely considering the CO_2 emissions in German traffic, the values remained nearly constant during the last 27 years [127].

There are about 45.8 million passenger cars in Germany with an average age of 9.3 years. Governmental incentives on EVs are thus not effective due to the slowly changing traffic sector. The current stock of EVs in Germany amounts to about 200 000 passenger cars, with forecasts predicting an increase to 6 million EVs until 2030, which would just account for about 13% of the total amount of passenger cars [156]. This already indicates that combustion engines will most likely be still the main propulsion technology in the near future. As the electrification of heavy-duty vehicles, ships and planes is presumed to be not feasible, they will also remain consumers of liquid fuels in the future. Therefore, just considering the contribution of E-mobility, the international climate objectives cannot be fulfilled. Since a change in consumer behaviour is not conceivable, the DECHEMA, a German association dealing with the development of chemical technologies, proposed three different approaches to solve these issues in Germany. Firstly, the fleet consumption could be distinctly reduced by combustion engines with significantly higher efficiencies. These progresses, however, did not lead to lower CO_2 emissions in the past, as current passenger cars tend to possess more powerful engines, to be heavier and to provide greater comfort as well as passenger security. Secondly, the amount of biofuels used as alternative to fossil fuels should be increased. Since the DECHEMA mainly promotes E-fuels due to its industrial cooperations with E-fuel producers, biofuels are just mentioned in passing. To increase the share of biofuels in the fuel sector, however, much larger cultivation areas are necessary. The third and as most promising promoted approach is the implementation of E-fuels into the transportation sector. The DECHEMA emphasises that electricity from sustainable resources is essential for the production of E-fuels. With the plans of the German government to further extend renewable energy in the electricity sector, valid since 2016, a maximum of 47.5 TWh from photovoltaics and 170.6 TWh from wind energy could be produced in 2030, assuming current technologies. Further contributors are hydro power and biogas, whose capabilities are mostly exhausted, and other energy sources like geothermal energy, whose shares are not considerable. The share of renewable sources on the total electricity used in the German transportation sector could thus be up to 53.7%. Nevertheless, this amount can just be achieved, when the necessary electricity of other sectors is excluded. To make this desperate situation even more obvious, an available amount of 25 TWh sustainable electricity for the production of E-fuels in 2030, which is a reasonable value, leads to a maximum of 1 million tonnes of E-fuel. Considering the fuel consumption of solely Germany, which is currently above 50 million tonnes of fossil fuel, more than 1 000 world-scale power plants would be necessary to produce enough electricity for the sufficient production of E-fuels [127].

Due to this critical situation, the DECHEMA suggests the development and construction of industrial complexes that produce sustainable electricity, which is subsequently used to synthesise E-fuels. Such complexes could be located on coasts next to offshore wind

farms or in Southern Europe close to photovoltaic power plants. So far, there are only a few projects promoted by European governments like the Power-to-X (P2X) project of Germany [157]. Besides huge costs to build these complexes and the lacking collaboration of the affected industrial sectors, which is also known as integrated energy, the availability of the required resources, in particular CO_2 and water, is the main challenge. Since highly purified CO_2 is necessary in huge amounts for the synthesis of many E-fuels, other companies that produce CO_2 continuously like cement plants should be close. Assuming that the total CO_2 emissions will distinctly decrease in the next years due to the international climate objectives, however, its availability will become even worse. When including Southern Europe, the high amounts of required water should not be underestimated. As known from China, for example, water is the limiting factor in arid regions due to the high consumption of the chemical industry.
This detailed evaluation shows that, although E-mobility and E-fuels have already been dominating the media since a few years, they are still far away from a comprehensive implementation. This conclusion leads to the confirmation that, at least currently, biofuels are a significantly better alternative to fossil fuels. In particular, the production processes should be kept simple and at best, existing and industrially applied processes should be combined to avoid problems regarding integrated energy.

2.1.3 Important parameters for fuel characterisation

The detailed comparison between biofuels and E-fuels in chapter 2.1.1 and 2.1.2 makes clear that most of the fuel's properties can be deduced from just a few physicochemical parameters. In particular, this section outlines the influence of the kinematic viscosity, low-temperature phase behaviour, heating values and oxidative stability of the fuel on its properties. As all formulated biofuels of this thesis are multi-component systems, the characterisation of the individual components concerning their advantages and drawbacks is essential. Further, different methods, applied during the engine tests, to obtain precise information on the ignition, combustion and emission properties of the formulated biofuels are explained.

2.1.3.1 Kinematic viscosity

The viscosity of a fluid can be described as the resistance that occurs, when the substance is irreversibly deformed. It determines the flow behaviour of liquid as well as gaseous compounds and the resistance that is opposed to a solid, which moves inside a fluid [158]. In particular, this viscosity is called dynamic or shear viscosity η_{dyn}. An easy and precise apparatus to measure η_{dyn} of a fluid is the rolling ball viscometer (see Fig. 11).

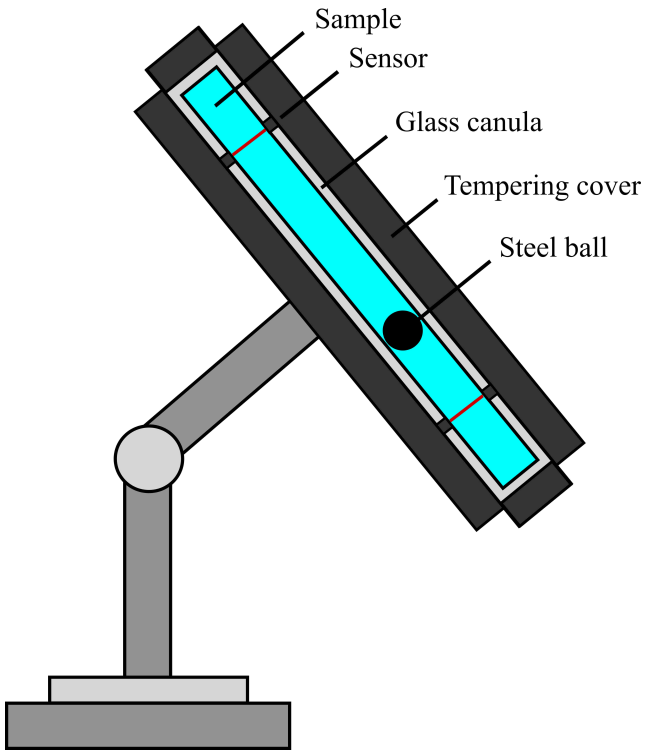

Figure 11: Common setup of an automated rolling ball viscometer.

With this method, the sample with the density ρ_{sample} is filled into a glass canula. The viscometer tilts this canula at a specific angle, while the temperature of the sample is controlled by a tempering cover. During this measurement, the time t is determined, until a steel ball with the density ρ_{ball} passed through a certain distance of the canula. This distance is predefined by magnetic induction sensors. Based on the friction law of Stokes for a ball falling through a liquid, this process is driven by gravity and the density difference between the steel ball and the sample. The apparatus possesses a technical constant K, which is determined by calibration oils with known dynamic viscosities [159]. These parameters lead to Eq. 21 for the calculation of the dynamic viscosity of the sample $\eta_{\text{dyn,sample}}$:

$$\eta_{\text{dyn,sample}} = K \cdot (\rho_{\text{ball}} - \rho_{\text{sample}}) \cdot t \tag{21}$$

$$\tau = \eta_{\text{dyn}} \cdot \frac{dv}{dy} \tag{22}$$

In general, η_{dyn} is the proportionality constant between the shear stress τ and the velocity gradient dv/dy perpendicular to the direction of motion (see Eq. 22). This equation shows that the density of the sample ρ_{sample} is necessary to obtain its dynamic viscosity. Thus, a densitometer is required, which is commonly based on the oscillating U-tube method. In this process, the sample is filled in a U-shaped tube, which is electronically excited to oscillate in its characteristic frequency. This frequency depends on the density of the sample, which in turn is distinctly influenced by the temperature. Therefore, a precise temperature control is essential for density measurements [160]. The sample's density is also necessary to convert the dynamic viscosity into the kinematic viscosity η_{kin} (see Eq. 23). It describes the flow behaviour of the fluid with respect to gravity and inertia. Further, it is the common viscosity parameter for standardisations in fuel industry [158].

$$\eta_{\text{kin}} = \frac{\eta_{\text{dyn}}}{\rho} \tag{23}$$

Since the viscosity of a fuel has a huge impact on its ignition, combustion and emission properties, it was the most important parameter of this thesis to ensure the applicability of the formulated biofuels. Thus, a detailed look into the consequences of high as well as low fuel viscosities is required. A high viscosity, as occurring for most of the vegetable oils explained in section 2.1.1.2, causes bad flow behaviour of the fuel in the engine. This increases fuel spray penetration, which is partly responsible for engine deposits and thickening of the lubricating oil [8]. The bad flow behaviour also leads to carbon deposits on the injection nozzles, valve seat and in the combustion chamber. Further, the lubricating oil can be contaminated with unburnt residues and the injection rate can be decreased because of heat losses in the fuel injection pumps and filters [58,59,67]. Another drawback

of a high viscosity is the poor spray behaviour from the injector. It reduces fuel atomisation, which leads to incomplete combustion in the engine because of larger droplet sizes and therefore higher soot emissions and lower efficiency [161–163]. Since a high viscosity is often coupled with a low volatility, it can cause poor cold engine start-ups, ignition delays and misfires [7]. These aspects explain, why highly viscous fluids are not suitable in modern diesel engines without any modification. One way to avoid at least some of these issues and to reduce the viscosity is heating up the fuel, before reaching the fuel pump and injectors [60].
Due to the considerable influence of the viscosity on the fuel properties, there are many different viscosity standardisations depending on the continent, country, climate and temperature. They certify optimal fuel properties, when used in engines and allow predictions concerning the potential impact of the fuel on the environment. Within the scope of this thesis, two different biodiesel standards are taken into consideration for the biofuel formulations: the American standard ASTM D6751 and the European standard EN 14214. While the American standard accepts viscosity values between 1.9 to 6.0 mm^2/s at 40 °C, the European standard applies to 3.5 to 5.0 mm^2/s at 40 °C [59]. At this point, it is important to mention that there are already some standards for vegetable oil containing fuels. However, they are by far less stringent than current biodiesel standards. Typical examples are the DIN 51623 for vegetable oil fuels and the DIN 51605 for rapeseed oil biofuels, which sets the maximum of the kinematic viscosity to 36.0 mm^2/s at 40 °C, which simply is the average value of pure rapeseed oil's viscosity [164]. As these standards do not ensure a direct usage in an unmodified up-to-date diesel engine, they are not considered in this thesis.

2.1.3.2 Low-temperature phase behaviour

A common problem of using biofuels is their low-temperature phase behaviour. The examples in section 2.1.1.2 already showed that predicting this property for fuels and in particular biofuels is not evident. Thus, some distinctive conditions were chosen to characterise and compare fuels regarding their low-temperature phase behaviour. The most important parameter to determine this property is the cloud point. It describes the temperature, at which the crystallisation process or phase separation of the fuel starts to occur. There are automated apparatus, which cool down the sample and determine the cloud point with optical detectors. Another parameter is the pour point, which is defined as the lowest temperature, at which the substance is still fluid, even if there are already some crystals in the liquid [19]. Thus, the pour point is always lower than the cloud point. Vegetable oils do not only have unsuitably high viscosities, as mentioned in the section

above, but also high cloud and pour points. These can cause engine durability problems like sticking of piston rings and coking of injector nozzles [7, 49]. Therefore, additives are necessary to achieve low-temperature properties similar to fossil fuels. Currently, so-called pour point depressants like polymethacrylates, polyacrylates and alkalated naphthalenes are used to inhibit crystal formation in the fuel at low temperatures. They adsorb on the crystal's surface and prevent its growth by forming a surface layer. Nevertheless, their influence on the cloud and pour point is not distinct enough to use these mixtures as biofuels [165, 166]. There are also standards that regulate the low-temperature phase behaviour of fuels like the European standard EN 590 for diesel fuels. It defines that a winter diesel, for example, must have a cold filter plugging point of −20 °C in Central and Western Europe [74]. This point usually occurs between the cloud and the pour point and describes the lowest temperature, at which a fluid still passes through a standardised filter [49]. Within the scope of this thesis, these standards are considered regarding the cloud and pour points of the formulated biofuels, but without having a standardised measuring device in the laboratory.

2.1.3.3 Oxidative stability

Besides their high viscosities and cloud points, their low stability towards oxidation is another drawback of biofuels like vegetable oils and biodiesel. This stability can be described as the time necessary to attain a critical point either associated with a sensorial change or an abrupt acceleration of the oxidation process [167]. Since it distinctly affects the quality and durability of liquids derived from vegetable plants, a closer look to this process is essential. In general, there are two different mechanisms: autoxidation and photooxidation. The autoxidation is a free radical chain reaction (see Fig. 12). In the initiation step, a hydrogen atom is removed from e.g. an acylglycerol like rapeseed oil or a fatty acid chain occurring in biodiesel [168]. The required energy of this process strongly depends on the position of the hydrogen in the molecule. As mentioned in section 2.1.1.2, vegetable oils and especially rapeseed oil as well as biodiesel mostly consist of unsaturated fatty acids. Removing a hydrogen atom adjacent to a double bond of the fatty acid residue leads to a stabilised allylic radical. In the case of linoleic acid, which is a common fatty acid of rapeseed oil's triglycerides, the hydrogen atom at the C_{11}-position is even more favoured due to the formation of a bis-allylic radical (see Table 1). Additionally, heat, light and metal catalysts can even accelerate this initiation process. In the presence of air, the formed radical R• can react with atmospheric triplet oxygen $^3O_2$. Due to its two unpaired electrons in the antibonding orbitals, $^3O_2$ is a radical as well and thus reacts with R• to form a peroxy radical ROO•.

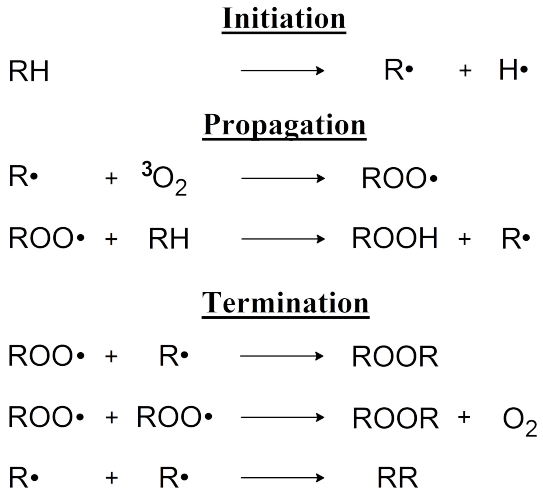

Figure 12: Mechanism of autoxidation divided in initiation, propagation and termination steps. In the case of a vegetable oil or biodiesel, R implies an acylglycerol or fatty acid methyl ester, respectively [168].

Since this peroxy radical can again remove a hydrogen atom from an acylglyceride or fatty acid chain, another R• can be formed, which leads to a radical chain reaction and a propagation of the autoxidation [168]. During this propagation, hydroperoxides, which are the primary oxidation products, can decompose and thus produce e.g. aldehydes and ketones. Especially in rapeseed oil, this secondary product formation is distinctly pronounced [169]. The chain reaction stops, when two radicals react with each other, leading to nonradical substances. In the second oxidation process, the photooxidation, singlet oxygen $^1O_2$ must be produced by either sensitisers or specific and harsh conditions in the laboratory, thus making it less important in the scope of this thesis. Since one of its antibonding orbitals is filled with paired electrons and the other one is empty, $^1O_2$ is electrophilic. Therefore, it reacts with substances with high electron densities like the double bonds of unsaturated fatty acids. This in turn leads to allyl hydroperoxides as primary oxidation products, which are again further oxidised similarly to the autoxidation process [168, 170].
There are two major methods to determine the oxidative stability of fuels: the Rancimat method and the PetroOxy method. In the Rancimat method, the reaction vessel, which is filled with the sample, is rinsed with air at a constant temperature. This accelerates the oxidation process and the volatile products are transported into the measuring vessel by the air stream. This vessel contains deionised water and its electrical conductivity, which is increased by the oxidation products, is continuously measured [171]. Once the secondary oxidation products are detected, the induction time is reached. Since the stability towards oxidation is one of the key problems of biofuels and in particular biodiesel, it is regulated by several standards. The European standard EN 14112 as well as the American standard ASTM D6751 for biodiesel prescribe, among other parameters, the measuring conditions of the Rancimat method. The temperature in the reaction vessel

is set to 110 °C and the minimum induction period to 8 h by the European and 3 h by the American standard [172]. The PetroOxy method is another standardised accelerated oxidation test, which was invented just ten years ago. The sample is put into a reaction vessel, filled with oxygen and then heated up to a specific temperature. Due to the oxidation of the sample and thus consumption of oxygen, the pressure inside the chamber decreases over time [173]. The setup for this method is prescribed by the DIN standard DIN EN 16091, which demands an oxygen pressure of 700 kPa at 140 °C. The induction time is reached, once the pressure drops by 10%, compared to the maximum pressure in the reaction vessel [172]. The PetroOxy method is a significantly faster alternative to the Rancimat method. Further, the results of the latter are incomplete, as just the highly volatile compounds are detected. The PetroOxy method, on the other hand, considers all volatile as well as non-volatile substances [173, 174]. In 2017, the PetroOxy was upgraded to the RapidOxy, which allows the usage of much smaller sample volumes [175]. As the PetroOxy and thus also the RapidOxy method were recently developed, a standardised minimum value for the induction time has yet to be accepted. Nevertheless, there are several empirical studies that investigate the correlation between the Rancimat and the PetroOxy method. Regarding the used compounds in this thesis, the following regression model is most suitable:

$$t_{\text{Rancimat}} = (31.89 - 20.63 \cdot f) \cdot t_{\text{PetroOxy}} + (-214.65 + 319.68 \cdot f) \tag{24}$$

with the induction times of the Rancimat and the PetroOxy method in minutes t_{Rancimat} and t_{PetroOxy} and $f = 0$, if no additives are used and $f = 1$ in the presence of additives. According to this equation, the necessary induction time of a biofuel measured by the PetroOxy and RapidOxy method to be in agreement with the European standard EN 14112 is reduced to 33.3 min. This impressively shows the much shorter duration for the determination of the oxidative stability of these methods compared to the Rancimat method [174].

Especially biodiesel's susceptibility towards oxidation retards its consolidation into the world energy matrix. During long-term storage, the autoxidation process and its consequent oxidation products drastically harm its fuel properties [176]. They lead to sediment and gum formation, which e.g. cause fuel filter plugging, and corrosion damage to the engine [177, 178]. To delay this oxidation process, so-called antioxidants are added to the biofuel [176]. In general, antioxidants capture free radicals like peroxy or alkyl radicals, control transition metals, quench singlet oxygen and inactivate sensitisers [168]. They donate hydrogen atoms to the radicals, converting them to nonradical compounds [179]. As they are typically sterically hindered phenols or secondary aromatic amines, the antioxidant radical has lower energy than the peroxy and alkyl radical due to resonance sta-

bilisation [168]. The ability of antioxidants to prevent oils from oxidation mainly depends on their chemical structure. As they act differently in oils and oil-in-water emulsions, the *polar paradox theory* was proposed. It summarises the empirical observations that polar antioxidants are more effective in less polar media and vice versa. It is assumed that the presence of polar antioxidants leads to association colloids in the oil. Thus, they are not located on the oil-air interface, but on the surface of the colloids. Non-polar antioxidants, on the other hand, dissolve in the oil and therefore do not prevent it from oxidation [180].

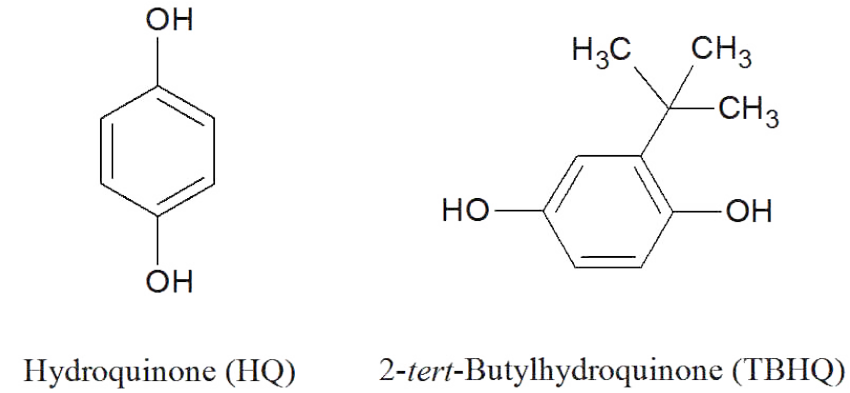

Figure 13: Chemical structures of the synthetic antioxidants hydroquinone (HQ) and 2-*tert*-butylhydroquinone (TBHQ).

Table 3: Composition of the commercially sold and as green promoted antioxidant mixture inaAOX1 from inaCHEM GmbH [182].

Compound	$\omega_{\mathbf{Compound}}$**(wt%)**
Hydroquinone	10
2-*tert*-Butylhydroquinone	30
L-Ascorbic acid	0.4
Solketal (as solvent)	60
Inorganic ash	0.02

In commercial biodiesel, hydroquinone and its derivatives are used, as they are obtained from petrochemistry and are thus very cheap (see Fig. 13). As hydroquinone is classified as carcinogenic, mutagenic and highly aquatoxic, it should not be used as additive for biofuels. Nevertheless, there are several current publications and patents that either deal with the stabilisation of biofuels with hydroquinones or even promote mixtures of natural antioxidants and hydroquinones as green and sustainable. In these mixtures, the actual effect of natural antioxidants needs to be questioned, as they are used in very small amounts compared to the hydroquinones [176, 181]. A typical example is the patented

antioxidant mixture inaAOX1 from inaCHEM GmbH (see Table 3). Although the amount of L-ascorbic acid, also known as vitamin C, is less than 1% of the total amount of antioxidants in the mixture, with the rest being highly toxic hydroquinones, it is promoted as "natural stabilisation of biodiesel". A closer look at the corresponding patent shows that, indeed, the hydroquinones are used due to their effectiveness and ascorbic acid just acts as their regenerating agent. Additionally, pictures of oranges are part of its advertising campaign to make the customer think that vitamin C is a main component of this mixture [182]. Besides ascorbic acid, a lot of different natural antioxidants are already known like phenolic acids, carotenoids and vitamins [183]. Research groups that dealt with the implementation of natural antioxidants into biofuels faced the problem of insufficient solubility of the hydrophilic antioxidants. Therefore, they also had to use hydroquinones in high amounts compared to the natural antioxidants, similar to the patent of inaCHEM, to still fulfil the standards. This in turn increased the total amount of antioxidants to up to 1 wt% of the biofuel [174,176,184]. To sum up, the usage of natural antioxidants in biofuels is hindered by their bad solubility, making hydroquinones and other synthetic antioxidants indispensible. In combination with natural antioxidants, however, their total quantity increases to industrially inappropriate amounts. There are different ideas to solve these problems like adding co-solubilisers or surfactants to implement the natural antioxidant into the oil [177]. The most promising approach is the utilisation of the synergistic effect of two different antioxidants in radical trapping chain transfer reactions [176, 185]. When using a very effective and a rather ineffective antioxidant simultaneously in a formulation, the ineffective one can sometimes regenerate the effective antioxidant, thus increasing the overall antioxidative capacity of the system [185]. This synergism could already be observed in mixtures of synthetic as well as natural antioxidants [186, 187]. Therefore, the usage of this synergistic effect could possibly compensate the bad solubility of natural antioxidants in biofuels, which obviates synthetic and toxic hydroquinones.

2.1.3.4 Heating value

There are various technologies to convert fuels obtained from biomass to energy. Since combustion is the most developed and common one, significant parameters of combustion systems are inevitable. Especially for a fuel, regardless of whether it is a complete biofuel or a drop-in fuel, its so-called heating value is essential [188]. This parameter can be calculated by two different approaches leading to either the higher heating value or the lower heating value. With the assumption that the fuel consists of hydrocarbons exclusively, following combustion equation can be used to explain the difference between the two values:

$$Fuel + x\,O_2 \rightarrow y\,CO_2 + z\,H_2O \tag{25}$$

While both heating values refer to the heat released from the fuel combustion, they differ in the final temperature of the combustion products. This in turn changes the state of aggregation of the produced water. The approach leading to the higher heating value considers the combustion products at 25 °C. Thus, water is in a condensed state and its latent heat of evaporation is taken into account. With the lower heating value approach, however, the products are considered at 150 °C and therefore, water is treated as vapour and its latent heat of evaporation is not recovered [189].
Commonly, an adiabatic bomb calorimeter is used to determine combustion energies and enthalpies. For that, a definite amount of sample is put into a crucible with cotton threads to enable a contact with the ignition device. To ensure a quick and complete combustion, the chamber is filled with oxygen. After placing the bomb into a thermostatically controlled water bath, the sample is ignited and the temperature of the water bath is recorded [190]. Due to the adiabatic insulation and the isochoric combustion in the bomb, the molar combustion energy at room temperature $\Delta_C U_{298}$ can then be calculated as follows:

$$\Delta_C U_{298} = -\frac{C_{\mathrm{cal}} \cdot \Delta T + \sum_{\mathrm{i}} q_{\mathrm{i}}}{n} \tag{26}$$

with the calibration constant C_{cal}, the measured temperature difference ΔT, further contributions q_{i} to the combustion energy like the usage of the cotton threads as ignition promoters and the ignition energy itself, and the amount of substance n. The combustion energy of a cotton thread and the ignition energy correspond to 50 J and 70 J, respectively. C_{cal} already indicates that the calorimeter needs to be calibrated with a substance with a known combustion energy, typically benzoic acid. The combustion enthalpy at room temperature $\Delta_C H_{298}$ can then be obtained with following equation:

$$\Delta_C H_{298} = \Delta_C U_{298} + RT\Delta_C n \tag{27}$$

with the general gas constant R, the reference temperature T and the change of the amount of substance in the gas phase during combustion $\Delta_C n$. With Eq. 25 and assuming a complete combustion of the sample, which can be at least visually detected by looking at the crucible after the combustion, $\Delta_C n$ can be determined as follows:

$$\Delta_C n = y - x \tag{28}$$

Eq. 28 shows that the produced water is assumed to be condensed in this approach. Thus, these calculations lead to the higher heating value of the sample.

2.1.3.5 Engine tests

As it is not only the scope of this thesis to formulate new biofuels, but also to develop them to be directly applicable in unmodified up-to-date diesel engines, detailed combustion tests are essential. A modern engine control unit regulates up to 40 000 components [191]. Thus, a specific choice of engine test methods and investigated parameters is necessary to simplify the evaluation of new fuels. Regarding the characterisation of the formulated biofuels of this thesis, ignition delay and exhaust gas recirculation (EGR) measurements are performed and their combustion process and behaviour is examined.

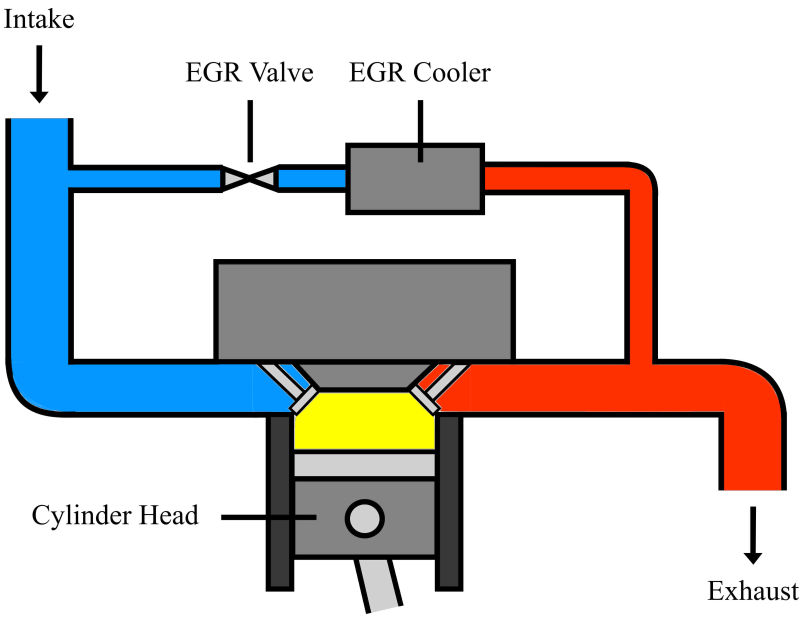

Figure 14: Simplified illustration of an engine with exhaust gas recirculation (EGR). The colours of the pipes indicate the temperatures of the gases with blue implying the cold intake air and red the hot exhaust gases [192].

Ignition delay measurements give information about the combustibility of the fuel. Ignition delay describes the period of time between the injection of the fuel and the start of combustion. An important parameter for the ignition quality of biofuels in diesel engines is the dimensionless cetane number (CN) [1]. To compare different fuel components using their CN, hexadecane, which is also called cetane and possesses a very short ignition delay, obtained a CN of 100. Saturated and unbranched long-chain hydrocarbons have high CNs and a good ignition quality, whereas branched hydrocarbons and aromatic compounds have low CNs and a poor ignition quality. Thus, the higher the CN, the shorter the ignition delay time. Too high as well as too low CNs can cause operational problems. In the case of a too high CN, the combustion starts, before fuel and air are properly mixed, leading to an incomplete combustion and smoke. With a too low CN, misfiring, slower

engine warm-up and an incomplete combustion occur [49]. Since biofuels usually tend to have low CNs, the respective standards just give minimum values for the CN. Regarding biodiesel, the European standard EN 14214 prescribes a lower limit of 51, whereas the American standard ASTM D6751 sets the minimum to 47 [74, 193]. To increase the CN of biofuels, ignition promoters are added to the formulations. Since these are currently hazardous compounds like 2-ethylhexylnitrate or organic peroxides, this topic is of main interest for many research groups [15, 194].

The EGR method is commonly used in diesel combustion engines to reduce NO_x emissions. During the combustion process, the hydrocarbons of the fuel are oxidised by atmospheric oxygen. As the oxygen is completely consumed by this combustion, there is no oxygen left in the exhaust gases. By adding a defined part of these exhaust gases to the intake air, the amount of oxygen in the mixture is reduced (see Fig. 14). Therefore, less fuel has to be injected to achieve a complete and slower combustion, which in turn reduces the in-cylinder peak temperatures [195, 196]. Since the formation of NO_x depends exponentially on the combustion temperature, according to the Zeldovich mechanism, less NO_x emissions are produced due to the EGR [197]. With the NO_x emissions being controlled by this method, the THC, CO and soot emissions as well as the fuel consumption and the air/fuel balance can be detected simultaneously with respect to a given NO_x emission. The air/fuel balance describes the mass ratio of air and fuel during combustion. By changing the load and EGR conditions at a constant engine speed, the combustion process and behaviour of the fuel can be analysed as well.

2.1.4 Nanostructuring in biofuels

With one of the main research topics of Kunz *et al.* being the miscibility and compatibility in solutions, including the influence of surfactants as well as hydrotropes and thus structured systems, a closer look was taken at several miscibility problems of fuel formulations. After briefly explaining the fundamental effects leading to surfactant-free microemulsions, the research concerning nanostructured fuels is summarised. In this context, water containing fuels, so-called hydrofuels, are mentioned and critically evaluated regarding the principles of green chemistry. Since the required measuring techniques and their interpretations, in particular light and X-ray scattering methods as well as conductivity measurements, are rather demanding, they are also outlined in the following sections.

2.1.4.1 Existing miscibility problems in fuel formulations

A kinetically stabilised system of two immiscible liquids is called macroemulsion. Due to the addition of so-called surfactants, surface active reagents, its stability can be sustained for a long time. Surfactants are amphiphilic molecules, thus containing hydrophilic as well as hydrophobic properties, which enable simultaneous interactions with polar and nonpolar liquids, generally referred to as aqueous and oil phases. These amphiphiles adsorb to the interface of both phases, which significantly reduces the interfacial tension. As the polar and nonpolar parts of the surfactants point to the respective phase, repulsive interactions occur between the formed aggregates. These interactions, however, are not strong enough to prevent coalescence and finally a macroscopic phase separation. Once a specific surfactant concentration, i.e. the critical micellar concentration (cmc), is reached, thermodynamically stable aggregates, called micelles, are formed by a spontaneous and reversible self-assembly [198, 199]. These homogeneous, isotropic and optically transparent mixtures are known as microemulsions. Their stability is strongly attributed to their droplet sizes. While aggregates of microemulsions possess sizes in the nanometre range, also known as mesoscale, macroemulsions contain larger droplets with a typical size of a few micrometres [200, 201].
In 1976, Barden *et al.* noticed that the ternary system water/2-propanol/hexane forms structures at the mesoscale, which leads to properties identical to microemulsions, although there is no surfactant present [202, 203]. This discovery proved that the addition of surfactants is not essential to obtain microemulsions. A typical surfactant-free microemulsion (SFME) consists of two immiscible liquids and a third component, which is completely miscible with both liquids and thus also amphiphilic. These so-called hydrotropes usually possess small hydrophobic parts, e.g. short hydrocarbon chains, compared to common surfactants, but their properties also differ from those of co-solvents [204, 205].

Due to their less pronounced amphiphilic character, higher amounts of hydrotropes are necessary to form SFMEs [206]. Coming back to the insufficient miscibility of ethanol with diesel, already mentioned in section 2.1.2.4, many research groups investigated different approaches to close the miscibility gap of this mixture. At lower temperatures, phase separation occurs and thus, the miscibility gap increases. This process can be prevented by using additional components, in particular either emulsifiers or co-solvents. An emulsifier, i.e. surfactant, causes a fine distribution of small ethanol droplets in diesel, whereas a co-solvent like tetrahydrofuran enables a molecular compatibility of ethanol and diesel, leading to a homogeneous mixture [18,144]. Already in 1980, Moses *et al.* added a surfactant to blends of aqueous ethanol and diesel and reported that they obtained thermodynamically stable mixtures [207]. Most of the investigated fuel blends, however, needed high amounts of surfactants and even higher ratios of co-solvents to prevent phase separation. In particular, about 2–10 wt% of surfactants were added, depending on the climatic conditions [18]. Due to their high prize and high affinity towards surfaces, the usage of surfactants in fuels is not favourable on an industrial scale. Therefore, reports about SFMEs as fuels increased rapidly [69]. In 2007, Silva *et al.* were the first to explicitly investigate mixtures of ethanol, diesel and different additives regarding the formation of SFMEs by performing light scattering experiments. Although solely light scattering is not sufficient to prove the existence of nanostructures, they concluded that such structures are formed, similar to those of water-in-oil microemulsions [208]. In contrast to that, Kayali *et al.* claimed that there is no structuring in similar biofuel mixtures by using NMR self-diffusion measurements [209]. Most importantly, however, the existence and type of nanostructures in SFMEs of biofuels as well as their influence on decisive parameters of fuel formulation could not be proven so far.

2.1.4.2 Hydrofuels

During the past 20 years, the implementation of water into fuel formulations was intensively investigated. It is well known that the presence of water in fuel combustion processes significantly reduces NO_x and soot emissions due to its high heat capacity and influence on combustion reactions. In particular, water lowers the combustion temperature and therefore, less thermal NO_x emissions are produced according to the Zeldovich mechanism [197, 210]. Further, the combustion of water containing fuels generates radicals that accelerate the decomposition of hydrocarbons, thus minimising their soot emissions [211]. These two effects show that the NO_x-soot trade-off, explained in 2.1.1.1, is overcome by adding water to the fuel [210]. Especially in combustion applications, sufficient mixture formation and long-time stability are essential parameters for consistent combustion

properties [212]. Similar to ethanol containing fuels mentioned in the section above, surfactants are required to obtain microemulsions consisting of water and fuels. Due the volatility difference between the small water droplets, distributed in the microemulsion, and the fuel, the combustion is often coupled with the microexplosion phenomenon, leading to an increased combustion efficiency [213]. Strey *et al.* patented several approaches to produce water-in-fuel microemulsions in the presence of surfactants and implemented the term hydrofuels for these mixtures. In general, they use nonionic surfactants like ethoxylated alkyl polyethylene glycol ethers, sold as Lutensol by BASF [211, 214]. Besides their high costs making them economically inapplicable on an industrial scale, Fig. 15 shows the fuel consumption of diesel and a typical hydrofuel consisting of diesel, water and about 7–10 wt% of a nonionic surfactant, depending on the amount of water and load conditions at different engine speeds.

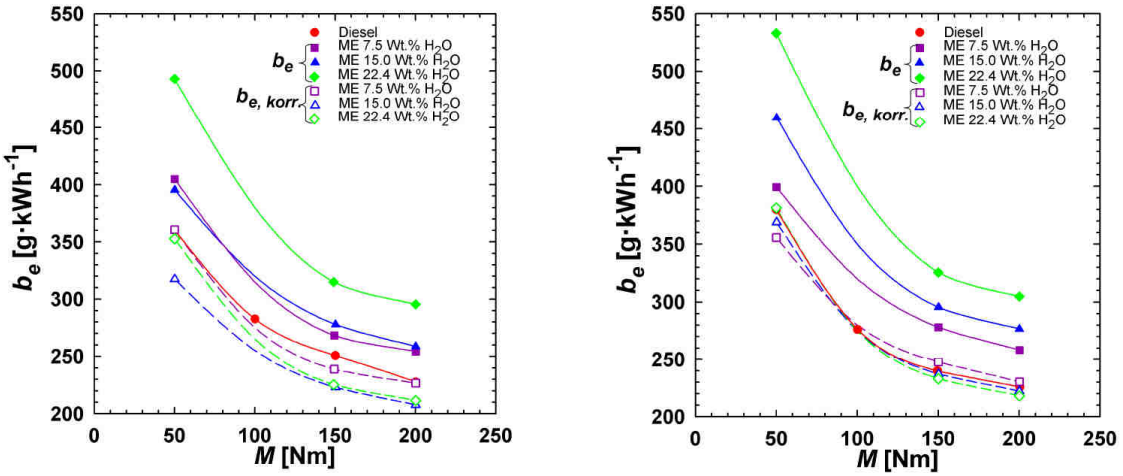

Figure 15: Effective, specific consumption b_e of diesel as well as formulated microemulsions (ME) consisting of diesel, different amounts of water and about 7–10 wt% of an ethoxylated alkyl polyethylene glycol ether as surfactant versus the load conditions. Besides showing these consumptions at engine speeds of 1500 rpm (left) and 1800 rpm (right), b_e is adjusted to obtain the actual value of the energy supplying compounds $b_{e,korr.}$, since the presence of water and surfactant distinctly increases the total fuel consumption [210, 211].

Compared to diesel, the effective, specific consumption b_e of the formulated hydrofuel is already distinctly higher in the presence of 7.5 wt% of water. Further, there is no linear dependence of b_e on the water content, as 22.4 wt% of water increase b_e by 37.5% at 1500 rpm (see Fig. 15). At a slightly higher engine speed of 1800 rpm, the increase is even 40.8% for the same mixture. These results can be explained by the low heating values of water and surfactant. Especially the surfactant is important to mention, as the increase of b_e is even higher than the amount of added water. This shows that the microexplosion phenomenon does not compensate the bad combustion properties of the surfactant, thus

resulting in higher consumptions than expected. Strey *et al.* deal with this issue by adjusting b_e with respect to the low heating value of water and, of course, obtain values for $b_{e,korr.}$ that are below the results of pure diesel [210, 211]. Instead of pointing out that the presence of surfactants is negatively affecting the fuel consumption, it is, unfortunately, not discussed any further in their patents and publications. Additionally, several injection and ignition tests were performed by Dittmann *et al.* with the same hydrofuel, proving that this mixture leads to considerable cavitational wear of the valves. The nozzle cross-section also needs to be adjusted to compensate the reduced heating value, which in turn distinctly increases the ignition delay of the hydrofuel [212]. To conclude, a nanostructured hydrofuel without any surfactants would be an interesting option, particularly SFMEs.

2.1.4.3 Dynamic and static light scattering

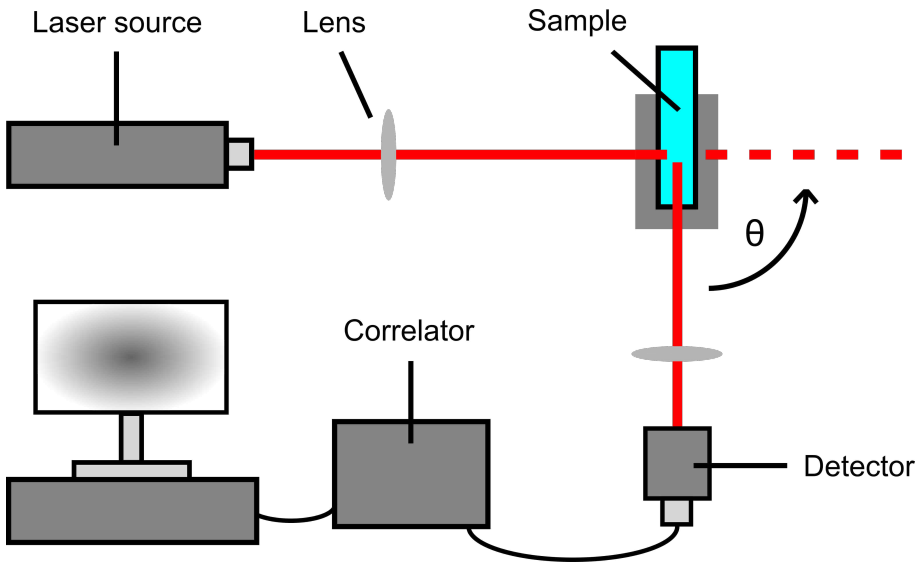

Figure 16: Common setup for dynamic light scattering (DLS) as well as static light scattering (SLS) used in this thesis.

To investigate colloidal structures like micelles and polymers in solutions, light scattering experiments are approved methods. In general, light is scattered by particles in solution, as long as they are smaller than the wavelength of the irradiated light. With the difference in the refractive indices between the dispersed, moving particles or aggregates and the dispersion medium, intensity fluctuations of the scattered light occur. Within the dynamic light scattering (DLS) method, these fluctuations are investigated in a sufficiently small measuring field and a time resolution of a few microseconds [215]. As shown in Fig. 16, a laser source and optical devices are used to produce a monochromatic, coherent and

vertically polarised laser beam, which irradiates the thermostatically controlled sample. Due to the presence of aggregates in the sample, the light is scattered and a specific scattering angle θ is chosen to measure its intensity by a photon detector.

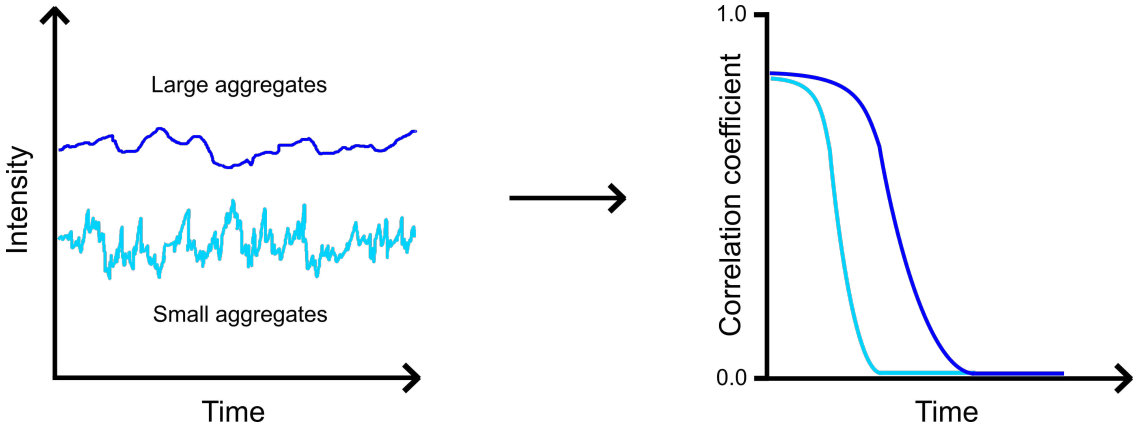

Figure 17: Data acquisition and processing by the detector and correlator: After measuring the intensities of the scattered light over a specific period of time (left), normalised electric field correlation functions can be derived (right). Within this thesis, these functions are called correlation coefficients for reasons of simplification. The different results obtained for large and small aggregates are shown, but it needs to be mentioned that the difference in the absolute values of the intensities is qualitative and just for a better illustration.

Coming back to the intensity fluctuations of the scattered light, the particles move due to the Brownian motion, which depends on their size and nature as well as on the temperature and viscosity of the medium. Therefore, the distance between the aggregates changes constantly, causing constructive and destructive interferences of the scattered light and thus intensity fluctuations. Their time-dependent progression obtains information on the motion, size and distribution of the particles (see Fig. 17). Since small aggregates move faster than big ones, their intensity fluctuation is more pronounced. A digital autocorrelator compares the intensities at different time intervals. Considering a specific intensity of the scattered light at the time t, the autocorrelator compares this value with the intensity just a very short moment $t + \tau$ later. In this case, a strong correlation is observed, which decreases with increasing time intervals between the measuring points. Therefore, the resulting normalised electric field correlation function remains for a longer period of time, when large aggregates are present in the solution [215, 216].
Assuming monodisperse aggregates, this time correlation function $g^1(q, \tau)$ is described with following equation:

$$g^1(q, \tau) = a_0 + [a_1 \cdot e^{(-a_2 \tau)}]^2 \tag{29}$$

with the delay time τ, the constant baseline value a_0, which is typically 1, the dynamic part of the amplitude a_1 and the decay rate a_2. The scattering vector q is the difference

between the propagation vectors of the irradiated and the scattered light. a_2 is linked to the diffusion coefficient D and q (see Eq. 30).

$$a_2 = Dq^2 \tag{30}$$

q is defined as:

$$q = \frac{4\pi n}{\lambda} \sin \frac{\theta}{2} \tag{31}$$

with the refractive index n, the wavelength of the irradiating light λ and the detection angle θ. Assuming spherical aggregates, the hydrodynamic radius r_h can be derived from the diffusion coefficient D, using the Stokes-Einstein equation:

$$D = \frac{k_\mathrm{B} T}{6\pi\eta r_\mathrm{h}} \tag{32}$$

with the Boltzmann constant k_B, the temperature T and the dynamic viscosity η. Therefore, η and n need to be measured additionally to obtain r_h, which provides information on the size of the aggregates in the system. While a viscometer, described in section 2.1.3.1, is used to determine η of a liquid, a refractometer, based on the critical angle for total internal reflection, is utilised to measure n [215, 216]. In contrast to real-time scattering intensities obtained by DLS, time-averaged scattering intensities are measured for different scattering angles during static light scattering (SLS) experiments. This enables the determination of the molecular weight of an aggregate or macromolecule and its root mean square radius, also known as radius of gyration. Since larger aggregates cannot be considered as isotropic scatterers, their scattering intensity is dependent on the scattering angle [199]. This dependence is explained within the Rayleigh theory, which needs to be adjusted to SFMEs with following equation:

$$M_\mathrm{app} = M \cdot S(q) = \frac{R_\mathrm{sample}}{Kc} \tag{33}$$

with the apparent and unchanged molar masses of the aggregates M_app and M, the structure factor $S(q)$, which considers the influence of the aggregates' interactions on the light scattering, the Rayleigh ratio of the sample R_sample, which is further described in Eq. 35, and the concentration of the aggregates in the system c. The parameter K can be obtained from Eq. 34:

$$K = \frac{4\pi^2 n^2}{\lambda^4 N_\mathrm{A}} (\frac{dn}{dc})^2 \tag{34}$$

with the refractive index increment dn/dc and Avogadro's number N_A. R_sample, which depends on the scattering angle, is calculated by using the data of the SLS experiments:

$$R_{\text{sample}} = \frac{I_{\text{sample}} - I_{\text{solvent}}}{I_{\text{standard}}} \cdot R_{\text{standard}} \cdot \left(\frac{n_{\text{solvent}}}{n_{\text{standard}}}\right)^2 \tag{35}$$

with the scattering intensities of the sample I_{sample}, solvent I_{solvent} and standard I_{standard}, which is toluene, and the correction factor $(n_{\text{solvent}}/n_{\text{standard}})^2$ of the scattered volume due to diffraction effects [217]. By assuming spherical aggregates and measuring their density $\rho_{\text{aggregate}}$, which is considered to be the density of the inner phase, their radius r is obtained from following equation [199, 218]:

$$V_{\text{sphere}} = \frac{M_{\text{app}}}{N_{\text{A}} \cdot \rho_{\text{aggregate}}} = \frac{4}{3}\pi r^3 \tag{36}$$

2.1.4.4 Small- and wide-angle X-ray scattering

While light is scattered by nanostructured mixtures due to fluctuations of the refractive index, an X-ray beam is scattered because of differences in the electronic densities of a structured medium. The small- and wide-angle X-ray scattering technique (SWAXS) is a powerful, but elaborate method to investigate the structuring of mixtures in detail. Fig. 18 shows the simplified measuring principle, in which a monochromatic and collimated X-ray beam irradiates the sample. The scattered X-rays are collected by a two-dimensional detector at a modifiable distance. The closer the detector is positioned to the sample, the bigger the investigated scattering angle.

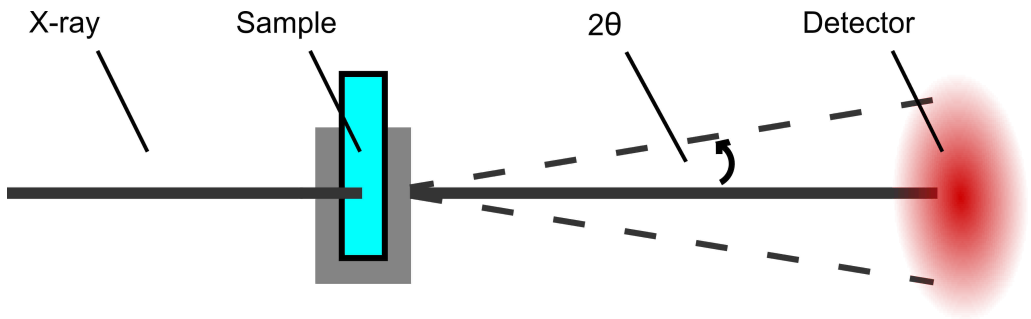

Figure 18: Simplified setup for small- and wide-angle X-ray scattering (SWAXS) measurements.

In general, the intensity of the scattered X-rays of isotropic scatterers can be described by following equation:

$$I(q) = nV^2 \cdot \Delta\rho^2 \cdot P(q)S(q) \tag{37}$$

with the particle concentration n, the volume of the aggregates V, the electron density difference between the scattering aggregate and the solvent $\Delta\rho$, also known as scattering

length density, the form factor $P(q)$ and the structure factor $S(q)$, which both depend on the scattering vector q [219]. While the shape of the aggregate is considered by $P(q)$, $S(q)$ takes into account the interactions between the aggregates in the mixture. There are many models to derive $P(q)$ and $S(q)$ from the experiments, but evaluating and choosing the most suitable one, depending on the fitting quality, is often complex. Particularly for SFMEs, the scattering intensity at low q-values is of interest, as it describes the interactions between structures and particles in solution. X-ray scattering at higher q-values, on the other hand, enables information on interactions between the molecules. Since SWAXS experiments were just performed once within the scope of this thesis and in collaboration with scattering experts from France, in particular Diat *et al.* and Bauduin *et al.*, this method and its principles are not further explained. To describe SWAXS data of SFMEs for q-values below $1\,\mathrm{nm}^{-1}$, a rather simple Ornstein-Zernike equation is sufficient:

$$I(q) = \frac{I_0}{1 + q^2\xi^2} \tag{38}$$

With this equation, the correlation length ξ of the aggregates can be determined with the forward scattering I_0 at $q = 0$ [220, 221].

2.1.4.5 Conductivity and percolation models

To obtain information on the structure formation and type of microemulsions, conductivity measurements are the method of choice. There are different types of microemulsions, which depend on the composition of the mixture, in particular the water and oil content. Generally, at high amounts of water, the oil molecules are in the inner phase of the microemulsion (o/w, oil-in-water), whereas the oil is the continuous phase, if it is the main component of the system (w/o, water-in-oil). During the transition from o/w to w/o, the microemulsion is bicontinuous, as the water and the oil phase form a sponge-like network [222, 223]. Fig. 19 illustrates the typical conductivity behaviour κ of a mixture consisting of water, oil and an ionic surfactant with an increasing volume ratio of water $\phi(W)$. At low $\phi(W)$ values, there is nearly no conductivity measurable, as the conductive water pseudo-phase is in the inner phase of a just forming w/o microemulsion. With further addition of water, κ slowly increases, until the percolation threshold ϕ^{P} is reached. After that critical point, κ increases proportionally to $\phi(W)$ because of a higher probability of charge transport due to micelle collisions [224]. Once the slope of the curve decreases and a maximum of κ is reached, bicontinuous structures are present [223]. At this point, any further addition of water leads to the transition to o/w microemulsions and κ decreases due to dilution effects [225, 226].

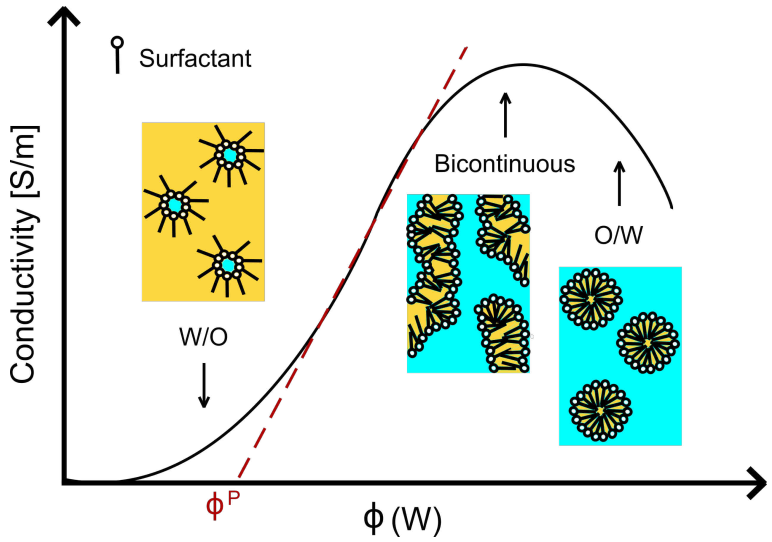

Figure 19: Conductivity of a mixture consisting of water (W), oil (O) and a surfactant versus the volume ratio of water ϕ(W). The red dashed line indicates the determination of the percolation threshold ϕ^{P}.

The percolation threshold ϕ^{P} indicates the formation of the first infinite cluster of aggregates, whose number rapidly increases with further addition of water. The correlation between the structural change of the mixture and the distinct increase of the conductivity can be described with two asymptotic scaling power laws (see Eq. 39 and 40). These equations contain two different exponents s and t, which provide information on the arrangement of the aggregates below and above ϕ^{P} [224, 227].

$$\kappa \propto (\phi^{\mathrm{P}} - \phi(W))^{-\mathrm{s}} \quad \forall\, \phi(W) < \phi^{\mathrm{P}} \tag{39}$$

$$\kappa \propto (\phi(W) - \phi^{\mathrm{P}})^{\mathrm{t}} \quad \forall\, \phi(W) > \phi^{\mathrm{P}} \tag{40}$$

There are two theoretical approaches to explain the percolation mechanism in microemulsions. The *static percolation model*, applying for $s \approx 0.6$ and $t \approx 1.9$, assumes that bicontinuous oil and water structures are formed, leading to higher conductivities due to connected water paths. Within the *dynamic percolation model*, applying for $s \approx 1.2$, the attractive interactions between water-rich aggregates cause the formation of percolation clusters. This model considers structural rearrangements due to Brownian motion and the high kinetics of microemulsions, with the charge being transported by the rearranging clusters. The exponent t just helps proofing the presence of a static percolation and therefore does not provide any further information concerning a dynamic percolation [222, 224]. As aggregates of SFMEs are known to be formed and destroyed on a microsecond scale, this model is particularly interesting for these systems. Up to now, there are just a few publications about conductivity measurements of low-conductive SFMEs and especially no comparable experiments concerning biofuels.

2.1.5 Towards a new concept of biofuels

As exemplified in detail in the previous chapters, opportunities to get rid of the dependence on fossil fuels do not only have to be further developed, but also implemented into everyday life in the next years. If this is not achieved, the international climate objectives will not be fulfilled. Driven by the "Dieselgate" scandal and the still fundamental problems of E-mobility, this thesis focuses on the applicability of new biofuel formulations that are not related to fossil fuels. During my master thesis, a first approach to a new kind of completely green biofuels was already developed [228]. After briefly outlining its main results, the motivation and strategy concerning the main topic of this PhD thesis, biofuel formulations, are explained.

2.1.5.1 First approach to completely sustainable biofuels

Within the scope of my master thesis, biofuels with a vegetable oil as main component had to be formulated, which are directly applicable in an unmodified up-to-date diesel engine and fulfil the principles of green chemistry, i.e. they do not contain any environmentally harmful additives. When using vegetable oils in biofuels, especially η_{kin} and the low-temperature phase behaviour must be precisely adjusted, as described in chapter 2.1.3, to ensure that the respective standards are met. To enable the direct usage of the formulated biofuels in diesel engines, the current biodiesel standard of the United States, ASTM D6751, as well as the European standard EN 14214 were taken into consideration. In particular, mixtures of rapeseed oil and FAME obtained from rapeseed oil were investigated. On the one hand, the usage of FAME was assumed to be inevitable due to its low viscosity and high CN, but on the other hand, its cloud and pour point are even higher compared to rapeseed oil. To overcome these problems, two different formulation approaches were performed. The first set of formulations consisted of rapeseed oil, its FAME and the furan derivatives 2-methyltetrahydrofuran (2-MTHF), 2,5-dimethylfuran (DMF) and 2-methylfuran (2-MF) as oxygenates (see Fig. 20). The aim with these compositions was to ensure rapeseed oil as main component and simultaneously to reduce the amount of necessary FAME in the formulations. The furan derivatives are environmentally promising substances, since they can be produced from sugar or cellulose, i.e. from the waste of vegetable oils [229, 230]. Thus, these mixtures constitute a combination of first and second generation biofuels, promoting the potential of bioresources. In the second approach, the terpenes D-limonene, α-pinene and farnesene were added to rapeseed oil in order to completely avoid the usage of FAME (see Fig. 20 again). Due to their chemical structure, in particular the high number of carbon atoms and the absence of heteroatoms, their favourable combustion properties were already known and therefore, FAME was not required [231].

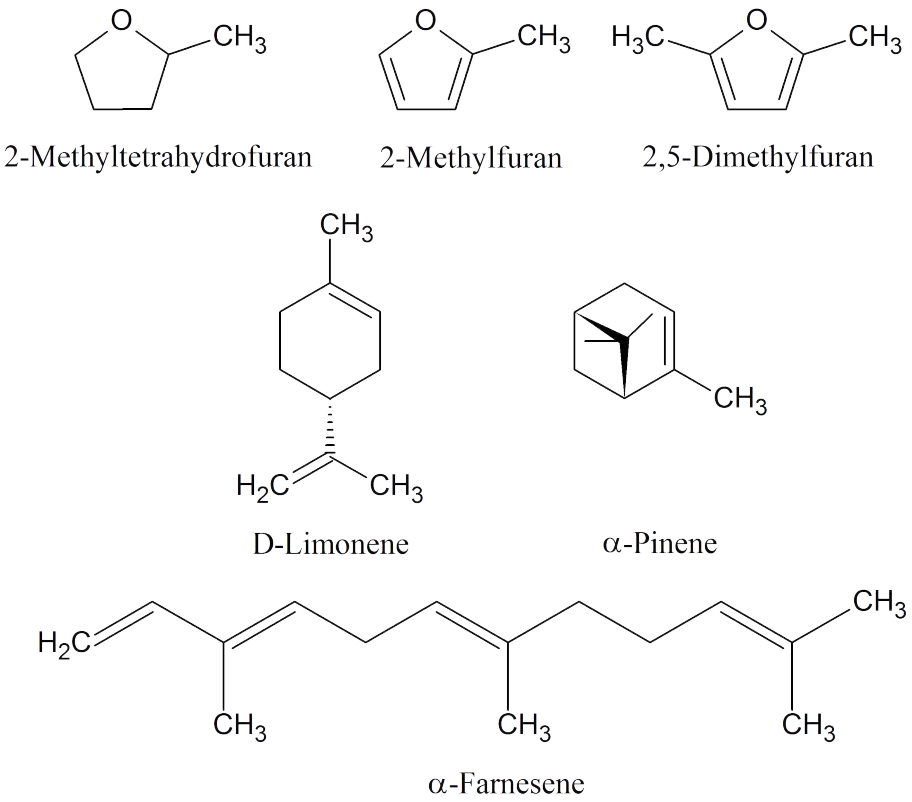

Figure 20: Structure of the investigated furan derivatives and terpenes as potential biofuel components.

As the furan derivatives as well as the terpenes are completely miscible with rapeseed oil and FAME at room temperature, no emulsifiers like in ethanol-containing fuels were necessary. Without going too far into detail, the main results and optimisation steps towards the final biofuel formulations are briefly summarised: It could be shown that the addition of a furan derivative distinctly reduces η_{kin} and the cloud point of the mixture, as expected. As 2-MF led to the lowest η_{kin} as well as cloud point and possessing the shortest synthesis route of the investigated furans, it was chosen as most suitable furan derivative [229]. Since the amount of rapeseed oil should be as high as possible and the amount of expensive 2-MF as low as possible, FAME was still necessary. Therefore, an exemplary biofuel formulation consisted of about 62 wt% of rapeseed oil, 10 wt% of FAME and 28 wt% of 2-MF. While the addition of the terpenes reduced η_{kin} to a lesser extent than the furans, they significantly decreased the cloud point of rapeseed oil. Thus, higher amounts of terpenes were required to fulfil the viscosity standards.
In order to obtain more information on the combustion and emission properties of the formulated biofuel with the composition mentioned above, measurements at an engine test bench were essential. These experiments were carried out in cooperation with the chair of combustion engines of Prof. Dr. Hans-Peter Rabl at the Ostbayerische Technische Hochschule Regensburg. Due to the self-imposed requirements for the formulated biofuel

to fulfil biodiesel standards, an unmodified up-to-date diesel engine could be used. Several injection pressure variation, ignition delay and EGR measurements showed that most properties of the biofuel are close to diesel and especially the THC and soot emissions are even lower. The slightly higher consumption of the biofuels can be justified with its complete sustainability and therefore possibly lower price in the future compared to fossil fuels. In general, this work points out that new kinds of completely green biofuels can be developed by using solely sustainable compounds. If the formulations are then adjusted to fulfil current standards regarding their physicochemical properties, their combustion behaviour, like in this case, can lead to unexpectedly favourable results [228].

2.1.5.2 Goals of the biofuel formulations within this thesis

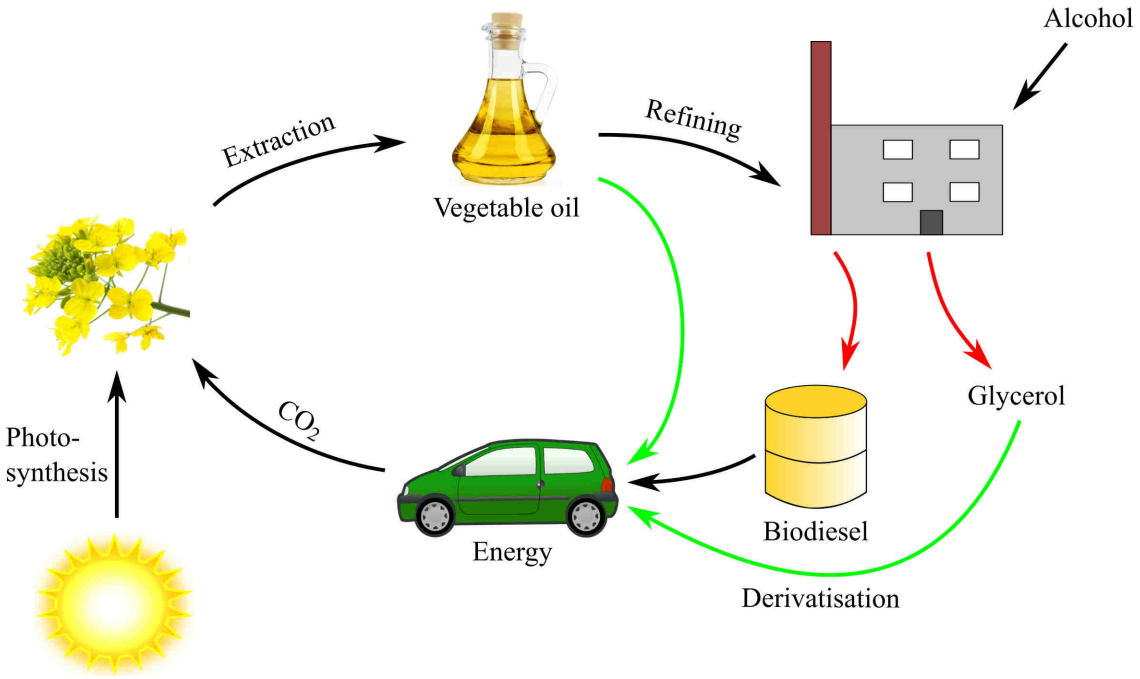

Figure 21: Scheme of the FAME production process including the developed optimisations within this thesis. The common production and consumption cycle of FAME is illustrated by black and red arrows. Red arrows indicate the most important drawbacks of this process, whereas green arrows show the considered optimisations steps, which distinctly increase the production profitability of FAME.

Even though the formulation approach during my master thesis was successful, there are still some problems to solve concerning these biofuels: due to their limited availability, high costs are associated with the usage of terpenes. The same applies to the furan derivatives, since they have to be produced by chemical conversion of crude materials. Therefore, the usage of 28 wt% of 2-MF, like in the formulated biofuel for the engine tests, is not

applicable on an industrial scale. Within this PhD thesis, I decided to focus more on the industrially established FAME production. Indicated by red arrows, Fig. 21 illustrates the two major drawbacks of this process that harm the environment. Firstly, it is evident that the process itself has some disadvantages, since refineries are necessary to synthesise FAME from methanol and a vegetable oil. Secondly, this transesterification reaction is coupled with the production of glycerol as by-product, explained in section 2.1.1.2, which lacks industrial large-scale applications that could consume its high production volume. To increase the efficiency of this process and to diminish its drawbacks, Fig. 21 also shows our ideas of maximising its profitability, indicated by green arrows. The direct usage and implementation of pure vegetable oils into the biofuel formulation make their chemical transformation to FAME obsolete and thus the production of glycerol. This approach was obviously already examined and implemented during my master thesis. Additionally, investigations regarding the compatibility of glycerol with fuel components should be performed to evaluate its potential as biofuel source. Since glycerol is the main waste product of FAME production, a concept dealing with its implementation into biofuels consisting of vegetable oils and FAME would distinctly increase FAME's competitiveness. In particular, the glycerol derivatives described in Fig. 9 are used for these investigations.
Besides this already challenging issue, the two fundamental problems of biofuels for diesel engines should also be faced within this thesis: their low stability towards oxidation and their high NO_x emissions during combustion. These two drawbacks should be taken into consideration by solubilising natural antioxidants in the biofuels without reducing the stability towards oxidation compared to commercially used and highly toxic hydroquinones (see section 2.1.3.3). Further, this new biofuel concept should enable the implementation of water to decrease the NO_x emissions without using surfactants. By completely fulfilling these demands, this biofuel concept would not only significantly increase the profitability of many industrial processes, but also enable a wide range of possible applications.
As the usage of water in these biofuel formulations leads to investigations on SFMEs, further experiments are performed to prove the existence of nanostructures in ethanol-containing, but surfactant-free biofuels. Moreover, the influence of these structures on the most important physicochemical parameters of the biofuel, in particular the viscosity and low-temperature phase behaviour, should be verified as well.

2.2 Further applications of glycerol derivatives

2.2.1 Extraction systems based on glycerol derivatives

Besides the development of a new biofuel concept, where glycerol derivatives should play a major role, further uses of these compounds were investigated concerning completely different fields of application. In particular, glycerol derivatives were examined in terms of replacing currently used, toxic or environmentally harmful substances. As their mixing and solubilising behaviour is extensively characterised within the biofuel formulations, specific applications were chosen, whose further development is inhibited due to miscibility or compatibility issues. In this chapter, the usage of glycerol derivatives as alternative, sustainable extracting agents is evaluated. Since several research articles of our group, dealing with sustainable extraction processes, were published in the past years, correlations between the mixing properties of the extracting agents, e.g. the amphiphilic character of surfactants or hydrotropes, and the extraction process could be identified [232–234]. After outlining the industrial status quo of improvable processes like the extraction of antioxidants from vegetable oils, high-performance liquid chromatography (HPLC) as research method and different approaches to purify and isolate the respective extract are briefly described.

2.2.1.1 Extraction of antioxidants from vegetable oils

Antioxidants have been known for their anti-aging properties for many years. Besides being popular in cosmetics due to their positive impact on skin aging, they also decrease the risk of cardiovascular diseases and cancer [235]. Since many synthetic antioxidants are toxic and do not fulfil the guidelines of the cosmetic and food industry, natural antioxidants are required for these applications [236]. Especially vitamin E, which consists of tocopherols and tocotrienols, is considered as most promising food approved antioxidant mixture, nowadays [237]. In this context, rapeseed oil plays an important role, as it contains high amounts of α-tocopherol, the most active form of vitamin E in vivo, with about 0.02 wt% [237, 238]. For comparison, soybean oil consists of about 0.007 wt% of α-tocopherol [239]. Concerning the objectives of the biofuel formulations within this thesis, high amounts of vegetable oil and in particular rapeseed oil should be used. Therefore, rapeseed oil is simply combusted with its constituents like α-tocopherol. Considering the *polar paradox theory*, this very hydrophobic antioxidant does not efficiently contribute to rapeseed oil's stability towards oxidation and thus, it can be removed without hindering the biofuel formulations (see Fig. 22). Since tocopherols are sensitive to heat, light and air, gentle methods are necessary to isolate the antioxidants from vegetable oils [237, 240]. Extraction is the most

common process to obtain sensitive or bioactive compounds from plant materials. As rapeseed oil is used in this work, the liquid-liquid extraction process is chosen, in which an extracting agent, i.e. solvent, is used to remove the extract from another liquid based on its solubility. The efficient application of this method requires intensive investigations, with the yield of extractions depending on a variety of parameters like type of solvents, temperature, time and extract-to-solvent ratio [241].

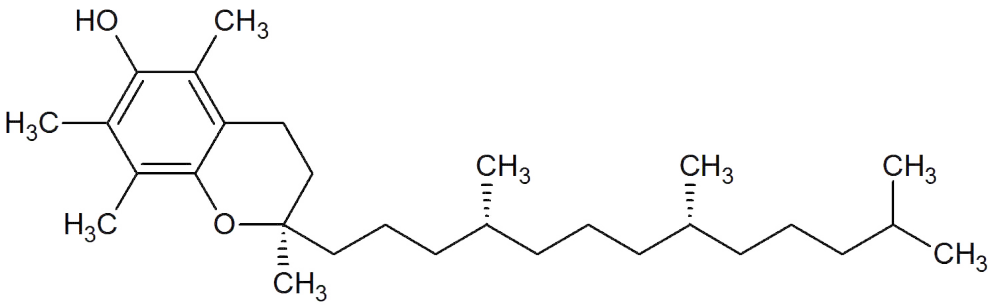

Figure 22: Chemical structure of α-tocopherol.

n-Hexane is typically used as extracting agent for antioxidants from vegetable oils. Besides being mainly obtained from fossil oil, its toxicity caused strict regulations for the usage of this alkane in the past years [242–244]. This in turn led to investigations on replacing *n*-hexane by less toxic and sustainable substances like ethanol and acetone. Consequently, many different extraction methods are currently performed to obtain antioxidants from either the oil plant or the vegetable oil [236, 245, 246]. When using the most promoted sustainable extracting agents, methanol and ethanol, high amounts of these alcohols, extraction times varying from half an hour to up to several weeks, increased temperatures and their subsequent evaporation is necessary to extract and isolate the antioxidants [245, 247]. There are, of course, many other extraction techniques including ultrasound-assisted and supercritical fluid extraction, which are beyond the scope of this thesis [236, 241, 248]. Additionally to their flammability and still toxic or at least harmful properties, the usage of these alternatives often requires the addition of surfactants, similar to some ethanol-containing fuels (see section 2.1.2.4). Since these compounds need to be approved for the cosmetic and food industry as well, sorbitan esters like Tween and Span are commonly utilised [249–251]. Even if these methods are industrially applicable and more environmentally friendly than *n*-hexane-based extraction processes, they are still very energy consuming and partially harmful for the environment. Therefore, the usage of non-toxic and sustainable extracting agents, which simultaneously leads to a significant process simplification, should be further investigated. For that reason, the potential of glycerol derivatives as extracting agents of antioxidants is examined in this chapter.

2.2.1.2 High-performance liquid chromatography

Chromatography is one of the most important separation techniques in industry. In general, the sample is dissolved in a mobile phase, which can be liquid, gaseous or supercritical, and separated due to different interactions of the components with the stationary phase. The more a compound interacts with the surface of the stationary phase, the longer it takes, until it passed through the column. This specific time is also known as the retention time of the compound. Depending on the mobile phase, this method is called liquid chromatography (LC), gas chromatography (GC) or supercritical fluid chromatography (SFC). In vegetable oil-containing systems, high-performance liquid chromatography (HPLC) is the most suitable method. Within this separation technique, high pressures are applied to move the mobile phase through the densely packed stationary phase. A UV/Vis-detector is commonly used to identify the different compounds of the sample depending on their light absorption behaviour at specific wavelengths [252, 253]. To particularly detect the α-tocopherol content of the sample, wavelengths between 290 and 295 nm are commonly used. A precise description of the HPLC settings is given in the experimental part of this thesis in section 3.2.1.2.

2.2.1.3 Purification and isolation of extracted antioxidants

After successfully extracting the desired antioxidants with another liquid, different methods are required to purify and isolate them. As already mentioned before, typical sustainable extracting agents like methanol, ethanol or acetone are evaporated after extraction processes in food industry, since they need to be completely removed in the final product [243, 254]. By using nontoxic, sustainable and even food approved extracting agents like triacetin, shown in Fig. 9, this energy-consuming step would become obsolete. However, as solketal and tributyrin are not food approved and as there is not much data about the extraction as well as miscibility properties of the investigated glycerol derivatives in general, many different purification and isolation techniques are considered within this thesis. In particular, centrifugation and additional extraction experiments as well as salting-out and temperature effects are examined, further explained in section 3.2.1.4.

2.2.2 Alternatives to ethanol as freezing point depressant

Freezing point depression is another completely different field of application, in which non-sustainable or harmful substances will be replaced by sustainable and non-toxic alternatives in the next years. Since the desired performance at low temperatures mostly depends on the miscibility properties of the components, this topic fits well to the other chapters of this thesis. With the presence of ethanol being the main issue due to its flammability, glycerol derivatives could again be suitable alternatives. After briefly explaining the concept of freezing point depression and the used measurements, the initial situation of the company WIGO Chemie GmbH is outlined, which requested for help to replace ethanol as main component of their winter windscreen cleaners.

2.2.2.1 Freezing point depression

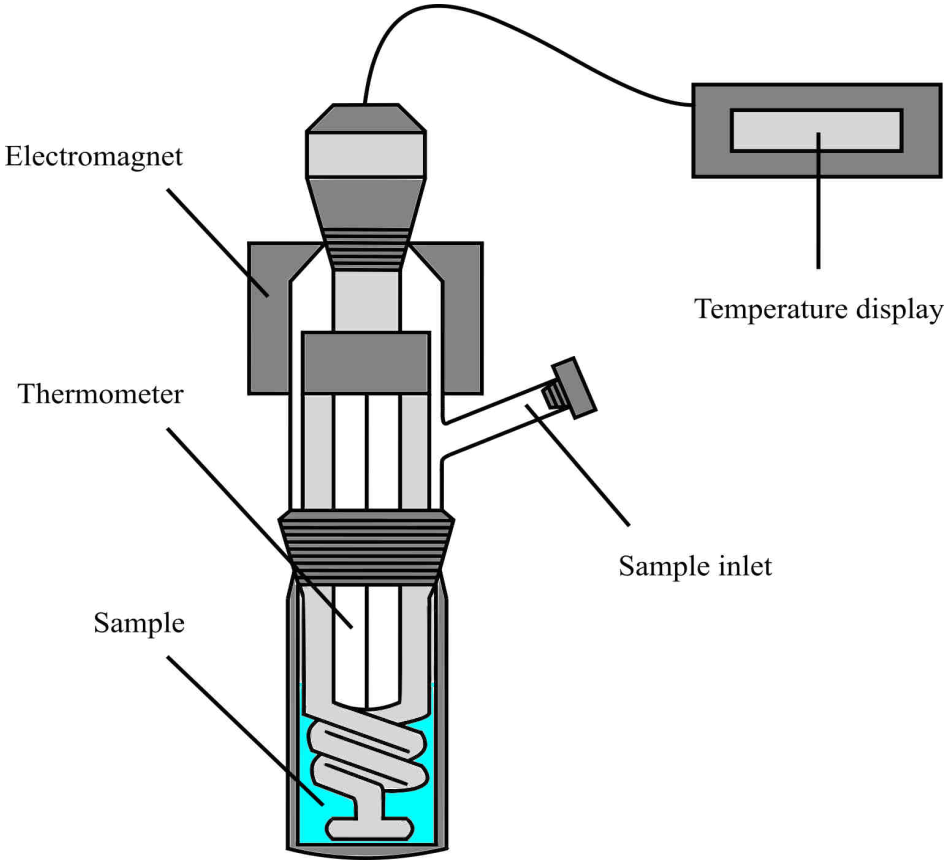

Figure 23: Used setup of a cryoscopic apparatus according to Beckmann to prevent humidity and supercooling effects.

If two liquids mix spontaneously, the Gibbs free energy of mixing $\Delta_{\text{mix}}G$ has to be negative. The entropy of mixing $\Delta_{\text{mix}}S$ is the driving force of this process, as the entropy of a mixture, e.g. of a solvent and a solute, is higher than the entropy of a pure solvent (see Eq. 41). This in turn is also the reason for the chemical potential of the mixture being lower than that of the pure solvent, which leads to a reduced freezing point and increased boiling point of the mixture compared to the pure solvent. If a physical parameter depends on the amount of the solute like the freezing point, it is also called a colligative property [255].

$$\Delta_{\text{mix}}G = G_{\text{after}} - G_{\text{before}} = \Delta_{\text{mix}}H - T\Delta_{\text{mix}}S \tag{41}$$

Since the investigated mixtures are aqueous multi-component systems, the determination of their freezing point is challenging due to humidity and supercooling effects. Within this thesis, several measuring techniques like light microscopy, differential scanning calorimetry (DSC) and cryoscopic processes were used and optimised. Especially the cryoscopic apparatus according to Beckmann, shown in Fig. 23, is further described, as it led to the most reliable results. The thermally insulated sample is stirred with a magnetic lifting mixer. By cooling down the sample with a mixture consisting of water, ice and sodium chloride, the sample's temperature reaches a minimum, before it will increase significantly due to the released heat of crystallisation. After adding a glass case, the sample is cooled down again, but with a distinctly slower speed. Once a constant temperature is recorded by the installed thermometer, the freezing point is reached [256, 257].

2.2.2.2 Current state of windscreen cleaners

The German company WIGO Chemie GmbH, which is part of the Berner Group, is specialised in cleaning agents for specific surfaces like glass and interiors of containers as well as the production of AdBlue. Within their patent on winter windscreen cleaners, they sum up the requirements of their products: a thorough and lasting cleaning, a sufficiently reduced freezing point, a low viscosity, a production from environmentally friendly as well as cheap resources and physiological safety. A closer look at the composition of this cleaning mixture shows that the product mostly consists of ethanol and water (see Table 4). Both substances act as solvents for the other components and ensure a sufficiently low viscosity, which is increased by the presence of glycerol and 1,2-propanediol. Along with ethanol, these three compounds are used as freezing point depressants due to their hydroxy groups. Further, glycerol and 1,2-propanediol are known to solubilise insect residues and to form a thin layer on the surface, which inhibits refreezing. Since glycerol is obtained from renewable resources and cheaper than the diol, it is used in higher amounts to replace 1,2-propanediol. Considering glycerol's high viscosity, shown in Table 2, this in turn explains

the necessity of more than 50 wt% of ethanol. Anionic and zwitterionic surfactants are primarily used to enable the miscibility of the components. In the case of special requests, nonionic surfactants, in particular alkyl polyglycosides, are necessary. Small quantities of complexing agents and fragrances complement this product formulation [258].

Table 4: Composition of the patented and commercially sold winter windscreen cleaner of WIGO Chemie GmbH [258].

Compound	$\omega_{\mathbf{compound}}$**(wt%)**	**Task**
Ethanol	52–58	Solvent, freezing point depression
Water	23-32	Solvent
Glycerol	10-12	Freezing point depression, solubilisation of insect residues, replacement of 1,2-propanediol
Surfactants	3	Miscibility of the components
1,2-Propanediol	2.5	Freezing point depression, solubilisation of insect residues
Nitrilotriacetic acid	0.5	Complexing agent
Terpenes	0.25	Fragrance

Due to the high ethanol content, this winter windscreen cleaner has a low flash point, which leads to the labelling as hazardous product. Besides the increasing demand for sustainable and environmentally friendly components in product formulations, requesting alternatives to ethanol, WIGO's highest costs arise from the hazardous materials transportation of huge amounts of ethanol [259]. Based on this problem, WIGO contacted the SKH GmbH, an associated institute of the University of Regensburg with Prof. Dr. Werner Kunz as chief executive, to find suitable, sustainable alternatives to ethanol. As glycerol derivatives are already investigated to replace ethanol in biofuel formulations within this thesis, taking into account the viscosity and low-temperature phase behaviour of the mixture, WIGO's research contract fits the scope of this thesis. The experiments should be performed according to the standard test method for freezing points of aqueous engine coolants ASTM D1177-12, which is further described in the experimental section 3.2.2.4 [260].

3 Experimental

3.1 Investigations on completely green biofuels

3.1.1 Chemicals

Acetylsalicylic acid (≥99%), ascorbic acid (AA, ≥99%), benzoic acid (≥99.5%), *tert*-butylhydroquinone (TBHQ, ≥97%), caffeic acid (CA, ≥98%), *p*-coumaric acid (≥98%), ethanol (purity ≥99.8%), *trans*-ferulic acid (≥99%), gallic acid (GA, ≥98%), ethyl gallate (≥96%), propyl gallate (≥98%), octyl gallate (≥99%), lauryl gallate (≥99%), (R)-(+)-limonene (≥97%), hydrocinnamic acid (≥99%), 3-hydroxybenzoic acid (≥99%), 4-hydroxybenzoic acid (≥99%), methyl *tert*-butyl ether (MTBE, ≥99.8%), tannic acid (≥98%), tributyl citrate (TBC, ≥97%), vanillic acid (≥97%) and the glycerol derivatives glycerol triacetate (triacetin, 99%) as well as tributyrate (tributyrin, 97%) were purchased from Sigma-Aldrich GmbH (Steinheim, Germany). Hydroquinone (HQ, ≥99%) was purchased from Fluka Chemika (Buchs, Switzerland). 1-Heptanol (HepOH, ≥99%) and anhydrous lithium perchlorate (≥99.5%) were purchased from Alfa Aesar (Karlsruhe, Germany). Ethyl *tert*-butyl ether (ETBE, ≥95%) was purchased from Tokyo Chemical Industry (Zwijndrecht, Belgium). 2-Ethylhexylnitrate (EHN, ≥97%) was a generous gift from EURENCO (Avignon, France). Pure rapeseed oil from Rapso Österreich GmbH (Aschach, Austria) was purchased in local grocery stores. The furan derivatives 2,5-dimethylfuran (DMF, ≥98.7%), 2-methylfuran (2-MF, ≥98%) and 2-methyltetrahydrofuran (2-MTHF, ≥99%)

as well as rapeseed oil FAME-biodiesel and isopropylidene glycerol (solketal, 98.5%) were respectively generous gifts from Penn A Kem Chemical Company (Memphis, USA), Tecosol GmbH (Ochsenfurt, Germany) and GLACONCHEMIE GmbH (Merseburg, Germany). All chemicals were used without further purification, except for water, which was obtained from a Millipore purification system.

3.1.2 Sample preparation

In general, every sample was prepared at room temperature, since the formulation of the biofuels should be realisable with a least possible effort, including standard conditions during their preparation. Exceptions were just necessary to solubilise a few antioxidants in different solvents, which required increased temperatures of up to 35 °C and vigorous stirring. Concerning most of the characterisation experiments, which consume just a few millilitres, tightly closed glass tubes with a maximum volume of 10 mL were commonly used. Particularly during the biofuel formulations consisting of several components, a specific compound was changed in 10, 5, 2 or 1 wt% steps within a measurement series, while the weight ratio of the others was kept constant. The closer the samples approached the optimal formulation, the smaller was the chosen difference in weight between them.

3.1.3 Dynamic and static light scattering

To prepare the samples for light scattering experiments, a few millilitres were filtered using a 0.2 µm PTFE membrane filter and put into cylindrical light scattering cells. The measurements were performed with a temperature-controlled CGS-3 compact goniometer from ALV (Langen, Germany) combined with an ALV-7004/Fast Multiple Tau digital correlator and a vertically-polarised 22 mW HeNe-laser with a wavelength of 632.8 nm. Every experiment was conducted at 25 ± 0.1 °C and a measuring time of 300 s. Concerning the DLS experiments, the measuring angle was set to 90°, whereas SLS measurements were performed at 45°, 90° and 135°. To determine the critical points of some biofuel mixtures, further described in chapter 3.1.6, the input count rate of signals (SI for scattering intensity) was considered, i.e. the scattered light impulses that reach the detector at constant attenuator settings.

3.1.4 Small- and wide-angle X-ray scattering

Concerning the SWAXS experiments, a X-ray bench from Xenocs is used with a sealed molybdenum tube as radiation source working with a wavelength of 0.071 nm. The collimation is performed by a 12:∞ multilayer mirror from Xenocs coupled with two scatterless pairs of slits from Forvis leading to a $0.8 \cdot 0.8\,\mathrm{mm}^2$ X-ray beam at the sample position. To detect the X-ray scattering, an off-centered 2D-detector MAR 345 from MAR Research with a diameter of 345 mm is used with a sample-to-detector distance fixed at 750 mm that allows covering two orders of magnitude of the scattering angle. A high-density polyethylene film from Goodfellow with a thickness of 2.36 mm is used as calibration standard ($4.9\,\mathrm{cm}^{-1}$ at the small angle scattering peak) with a measuring time of 600 s [261]. Scattering data are plotted in absolute units (in cm^{-1}), taking into account the transmission and sample thickness normalisation as well as the empty cell subtraction. These experiments were performed at the Institut de Chimie Séparative de Marcoule (ICSM) in Marcoule, France, by the research groups of Dr. Olivier Diat and Dr. Pierre Bauduin.

3.1.5 Conductivity measurements

The conductivity measurements were performed with a Cond 730 conductometer and a TetraCon 325 electrode from WTW GmbH (Weilheim, Germany) with an alternating current frequency of 140 Hz at 25 °C. 0.3 wt% of $LiClO_4$, which is soluble in alcohols, were added to every sample to measure the conductivity of vegetable oil-containing, organic mixtures. Since multi-component systems were investigated and the salt content had to be constant, no diluting method was applicable. Therefore, 20 mL of each sample were used to measure their conductivities separately.

3.1.6 Preparation of phase diagrams

To investigate the miscibility of the different compounds and to enable predictions about the compatibilities of additional components, ternary phase diagrams are essential. To obtain these diagrams, screw top tubes and a thermostatically controlled test tube rack were used at 25 °C. Binary mixtures had been prepared as starting points, before the third component was added dropwise with Pasteur pipettes. This process was continued, until the mixture changed from biphasic to monophasic, which was visually detected by a change from turbid to transparent and vice versa. Especially for the characterisation of the nanostructured biofuels, the *critical point* (CP) of the respective system was important. It is defined as the point of the phase boundary between the monophasic and

biphasic region with the length of the tie line approaching zero. Thus, the miscibility gap disappears and both liquid phases have the same composition [199]. Besides being indicated by the phase diagram itself and some dynamic light scattering results, the CP was determined by an additional method. Monophasic samples with compositions close to phase separation and with the highest SIs were prepared in glass tubes with volume scaling. By adding two of the three components of the mixture dropwise to the tubes, the biphasic region was reached. After the complete separation of the two phases, the samples were thermostatically controlled until the next day to obtain a sharp and easily identifiable phase boundary. If the ratio of the volume of the lower phase divided by the total volume was 0.5, the corresponding mixture was considered to be close to the CP of the system. The final composition of the CP was obtained by taking into account the average weight of one drop of each component and the number of drops used to achieve phase separation. Further, the influence of the temperature on the liquid/liquid phase organisation close to the CP was investigated for several biofuels. Within the temperature range between −10 and 30 °C, the volume ratio of the lower phase was determined. For that, the biphasic samples were put into the cryostat, described in chapter 3.1.8.

3.1.7 Viscosity measurements

An automated rolling ball viscometer AMVn from Anton Paar GmbH (Graz, Austria) was used to measure the dynamic viscosity of the mixtures at 40 °C. To obtain the kinematic viscosity from the dynamic viscosity of the samples, their densities were determined with a DMA 5000 M densitometer from Anton Paar GmbH (Graz, Austria). Every density measurement was performed one time, as its inaccuracy is small enough ($\pm 5 \cdot 10^{-3}$ kg/m^3), according to the manufacturer. Concerning the viscosity measurements, each experiment was repeated five to ten times, which led to deviations of about 0.01%. Depending on the viscosity of the samples, either a canula with a diameter of 1.6 mm, which had to be calibrated with deionised water or with 1.8 mm, which had its own calibration oil, was used. In general, the measuring process was predefined by the considered standards, mentioned in section 2.1.3.1.

3.1.8 Low-temperature phase behaviour

Concerning the low-temperature phase behaviour of the formulated biofuels, a small amount of every investigated mixture was put into tightly closed glass tubes and placed into different cryostats. In most cases, an Alpha RA 8 refrigerated circulator from LAUDA

GmbH & Co. KG (Lauda-Königshofen, Germany) with a cooling liquid consisting of water and ethylene glycol, suitable for temperatures down to −20 °C, was used. For some specific mixtures, a cooling thermostat RK 20 from LAUDA GmbH & Co. KG (Lauda-Königshofen, Germany) with silicone oil was necessary to obtain temperatures down to −40 °C. The phase behaviour of the samples, including cloud and freezing points, was visually observed over a period of several days and even weeks.

3.1.9 Calorimetry

The higher heating values of the biofuel mixtures as well as the single components of these formulations were determined with an IKA C200 calorimeter from IKA-Werke GmbH & Co. KG (Staufen, Deutschland). After calibrating the device with benzoic acid, the samples were combusted with an oxygen pressure of 24 bar. Two cotton threads were used for every sample to ensure a sufficient contact with the ignition device. Further, the settling time was set to 8 min and the combustion time to 11 min for every single measurement. The completeness of the combustion was at least visually detected during the cleaning and disassembling after each experiment. If the crucible was empty without any soot deposits on the brackets after the measurement, the sample was considered to combust completely.

3.1.10 Oxidative stability

The stability of the mixtures and pure components towards oxidation was measured with a RapidOxy Oxidation Stability Tester from Anton Paar GmbH (Graz, Austria) according to the DIN standard DIN EN 16091. 5 mL of each sample were oxidised with an oxygen pressure of 700 kPa and a temperature of 140 °C. Although the device itself is not suitable for a quantitative analysis and a precise investigation of the oxidation processes, it is sufficient to determine the overall stability of a sample towards oxidation and to draw comparisons to similar mixtures, as validated by the standard.

3.1.11 Engine tests

Similar to my master thesis, the whole engine tests of the formulated biofuels were performed at the chair of combustion engines of Prof. Dr. Hans-Peter Rabl at the Ostbayerische Technische Hochschule Regensburg. The engine test bench consisted of an up-to-date

2.2 L diesel engine with a two stage turbocharging concept, an AVL-IndiCom cylinder pressure indication, an AVL PUMA Open test bench control, both from AVL List GmbH (Graz, Austria), and an INCA 7.0 application software from ETAS GmbH (Stuttgart, Germany). In total, the ignition, combustion, emission and consumption behaviour of two different formulated biofuels, 40 L each, was investigated. The ignition delay measurements of both biofuels and diesel were performed at an engine speed of 1500 rotations per minute (rpm) and a torque of 80 Nm. The ignition delay can be calculated by using the injection rates and the combustion start with 5% turnover. In particular, the injection start is defined as the point with an injection rate higher than 1.5 g/s. The difference between this point and the combustion start with 5% turnover constitutes the ignition delay in milliseconds. Further, a constant injection volume of 10 mg at 5° crankshaft angle before top dead centre was used. By plotting the calculated ignition delay versus the injection pressure and the relative boost pressure, a three-dimensional ignition delay profile is obtained.
EGR measurements were carried out to get more information on the emission and consumption properties of the formulated biofuels. By adjusting the injection start, the combustion time with 10% turnover was kept constant during the EGR experiments. The NO_x, THC, CO and soot emissions as well as the air/fuel balance of both biofuel mixtures, diesel and rapeseed oil were detected by a HORIBA MEXA-9100H exhaust gas measurement device from HORIBA Europe GmbH (Oberursel, Germany) and an AVL 415 Smoke Meter from AVL List GmbH (Graz, Austria). Their consumption was gravimetrically determined by a fuel scale. Their combustion process and behaviour was investigated by setting the engine speed to 1500 rpm with two different load conditions. Low load conditions were represented by 80 Nm torque, 200 mbar relative boost pressure and 100 MPa injection pressure, whereas medium load conditions were represented by 240 Nm torque, 700 mbar relative boost pressure and 140 MPa injection pressure. Additionally, these measurements were performed without and with the highest drivable EGR rate. The injection rate was further investigated by a HDA injection analyser from Moehwald GmbH (Homburg, Germany). With the cylinder pressure indication, the rate of heat release was calculated with a polytropic exponent of 1.37 for all fuels. These parameters were evaluated for different driving and EGR conditions.

3.2 Further applications of glycerol derivatives

3.2.1 Extraction systems based on glycerol derivatives

3.2.1.1 Chemicals

1-pentanol (≥99%), potassium pyrophosphate (97%), sodium chloride (99.9%) and α-tocopherol (≥95.5%) as well as the surfactants lecithin (≥99%), Tween 20 (≥97%), Tween 40 (≥97%), Tween 60 (≥97%), Tween 80 (≥97%), Span 40 (≥97%) and Span 80 (≥97%) were purchased from Sigma-Aldrich GmbH (Steinheim, Germany). Span 65 (≥97%) was obtained from Kolb Distribution AG (Hedingen, Switzerland). Ammonium sulfate (≥99.5%), hexane (98.5%) and methanol (≥99.9%, gradient grade for liquid chromatography) were purchased from Merck KGaA (Darmstadt, Germany). Every further chemical, used within this topic, was already mentioned in chapter 3.1.1.

3.2.1.2 Extraction process and sampling

To determine the most suitable extraction system, phase diagrams of binary mixtures consisting of rapeseed oil and a glycerol derivative as well as ethanol as reference system were prepared. Concerning the food approved triacetin, the influence of edible surfactants, in particular different Tweens and Spans, was investigated with respect to the miscibility gap between rapeseed oil and triacetin. In general, the extraction of α-tocopherol from rapeseed oil was carried out for different compositions taking into account the influence of the extraction as well as cooling temperature, extraction duration and phase separation process. While the extraction temperatures varied from room temperature to 100 °C as well as the cooling temperature from 4 °C to room temperature, the durations of the extraction and cooling process varied from a few hours to several days. Since these parameters differ for every examined extraction system, they are explicitly described in the respective results and discussion sections.

3.2.1.3 High-performance liquid chromatography

A HPLC consisting of a Waters 717plus Autosampler, a Waters 515 HPLC Pump, a Waters Pump Control Module 2, a Waters 2487 Dual λ Absorbance Detector, a Waters C_{18} reversed-phase column and a Waters Empower Chromatography Data Software from Waters Corporation (Milford, U.S.) was used to measure the amount of extracted α-tocopherol. After the extraction process, 200 µL of either both existing phases due to phase

separation or of solely the phase of the extracting agent were taken with an Eppendorf pipette. These samples were dissolved in 3 mL of 1-pentanol, since every component of the system, including methanol, which was used as mobile phase, was miscible with 1-pentanol, and put into the autosampler. Before the chromatography was performed with an isocratic methanol elution with a flow speed of 1 mL/min at 25 °C, the methanol had been degassed for 10 min in an ultrasonic bath. The UV/Vis detector was set to a wavelength of 295 nm, as α-tocopherol shows, by far, the strongest absorbance of all components at this wavelength. With these settings, the reference samples with ethanol as extracting agent were measured for 20 min, whereas the others had a measuring time of 14 min.

3.2.1.4 Purification and isolation processes of the extracted α-tocopherol

In the case of extracting agents that are not food approved, the extracted α-tocopherol needs to be isolated. Concerning particularly the system with solketal as extracting agent, the effect of an additional liquid-liquid extraction with water was investigated. Since α-tocopherol is immiscible and solketal completely miscible with water, an isolated α-tocopherol phase was expected. For that, the influence of the amount of water, the α-tocopherol content in solketal, the temperature and the extraction duration on the second liquid-liquid extraction was examined. After determining the most suitable conditions, different process optimisations were evaluated to decrease the extraction duration with water and to increase the amount of isolated antioxidant. Besides using a centrifuge to accelerate the phase separation, different salts were added to the mixtures to make use of their salting-out properties. Due to the addition of electrolytes, the interaction between water and in this case α-tocopherol is even further reduced.

3.2.2 Alternatives to ethanol as freezing point depressant

3.2.2.1 Chemicals

Betaine (≥99%) as well as quartz sand (≥99.9%), dimethyl sulfoxide (≥99.9%), fructose (≥99%) as well as phosphorus pentoxide (Sicapent, ≥99.9%), 1,2-propanediol (≥99.5%) and γ-valerolactone were purchased from Sigma-Aldrich GmbH (Steinheim, Germany), Thermo Fisher Scientific (Waltham, U.S.), Merck KGaA (Darmstadt, Germany), VWR International (Radnor, U.S.) and Chemical Point UG (Oberhaching, Germany), respectively. All chemicals were used without further purification. Every other substance of this section was already mentioned in chapter 3.1.1.

3.2.2.2 Differential scanning calorimetry

A Perkin Elmer DSC 8000 differential scanning calorimeter combined with a Perkin Elmer Intracooler 2 Cooling Accessory from Perkin Elmer (Waltham, U.S.) was one of the used devices to determine the freezing points of the investigated mixtures. Every sample had been cooled down to −60 °C with a rate of 2 °C/min, before being heated up to 25 °C with a rate of 10 °C/min. This process was repeated one time and only the freezing point of the second measurement was considered, since the first one is known to be inaccurate. Due to several performance issues within these experiments, closed as well as opened pans were used as measuring vessels.

3.2.2.3 Polarisation microscopy

Additionally to the calorimetric measurements, a JVC TK-C1380 camera from Victor Company of Japan Limited (Yokohama, Japan) combined with a Linkam liquid nitrogen pump from Linkam Scientific Instruments (Waterfield, England) was used. One drop of a sample was put on an object slide and cooled down to −45 °C with a rate of 3 °C/min. By using the polarisation microscope, the formation of single crystals as well as the complete freezing process could be visually observed. To prevent the influence of the ambient humidity on the freezing behaviour of the samples, a glove box with a nitrogen flux and Sicapent as drying agent was installed around the microscope.

3.2.2.4 Cryoscopic measurements

A cryoscopic apparatus according to Beckmann, shown in Fig. 23, was used to determine the freezing points of the investigated systems without supercooling effects. A mixture of ethanol and dry ice with a temperature of about −78 °C was utilised in a Dewar flask to cool down the samples. By measuring the temperature of 20 mL of the sample and a spatula tip of quartz sand as crystallisation seed over time, the resulting temperature-time profile indicates its freezing point according to the standard ASTM D1177-12. It defines the freezing point as the intersection of the cooling curve and the horizontal plateau occurring during freezing. If the sample shows supercooling, the freezing point is defined as the maximum temperature reached immediately after supercooling [260]. During a business trip to the head office of the client WIGO Chemie GmbH in Bad Kreuznach, several reference values could be measured with their standardised test method. They use a LAUDA Proline RP 890 cryostat with a Lauda Command control unit and a LAUDA Wintherm Plus software from LAUDA GmbH & Co. KG (Lauda-Königshofen, Germany) combined with a digital lifting mixer with a Simatic Panel control unit from Siemens AG (Munich, Germany). The temperature of the cooling bath is manually set to about 15 °C below the expected freezing point of the sample. About 25 mL of a mixture and a spatula tip of quartz sand are necessary for their test method.

4 Results and discussion

4.1 Investigations on completely green biofuels

4.1.1 Proof and impact of nanostructures on biofuels

Within this topic, the presence of nanostructures in ethanol-containing biofuels, which was the subject of extensive debates in the last years with several proving and also refuting publications, is finally indisputably verified [208, 209]. To define the required properties of the mixtures to overcome the miscibility problems of ethanol-containing fossil fuels and biofuels, the term *ethanolotrope* is introduced. For the first time in fuel and particularly biofuel science, a combination of SWAXS and conductivity experiments is used [262]. Due to the precise specification of the structured areas in several biofuel formulations, investigations on the impact of these structures on relevant physicochemical parameters of the biofuels were possible [263].

4.1.1.1 Proof of nanostructured biofuels

Proceeding from the first investigations of Khoshsima *et al.*, who screened several biomass-derived substances concerning their potential to close miscibility gaps in fuel formulations, the ternary system consisting of ethanol, rapeseed oil and 1-heptanol (HepOH) was used

in the following experiments [264]. The phase diagram of this system is represented in a typical triangular plot in Fig. 24. Due to the poor miscibility of rapeseed oil with ethanol, further explained in the sections 2.1.2.4 and 2.1.4.1, a biphasic region is obtained at low amounts of HepOH, indicated by the darkened area. With an increasing amount of HepOH, in particular higher than 15 wt%, ethanol and rapeseed oil become miscible in every ratio. The illustrated paths ***a*** and ***b*** contain the mixtures being precisely examined by SWAXS and conductivity measurements. While a constant amount of 20 wt% of HepOH is used along path ***a***, the amount of HepOH varies within path ***b***, which includes measuring points with high shares of rapeseed oil.

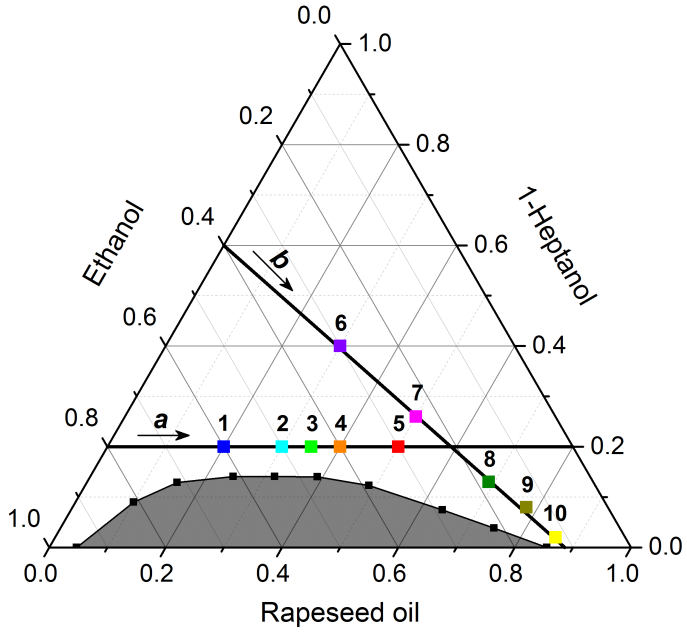

Figure 24: Ternary phase diagram consisting of rapeseed oil, ethanol and HepOH at 25 °C, as taken from [264]. The darkened area represents the biphasic region of the system. The performed SWAXS measurements along path ***a*** and ***b*** are illustrated by the coloured and numbered points of the diagram. The conductivity experiments were performed along path ***a***. The values are given in mass fractions.

Fig. 25a shows the SWAXS spectra along path ***a***. The high scattering intensity at low q-values ($q < 1\,\mathrm{nm}^{-1}$) indicates the presence of nanostructures. By subtracting the contribution of the solvent, one can assume that the scattering intensity in this q-range decays with a slope close to 2. These values are expected for the scattering of sub-nanometric structures ranging from dynamically percolated to bicontinuous-like clusters [265]. In the high q-range for $q > 9\,\mathrm{nm}^{-1}$, where both interatomic and intermolecular correlations are examined, a broad and intense peak is observed. This peak typically originates from C-C correlations between liquid alkyl chains. This peak shape, centre and intensity remain unchanged for all measured samples, indicating that the structure at the molecular level,

i.e. the chemical environment in terms of local electron density, is not altered and independent of the concentration in the ternary system. In the middle q-range between 5 and 9 nm^{-1}, a broad shoulder appears with increasing ethanol content (from red to blue). This shoulder is related to the structure of bulk liquid ethanol and emerges mainly from the correlation between oxygen atoms in the ethanol [266]. The presence of this shoulder in the spectrum of a mixture indicates that ethanol is either the continuous phase or present as a pseudo-phase. By increasing the amount of rapeseed oil in the mixture from blue to red in Fig. 25a, this shoulder vanishes. In this case, ethanol is no longer in the bulk phase. Simultaneously to this process, a peak appears at q-values around 3 nm^{-1}.

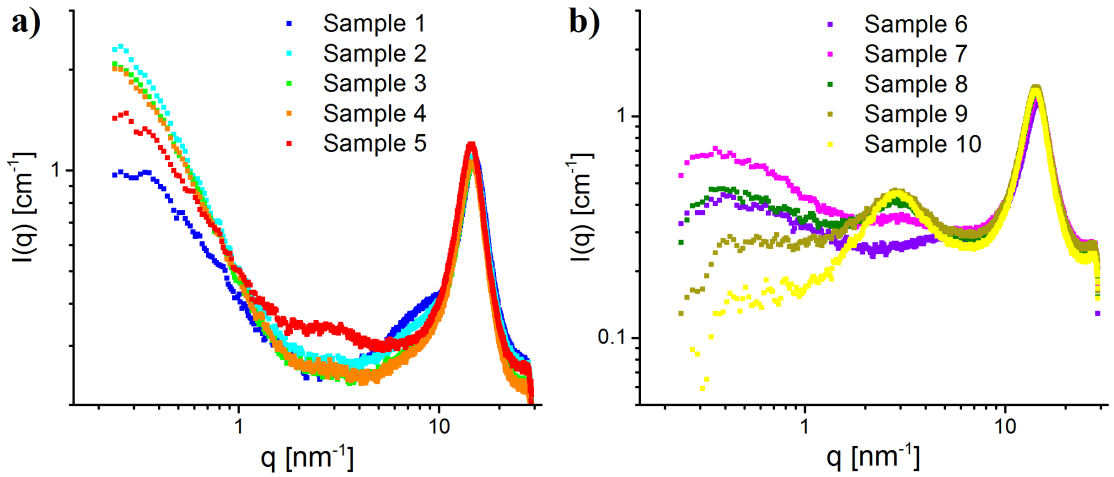

Figure 25: SWAXS spectra on a double logarithmic scale of the measured intensities I versus the scattering vector q in absolute scale for samples along path ***a*** (Fig. 25a) and along path ***b*** (Fig. 25b) of the phase diagram. The different colours correspond to the points of the ternary phase diagram shown in Fig. 24.

This peak is present in the spectrum of pure rapeseed oil and its origin arises from the correlation between the polar parts, i.e. high electron density, and the alkyl chains of the triglycerides, i.e. low electron density, which are the main components of rapeseed oil [264]. In this mixture, this peak proves that domains of liquid rapeseed oil are present. Along path ***b***, the intensity of this peak increases significantly with an increasing rapeseed oil content (see Fig. 25b). This evolution is distinctive of rapeseed oil in the bulk phase, which means that the bulk changes from an ethanol-rich to a rapeseed oil-rich pseudo-phase with increasing rapeseed oil concentrations [267]. Therefore, these experiments show that the solubility of ethanol in rapeseed oil at high amounts of rapeseed oil is coupled with the formation of nanodroplets, presumably made of an ethanol-rich pseudo-phase. Thus, these SWAXS results indicate that water-free and surfactant-free microemulsions are present in such ternary systems.

Table 5: Forward scattering I_0 and correlation length ξ of sample 1 to 5 along path ***a***, calculated with an Ornstein-Zernike equation (see Eq. 38).

Sample	I_0 **[nm^{-1}]**	ξ **[nm]**
1	1.15	2.05
2	3.30	2.84
3	2.60	2.60
4	2.74	2.66
5	1.60	2.10

Table 5 shows the obtained values of the forward scattering I_0 and the correlation length ξ of sample 1 to 5 along path ***a***, calculated with an Ornstein-Zernike equation (see Eq. 38). These parameters are related to the size of the nano-domains, i.e. aggregates or droplets, which lead to electron density inhomogeneities in the mixture. In this case, ξ describes the maximum distance of correlated dynamics of two molecules of the same phase. Thus, ξ can be used as indicator of the range of intermolecular interactions. The calculations lead to values of a few nanometres, with a maximum for sample 2, which implies that the pseudo-phases consist of very small aggregates.

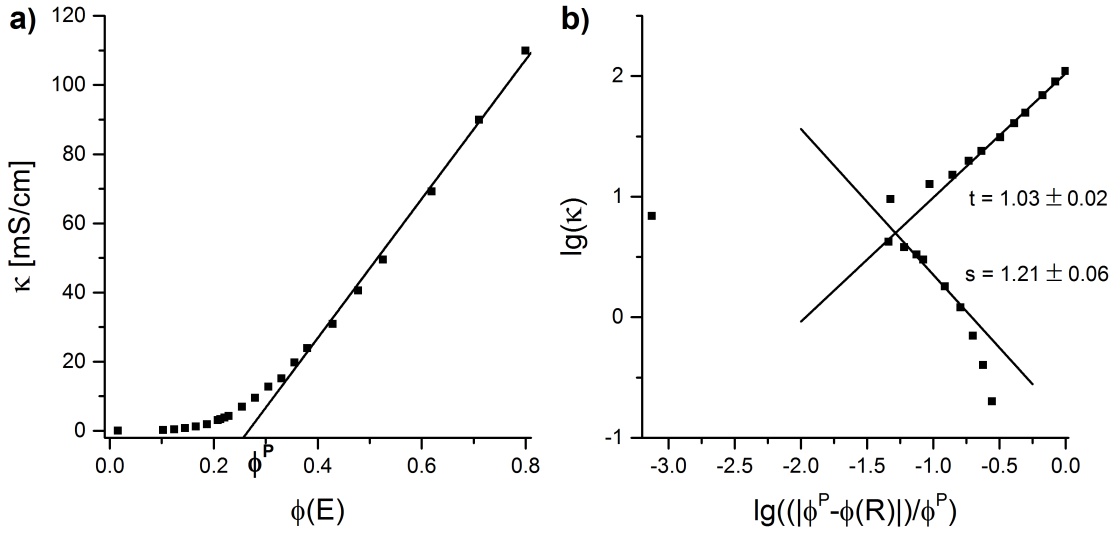

Figure 26: Conductivity measurements performed along path ***a*** at 25 °C: a) Conductivity κ versus the volume fraction of ethanol $\phi(E)$. Extrapolating the linear fit for high amounts of ethanol leads to the percolation threshold ϕ^P; b) Specific plot according to Eq. 39 and 40 to determine the critical exponents of the percolation process with the volume fraction of rapeseed oil $\phi(R)$.

To verify the results of the SWAXS experiments, conductivity measurements were performed along path ***a***. Due to the addition of 0.3 wt% of $LiClO_4$ to every sample of the organic mixture, it was even possible to determine its percolation threshold and to charac-

terise its percolation behaviour. The measured conductivity κ versus the volume fraction of ethanol $\phi(E)$ along path $\boldsymbol{a}$ is illustrated in Fig. 26. Logically, the higher the amount of ethanol, the higher the conductivity. Since κ increases linearly at higher amounts of ethanol, a percolation threshold ϕ^P can be determined, which occurs at 25.4 vol%, i.e. 22.5 wt%, of ethanol. Further, the change of the bulk pseudo-phase from rapeseed oil-rich to ethanol-rich is reflected by the transition from low to high values of κ. To have a closer look into the nature of the percolation, a specific plot according to Eq. 39 and 40 is used (see Fig. 26b). According to the dynamic percolation model, further explained in section 2.1.4.5, the following power laws can be applied [224, 227]:

$$\kappa \propto \frac{\left|\phi^P - \phi(R)\right|^{-s}}{\phi^P} \forall \phi^P < \phi(R) \tag{42}$$

$$\kappa \propto \frac{\left|\phi^P - \phi(R)\right|^{-t}}{\phi^P} \forall \phi^P > \phi(R) \tag{43}$$

Below the threshold, the critical parameter $s = 1.21 + 0.06$, which is obtained by a linear fit of the part of the conductivity curve with the highest curvature, is in very good agreement with the dynamic percolation model. This means that the nanostructures rearrange dynamically due to Brownian motion and are not statically linked to each other [224, 268]. With the proof of highly dynamic association processes within these mixtures, which is in line with the small correlation lengths measured with SWAXS, the presence of different nanostructures in ternary, ethanol-containing biofuel systems is indisputably proven [262].

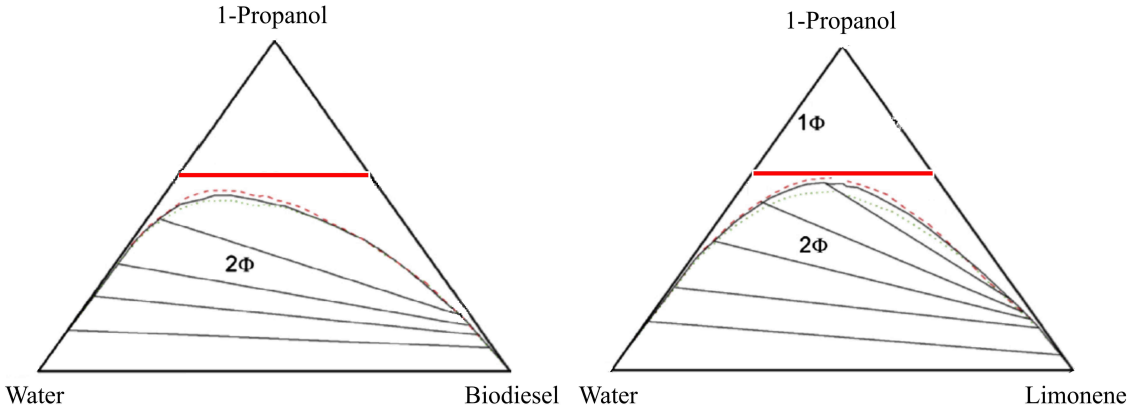

Figure 27: Ternary phase diagrams investigated by Kayali *et al.* consisting of water, 1-propanol and either biodiesel (left) or limonene (right) at 25 °C based on [209]. The red lines indicate the investigated compositions of the DLS and SLS experiments. The diagrams are plotted in mass fractions.

This in turn also verifies the work of Silva *et al.*, who stated the presence of microemulsions in such systems by solely light scattering experiments, which was falsely refuted by other research groups like Kayali *et al.* [208, 209]. The latter examined several ternary systems consisting of 1-propanol, water and hydrophobic components like biodiesel and limonene (see Fig. 27). By using NMR self-diffusion measurements for different samples of each system, they investigated the presence of aggregates in these mixtures. Since the measured diffusion coefficients were high for every component regardless of the sample, they stated that these mixtures are structureless solutions. They even mentioned that SFMEs could also just be "enhanced concentration fluctuations in near-critical conditions" [209]. Proceeding from the verified nanostructuring of the ethanol-containing biofuels, DLS and SLS experiments were performed in the same systems with constant 60 wt% of 1-propanol, indicated by the red lines in Fig. 27.

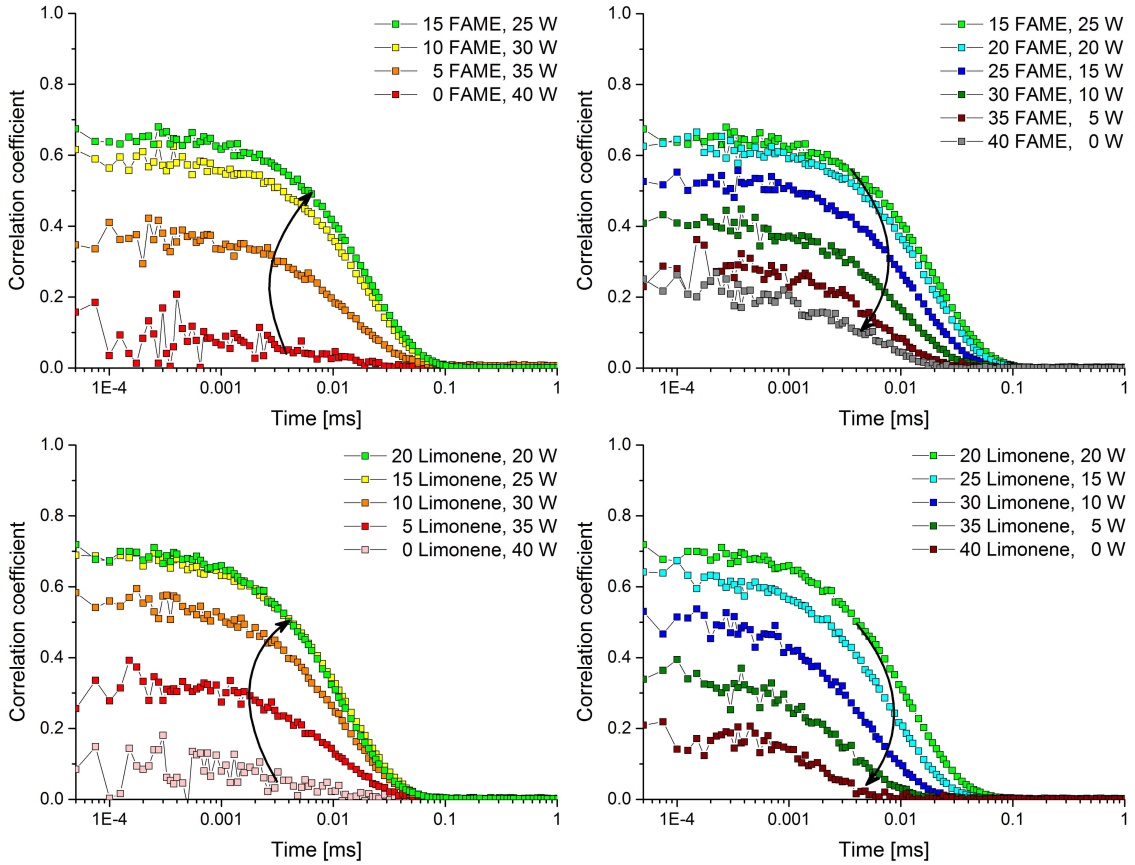

Figure 28: Time-dependent autocorrelation functions obtained by DLS experiments of the ternary system 1-propanol/water (W)/FAME (top) and 1-propanol/water/limonene (bottom) with constant 60 wt% of 1-propanol, according to the red lines in Fig. 27, at 25 °C. The samples are arranged according to their correlation coefficient. In the system containing FAME, a maximum correlation is observed at 15 wt% of FAME, whereas 20 wt% of limonene lead to the maximum correlation in the second system.

Fig. 28 depicts the time-dependent autocorrelation functions of the DLS experiments of both ternary systems. Already without any further calculations, the presence of defined correlation functions implies an aggregation of the mixtures. The evolution of the correlation coefficients shows that, in the FAME-containing system, a maximum correlation is observed at 15 wt% of FAME, whereas 20 wt% of limonene lead to a maximum correlation in the second system. After determining the dynamic viscosities, densities and refraction indices of the samples and performing additional SLS experiments, the radii of the aggregates can be calculated, assuming spherical geometry (see Fig. 29). The present aggregates possess radii in the range of 0.8 – 1.6 nm and are thus very small. The obtained radii of the SLS experiments are bigger than the hydrodynamic radii of the DLS measurements, which means that the assumption of a spherical shape is wrong. Further, the aggregate size is too small to commit to the calculated radii. In any case, these results show that NMR self-diffusion experiments with a time resolution of microseconds are too slow to detect highly dynamic aggregations, as present in these biofuel mixtures. Light scattering measurements, however, possess a time resolution in the nanosecond scale and are thus capable of detecting highly dynamic processes.

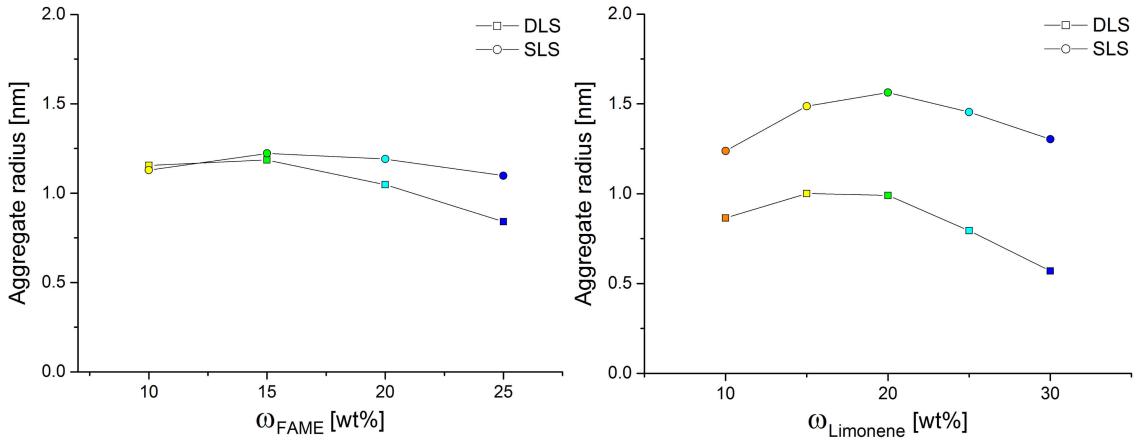

Figure 29: Calculated radii of the scattering aggregates within the DLS and SLS experiments versus the weight percentage of FAME (left) and limonene (right), assuming spherical geometry.

Since many substances apart from HepOH are used within the following section to increase the miscibility of ethanol with rapeseed oil, the term *ethanolotrope* is introduced, referring to a hydrotrope. An *ethanolotrope* increases the miscibility of organic compounds in ethanol without being a surfactant. This in turn is often coupled with a nanostructuring of the mixture, as recently shown in the hydrotrope-containing system 1-octanol/ethanol/water [269]. With the structures being precisely determined, their impact on relevant fuel parameters is investigated in the next section.

4.1.1.2 Influence of the nanostructuring on the properties of biofuels

To determine possible correlations between the type of nanostructuring in the mixture and fuel properties like the kinematic viscosity η_{kin} and the low-temperature phase behaviour, many different ternary systems were examined. In particular, every biofuel formulation consisted of ethanol and rapeseed oil, but the *ethanolotrope* was varied. Fig. 30 shows some of the used *ethanolotropes* for these experiments. Methyl (MTBE) and ethyl *tert*-butyl ether (ETBE) were chosen, as they are already used as renewable gasoline and diesel additives [270, 271]. 2-Ethylhexyl nitrate (EHN) is a well-known cetane improver, whereas tributyl citrate (TBC) and 1-heptanol (HepOH) are obtained from biomass [272]. Additionally to these compounds, the furan derivatives 2-MTHF, 2-MF and DMF as well as FAME were utilised as *ethanolotropes*, due to their sustainability (see also section 2.1.1.2 and 2.1.5.1).

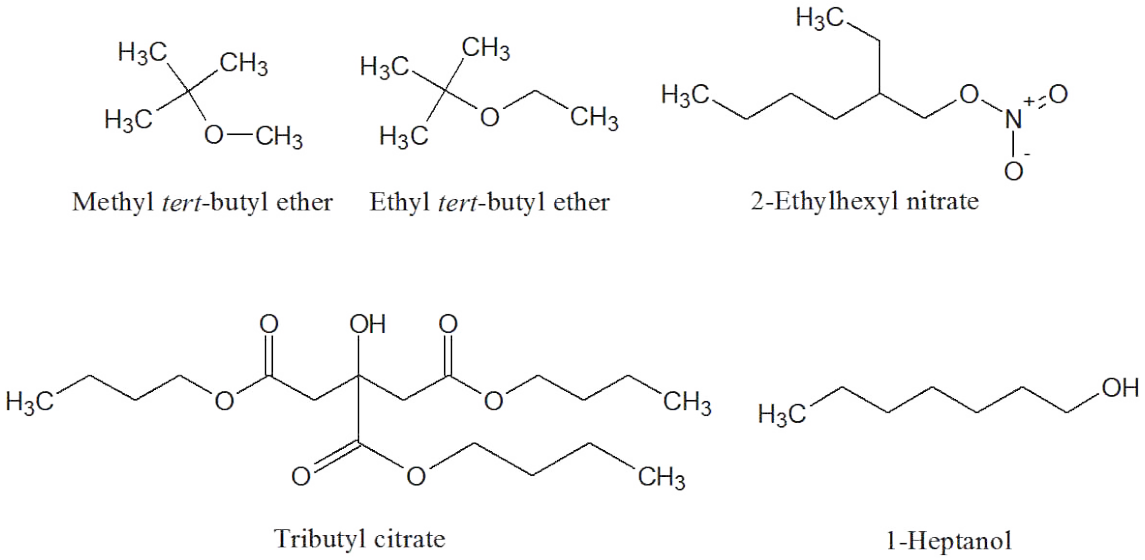

Figure 30: Chemical structures of the used *ethanolotropes* methyl *tert*-butyl ether (MTBE), ethyl *tert*-butyl ether (ETBE), 2-ethylhexyl nitrate (EHN), tributyl citrate (TBC) and 1-heptanol (HepOH). Additionally to these compounds, FAME (see Fig. 7) as well as the furan derivatives 2-MTHF, 2-MF and DMF (see Fig. 20) were utilised.

To compare the potential of the used compounds as *ethanolotropes*, all investigated ternary systems are combined in Fig. 31. Every *ethanolotrope* is indeed able to close the miscibility gap between ethanol and rapeseed oil. It is also completely miscible with both ethanol and rapeseed oil. Nevertheless, they can be divided into two groups, which are indicated by filled and empty symbols. The ternary systems containing *ethanolotropes* marked by filled symbols, in particular MTBE, ETBE, HepOH and 2-MTHF have a smaller biphasic region than the ones with *ethanolotropes* marked by empty symbols, i.e. FAME, TBC,

EHN, 2-MF and DMF. Thus, to ensure comparable results during the experiments, which means that the distance to the biphasic region must be similar, higher amounts of the less efficient ethanolotropes are necessary. This is illustrated by path ***a*** and ***b***. While a constant amount of 20 wt% of *ethanolotrope* is used for the systems indicated by filled symbols (path ***a***), constant 30 wt% are utilised for the ones with empty symbols (path ***b***).

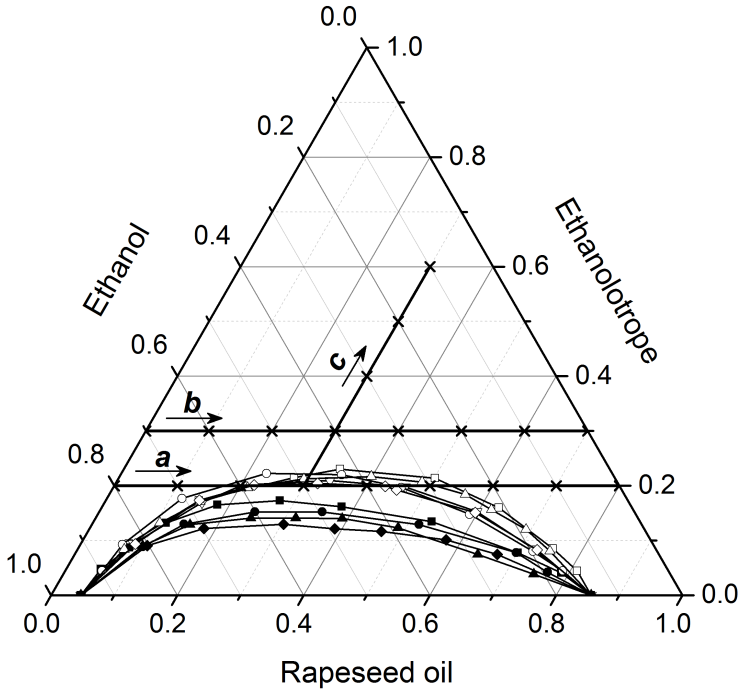

Figure 31: Ternary phase diagrams consisting of rapeseed oil, ethanol and an *ethanolotrope* at 25 °C. The different represented liquid-liquid demixing borders are obtained using the following substances as *ethanolotropes*: FAME (□), TBC (○), EHN (△), 2-MF (◇), DMF (▽), MTBE (■), ETBE (●), HepOH (▲), 2-MTHF (◆). The kinematic viscosity and the low-temperature phase behaviour are determined along paths ***a***, ***b*** and ***c***. The values are given in mass fractions.

Before starting with the characterisation of the ternary mixtures, the temperature dependence of the miscibility gap between ethanol and rapeseed oil was examined (see Fig. 32). As expected, the higher the temperature, the smaller the biphasic region, even though the impact of the temperature is surprisingly weak. This observation is in agreement with work performed by Follegatti-Romero *et al.*, who investigated different vegetable oils except rapeseed oil [273]. This phase diagram is also of importance for the topic dealing with alternative extraction systems, further explained in section 4.2.1.1.
The low-temperature phase behaviour of rapeseed oil/ethanol/*ethanolotrope* mixtures at 0, −15 and −20 °C along path ***a*** is summarised in Table 6. It indicates that the binary mixtures ethanol/*ethanolotrope* do not show any phase transitions and stay monophasic and clear regardless of the applied temperature.

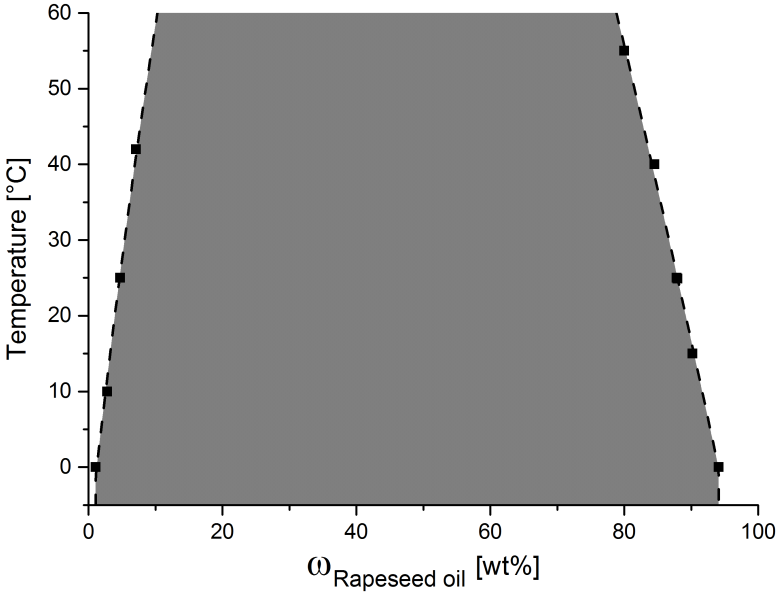

Figure 32: Phase separation temperatures versus the weight percentage of rapeseed oil in the binary system consisting of rapeseed oil and ethanol. The darkened area represents the biphasic region of the system.

Table 6: Phase behaviour of rapeseed oil/ethanol/*ethanolotrope* mixtures at 0, −15 and −20 °C along path ***a*** with HepOH, MTBE, ETBE and 2-MTHF as *ethanolotropes*. In total, monophasic and clear (1ϕ) or biphasic mixtures (2ϕ) as well as solid phases (s) were obtained.

Ethanolotrope	**T** [°C]	$\omega_{\textbf{Rapeseed oil}}$[wt%]								
		0	10	20	30	40	50	60	70	80
HepOH	0	1ϕ	2ϕ	2ϕ	2ϕ	2ϕ	1ϕ	1ϕ	1ϕ	1ϕ
	−15	1ϕ	2ϕ	2ϕ	2ϕ	2ϕ	2ϕ	2ϕ	1ϕ	1ϕ
	−20	1ϕ	s	s	s	s	s	s	s	s
MTBE	0	1ϕ	2ϕ	2ϕ	2ϕ	2ϕ	2ϕ	1ϕ	1ϕ	1ϕ
	−15	1ϕ	2ϕ	2ϕ	2ϕ	2ϕ	2ϕ	2ϕ	1ϕ	1ϕ
	−20	1ϕ	2ϕ	2ϕ	2ϕ	2ϕ	2ϕ	2ϕ	2ϕ	2ϕ
ETBE	0	1ϕ	2ϕ	2ϕ	2ϕ	2ϕ	2ϕ	2ϕ	1ϕ	1ϕ
	−15	1ϕ	2ϕ	2ϕ	2ϕ	2ϕ	2ϕ	2ϕ	1ϕ	1ϕ
	−20	1ϕ	2ϕ	2ϕ	2ϕ	2ϕ	2ϕ	2ϕ	2ϕ	2ϕ
2-MTHF	0	1ϕ	1ϕ	1ϕ	2ϕ	2ϕ	2ϕ	1ϕ	1ϕ	1ϕ
	−15	1ϕ	2ϕ	2ϕ	2ϕ	2ϕ	2ϕ	1ϕ	1ϕ	1ϕ
	−20	1ϕ	2ϕ	2ϕ	2ϕ	2ϕ	2ϕ	2ϕ	2ϕ	s

Using HepOH as *ethanolotrope*, a liquid-liquid phase separation is observed at 0 °C for the ternary mixture between 10 and 40 wt% of rapeseed oil, whereas above 50 wt% of rapeseed oil, the mixtures remain monophasic and clear. The miscibility gap increases to 10-60 wt% at −15 °C. The mixtures remain monophasic and clear in presence of 70 wt% of rapeseed oil. At −20 °C, the freezing point, particularly the temperature at which precipitation occurs and at least one solid phase is observed, is reached for mixtures containing between 10 and 80 wt% of rapeseed oil. In presence of MTBE as well as ETBE, liquid-liquid phase separation occurs for mixtures containing 10-50 wt% and 10-60 wt% of rapeseed oil, respectively, at 0 °C, whereas the other mixtures are monophasic and clear. At −15 and −20 °C, the biphasic region increases similarly for the systems with MTBE and ETBE. With 2-MTHF, liquid-liquid phase separation is obtained for rapeseed oil concentrations between 30 and 50 wt% at 0 °C. At lower temperatures, this biphasic region increases, as already shown for other *ethanolotropes*. The comparison of these *ethanolotropes* leads to the assumption that the slightly greater hydrophilicity of HepOH especially shows up at lower temperatures, resulting in higher freezing points of the mixtures.
The phase behaviour of rapeseed oil/ethanol/*ethanolotrope* mixtures at 0, −15 and −20 °C along path ***b*** is reported in Table 7. The binary systems of ethanol and *ethanolotrope* do not show any phase transitions at 0, −15 and −20 °C, except for FAME. In presence of this compound, the freezing point of the binary mixture ethanol/FAME is reached for temperatures close to −15 °C. Using TBC or EHN as *ethanolotrope*, liquid-liquid phase separation occurs for rapeseed oil concentrations between 10 and 40 wt% or 20 and 50 wt%, respectively, at 0 °C. At −15 and −20 °C, the miscibility gap increases similarly for both systems. In presence of FAME, liquid-liquid phase separation is observed for mixtures containing 20-50 wt% of rapeseed oil at 0 °C. At −15 °C, the freezing point is reached for samples consisting of 0-80 wt% of rapeseed oil, leading to a white precipitate in these mixtures. These results already reflect the aforementioned bad low-temperature properties of FAME and FAME-containing biofuels (see section 2.1.1.2). Regarding the systems with either DMF or 2-MF, liquid-liquid phase separation occurs for rapeseed oil concentrations between 20 and 60 wt% or 10 and 60 wt%, respectively, at 0 °C. At lower temperatures, the biphasic region just slightly increases for the mixtures with DMF, whereas it stays the same for the system containing 2-MF. Investigations during my master thesis showed that the binary systems DMF/rapeseed oil and 2-MF/rapeseed oil stay monophasic and clear even at −20 °C [228]. Although the samples seem to be gel-like after several hours at −20 °C, they immediately become low-viscous and clear again after shaking. To sum up the results of Table 6 and 7, the investigated mixtures seem to be more sensitive to low temperatures in the bicontinuous-like region, leading to higher cloud and freezing points. In the region of reverse nanostructures, on the other hand, they are less sensitive. This is particularly pronounced for the systems containing HepOH or 2-MTHF as *ethanolotropes*.

Table 7: Phase behaviour of rapeseed oil/ethanol/*ethanolotrope* mixtures at 0, −15 and −20 °C along path ***b*** with TBC, EHN, FAME, DMF and 2-MF as *ethanolotropes*. In total, monophasic and clear (1ϕ) or biphasic mixtures (2ϕ) as well as solid phases (s) and gels (g) were obtained.

Ethanolotrope	**T [°C]**	$\omega_{\textbf{Rapeseed oil}}$**[wt%]**							
		0	10	20	30	40	50	60	70
TBC	0	1ϕ	2ϕ	2ϕ	2ϕ	2ϕ	1ϕ	1ϕ	1ϕ
	−15	1ϕ	2ϕ	2ϕ	2ϕ	2ϕ	2ϕ	1ϕ	1ϕ
	−20	1ϕ	2ϕ	2ϕ	2ϕ	2ϕ	2ϕ	2ϕ	2ϕ
EHN	0	1ϕ	1ϕ	2ϕ	2ϕ	2ϕ	2ϕ	1ϕ	1ϕ
	−15	1ϕ	2ϕ	2ϕ	2ϕ	2ϕ	2ϕ	1ϕ	1ϕ
	−20	1ϕ	2ϕ	2ϕ	2ϕ	2ϕ	2ϕ	2ϕ	2ϕ
FAME	0	1ϕ	1ϕ	2ϕ	2ϕ	2ϕ	2ϕ	1ϕ	1ϕ
	−15	s	s	s	s	s	s	s	s
	−20	s	s	s	s	s	s	s	s
DMF	0	1ϕ	1ϕ	2ϕ	2ϕ	2ϕ	2ϕ	2ϕ	1ϕ
	−15	1ϕ	2ϕ	2ϕ	2ϕ	2ϕ	2ϕ	2ϕ	1ϕ
	−20	1ϕ	2ϕ	2ϕ	2ϕ	2ϕ	2ϕ	2ϕ	g
2-MF	0	1ϕ	2ϕ	2ϕ	2ϕ	2ϕ	2ϕ	2ϕ	1ϕ
	−15	1ϕ	2ϕ	2ϕ	2ϕ	2ϕ	2ϕ	2ϕ	1ϕ
	−20	1ϕ	2ϕ	2ϕ	2ϕ	2ϕ	2ϕ	2ϕ	g

Table 8: Phase behaviour of rapeseed oil/ethanol/*ethanolotrope* mixtures with a constant amount of 30 wt% of rapeseed oil at 0, −15 and −20 °C along path ***c*** with 2-MTHF and HepOH as *ethanolotropes*. In total, monophasic and clear (1ϕ) or biphasic mixtures (2ϕ) as well as solid phases (s) were obtained.

Ethanolotrope	**T [°C]**	$\omega_{\textbf{Ethanolotrope}}$**[wt%]**				
		20	30	40	50	60
HepOH	0	2ϕ	1ϕ	1ϕ	1ϕ	1ϕ
	−15	2ϕ	2ϕ	2ϕ	2ϕ	1ϕ
	−20	s	s	s	s	s
2-MTHF	0	2ϕ	1ϕ	1ϕ	1ϕ	1ϕ
	−15	2ϕ	1ϕ	1ϕ	1ϕ	1ϕ
	−20	2ϕ	2ϕ	1ϕ	1ϕ	1ϕ

Table 8 reports the phase behaviour of rapeseed oil/ethanol/*ethanolotrope* mixtures with a constant amount of 30 wt% of rapeseed oil at 0, −15 and −20 °C along path ***c*** in presence of HepOH and 2-MTHF as *ethanolotropes*. These measuring series enable information on

the properties of the *ethanolotropes* as freezing point depressants. By replacing ethanol with 2-MTHF along path ***c***, the phase stability of the monophasic and clear mixtures is increased, leading to lower freezing points. Thus, it is possible to formulate mixtures containing 30 wt% of rapeseed oil that remain monophasic and clear at −15 and −20 °C. By using HepOH, the trend is similar, but it is distinctly less effective than 2-MTHF. Fig. 33a-d show the kinematic viscosity curves as a function of the weight percentage of rapeseed oil for the investigated ternary systems. Fig. 33a-b and c-d illustrate the results of path ***a*** using 20 wt% of *ethanolotropes* (i.e. HepOH, ETBE, MTBE and 2-MTHF) and path ***b*** using 30 wt% of *ethanolotropes* (i.e. TBC, FAME, EHN, DMF and 2-MF), respectively at 25 and 40 °C.

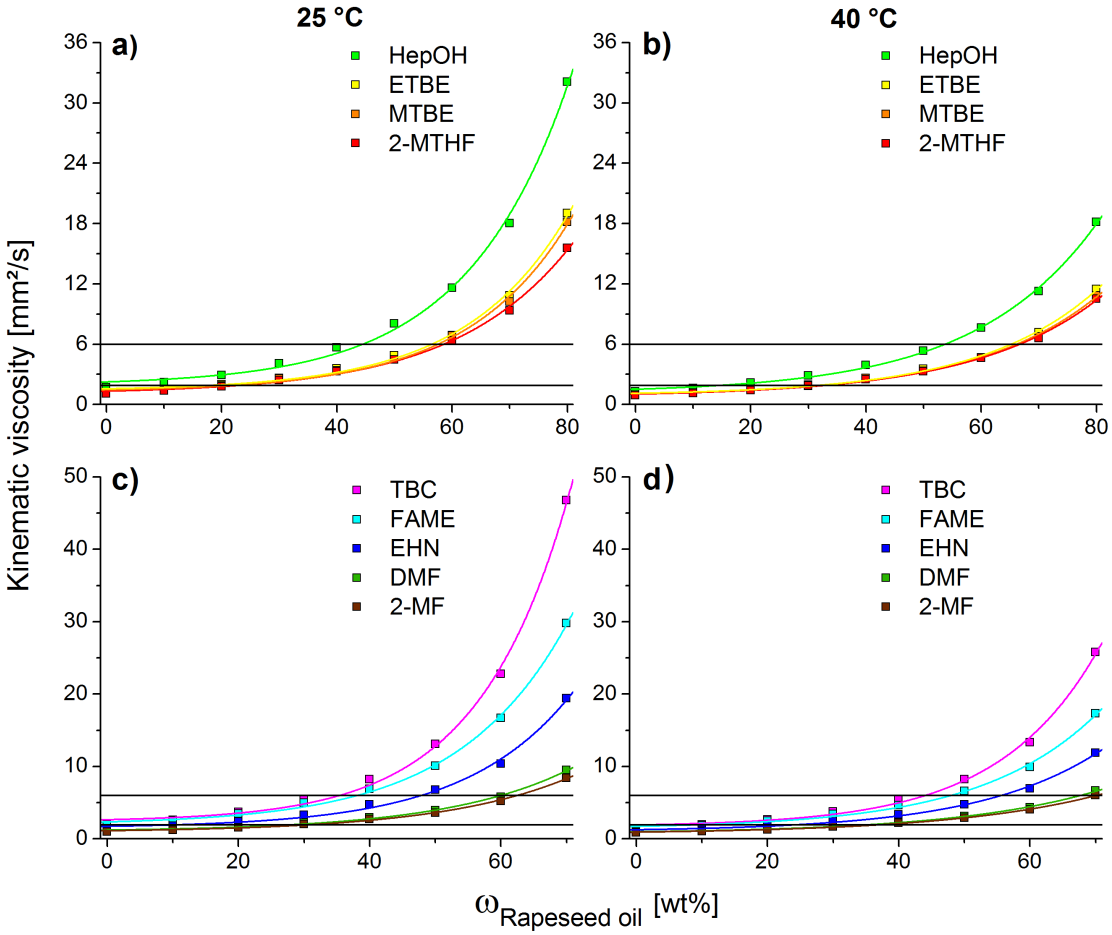

Figure 33: Kinematic viscosities along path ***a*** depending on the weight percentage of rapeseed oil at 25 °C (a) and 40 °C (b). In analogy, c) and d) depict the kinematic viscosities along path ***b*** at 25 °C and 40 °C, respectively. The horizontal lines indicate the required viscosity range (from 1.9 to 6 mm^2/s) according to the ASTM D6751 standard.

By comparing the results of the different *ethanolotropes*, it can be inferred that a temperature increase leads to a decrease of the kinematic viscosity, η_{kin}, of all studied mixtures, as expected by Eyring's approach [274]. The higher the amount of rapeseed oil along path ***a*** and ***b***, the higher the viscosity. The evolution of η_{kin} is exponential and dependent on the nature of the *ethanolotrope*. The values of η_{kin} decrease in the following order of *ethanolotropes*:

- along path ***a***: HepOH > ETBE > MTBE > 2-MTHF
- along path ***b***: TBC > FAME > EHN > DMF > 2-MF.

It turns out that the more voluminous the ethanolotrope, the higher the resulting η_{kin}. This effect is even more obvious, when using molar concentration instead of mass concentration. The greater effect of TBC compared to FAME can be explained by the three chains present in the TBC structure, compared to a more linear structure of FAME. Fig. 33 also shows that mixtures can meet the ASTM D6751 standard for every *ethanolotrope*, but their compositions are different. According to Fig. 33b, only mixtures containing about 50 wt% of rapeseed oil with HepOH as *ethanolotrope* fulfil the standard and are still monophasic and clear at 0 °C. None of the mixtures meets the kinematic viscosity standard and stays monophasic and clear at −15 and −20 °C (see Table 6). Considering η_{kin} and the low-temperature phase behaviour of the system with MTBE, only mixtures consisting of about 60 wt% of rapeseed oil and MTBE as *ethanolotrope* are within the viscosity range and stay monophasic and clear at 0 °C. However, at −15 and −20 °C, this standard can no longer be met by any compositions. Further, none of the studied mixtures containing ETBE could fulfil these conditions at 0 °C and, consequently, at even lower temperatures. By contrast, with 2-MTHF, even at −15 °C, mixtures consisting of 60 wt% of rapeseed oil stay monophasic and clear and fulfil the viscosity standard (see Fig. 33b and Table 6). Moreover, Fig. 33d shows that no mixture containing either TBC or EHN as *ethanolotrope* meets the viscosity standard and simultaneously stays monophasic and clear at 0 °C. Similar to the abovementioned *ethanolotropes*, no composition containing FAME fulfils the viscosity standard and stays monophasic and clear at low temperatures. In the presence of DMF or 2-MF, the clear and monophasic binary mixtures with rapeseed oil nearly meet the standard at −20 °C, but show a gel-like state.

Fig. 34 depicts η_{kin} as a function of the weight percentage of HepOH and 2-MTHF, respectively, in the presence of constant 30 wt% of rapeseed oil along path ***c***. The measurements are performed at 25 as well as at 40 °C. As previously, η_{kin} decreases with increasing temperature. Using HepOH as *ethanolotrope*, a continuous increase of η_{kin} appears with increasing amounts of HepOH in the mixture. This fact can be attributed to the higher η_{kin} of HepOH compared with ethanol. At 40 °C, η_{kin} of ethanol is 1.07 $\mathrm{mm^2/s}$, while it is 4.42 $\mathrm{mm^2/s}$ for HepOH [275]. At low amounts of HepOH, η_{kin} is close to the lower required

value of the ASTM D6751 standard. By increasing the amount of this component, η_{kin} reaches the upper limit of this standard. It can be noted that a mixture containing 30 wt% of rapeseed oil, 60 wt% of HepOH and 10 wt% of ethanol meets the viscosity standard and remains monophasic and clear at −15 °C. At low amounts of 2-MTHF, η_{kin} is even closer to the lower value required to reach the standard. In presence of more 2-MTHF, η_{kin} decreases and does not fulfil the standard due to the fact that 2-MTHF is less viscous than ethanol. At 40 °C, η_{kin} of 2-MTHF is 0.58 mm^2/s [276]. These results show that η_{kin} of the mixture can be controlled and predicted by the amount of used *ethanolotrope*. If the viscosity of the ternary system is too low, the addition of a component, which is more viscous than ethanol, will increase its η_{kin} and vice versa. With this method, it is easy to fulfil the requirements of a viscosity standard. In general, by adjusting the nature and the amount of *ethanolotrope* in these ethanol-containing biofuels, the high η_{kin} due to the presence of vegetable oils as well as the bad low-temperature phase behaviour due to ethanol can be overcome.

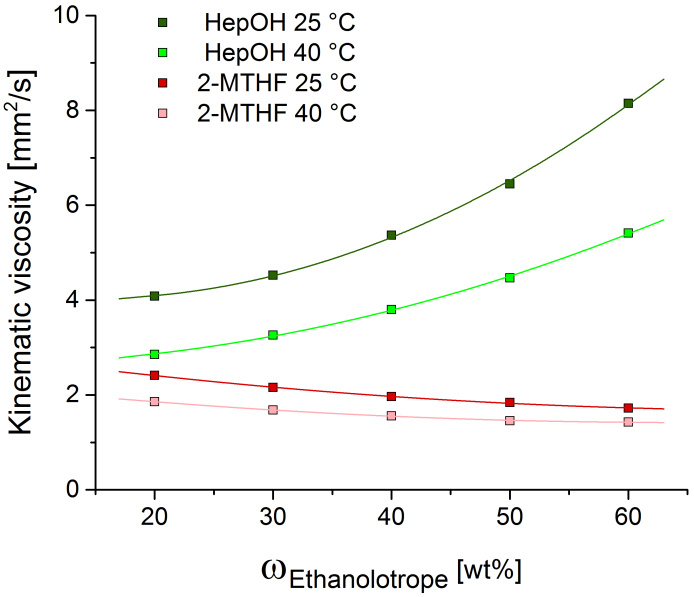

Figure 34: Kinematic viscosity along path ***c*** depending on the ratio of ethanol and the *ethanolotrope* HepOH (green) or 2-MTHF (red) with constant 30 wt% of rapeseed oil at 25 and 40 °C.

To investigate a possible correlation between these relevant fuel properties and the nanostructuring of the mixtures, DLS experiments were performed along path ***a*** and ***b*** (see Fig. 35). As expected due to the SWAXS results of Fig. 25, defined autocorrelation functions are obtained. In particular, the systems possess very similar maximum correlation coefficients, irrespectively of the *ethanolotrope*. This supports the aforementioned assumption that the existence of nanostructures in the HepOH-containing system can be also

transferred to some other *ethanolotrope*-containing biofuels. A closer look at the results shows, however, that the maximum autocorrelation functions are obtained at slightly different compositions. This in turn matches with the differences in the viscosities and low-temperature phase behaviours, which need to be considered within the overall comparison. For that, the mean scattering intensity (SI) within the DLS experiments of each sample is plotted in the subsequent comprehensive figure (see Fig. 37).

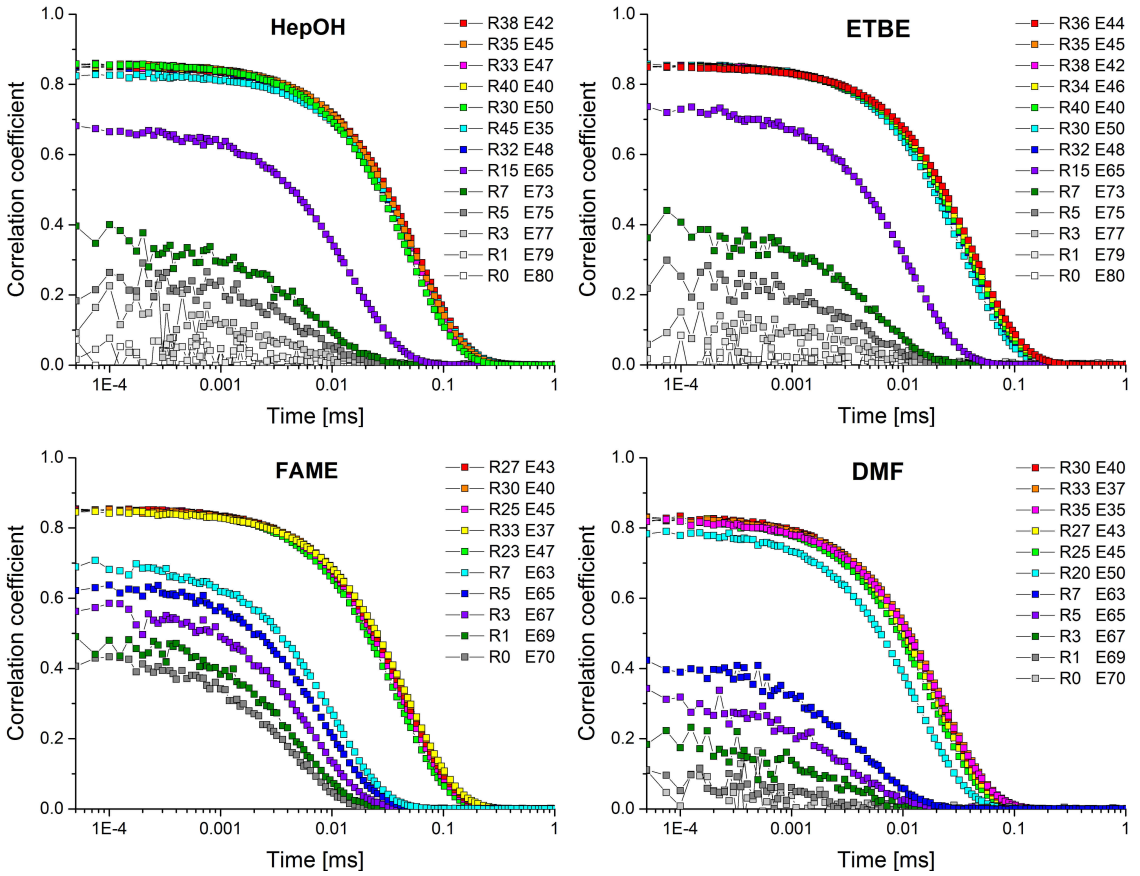

Figure 35: Time-dependent autocorrelation functions obtained by DLS experiments of mixtures containing either HepOH or ETBE along path ***a*** or FAME or DMF along path ***b*** at 25 °C. The composition of the samples is indicated by the amount of rapeseed oil (R) and *ethanolotrope* (E) of each mixture in wt%. The samples are arranged according to their correlation coefficient.

According to the procedure explained in chapter 3.1.6, the critical point (CP) of each ternary system was determined. After detecting the compositions with the highest SI and reaching the biphasic region of these samples, the mixtures appeared turbid (see Fig. 36 on the left). Since these samples were very sensitive towards temperature, it took about one day, until a sharp phase boundary was observable (see Fig. 36 on the right). The compositions of the CPs are represented in Table 9, which again show slight differences between the investigated systems.

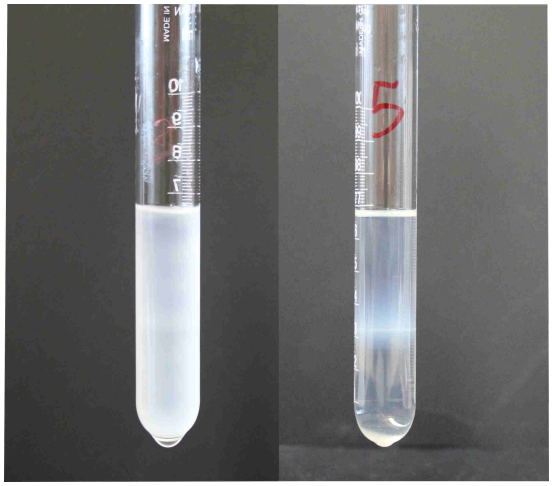

Figure 36: Determination of the critical point (CP) of the ternary system rapeseed oil/ethanol/HepOH, according to chapter 3.1.6, at 25 °C. Once the CP is reached, the mixture appears turbid (left), but after one day, a sharp phase boundary is observable (right).

Table 9: Composition of the CPs of the ternary systems consisting of rapeseed oil, ethanol and the *ethanolotropes* HepOH, ETBE, FAME and DMF at 25 °C.

Ethanolotrope	$\omega_{\textbf{Ethanolotrope}}$[**wt%**]	$\omega_{\textbf{Rapeseed oil}}$[**wt%**]	$\omega_{\textbf{Ethanol}}$[**wt%**]
HepOH	14.26	43.28	42.64
ETBE	16.31	37.25	46.44
FAME	22.60	28.59	48.81
DMF	21.87	34.86	43.27

Fig. 37a-d summarise every experiment concerning these systems and allow conclusions about possible correlations between the physicochemical parameters of the mixtures and their properties as fuels. In particular, the SIs, η_{kin} and the volume fractions of the lower phase of the samples directly after reaching the biphasic region are shown. Obviously, there is no precise SI maximum at a specific composition, but a high intensity plateau. This area is located between 32 and 40 wt% of rapeseed oil with HepOH as *ethanolotrope* and 32 to 36 wt% of rapeseed oil with ETBE (see Fig. 37a-b). The mixtures containing 30 wt% of FAME or DMF possess a less high intensity plateau at lower amounts of rapeseed oil. The maximum SI is obtained at about 25 wt% of the vegetable oil with FAME and 30 wt% of rapeseed oil with DMF (see Fig. 37c-d). The CPs of these systems, indicated by a volume ratio of 0.5 between the lower phase of the sample and the total volume, given in Table 9, are located close to the SI plateau at higher amounts of rapeseed oil (see Fig. 37a-d). The correlation between the SI and the CP becomes obvious, which enables predictions concerning the composition of the highly sensitive CP of similar ternary systems by just

performing light scattering experiments. Thus, the increasing SI is related to the approach to the CP. Concerning the viscosity curves of Fig. 37a-d, trend lines were inserted at very low and very high rapeseed oil concentrations. Surprisingly, their intersections correspond to the CP of the ternary systems containing HepOH, ETBE or FAME, whereas it is slightly shifted to higher amounts of rapeseed oil with DMF as *ethanolotrope*. In contrast to the viscosity curves of the HepOH and ETBE system along path ***a***, the mixtures consisting of 70 wt% of rapeseed oil were not considered in the FAME and DMF system along path ***b***, as they are just binary mixtures.

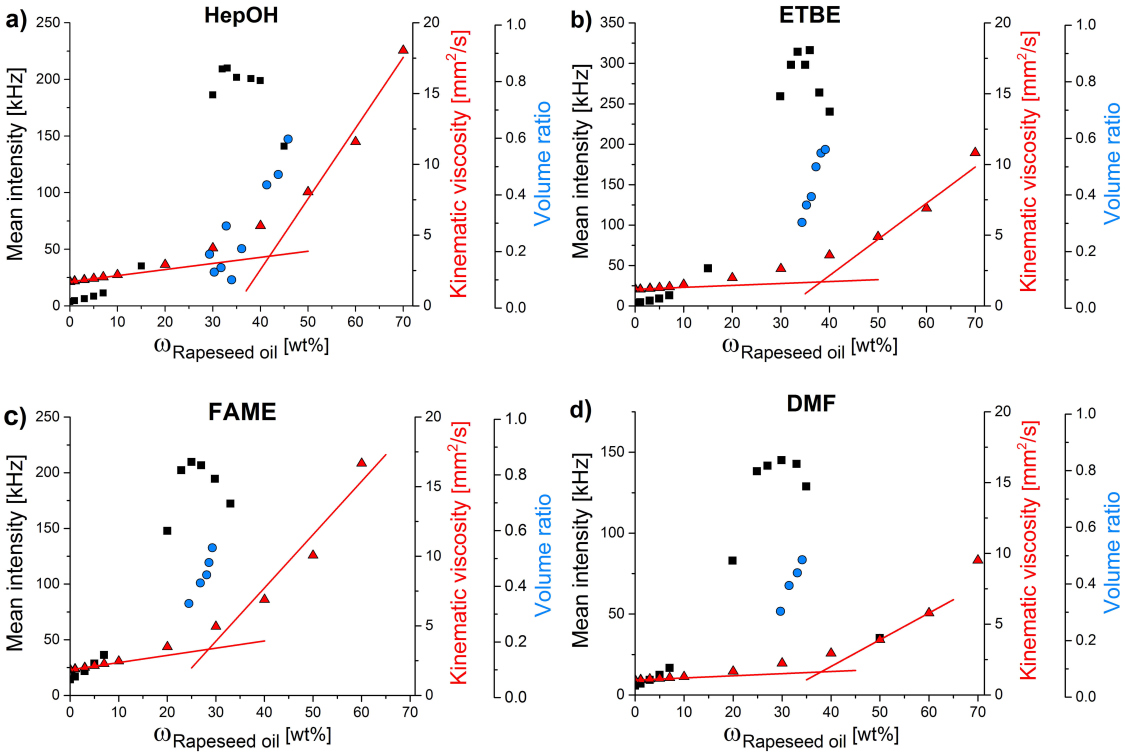

Figure 37: Mean scattering intensities obtained by DLS measurements (■) and kinematic viscosities (▲) along path ***a*** and ***b***, respectively, as well as the volume fractions of the lower phase (●), directly after reaching the biphasic region of the system versus the weight percentage of rapeseed oil in the ternary systems consisting of ethanol, rapeseed oil and HepOH (a), ETBE (b), FAME (c) and DMF (d) as *ethanolotropes* at 25 °C. The depicted viscosity trend lines indicate a pseudo-phase inversion close to or even directly at the critical points of the systems.

Coming back to the ternary system rapeseed oil/ethanol/HepOH and comparing these results with the proof of nanostructures, several conclusions can be drawn. Besides the already mentioned correlation between the SI and CP of the systems, their viscosity curves are directly related to their nanostructuring. The scattering and conductivity results showed that, with an increasing amount of rapeseed oil, the bulk changes from an ethanol-rich to a rapeseed oil-rich pseudo-phase. Due to the formation of a rapeseed oil continuum,

the rapid increase of η_{kin} close to the CP can be explained. These high viscosities correlate with the observed percolation of ethanol droplets, according to the dynamic percolation model. Further, the intersection of the viscosity trend lines in Fig. 37a-d even indicates a correlation between the slope of the viscosity curve and the CP of the system.

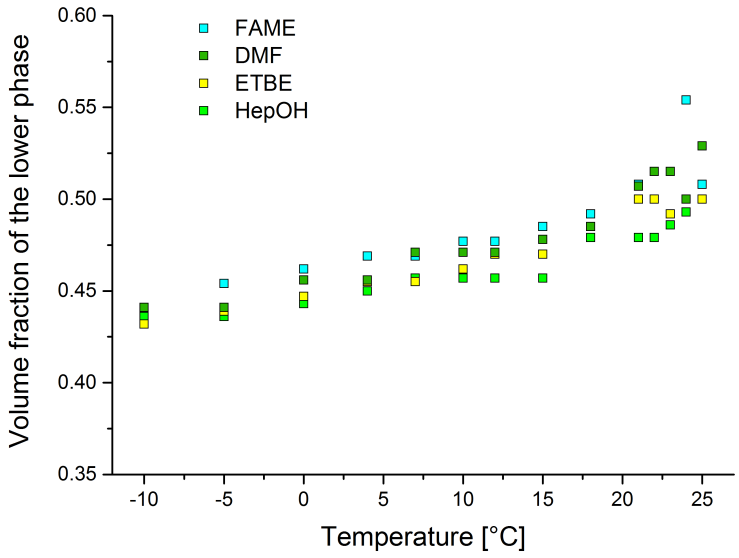

Figure 38: Temperature dependence of the volume fraction of the lower phase of liquid-liquid mixtures close to the CP of the systems containing rapeseed oil, ethanol and one of the *ethanolotropes* FAME (■), DMF (■), ETBE (■) and HepOH (■) from −10 to 25 °C.

For a closer look at the influence of the temperature on the location of the CP and thus also on the structuring of the system, the phase behaviour of these ternary mixtures was even further investigated. Fig. 38 shows the temperature dependence of the volume fractions of the lower phase of the ternary biofuels with their respective compositions at the CP at 25 °C from −10 to 25 °C. In general, every investigated system behaves similarly. By warming up the mixtures, they become clear and monophasic between 27 and 30 °C. The volume fraction of the lower phase decreases with declining temperatures for each of these ternary biofuels. At low temperatures, there is less ethanol in the lower, rapeseed oil-rich phase than in the upper, ethanol-rich phase. With increasing temperature, the solubility of ethanol in the phase consisting of rapeseed oil and *ethanolotrope* is enhanced. The driving force of the formation of the monophase seems to be an incorporation of ethanol in the oil phase by the third component of the system. This in turn leads to the work of Bauduin *et al.*, who described the term *reverse hydrotropes* for the first time, showing that the solubility of water in oil can be increased by using HepOH. They propose that this solubilisation is coupled with the insertion of water molecules into the network of the percolated *n*-alcohol [277]. This percolation phenomenon was shown by Glatter *et al.* and

other groups, who explain the aggregation of pure alcohols to oligomers due to a hydrogen bond network [278]. This concept is, once again, also in accordance with the previous scattering and conductivity results.

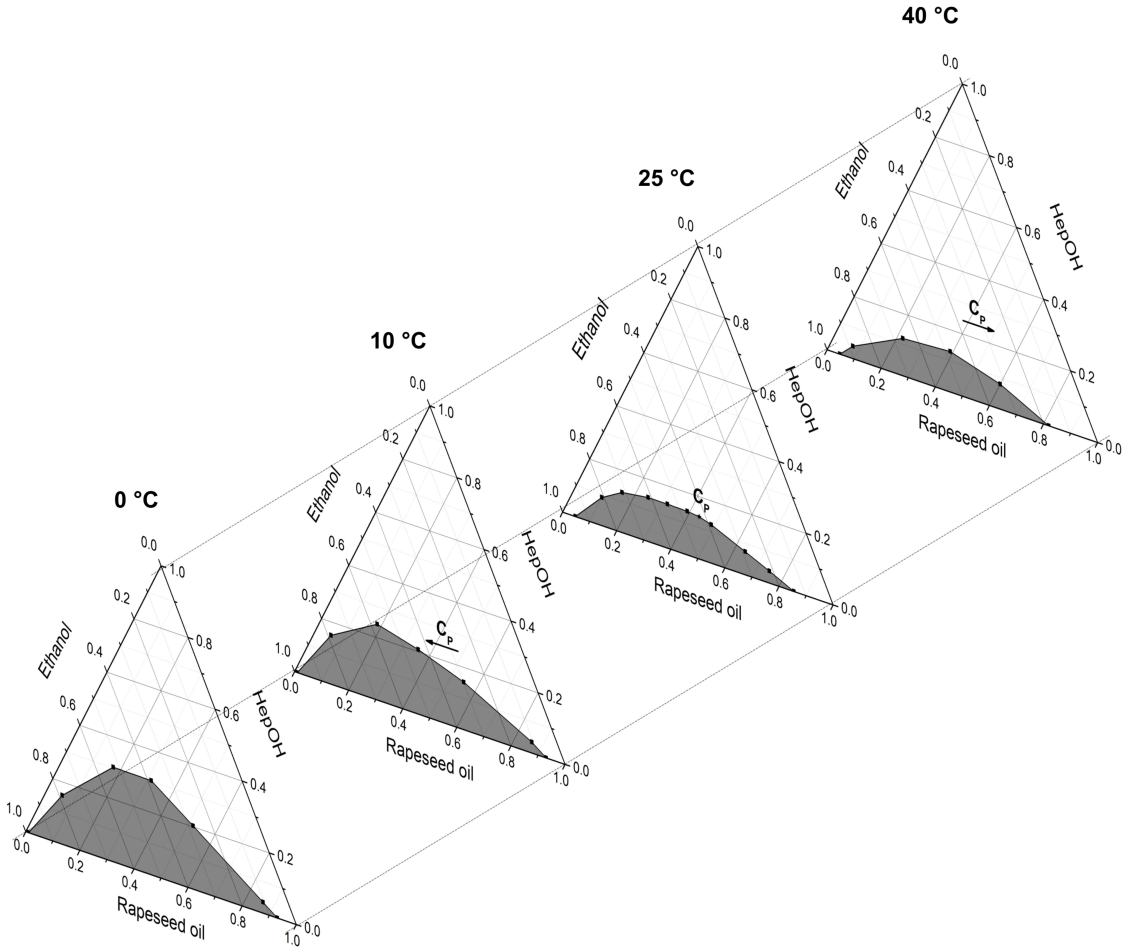

Figure 39: Phase prism of the ternary system consisting of rapeseed oil, ethanol and HepOH in mass fractions. The darkened areas represent the biphasic regions, determined at 0 °C, 10 °C, 25 °C and 40 °C. The change in the location of the CP is also indicated.

To complete these investigations, the temperature-dependent phase behaviour of a whole ternary system was studied. For that, a phase prism was prepared for the ternary biofuel consisting of rapeseed oil, ethanol and HepOH with four different temperatures (see Fig. 39). Similar to the binary phase diagram shown in Fig. 32, the phase prism shows that the biphasic region becomes smaller with increasing temperature. This observation is also in agreement with the observed low-temperature behaviour of this ternary system, represented by Table 6. Further, it illustrates the impact of the nanostructuring of the mixtures on the phase behaviour of the system. At low temperatures, the biphasic re-

gion strongly expands to lower amounts of rapeseed oil, whereas it just slightly changes at higher amounts of the vegetable oil, which is the region of reversed nanostructures. This in turn also corresponds to the previous low-temperature results of these mixtures. The change in the location of the CP is given in the phase prism as well, according to its temperature dependence shown in Fig. 38. To illustrate the expansion of the biphasic region with decreasing temperature, the phase diagrams of the phase prism are combined to a single ternary phase diagram in Fig. 40.

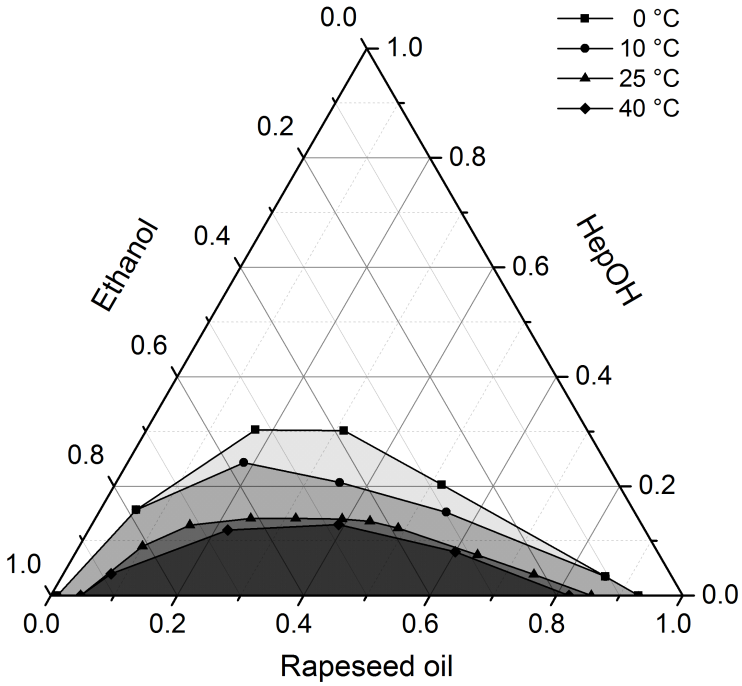

Figure 40: Ternary phase diagram of the system consisting of rapeseed oil, ethanol and HepOH at 0 °C (■), 10 °C (●), 25 °C (▲) and 40 °C (◆). The values are given in mass fractions.

Within this research topic, considerable contributions were made and published concerning the understanding of ethanol-containing biofuel formulations, their physicochemical characteristics and obstacles as well as their relevant fuel properties [262, 263]. *Ethanolotropes* improve the miscibility of ethanol with rapeseed oil and simultaneously reduce η_{kin} of the mixture. These compounds also favourably influence the low-temperature phase behaviour, leading to monophasic and clear mixtures even at −20 °C. Therefore, some of these formulations can be considered as potential summer or even winter biofuels. Due to the investigated correlations between η_{kin}, the SI, the CP and the phase behaviour with the nanostructuring of the mixtures, a better understanding of the substantial obstacles, when dealing with ethanol as biofuel component, was achieved.

4.1.2 New concept of biofuels

Based on the results within the scope of my master thesis, explained in section 2.1.5.1, this chapter deals with the optimisation of the biodiesel production process (see Fig. 21). After successfully implementing the waste product glycerol into the biofuel formulations, the subsequent investigations showed that its presence leads to several advantages during combustion and storage. Already at this point, these results were sufficient to be patented [279]. For the first time, natural antioxidants can be used in biofuel formulations without any surfactants, which completely replace the commonly used synthetic and highly toxic antioxidants. Additionally, glycerol derivatives have the potential to significantly contribute to the extensive commercialisation of hydrofuels [280].

4.1.2.1 Implementation of glycerol derivatives into biofuel formulations

As already described in section 2.1.5.2, the usage of the waste product of the biodiesel production, glycerol, as fuel component would distinctly increase the competitiveness of this process (see Fig. 21). In particular, the products of the derivatisation reactions to more hydrophobic glycerol derivatives, shown in Fig. 9, were used. To be able to develop new multi-component formulations like biofuels, detailed information about the miscibility of the substances is essential. Based on the results of section 4.1.1.2, the miscibility gap between a hydrophilic substance, e.g. ethanol, and vegetable oils can be closed by adding different sustainable components like FAME or 2-MF. Due to the either amphiphilic or less hydrophilic character of the investigated glycerol derivatives, a similar result was to be expected for their mixtures with rapeseed oil.
Fig. 41 indicates that, indeed, the biphasic region of ternary mixtures consisting of rapeseed oil, FAME and a glycerol derivative significantly depends on the hydrophilicity of the derivative. While the binary mixture of solketal and rapeseed oil possesses a rather small miscibility gap, the more hydrophilic triacetin is hardly miscible with the vegetable oil. The more hydrophobic tributyrin, however, is completely miscible with rapeseed oil at room temperature. Already small amounts of FAME are sufficient to close the miscibility gap in the solketal system, whereas very high amounts of FAME are necessary in the triacetin system. For comparison, the ternary system with ethanol as hydrophilic compound is also given in this figure. As explained before, the main problem concerning the usage of ethanol in fuel formulations is its bad miscibility with other relevant substances at lower temperatures. Since this is already indicated by the size of the biphasic region in the phase diagram at room temperature, the comparison with the triacetin system leads to the assumption that implementing triacetin in such formulations will be even more difficult.

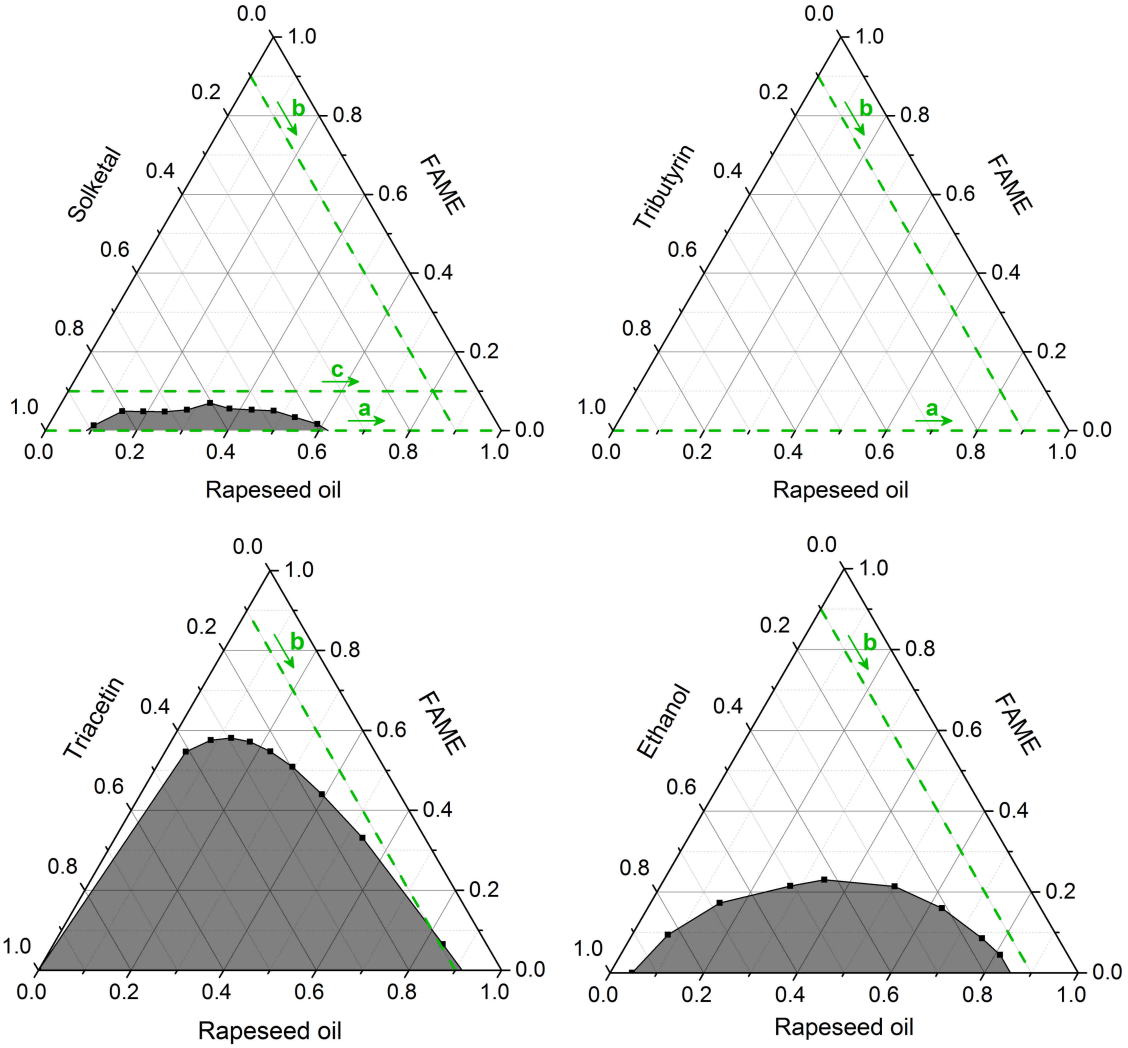

Figure 41: Ternary phase diagram of mixtures consisting of rapeseed oil, FAME and either solketal, tributyrin, triacetin or ethanol as hydrophilic compound at 25 °C. The darkened areas represent the biphasic regions of the systems. The further investigated compositions in the subsequent formulations are indicated by path ***a***, ***b*** and ***c***. The values are given in mass fractions.

These phase diagrams also show the investigated compositions in the subsequent formulations along path ***a***, ***b*** and ***c***. While path ***a*** relates to the properties of the binary mixture of the hydrophilic compound and rapeseed oil, path ***b*** represents reasonable biofuel compositions. Every sample along this path consists of challenging 10 wt% of the hydrophilic substance. Thus, the mass ratio between glycerol derivative and FAME is higher in every mixture than during FAME production. If these formulations possess properties that fulfil the respective standards, this will also apply for mixtures with lower amounts of glycerol derivatives. Comparing the phase diagrams of the solketal system with the ethanol system along path ***b*** regarding the fact that the biphasic region usually drastically increases with decreasing temperature, one can assume that the solketal system will have lower cloud

points. Concerning this system, several mixtures with a constant amount of 10 wt% of FAME, indicated by path ***c***, are also investigated regarding the presence of nanostructures analogously to the aforementioned results. To this purpose, DLS measurements were performed, which led to pronounced correlation functions with a correlation maximum for the mixture consisting of 60 wt% of solketal and 30 wt% of rapeseed oil (see Fig. 42). These already indicate the presence of nanostructures in this system. The calculation of the aggregate size for the mixtures with the highest correlation coefficients shows that both measurements result in values of a few nanometres. Similar to the radii in Fig. 29, the sizes obtained by the SLS experiments are bigger than the hydrodynamic radii of the DLS measurements, once again indicating that the assumption of a spherical shape is wrong. Since scattering experiments along path ***b*** led to no correlation functions, these structures exist at compositions that are not of interest for biofuel formulations, due to their high amount of solketal.

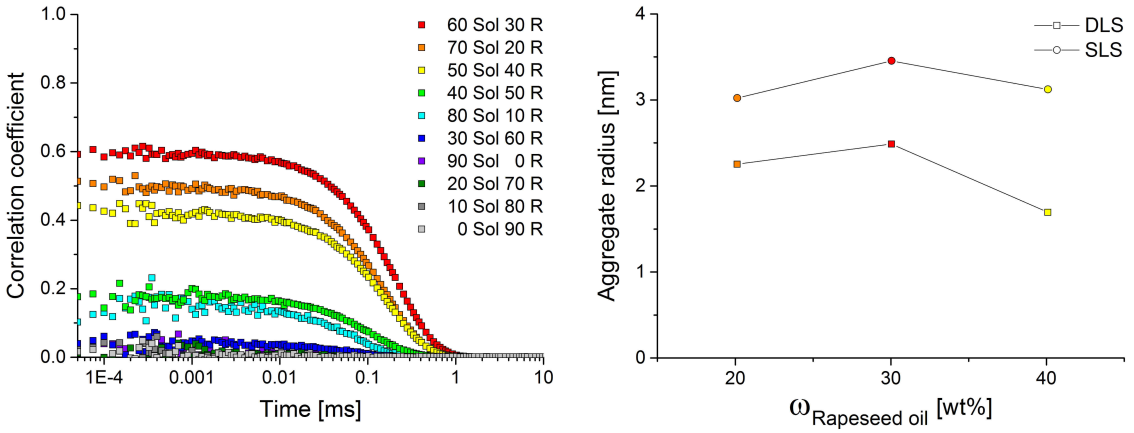

Figure 42: Left: time-dependent autocorrelation functions obtained by DLS experiments of mixtures consisting of rapeseed oil, solketal and 10 wt% of FAME along path ***c*** at 25 °C. The composition of the samples is indicated by the amount of rapeseed oil (R) and solketal (Sol) of each mixture in wt%. The samples are arranged according to their correlation coefficient. Right: Calculated radii of the scattering aggregates based on the DLS and SLS experiments versus the weight percentage of rapeseed oil assuming spherical geometry.

To obtain more information on the influence of the glycerol derivatives on the main physicochemical drawbacks of vegetable oils as biofuels, i.e. high viscosities and cloud points, Fig. 43a shows the viscosity curves of binary mixtures of them, along path ***a*** at 40 °C. Due to their much lower η_{kin} compared to glycerol, the derivatives solketal and tributyrin distinctly reduce the viscosity of rapeseed oil. The triacetin system could not be examined, as none of the samples was monophasic at 40 °C. This figure also indicates that the presence of the glycerol derivatives leads to nearly the same viscosity reduction as the presence of FAME. This already implies that the implementation of these waste materials does not inevitably cause further drawbacks, but could actually reduce the necessary

amount of additives, as explained in chapter 2.1.5. For comparison, the viscosity curve of the binary mixture with 2-MTHF was also added to illustrate the strong impact of the furan derivatives on η_{kin} of vegetable oils. The results of these experiments along path ***b*** are given in Fig. 43b. For these compositions, the investigated glycerol derivatives affect η_{kin} similarly. The influence of ethanol on η_{kin} is much stronger, which is one of the reasons, why ethanol is still considered as possible blending compound for biofuels, despite its high cloud point.

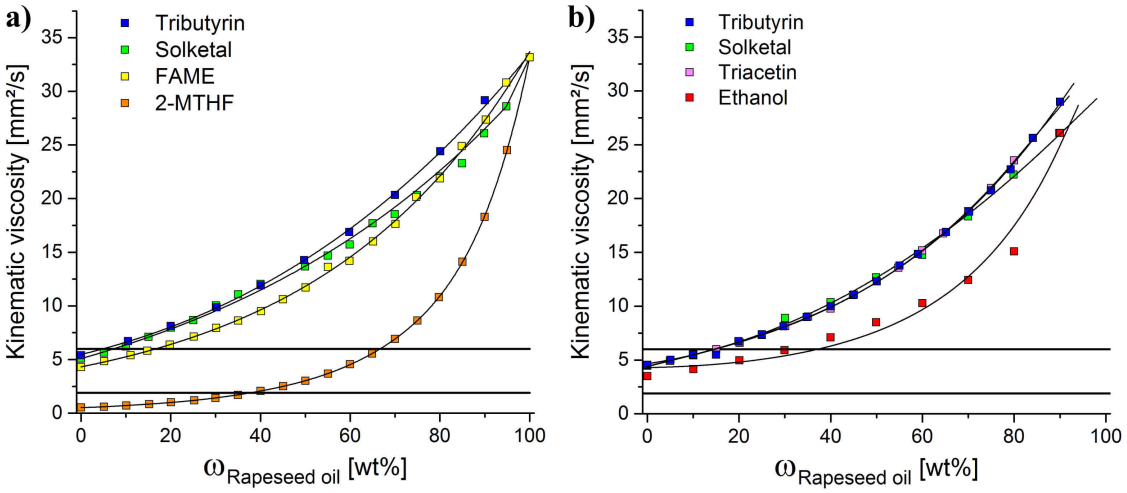

Figure 43: Kinematic viscosities versus the weight percentage of rapeseed oil along path ***a*** (a) and ***b*** (b) at 40 °C. For comparison, the viscosity curve of the system containing 2-MTHF or FAME along path ***a*** was added as well as the results of the ethanol system along path ***b***. The horizontal lines indicate the required viscosity range (from 1.9 to 6.0 mm^2/s), according to the ASTM D6751 standard.

The low-temperature phase behaviour of these ternary systems along path ***b*** and of the binary mixture of FAME and rapeseed oil is shown in Fig. 44. It becomes evident that, for systems with small miscibility gaps at room temperature, the cloud points decrease with increasing amount of rapeseed oil. FAME, on the other hand, leads to higher cloud points and thus a worse low-temperature phase behaviour of the fuel, as expected. The comparison of the glycerol derivatives confirms the assumption that triacetin is not suitable as biofuel component in our formulations, due to its poor miscibility with rapeseed oil. Firstly, the lowest cloud point in this system is −4 °C and secondly, none of the mixtures remain monophasic and clear after one month at 0 °C, which is indicated by green points. The same trend is observable for the ethanol system, but the cloud points are slightly lower and some samples even stay monophasic after one month at 0 °C. The solketal and tributyrin systems, however, show much more promising results. The presence of these two compounds distinctly reduces the cloud points of the mixtures, which had to be achieved by further additives, in particular furan derivatives, in our previous work [228].

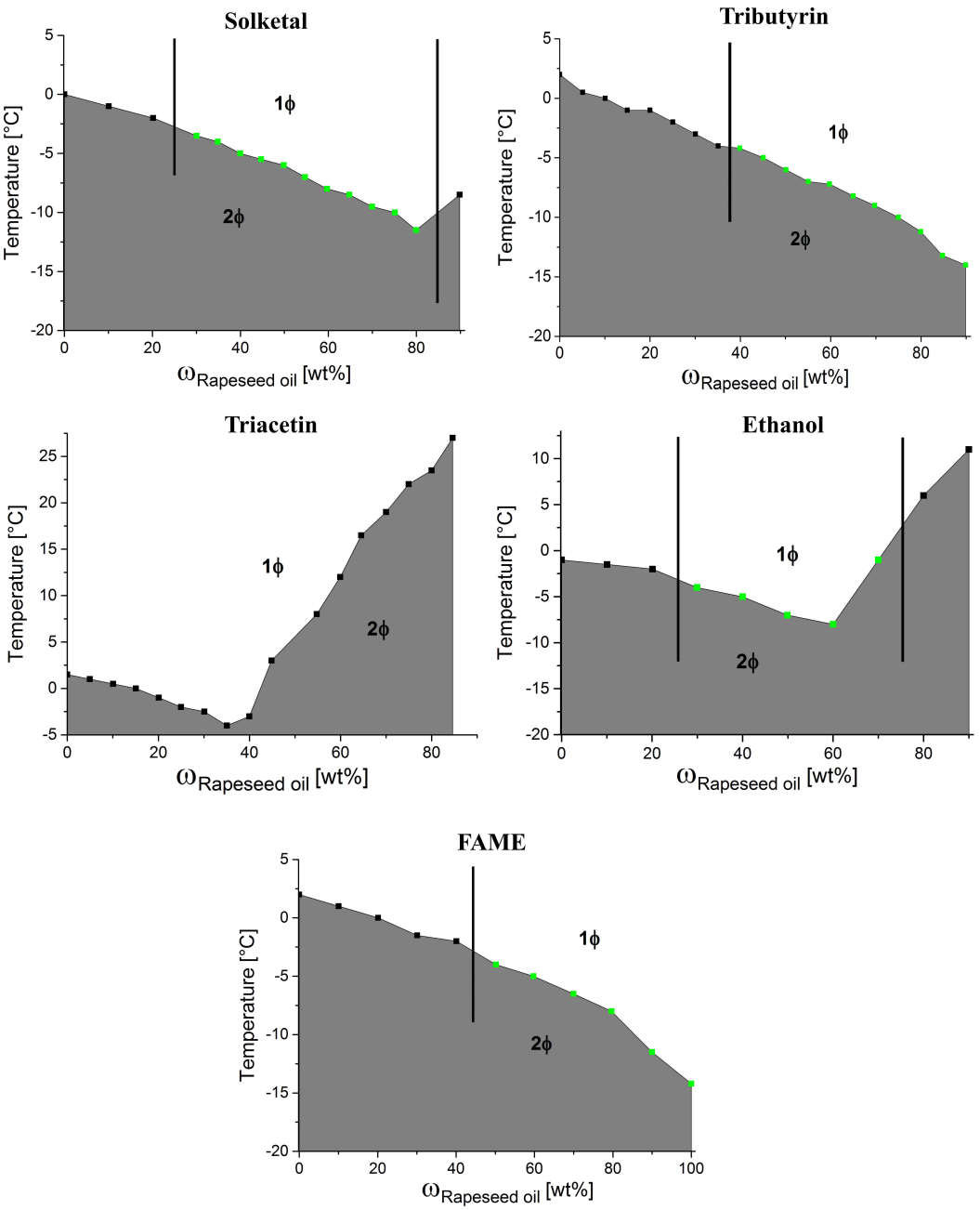

Figure 44: Cloud points versus the weight percentage of rapeseed oil for mixtures along path ***b*** as well as for the binary mixture of rapeseed oil and FAME (bottom). The darkened area represents the biphasic region of the system. The perpendicular lines and green points indicate mixtures, which remained monophasic after one month at 0 °C.

Although the melting point of solketal is much higher than the one of tributyrin, less rapeseed oil is necessary to obtain monophasic mixtures even after one month at 0 °C. Thus, 30 wt% of rapeseed oil are sufficient in the solketal system to achieve this, whereas at least 40 wt% of rapeseed oil are necessary in the tributyrin system. The comparison with

the binary system rapeseed oil/FAME shows that the usage of the derivatives enhances the properties of the biofuel formulation, although being produced from waste. Even though the usage of FAME in these formulations was intended, its presence even proves to be reasonable. While these biofuel formulations imply a processing of the glycerol to derivatives and then the usage of a mixture with FAME, increasing its production profitability, FAME reduces η_{kin} even further and increases the ignition quality due to its high CN. Since it also increases the cloud point of the mixture, the composition needs to be optimised for final formulations.

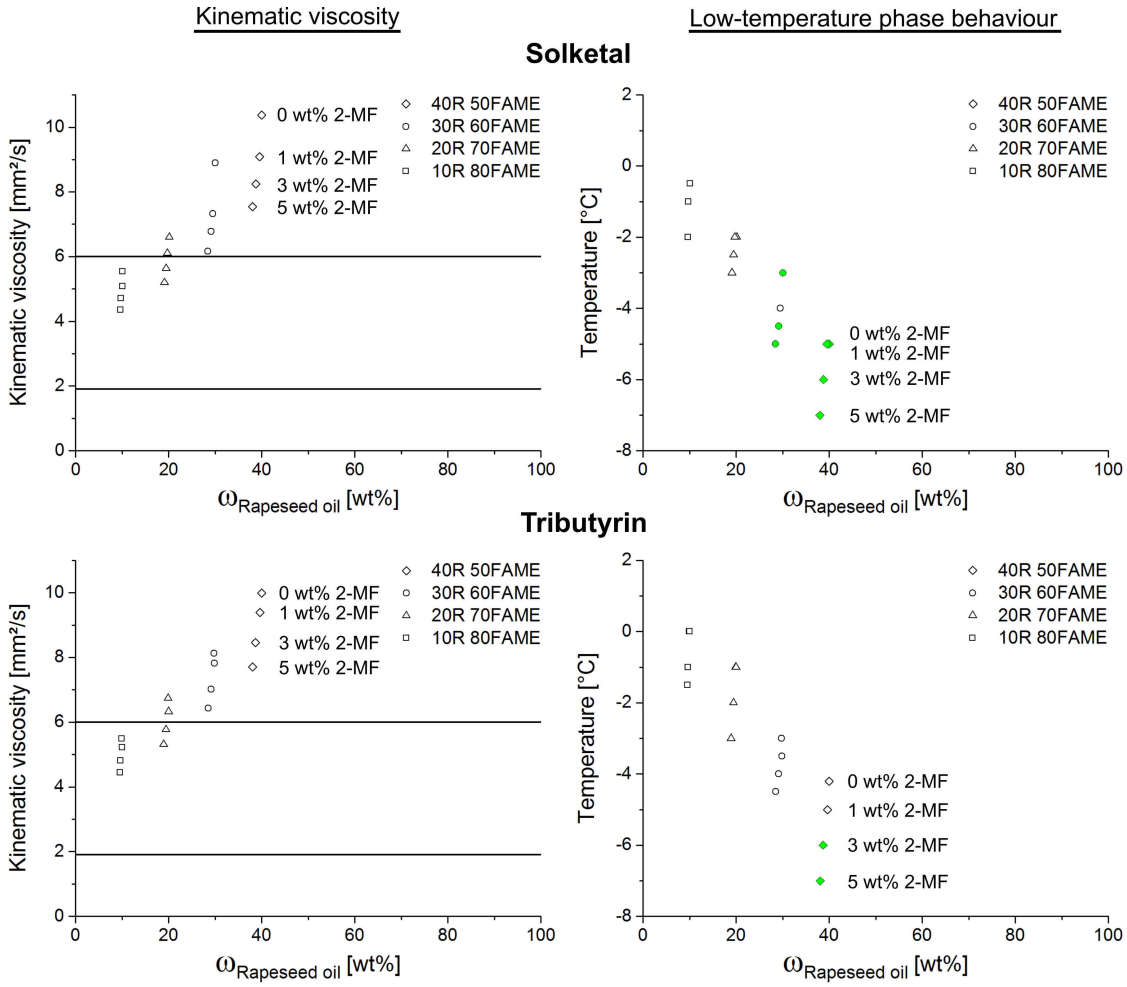

Figure 45: Kinematic viscosities and cloud points versus the weight percentage of rapeseed oil (R) for mixtures along path ***b*** of the solketal (top) and tributyrin system (bottom) with additional 0, 1, 3 and 5 wt% of 2-MF. The viscosities were measured at 40 °C and the horizontal lines indicate the required viscosity range (from 1.9 to 6.0 $\mathrm{mm^2/s}$), according to the ASTM D6751 standard. Regarding the low-temperature phase behaviour, the green points represent mixtures, which remained monophasic after one month at 0 °C.

With the compatibility problem of glycerol derivatives being already solved even with 10 wt% of them, compositions with lower amounts will fulfil the self-imposed requirements, too. In the case of lower amounts, miscibility and viscosity problems will not occur. Even higher ratios of glycerol derivatives will be viable, if the amount of rapeseed oil is decreased or the amount of FAME is increased, instead. Further, by replacing rapeseed oil with a much less viscous, more saturated vegetable oil like palm oil, the standards would be easily fulfilled as well. These results imply that this new class of biofuels enables adaptable compositions depending on the application.

Fig. 45 shows the influence of the addition of 2-MF on η_{kin} and on the cloud points of the biofuels with the glycerol derivatives solketal and tributyrin along path ***b***. Since the amount of vegetable oil should be as high as possible, due to economic reasons, 2-MF is added to samples containing 10 to 40 wt% of rapeseed oil. All predictions regarding the influence and necessary amount of 2-MF during the investigations of the binary and ternary mixtures prove to be correct. Already very small amounts of the furan derivatives distinctly improve the physicochemical properties of the formulations. The addition of 1 wt% of 2-MF leads to a considerable reduction of η_{kin} and the cloud points of both biofuels. Once a certain amount of 2-MF is used, further additions of 2-MF just slightly change these parameters. Thus, the desired viscosity and cloud point can be adjusted by changing the amount of 2-MF. This figure also points out that both biofuels are very similar concerning these parameters. The tributyrin biofuel possesses just slightly higher viscosities and cloud points as well as less monophasic compositions than the solketal biofuel after one month at 0 °C, indicated by green points. Further, the main goal of implementing glycerol derivatives and simultaneously reducing the necessary amount of 2-MF is achieved, even though the cloud points are no longer below −20 °C.

The influence of the biodiesel source on these biofuel formulations, examined by replacing FAME with MeC_{10}, is outlined in Fig. 46. Due to the much lower η_{kin} as well as freezing point of MeC_{10} and its good miscibility with the other biofuel components, the properties of the formulations are considerably enhanced (see also Table 2). The comparison of η_{kin} of binary mixtures of rapeseed oil with either FAME or MeC_{10} already indicates the difference between the biodiesels (see Fig. 46a). Using MeC_{10} instead of FAME for the formulations with 2-MF, one can firstly notice that even mixtures with 50 wt% of rapeseed oil become conceivable. Secondly, for biofuels consisting of 10 to 40 wt% of rapeseed oil, no 2-MF is necessary at all to reach the viscosity range to fulfil the American biodiesel standard, given by the horizontal lines (see Fig. 46b). Fig. 46c-d show the cloud points of binary mixtures of rapeseed oil with FAME and MeC_{10}, respectively. It is obvious that the presence of MeC_{10} distinctly improves the low-temperature phase behaviour of rapeseed oil. While the cloud points of mixtures with FAME decrease with increasing amount of rapeseed oil, it is just the opposite for the MeC_{10} system. Once the amount

of MeC_{10} is higher than 50 wt% in mixtures with rapeseed oil, the cloud point is even below −20 °C. Further, every investigated mixture remained monophasic after one month at 0 °C. These results also apply to the formulations with additional 2-MF, as the cloud points are around −20 °C even without 2-MF. Therefore, the potential of this biofuel concept becomes obvious, once alternative components are used [279, 280].

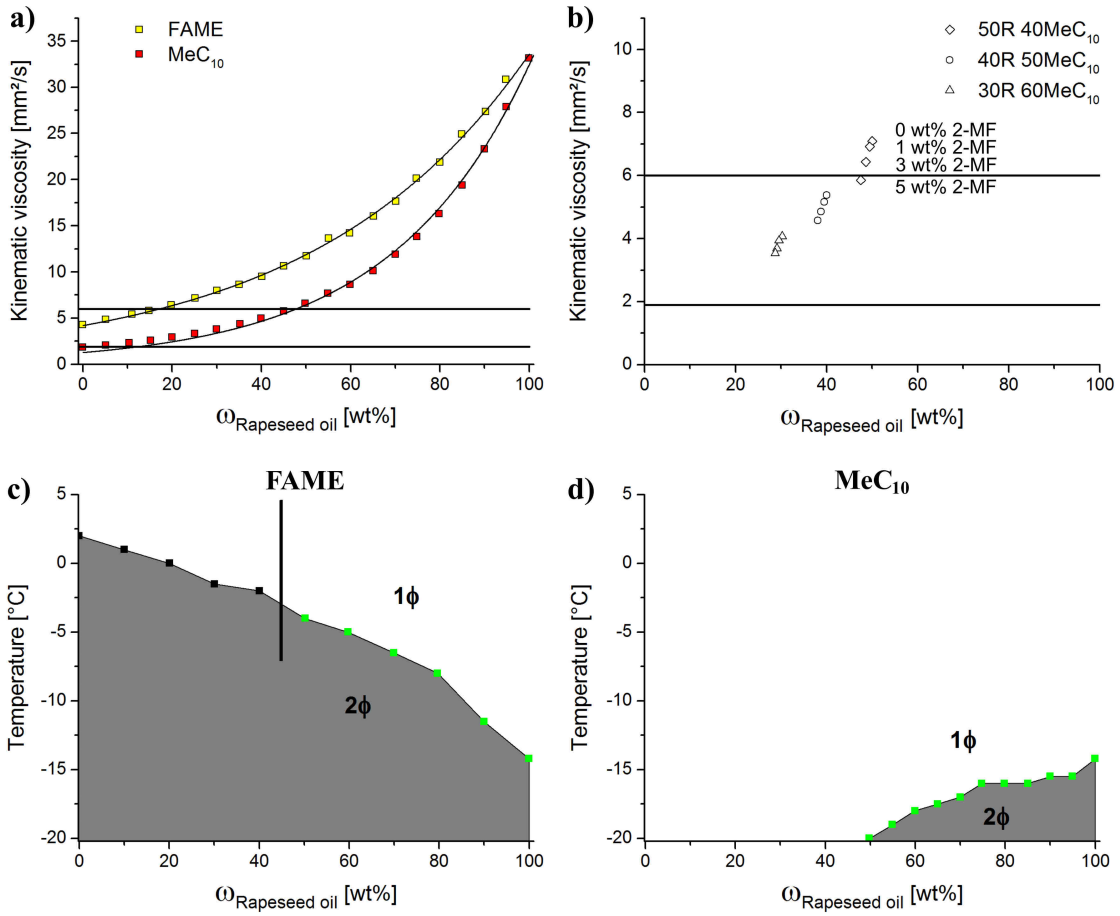

Figure 46: Influence of the biodiesel source on the biofuel formulations, examined by replacing FAME with MeC_{10}. (a) Kinematic viscosity versus the weight percentage of rapeseed oil for binary mixtures with either FAME or MeC_{10} at 40 °C. The horizontal lines indicate the required viscosity range (from 1.9 to 6.0 mm^2/s), according to the ASTM D6751 standard. (b) Similar measurements as for (a), but with mixtures consisting of 10 wt% of solketal, a varying ratio between rapeseed oil (R) and MeC_{10} as well as additional 0, 1, 3 and 5 wt% of 2-MF. (c-d) Cloud points versus the weight percentage of rapeseed oil for mixtures with either FAME (c) or MeC_{10} (d). The darkened area shows the biphasic region of the system. The perpendicular line and green points represent mixtures, which remained monophasic after one month at 0 °C.

4.1.2.2 Engine test results

Based on the results of these fuel formulations, two biofuels with either solketal or tributyrin as glycerol derivative were prepared for the subsequent engine tests. To investigate the influence of every possible compound, 3 wt% of 2-MF were added to the formulations. In particular, the biofuels consisted of 29.1 wt% of rapeseed oil, 58.2 wt% of FAME, 9.70 wt% of either solketal or tributyrin and 3.00 wt% of 2-MF (see Table 10).

Table 10: Compositions of the formulated and further investigated biofuels consisting of rapeseed oil (R), FAME, one of the glycerol derivatives (Glyc.deriv.) solketal as well as tributyrin and 2-MF.

Sample	$\omega_{\mathbf{R}}$**[wt%]**	$\omega_{\mathbf{FAME}}$**[wt%]**	$\omega_{\mathbf{Glyc.deriv.}}$**[wt%]**	$\omega_{\mathbf{2\text{-}MF}}$**[wt%]**
Solketal biofuel	29.1	58.2	9.70	3.00
Tributyrin biofuel	29.1	58.2	9.70	3.00

In these mixtures, the mass ratio between the derivative and FAME is 1:6 and therefore even higher than during FAME production with 1:10. Thus, the biofuels consisted of high amounts of exactly those components that could negatively affect the combustion or emission properties, namely rapeseed oil and the glycerol derivative. In the case of positive engine test results, one can assume that other possible mixtures with lower amounts of these two components will also have favourable properties. Regarding the vegetable oil content of a plant as well as the yields of FAME and the glycerol derivatives during their production, the fuel yield is increased from 89% to 98% within these formulations. With regard to the whole plant, the current yield of FAME is about 35.6%, whereas the developed concept leads to a fuel yield of 39.2% [281, 282].

Table 11: Measured densities ρ and kinematic viscosities η_{kin} at 40 °C and cloud points of the formulated biofuels as well as pure rapeseed oil and diesel.

Sample	ρ**[kg/m³]**	$\eta_{\mathbf{kin}}$**[mm²/s]**	$\mathbf{T_{Cloud}}$**[°C]**
Solketal biofuel	890	6.78	−4.5
Tributyrin biofuel	888	7.02	−4.0
Rapeseed oil	903	33.2	−14
Diesel	840	3.80	−10

Table 11 shows the most important physicochemical properties of the final formulations as well as rapeseed oil and diesel, which were used for comparison. The calorific data of the pure biofuel components and the final formulations, in particular the combustion energy

$\Delta_C U_{298}$ and enthalpy $\Delta_C H_{298}$, are given in Table 12. The obtained values for $\Delta_C H_{298}$, whose absolute values are the higher heating values, are close to literature, except for MeC_{10}. However, this substance does not influence the results of the formulations, since it is not part of them. With −34.0 and −32.3 MJ/kg, the combustion enthalpies of the solketal and tributyrin biofuel are just slightly below the enthalpy of FAME. This means that the simultaneous usage of high amounts of a vegetable oil and glycerol derivative does not necessarily lead to a significant loss in combustion enthalpy.

Table 12: Measured combustion energies, $\Delta_C U_{298}$, and enthalpies, $\Delta_C H_{298}$, of the pure biofuel components and the two final formulations at 25 °C. The enthalpies are compared to literature [7,71,109,283,284].

Sample	$\Delta_C U_{298}$ [MJ/mol]	$\Delta_C H_{298}$ [MJ/kg]	
		Used	**Literature**
Rapeseed oil	−37.4	−38.5	−39.7
FAME	−11.5	−35.4	−35.8
MeC_{10}	−6.01	−32.3	−36.7
Solketal	−3.29	−24.9	−25.9
Tributyrin	−7.36	−9.22	−8.12
2-MF	−2.01	−24.6	−27.6
Solketal biofuel	−16.3	−34.0	–
Tributyrin biofuel	−15.5	−32.3	–

Despite containing high amounts of a vegetable oil and glycerol derivative, both biofuels could be directly used in an unmodified up-to-date diesel engine due to their low viscosities. Fig. 47 shows the combustion start as a function of the injection pressure and the relative boost pressure for both formulated biofuels and diesel. By using three-dimensional graphics, it becomes obvious that firstly, the solketal and tributyrin biofuel possess very similar ignition behaviours. Secondly, the biofuels have ignition properties very close to those of diesel, which implies comparable CNs. Further, the higher the injection and boost pressure, the earlier the combustion starts. At very low injection and boost pressures, the combustion start takes slightly longer for the formulated biofuels, but since this time rapidly decreases with higher boost pressures, the ignition properties of diesel can be achieved.

To investigate the emission characteristics of the biofuels, the EGR rate is varied at 200 and 700 mbar relative boost pressure (see Fig. 48). A specific NO_x emission value is adjusted for every measurement as reference point to determine the other emission parameters of the formulations, diesel and pure rapeseed oil.

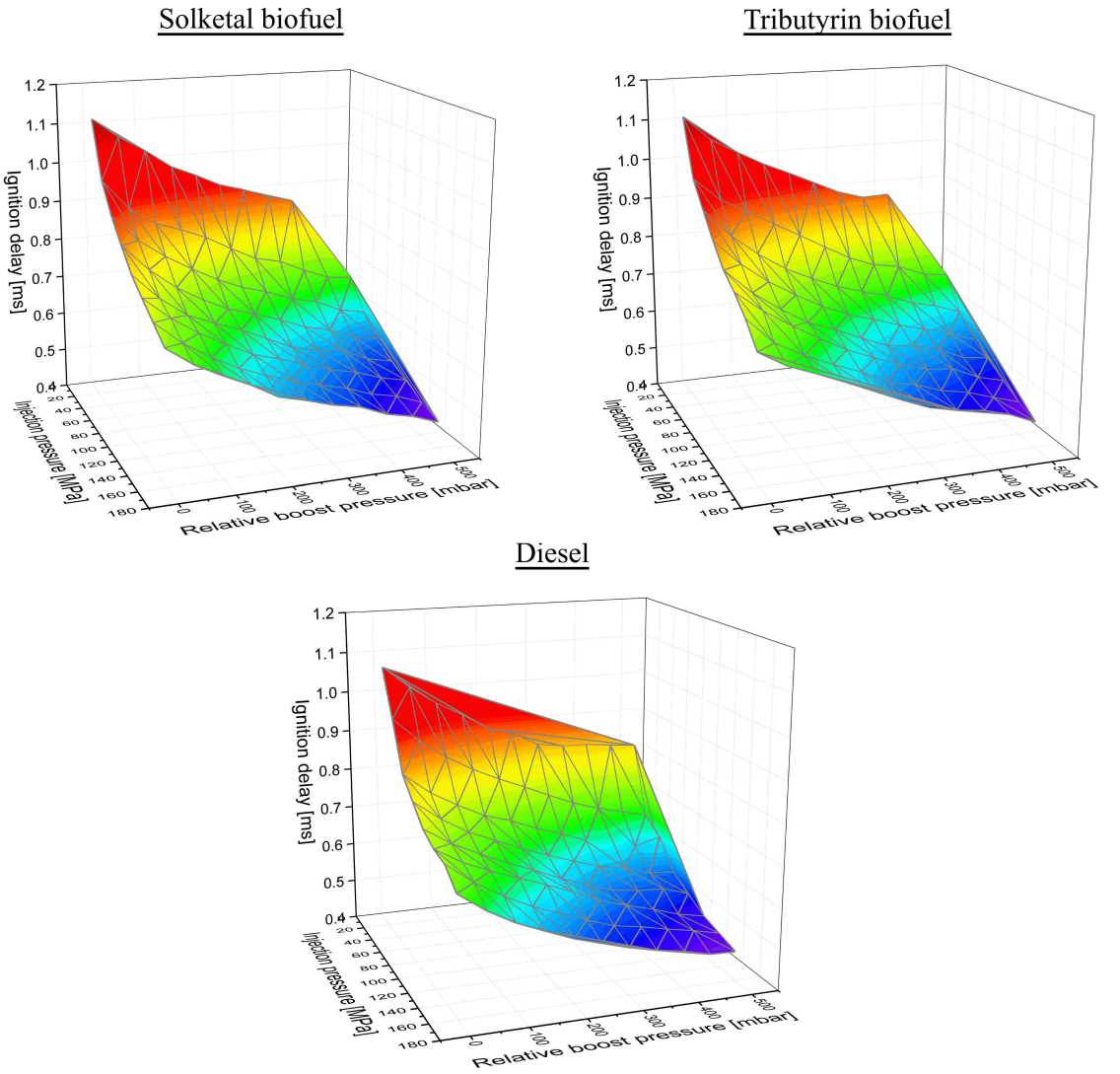

Figure 47: Ignition delay measurements of both formulated biofuels and diesel with an engine speed of 1500 rpm and a torque of 80 Nm. The ignition delay is calculated as difference between the point with an injection rate higher than 1.5 g/s and the combustion start with 5% turnover. This value is shown versus the injection pressure and the relative boost pressure with a constant injection volume of 10 mg at 5° crankshaft angle before top dead centre.

While both biofuels lead to just slightly higher CO emissions than diesel at low boost pressure, they possess distinctly lower ones than diesel at high boost pressure. The same applies to the THC emissions. By analysing the results without EGR, i.e. highest NO_x level, it is also observable that both biofuels possess comparable NO_x emissions to diesel, which is exceptional for biofuels. Further, the determination of the soot emission shows that the solketal and tributyrin biofuel as well as diesel do not lead to soot formation at low boost pressure. The combustion of pure rapeseed oil, however, causes increased soot emissions. At higher boost pressure, the formulated biofuels show better results than diesel again.

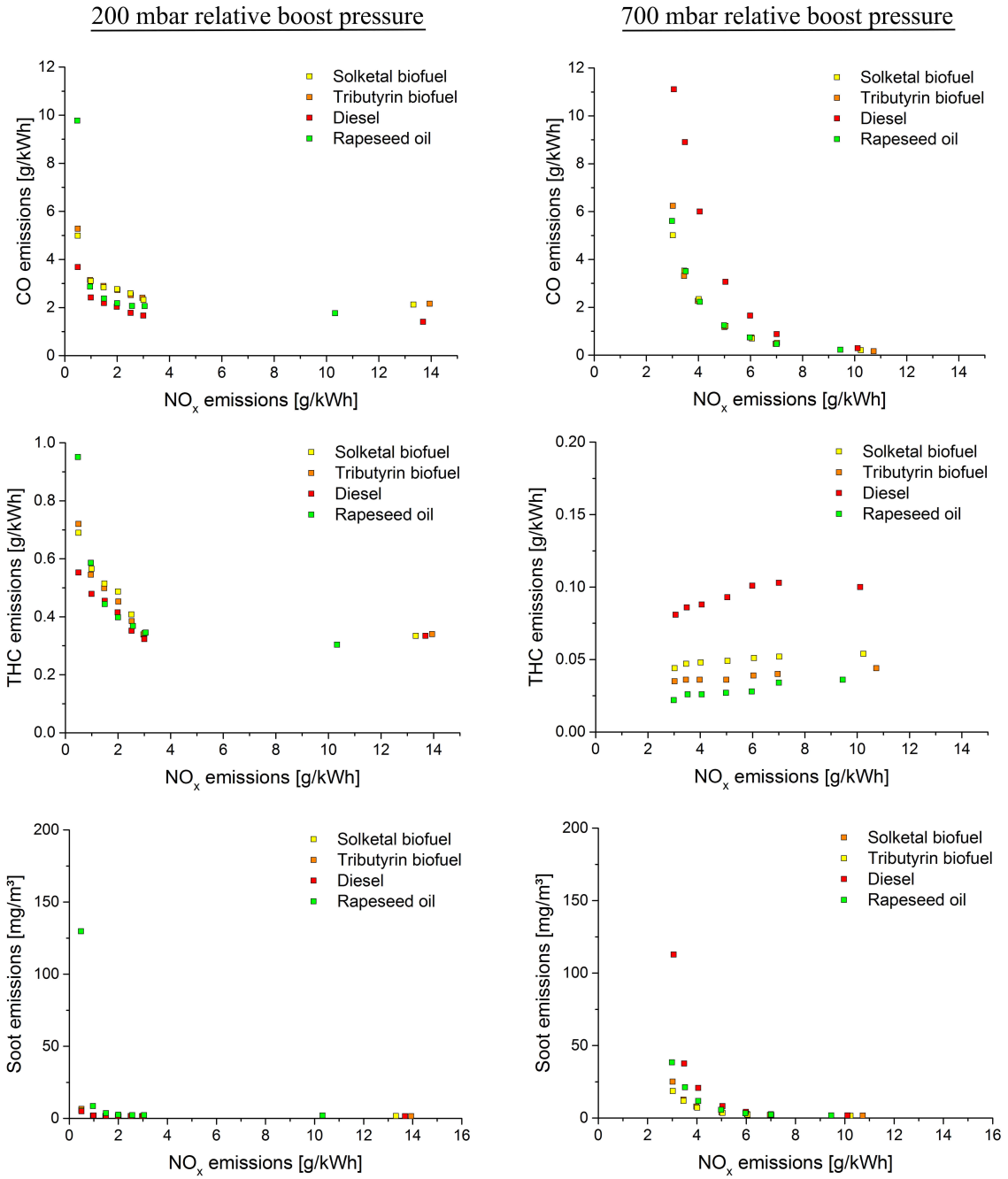

Figure 48: Results of the exhaust gas recirculation (EGR) measurements, in particular CO, THC and soot emissions versus NO_x emissions, of both formulated biofuels, diesel and rapeseed oil at 200 mbar (left) and 700 mbar (right) relative boost pressure.

The fuel consumption and the air/fuel balance during the EGR measurements are given in Fig. 49. The fuel consumption of the solketal and tributyrin biofuel is, analogously to other biofuels, slightly higher than diesel. This can be economically justified with its complete sustainability and therefore possible competitive price in the future, compared to

fossil fuels. The air/fuel balance, also known as λ, is nearly identical for every investigated liquid. The combustion processes, injection rates and heat release rates of both formulated biofuels, diesel and rapeseed oil are depicted in Fig. 50. The experiments are performed at low and medium load conditions as well as without and with the highest driveable EGR rate. At low load conditions and without EGR, diesel possesses the shortest combustion period, which could be addressed to a slightly improved mixture formation due to its low viscosity. The formulated biofuels show the same ignition delay as diesel and are very similar regarding the combustion properties. The combustion process of rapeseed oil, however, is strongly displaced due to its high viscosity and surface tension. Further, it has the longest combustion period, but the shortest ignition delay.

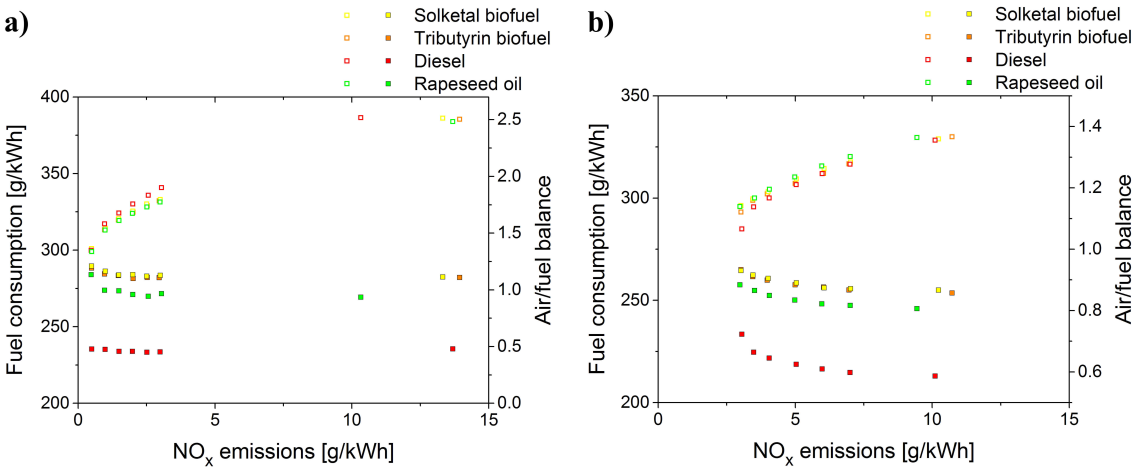

Figure 49: Fuel consumption and air/fuel balance of both formulated biofuels, diesel and rapeseed oil at 200 mbar (a) and 700 mbar (b) relative boost pressure. The unfilled points show the air/fuel balance of the samples, whereas the filled points indicate their consumption.

At complete EGR, i.e. distinctly reduced availability of oxygen in the combustion chamber, the formulated biofuels possess the shortest combustion period due to their high oxygen content. Because of the displacement of the heat release rate of diesel, rapeseed oil and diesel assimilate. Nevertheless, rapeseed oil still needs to be added at a later stage to provide the same performance compared to the other fuels. At medium load conditions and without EGR, rapeseed oil shows the shortest ignition delay again, leading to a reduced premixed combustion amount and an increased diffusive amount. Both formulated biofuels and diesel possess the same ignition delay and the same premixed combustion amount. Due to the highest driveable EGR rate, the heating processes flatten considerably. The burnout properties of the fuels assimilate, as the heating process of diesel is now also strongly displaced, because of the missing oxygen content. It is further necessary to mention that the injection period of all biofuels is increased due to the lower heating value and thus higher injection mass. This distinctly influences the diffusive combustion and burnout.

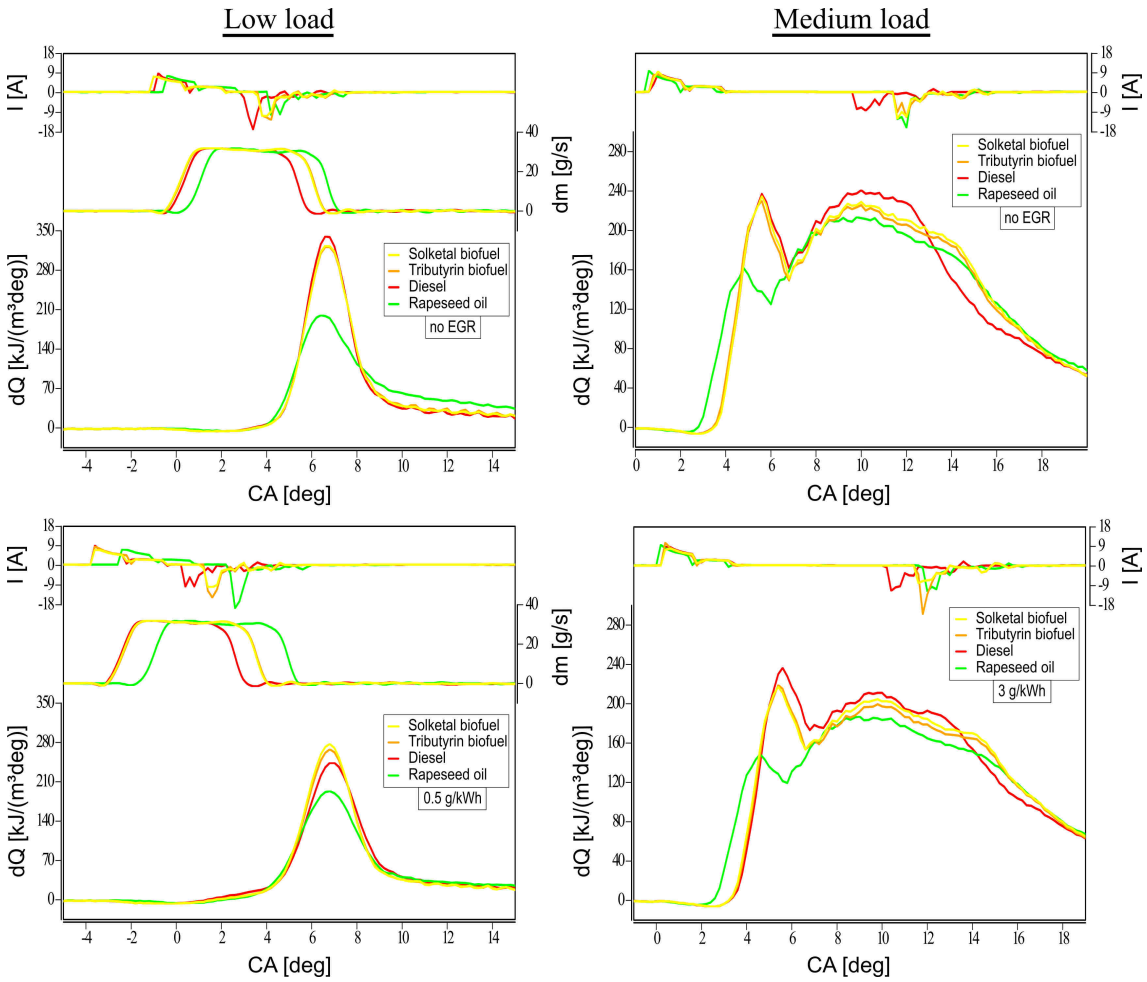

Figure 50: Combustion processes, injection rates and heat release rates versus crankshaft angle (CA) of both formulated biofuels, diesel and rapeseed oil at low load, i.e. 1500 rpm engine speed, 80 Nm torque, 200 mbar relative boost pressure and 100 MPa injection pressure (left), and medium load conditions, i.e. 1500 rpm engine speed, 240 Nm torque, 700 mbar relative boost pressure and 140 MPa injection pressure (right), without EGR (top) and with the highest driveable EGR (bottom).

These results show that the formulated biofuels can not only be used in an unmodified up-to-date diesel engine, but also possess very promising combustion, emission and ignition properties. Further, the presence of high amounts of vegetable oil as well as glycerol derivatives does not lead to any drawbacks that would make the formulations inappropriate for future biofuels [279, 280].

4.1.2.3 Oxidative stability

Due to the presence of a hydrophilic glycerol derivative like solketal within this biofuel concept, the implementation of natural antioxidants into these mixtures seems possible. As already explained in sections 2.1.3.3 and 2.1.5.2, the effective replacement of synthetic and toxic antioxidants by natural ones depends on their compatibility. Fig. 51 shows the solubilities of several natural antioxidants in solketal. To also obtain information on the hydrophilicity of solketal, the same solubility tests are performed with ethanol, for comparison.

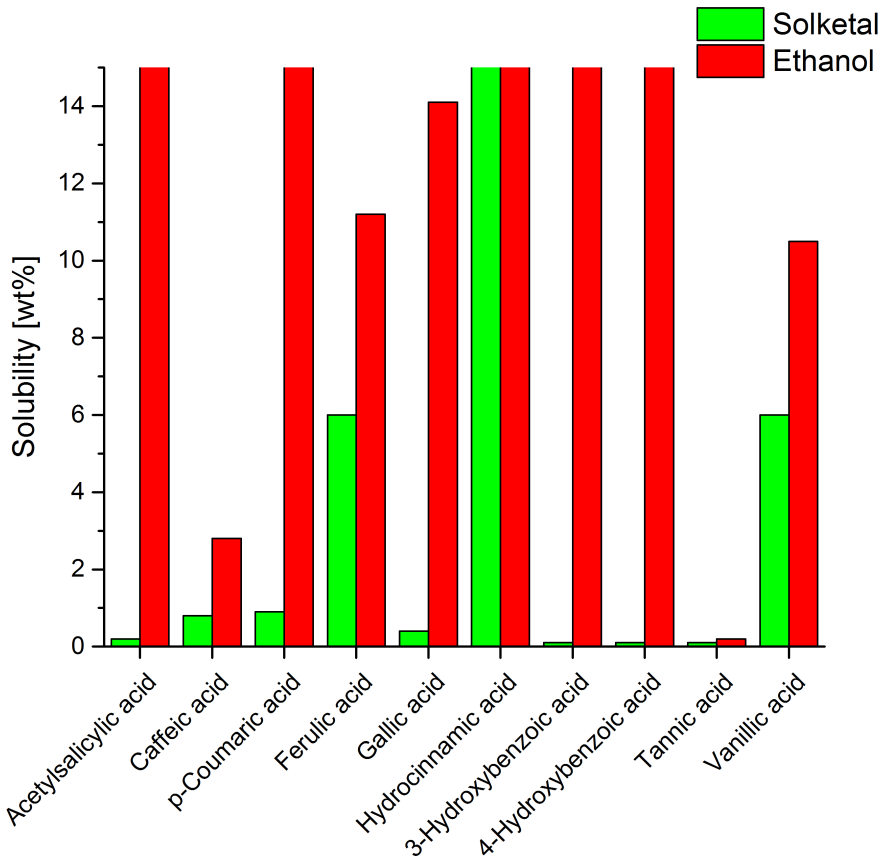

Figure 51: Solubilities of different natural antioxidants in either solketal or ethanol at 25 °C.

Even though the solubilities of the antioxidants are given in wt%, whereas they will be used in a three-digit ppm scale in the final formulations, acetylsalicylic acid, 3-hydroxybenzoic acid, 4-hydroxybenzoic acid and tannic acid are insufficiently soluble in solketal. While less than 1 wt% of caffeic, *p*-coumaric and gallic acid can be solubilised in solketal, about 6 wt% of ferulic as well as vanillic acid and even more than 15 wt% of hydrocinnamic acid are soluble in the glycerol derivative. Concerning every investigated antioxidant, much

higher amounts are soluble in ethanol, except for tannic acid. This indicates that on the one hand, solketal is hydrophilic enough to solubilise specific, natural antioxidants, but on the other hand, it is more hydrophobic than ethanol. This could in turn mean that no associated miscibility problems will occur, when adding the antioxidants into the biofuel formulations.

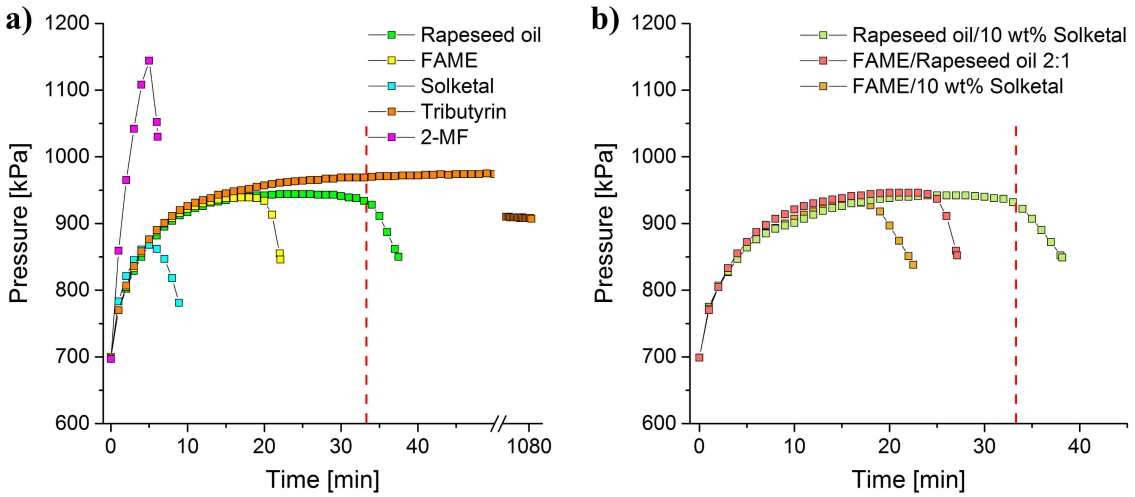

Figure 52: RapidOxy measurements of the single, pure components of both formulated biofuels (a) and binary mixtures of them (b) according to the standard DIN EN 16091. Every sample, for which the pressure dropped by less than 10% compared to its maximum value after 33.3 min, fulfils the standard illustrated by the red dashed line [174].

To be able to estimate the general stability towards oxidation of the single components of the biofuel formulations, RapidOxy measurements were performed with these pure substances (see Fig. 52a). While pure rapeseed oil fulfils the standard, indicated by the red dashed line, FAME is oxidised distinctly earlier, as expected. Especially solketal's sensitivity towards oxidation surprises, since it is oxidised nearly as fast as 2-MF, which was chosen as furan derivative, for comparison. Tributyrin, however, is insensitive towards oxidation. The jump in the measuring curve of tributyrin can be explained by the necessary break of the time scale within this experiment. This figure further shows that especially solketal and FAME are prone to oxidation. To gain even more information on the oxidative stability of these components in advance, the results of all possible binary mixtures of rapeseed oil, FAME and solketal are given in Fig. 52b. While the addition of rapeseed oil to FAME just leads to the expected increase of the oxidative stability, the presence of 10 wt% of solketal in rapeseed oil as well as FAME does not negatively affect the obtained results. In particular, the measured induction times of mixtures of either rapeseed oil or FAME with solketal are identical to the results of the pure components. This indicates that solketal's sensitivity towards oxidation is negligible, once it is used in mixtures.

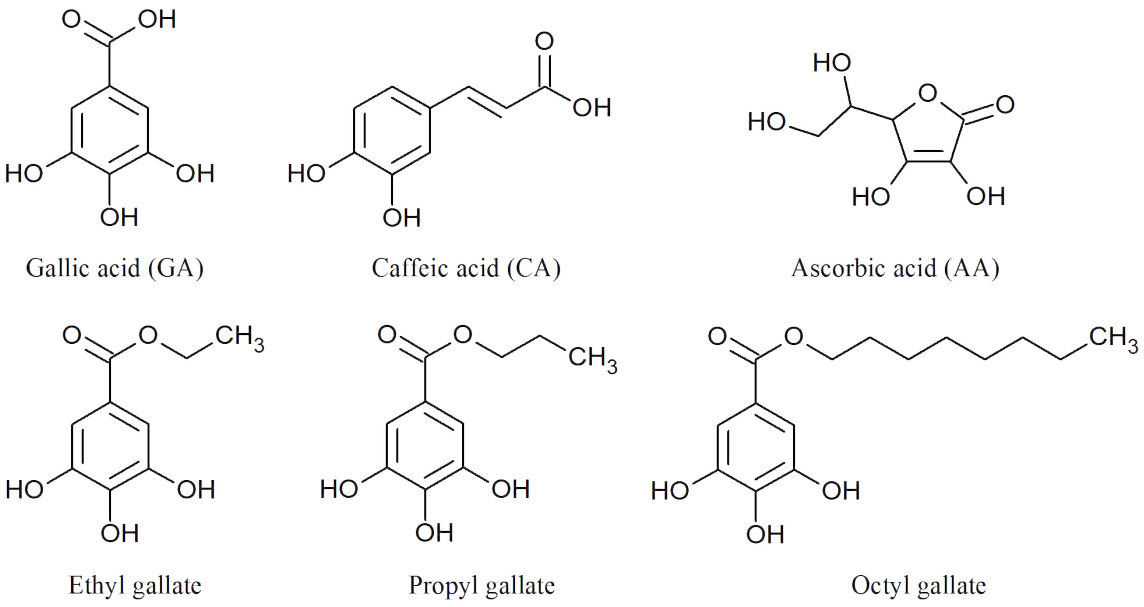

Figure 53: Selection of natural antioxidants that led to the best results concerning the oxidative stability of the formulated biofuels.

Even if every natural antioxidant of Fig. 51 was investigated by RapidOxy experiments, Fig. 53 just shows those compounds that led to the best results. The comparison of Fig. 51 with Fig. 53 makes clear that especially the hydrophilic antioxidants, i.e. caffeic and gallic acid, are promising for these formulations. The less hydrophilic behaviour of vanillic and ferulic acid can be explained by the *ortho*-position of the methoxy group in these molecules. Due to the formation of an intramolecular hydrogen bond, the hydrophilicity and therefore the effectiveness to increase the oxidative stability of hydrophobic mixtures like biofuels is decreased [285]. Concerning the different gallates, solubility tests were omitted, since they are more hydrophobic than gallic acid and thus better soluble in solketal.
Before measuring the biofuel formulations with natural antioxidants, the effectiveness of the synthetic antioxidants hydroquinone (HQ) and 2-*tert*-butylhydroquinone (TBHQ) was investigated as reference (see Fig. 54a). For these experiments, the solketal biofuel, shown in Table 10, was used. Regarding the results of the solketal system, it becomes obvious that additional antioxidants are indispensable to fulfil the standard. By adding 0.2 wt% of HQ, one of its derivatives or a mixture of them, the oxidative stability of the biofuel is distinctly increased, with TBHQ being much less effective than HQ. 0.2 wt% of antioxidants, however, are already very high amounts for fuel formulations and can only be justified by the currently low prices of these toxic substances. Therefore, another measurement with 160 ppm of HQ was performed, since this scale is also used for the subsequent investigations with natural antioxidants. Surprisingly, 160 ppm of HQ are not enough to fulfil the standard.

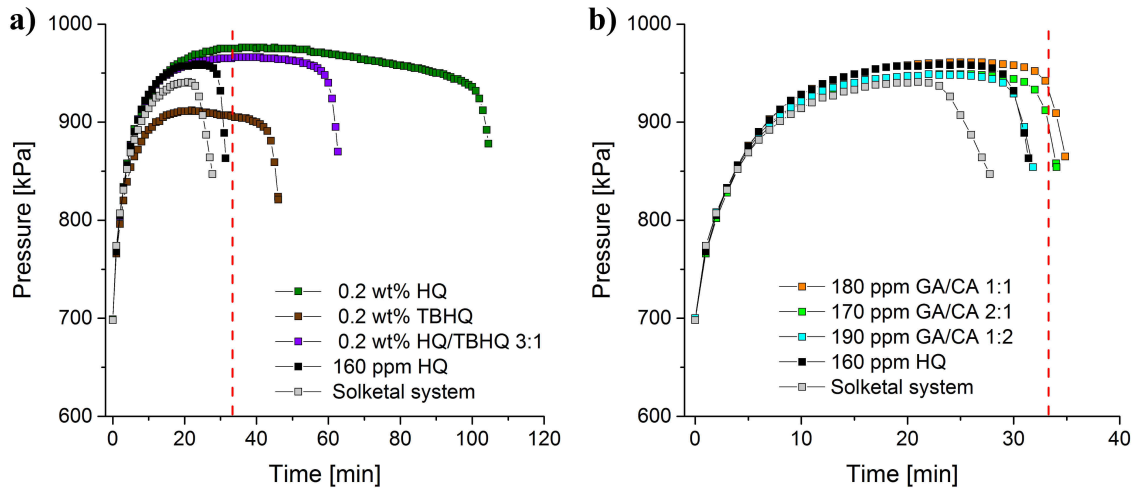

Figure 54: RapidOxy measurements of the solketal biofuel with the synthetic antioxidants hydroquinone (HQ) and 2-*tert*-butylhydroquinone (TBHQ) in different amounts and mass ratios (a) and with mixtures of the natural antioxidants gallic acid (GA) and caffeic acid (CA) in different mass ratios (b). The experiments were performed according to the standard DIN EN 16091. Every sample, for which the pressure dropped by less than 10% compared to its maximum value after 33.3 min, fulfils the standard illustrated by the red dashed line [174].

As it was, so far, not possible to use natural, hydrophilic antioxidants in biofuel formulations, the process of implementing them is crucial. For that, the antioxidants were solubilised in the glycerol derivatives first, before adding this mixture to the other fuel components. In this step, the difference between solketal and tributyrin is decisive, since solketal is more hydrophilic than tributyrin. Therefore, each biofuel system is able to solubilise different antioxidants. While gallic and caffeic acid are suitable for the solketal biofuel, the more hydrophobic alkyl gallates have to be used for the tributyrin biofuel. After several solubility and RapidOxy experiments with single natural antioxidants as additives for the solketal system, no biofuel formulation was able to fulfil the standard. In the next step, mixtures of the two most effective, natural antioxidants, gallic (GA) and caffeic acid (CA), were investigated according to the synergistic effect, when using two different antioxidants simultaneously (see also section 2.1.3.3) [176, 185]. Fig. 54b shows that there is, indeed, a synergistic effect between GA and CA, leading to a compliance with the standard with only 170 ppm and a mass ratio of either 1:1 or 2:1 of GA/CA for the solketal system. The amount of antioxidants slightly differs, as they clump easily. Nevertheless, the comparison of the induction times with 160 ppm HQ and 180 ppm GA/CA with a mass ratio of 1:1 shows that the natural mixture is nearly twice as effective as the synthetic antioxidant, which cannot be explained by the additional 20 ppm. In general, this means that the amphiphilic properties of solketal enable the usage of hydrophilic, natural antioxidants in biofuels with vegetable oils as one of the main components. Further, they are competitive with the highly toxic hydroquinones regarding their effectiveness.

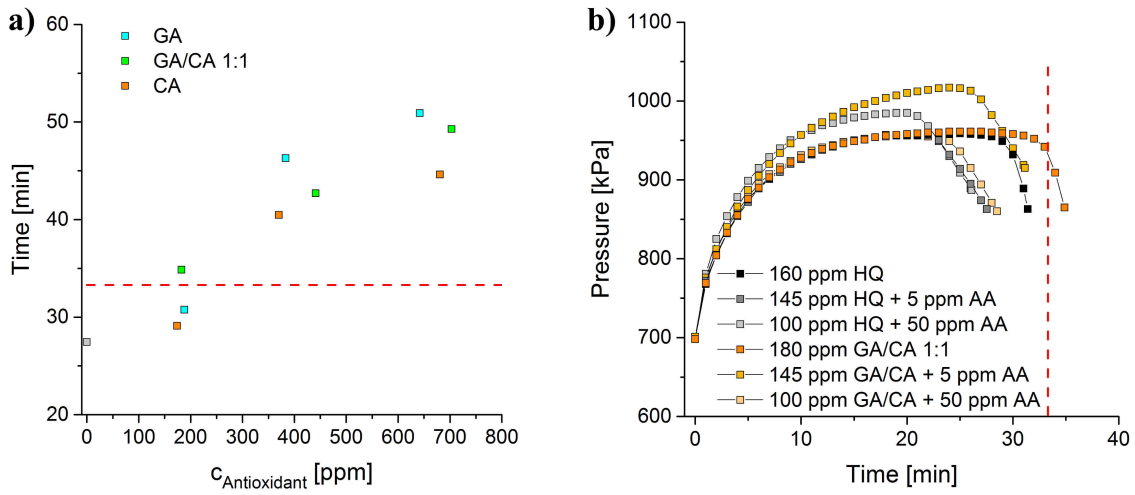

Figure 55: Measured induction times of the solketal system with the natural antioxidants gallic acid (GA) and caffeic acid (CA) as single components and as mixture with a mass ratio of 1:1 versus the concentration of the antioxidants in the mixture (a). RapidOxy measurements of the solketal biofuel with the synthetic antioxidant hydroquinone (HQ) and the natural antioxidants GA and CA as mixture with a mass ratio of 1:1 (b). To both investigated systems, 5 as well as 50 ppm of ascorbic acid (AA) were added and their influence on the oxidative stability of the mixture was examined. The experiments were performed according to the standard DIN EN 16091. Every sample, for which the pressure dropped by less than 10% compared to its maximum value after 33.3 min, fulfils the standard illustrated by the red dashed line [174].

To gain more information on the influence of the amount of used antioxidants on the stability of the biofuel, Fig. 55a shows the concentration-dependent induction times of the solketal system with GA and CA as single components and as mixture with a mass ratio of 1:1. As expected, higher concentrations lead to a better oxidative stability, with the 1:1 mixture being the most effective at low concentrations and pure gallic acid at higher concentrations. Since these natural antioxidants are much more expensive than the synthetic ones, the influence of ascorbic acid (AA), i.e. vitamin C, as alternative, which is the cheapest, natural antioxidant, was also investigated (see Fig. 55b). For that, 5 as well as 50 ppm of AA were added alternatively to the natural antioxidant mixture and to HQ in the solketal system. Fig. 55b shows that the higher the amount of AA in the antioxidant mixture, the lower the oxidative stability of the biofuel. Irrespective of the antioxidants, the presence of 5 ppm AA is already enough to distinctly reduce the stability towards oxidation. It is also important to emphasise that AA itself is insoluble in biofuels. Just due to the presence of hydrophilic antioxidants like GA or CA, AA becomes compatible with these formulations. These results explain the aforementioned low concentration of AA in the commercially sold, natural antioxidant mixture inaAOX1 from inaCHEM GmbH (see Table 3). While its small amount was presumed to be reasonable due to its low effectiveness, it is now obvious that higher amounts significantly decrease the overall oxidative stability of the mixture.

Since none of the investigated antioxidants of the solketal biofuel were either soluble or effective in the tributyrin system, alkyl gallates were used instead. Fig. 56 shows the influence of these soluble, less hydrophilic gallic acid esters on the oxidative stability of the tributyrin biofuel. It is obvious that every examined alkyl gallate is suitable for this application. Concerning the propyl gallate, the amount added to the formulation was varied to see the influence on the oxidative stability of the mixture. As expected, the higher the concentration of the antioxidant, the better the stability towards oxidation. These results show that, indeed, the presence of the glycerol derivatives enables the usage of natural, hydrophilic antioxidants in these biofuel formulations, which are even more effective than the synthetic and highly toxic hydroquinones [279, 280].

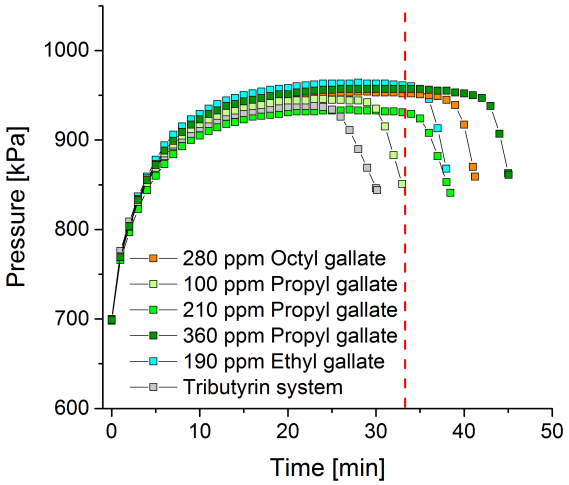

Figure 56: RapidOxy measurements of the tributyrin biofuel with different alkyl gallates as natural antioxidants. The experiments were performed according to the standard DIN EN 16091. Every sample, for which the pressure dropped by less than 10% compared to its maximum value after 33.3 min, fulfils the standard illustrated by the red dashed line [174].

4.1.2.4 New concept of water implementation for NO_x reduction

Before actually investigating the potential of glycerol derivatives to implement water into biofuel formulations, the system consisting of rapeseed oil, FAME and an aqueous mixture of 96 wt% of ethanol was examined to see the influence of small amounts of water on the miscibility in these systems (see Fig. 57). The comparison of the phase diagram with the one with pure ethanol in Fig. 41 shows that the biphasic region as well as the miscibility gap between rapeseed oil and the ethanol/water mixture is distinctly increased. The same applies to the low-temperature phase behaviour along path ***b*** compared with Fig. 44, with the presence of small amounts of water increasing the cloud point by several degrees. DLS measurements were also performed along path ***b***, but did not show any correlation functions. These results already indicate that hydrophobic biofuels are very sensitive to the presence of water, which in turn explains the usage of high amounts of surfactants in common hydrofuels (see also section 2.1.4.2).

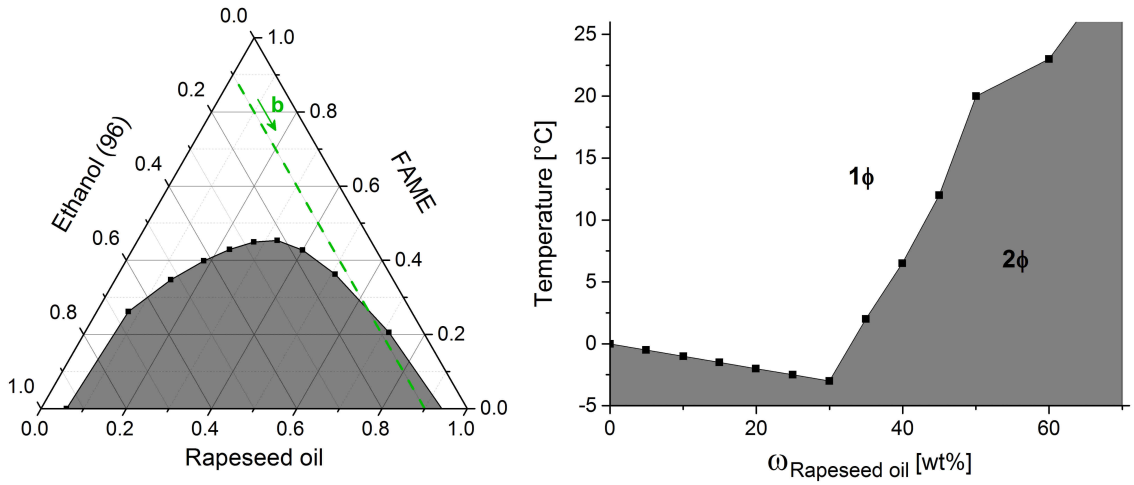

Figure 57: Left: Ternary phase diagram consisting of rapeseed oil, FAME and an aqueous mixture with 96 wt% of ethanol at 25 °C. Further investigations are performed along path ***b***. The values are given in mass fractions. Right: Cloud points versus the weight percentage of rapeseed oil for mixtures along path ***b***. The darkened areas represent the biphasic region of the system.

In the next step, the influence of small amounts of water on the solketal biofuel was investigated (see Fig. 58). Similarly to the system with an aqueous mixture of 96 wt% of ethanol, the ternary phase diagram of the solketal biofuel with an aqueous mixture of 96 wt% of solketal possesses a distinctly increased biphasic region. While the aqueous mixture is completely immiscible with rapeseed oil, there is also a miscibility gap with FAME. To gain first information on the presence of a surfactant-free microemulsion (SFME) in this system, DLS and SLS experiments were performed close to the biphasic region. By indicating a SFME, one could also expect the presence of microexplosions during combustion,

which is one of the main advantages of a hydrofuel. The obtained autocorrelation functions are on the one hand well defined, but at the same time do not lead to high correlation coefficients. A possible reason for this observation could be the typically highly dynamic processes of SFMEs. Since the resolution of these light scattering techniques is in the nanosecond scale, more precise SAXS or even neutron scattering experiments could be more suitable. With the autocorrelation functions being well defined, the size of the aggregates was calculated, assuming spherical geometry. The obtained radii are in the range of 4 to 7 nm, but as the results of the SLS measurements are similar to or even higher than the ones of the DLS experiments, the shape of the aggregates seems to be different.

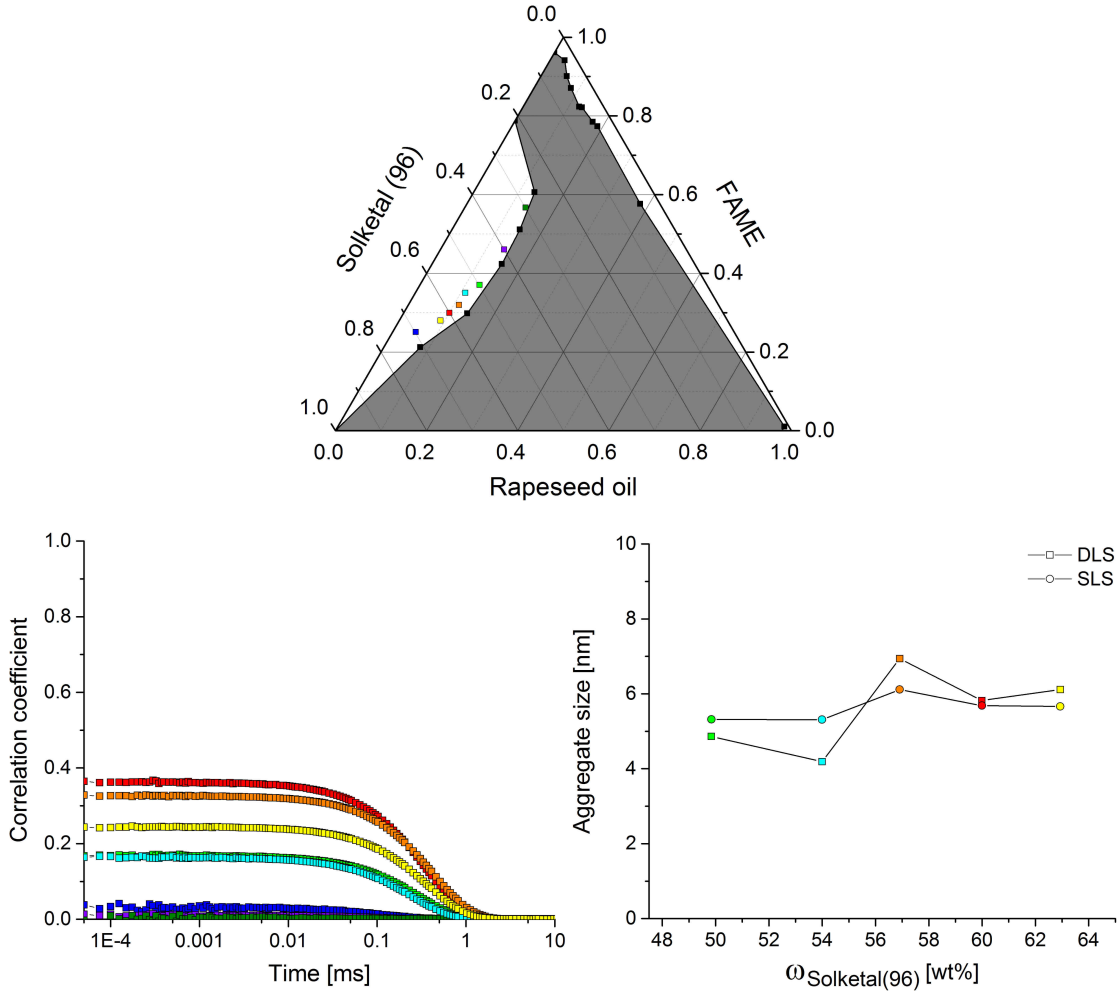

Figure 58: Top: Ternary phase diagram consisting of rapeseed oil, FAME and an aqueous mixture with 96 wt% of solketal at 25 °C. The darkened area represents the biphasic region of the system. The values are given in mass fractions. Bottom: Time-dependent autocorrelation functions obtained by DLS experiments at 25 °C and the calculated radii of the respective aggregates within the DLS and SLS measurements versus the weight percentage of rapeseed oil assuming spherical geometry. The colours of the measuring points correspond to the coloured compositions of the phase diagram.

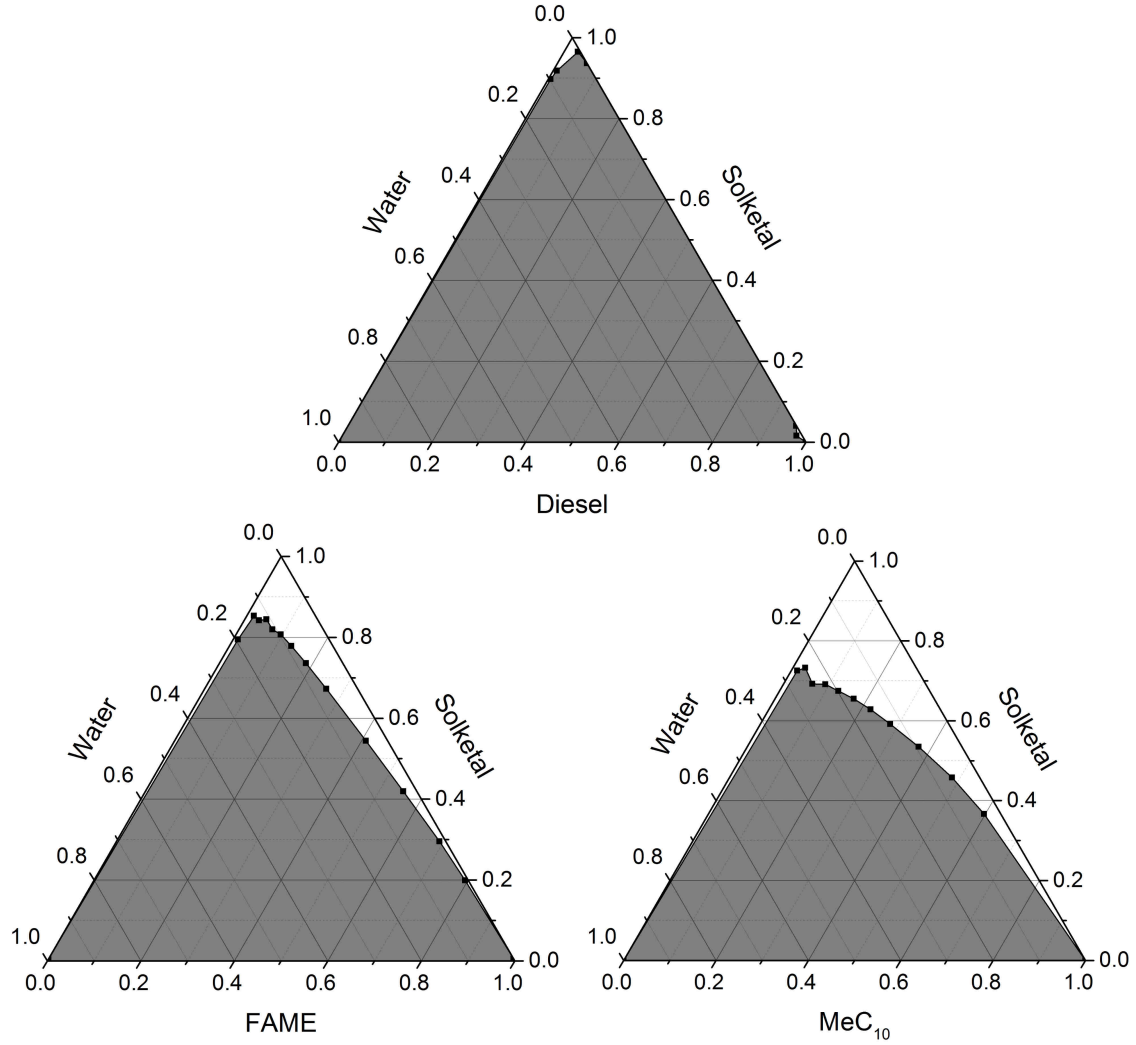

Figure 59: Ternary phase diagrams consisting of solketal, water and either diesel, FAME or MeC_{10} as hydrophobic fuel component at 25 °C. The darkened areas represent the biphasic regions of the systems. The values are given in mass fractions.

In general, the phase diagram of this system shows that water cannot be implemented into biofuels satisfactorily in the presence of very hydrophobic biofuels like rapeseed oil. To get closer to applicable hydrofuel formulations, mixtures consisting of water, solketal and a fuel component, which is less hydrophobic than rapeseed oil, were investigated (see Fig. 59). In these systems, the amphiphilic properties of solketal are essential to increase the miscibility of water with the fuel. As shown in Fig. 59, water and diesel are completely immiscible. By adding at least 90 wt% of solketal, the mixtures finally turn monophasic. Further, there is a very small monophasic region for mixtures consisting of about 1 wt% of water as well as solketal and 98 wt% of diesel. The comparison of the phase diagrams with either FAME or MeC_{10} instead of diesel as fuel component illustrates the influence of the hydrophobicity of the fuel on the size of the monophasic region of the mixtures. Replacing

diesel by FAME, the monophasic region distinctly increases. The lower the amount of water in mixtures with FAME, the less solketal is necessary. By using MeC_{10} instead of FAME, the monophasic area even further increases with the same tendency towards mixtures with low amounts of water. These results already show that the hydrotropy of solketal, indeed, enables the implementation of at least a few wt% of water into biofuels.

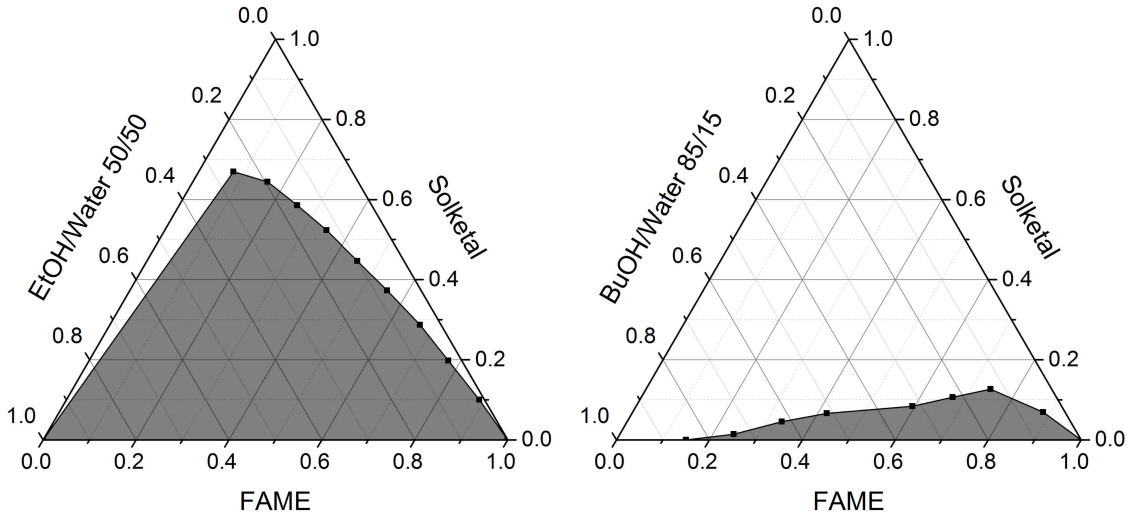

Figure 60: Ternary phase diagrams consisting of solketal, FAME and either a mixture of ethanol (EtOH) and water with a mass ratio of 50/50 or of butanol (BuOH) and water with a mass ratio of 85/15 at 25 °C. The darkened areas represent the biphasic regions of the systems. The values are given in mass fractions.

Nevertheless, since typical biofuel formulations with glycerol derivatives will not exceed amounts of about 10 wt% of the derivative, more hydrophilic substances are additionally necessary to increase the compatibility of water. Therefore, the phase diagrams consisting of solketal, FAME and either a mixture of ethanol and and water with a mass ratio of 50/50 or of butanol and water with a mass ratio of 85/15 are further examined. While the presence of ethanol as mixing agent for water just slightly increases the monophasic region of the system, the presence of butanol leads to a considerable monophasic area. Even mixtures with about 10 wt% of solketal are viable in this system. Since butanol is a very promising biofuel compound and currently intensively investigated by many research groups, this new possibility to implement water into biofuels becomes even more industrially interesting [280, 286].

4.2 Further applications of glycerol derivatives

4.2.1 Extraction systems based on glycerol derivatives

As explained in chapter 2.2.1, the potential of glycerol derivatives as alternative extracting agents was also investigated within this thesis. At first, the extraction systems and settings to extract α-tocopherol from rapeseed oil with different glycerol derivatives were determined and optimised. The subsequent extractions, especially with solketal as extracting agent, led to promising results, as shown via HPLC (see also section 3.2.1.3). Due to an optimised liquid-liquid extraction step with water afterwards, the antioxidant could be isolated from the glycerol derivative.

4.2.1.1 Antioxidant extraction from vegetable oils

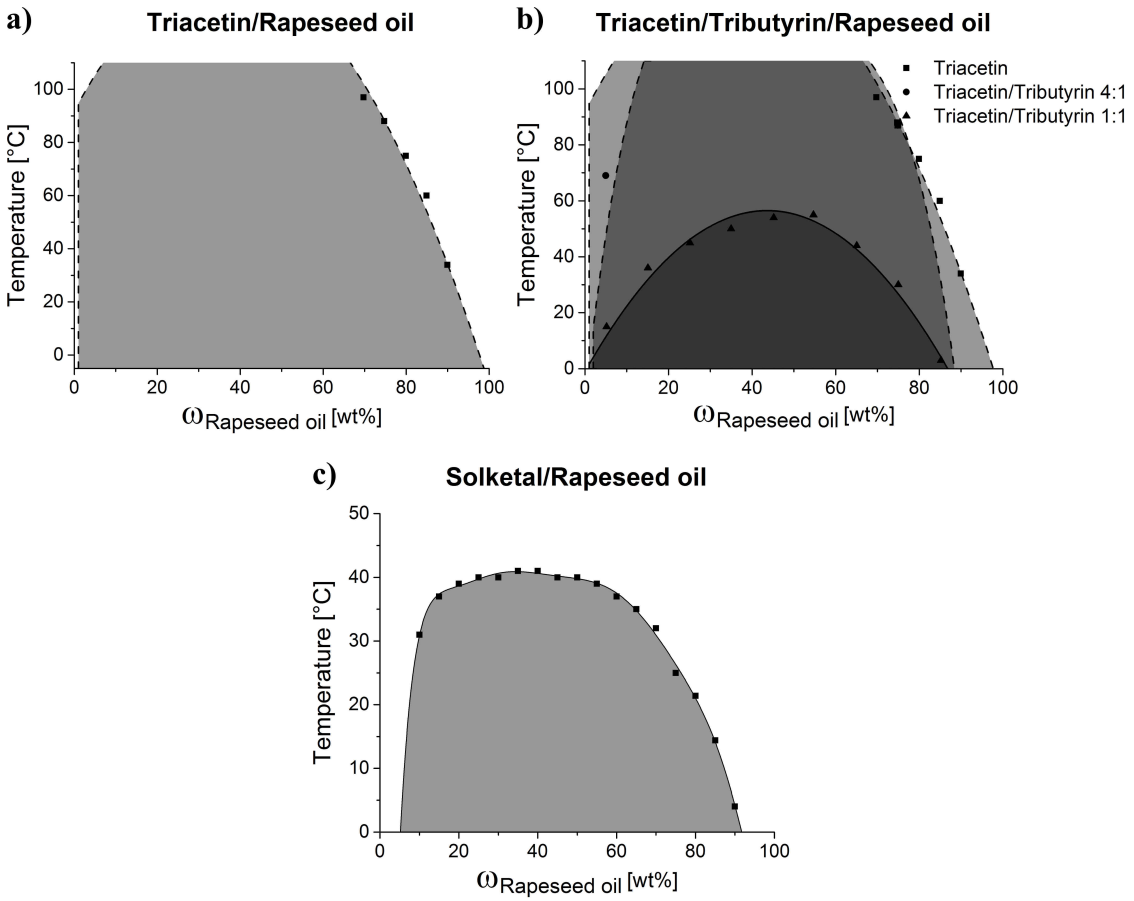

Figure 61: Phase separation temperatures versus the weight percentage of rapeseed oil in the binary and ternary systems consisting of the vegetable oil and either triacetin (a), mixtures of triacetin and tributyrin with different mass ratios (b) or solketal (c). The darkened areas represent the biphasic regions of these systems.

When developing new extraction methods, the miscibility behaviour of every component in the extraction system must be examined in detail first. To this purpose, mixtures consisting of rapeseed oil and different glycerol derivatives as well as combinations of them were investigated, according to the binary system of ethanol and rapeseed oil in Fig. 32. The binary phase diagram of the food approved triacetin and rapeseed oil is shown in Fig. 61b. In general, high temperatures are necessary to obtain monophasic mixtures in this system. While samples with high amounts of rapeseed oil become monophasic within the investigated temperature range of 20-100 °C, the remaining compositions are still biphasic. Since high temperatures facilitate the oxidation processes and thus lead to the degradation of the extractant, i.e. lower yield, this system cannot be used without further optimisations. With tributyrin showing no miscibility gap with rapeseed oil even at −10 °C, different mixtures of triacetin and tributyrin were examined (see Fig. 61b). In particular, the phase diagrams with triacetin/tributyrin mixtures with a mass ratio of 4:1 as well as 1:1 were compared with the triacetin/rapeseed oil system. As expected, the higher the amount of tributyrin, the lower the phase separation temperatures of the samples. In the case of a 1:1 mass ratio, these temperatures are between 0 and 55 °C, which are common extraction temperatures for industrial processes. The binary phase diagram consisting of solketal and rapeseed oil, depicted in Fig. 61c, possesses the most suitable phase separation temperatures of the investigated systems. With these temperatures being between 30 and 40 °C even at low amounts of rapeseed oil, which is important for the actual extraction, no further optimisations are necessary for this system. Concerning the developed biofuel concept, the extraction of the valuable α-tocopherol with solketal could be realised within the same facilities before the biofuel formulation, as solketal is added to the vegetable oil anyway.

To decrease the phase separation temperatures of the triacetin/rapeseed oil system, the influence of different, also food approved Tween and Span surfactants was examined. At first, the single surfactants were added to a triacetin/rapeseed oil as well as an ethanol/rapeseed oil mixture as reference with a mass ratio of 1:1. Since very high amounts of surfactants, partially more than 80 wt%, were necessary to obtain a monophasic mixture at room temperature, combinations of Tween and Span were investigated. With Span being more hydrophobic than Tween, it is evident that Span is more suitable for this system and should thus be used in higher amounts than Tween. After screening possible surfactant combinations in different mass ratios, a mixture of Tween 80 and Span 80 with a mass ratio of 1:4 showed the highest efficiency in decreasing the phase separation temperatures of both systems. Therefore, the influence of 5, 10 and 15 wt% of this surfactant mixture on the binary phase diagrams of rapeseed oil and either ethanol or triacetin was investigated. Fig. 62a shows that the higher the amount of surfactants added to mixtures consisting of ethanol and a maximum of 70 wt% of rapeseed oil, the lower their phase

separation temperatures. Above 70 wt% of rapeseed oil, these temperatures are increased. Unfortunately, these amounts of surfactants do not significantly change the phase separation behaviour of the system triacetin/rapeseed oil (see Fig. 62b). Just for very high amounts of rapeseed oil, the phase separation temperatures are reduced with increasing amount of surfactants. For the sake of completeness, 5 wt% of the surfactant mixture were also added to the solketal/rapeseed oil system (see Fig. 62c). Already in presence of this small amount of surfactants, the phase separation temperatures are reduced close to room temperature. Even if the subsequent extraction experiments with solketal are performed without surfactants, this result at least shows that the extraction temperature can be precisely adjusted by adding this surfactant mixture.

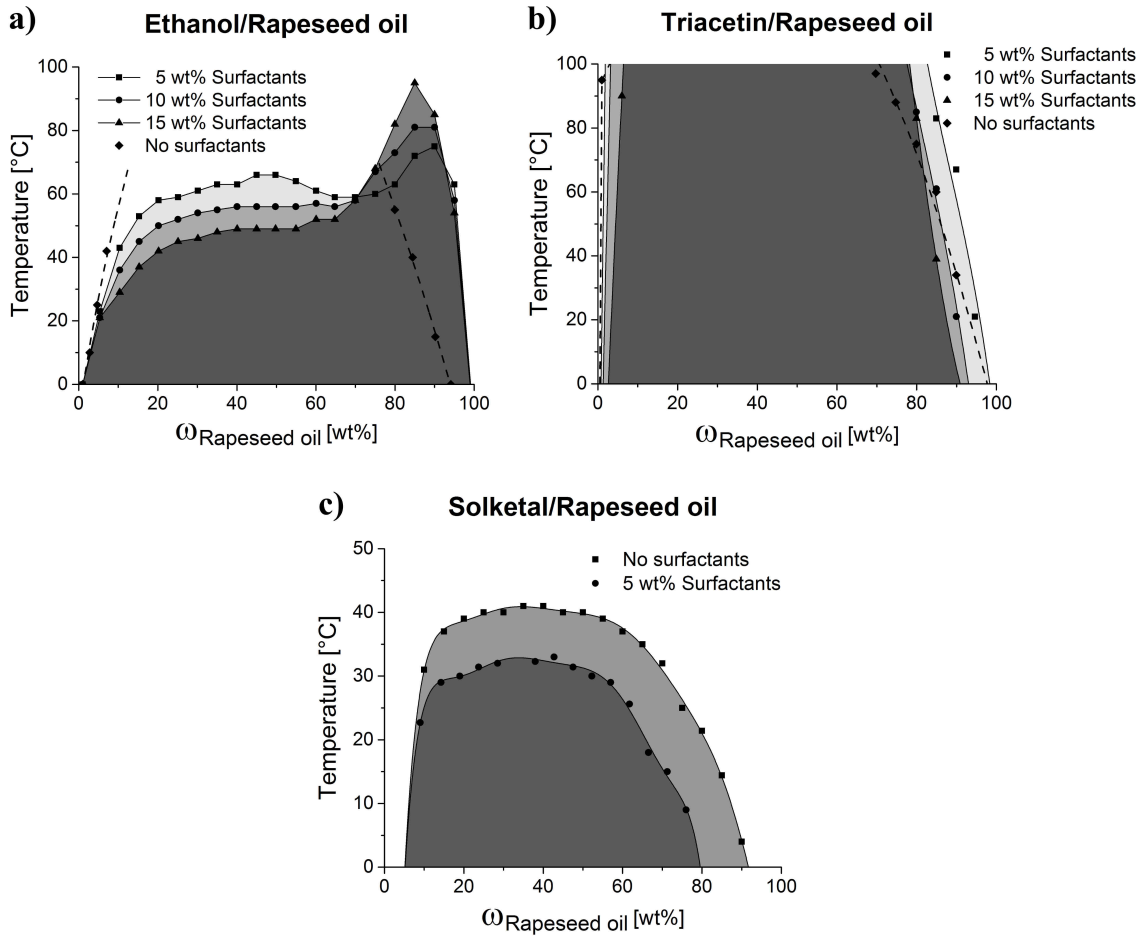

Figure 62: Influence of different amounts of a surfactant mixture consisting of Tween 80 and Span 80 with a mass ratio of 1:4 on the phase separation temperatures of binary mixtures composed of rapeseed oil and either ethanol (a), triacetin (b) or solketal (c). The darkened areas represent the biphasic regions of these systems.

Before investigating the extraction processes, the HPLC chromatograms of the single components, used within these experiments, were necessary. Fig. 63 shows that, with the chromatography settings described in section 3.2.1.3, α-tocopherol possesses a huge absorption peak at about 11 min. This peak is distinctly separated from any other signal of the different components in the system. While triacetin and ethanol do not show any absorption, the experiments with the surfactant mixture as well as pentanol just lead to small signals within the first minutes. The chromatogram of rapeseed oil shows two well defined, but small peaks. The first signal between 9 and 10 min refers to the absorption of the fatty acid chains of rapeseed oil, whereas the second one at about 11 min indicates the α-tocopherol content of this vegetable oil. Even if the conditions of the triacetin system were conceivably bad concerning the intended extraction experiments, further investigations were still performed, since this system would allow applications in food industry.

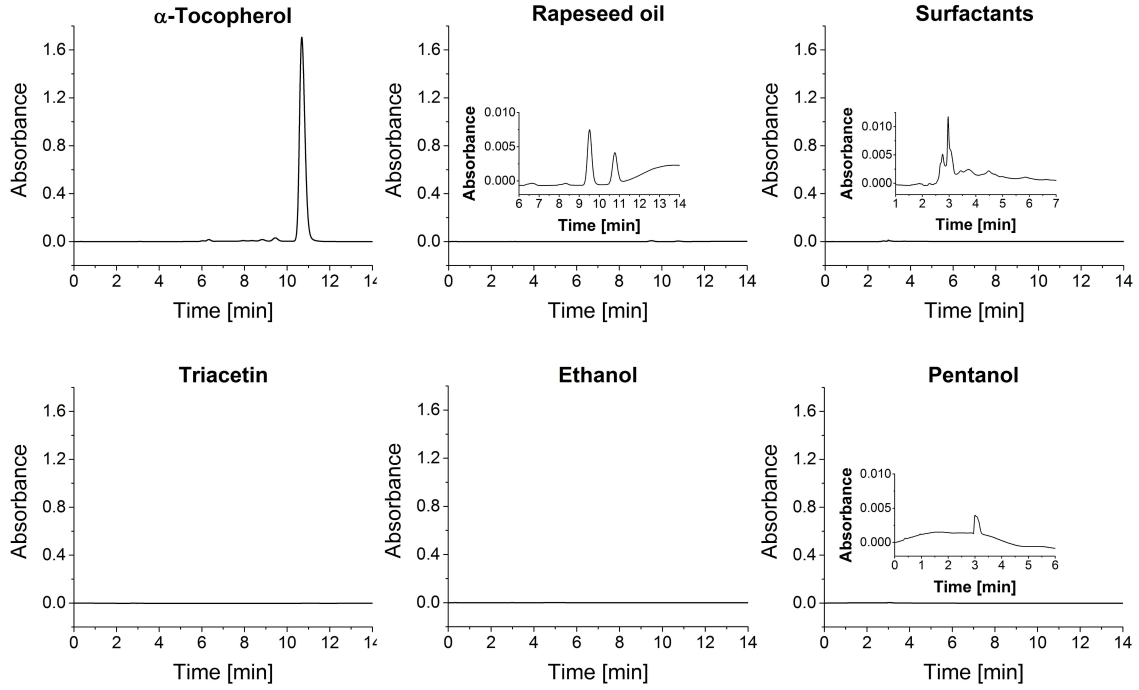

Figure 63: HPLC chromatograms of the single components used within the extraction experiments.

Table 13 shows the compositions of the prepared samples for the extraction experiments with triacetin (A) and ethanol (E). Due to limited possibilities because of the phase diagram, samples with very high amounts of rapeseed oil, in particular 80, 85 and 90 wt%, were used in the triacetin system as well as in the ethanol system for comparison. To all samples except A5, 0.1 wt% of α-tocopherol were added to the biphasic mixtures to facilitate the detection afterwards. Further, 10 wt% of the surfactant mixture were used for the samples A4 and E1-3 to increase the miscibility of the systems and to examine

the influence of the surfactants on the extraction process. All samples were heated up to 100 °C for one hour to become monophasic, with the ethanol mixtures being additionally sealed with parafilm, and cooled down to room temperature over night.

Table 13: Compositions of the investigated samples of the triacetin (A) as well as ethanol (E) extraction system. The surfactant mixture consists of Tween 80 and Span 80 with a mass ratio of 1:4.

Sample	$\omega_{\textbf{Rapeseed oil}}[\textbf{wt\%}]$	$\omega_{\alpha\textbf{-Tocopherol}}[\textbf{wt\%}]$	$\omega_{\textbf{Surfactants}}[\textbf{wt\%}]$
A1	80	0.1	–
A2	85	0.1	–
A3	90	0.1	–
A4	85	0.1	10
A5	85	–	–
E1	80	0.1	10
E2	85	0.1	10
E3	90	0.1	10
E4	85	0.1	–

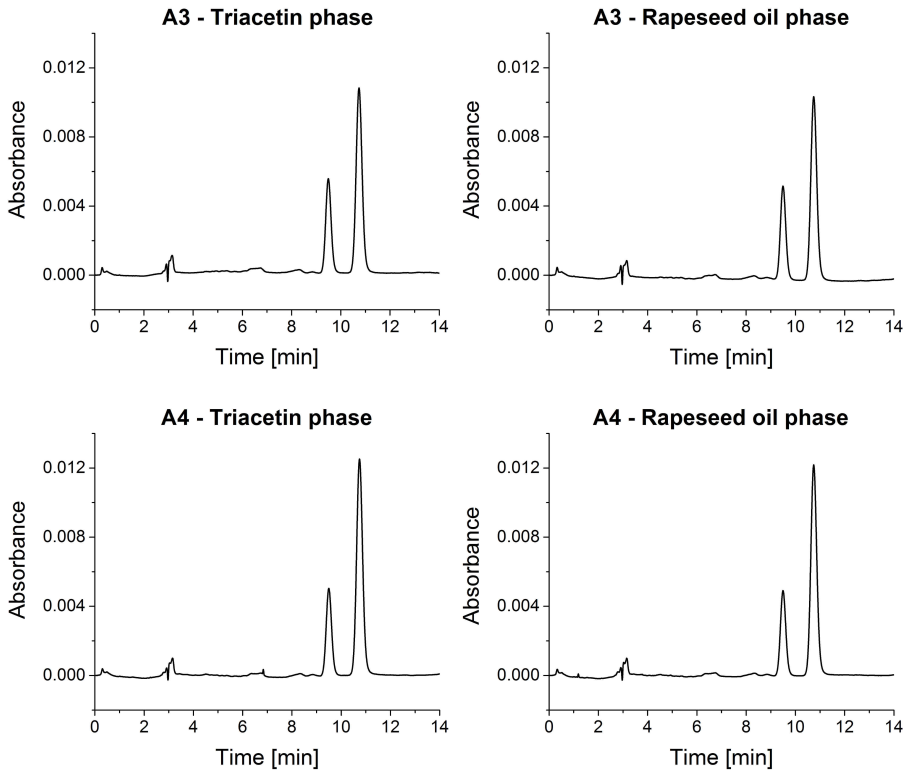

Figure 64: HPLC chromatograms of the separated triacetin as well as rapeseed oil phase of the samples A3 and A4.

This new phase separation is supposed to be the extraction process of the antioxidant. Since α-tocopherol possesses a rather hydrophilic part, the interactions with the extracting agent could be strong enough during the monophasic state to be extracted from the vegetable oil. Fig. 64 shows the best results of these experiments. Since cooling down to room temperature over night did not lead to a defined phase separation and thus sampling was very difficult, the rapeseed oil peak is present in the chromatogram of triacetin and vice versa. By comparing the peak ratios of the rapeseed oil and α-tocopherol peak in the chromatograms of both phases, conclusions can be drawn about the effectiveness of the extraction processes. In particular, there is 1.1 wt% more α-tocopherol in the triacetin phase than in the rapeseed oil phase for sample A3 and 0.4 wt% more α-tocopherol for sample A4. The extraction process did not work for the other triacetin samples, including A2, which is similar to A4, but without surfactants. This indicates that the presence of the surfactant mixture enhances the process. It is also remarkable that no antioxidant extraction was achieved within the ethanol system, irrespectively of the presence of surfactants.

Table 14: Compositions of the investigated samples of the solketal extraction system.

Sample	$\omega_{\textbf{Rapeseed oil}}$**[wt%]**	$\omega_{\textbf{Solketal}}$**[wt%]**
F1	10	90
F2	15	85
F3	20	80
F4	70	30
F5	75	25
F6	80	20

Obviously, these harsh extraction conditions and the unfavourable extraction system do not lead to striking results. Nevertheless, these experiments show that the developed, but very simple extraction process could work in principal and that further investigations on the usage of better miscible extracting agents, e.g. solketal, is worthwile. Therefore, different samples within the solketal extraction system were prepared (see Table 14). Due to its favourable phase separation temperatures, shown in Fig. 61, no surfactants were necessary for the extraction process. Table 14 further indicates that, again because of the phase diagram, a broad range of compositions was investigated. In particular, samples containing either high or low amounts of rapeseed oil were examined by heating them up to just 45 °C for one hour and cooling them down to room temperature for three days. These mild conditions already ensure that no degradation or other oxidation processes take place during the extraction process.

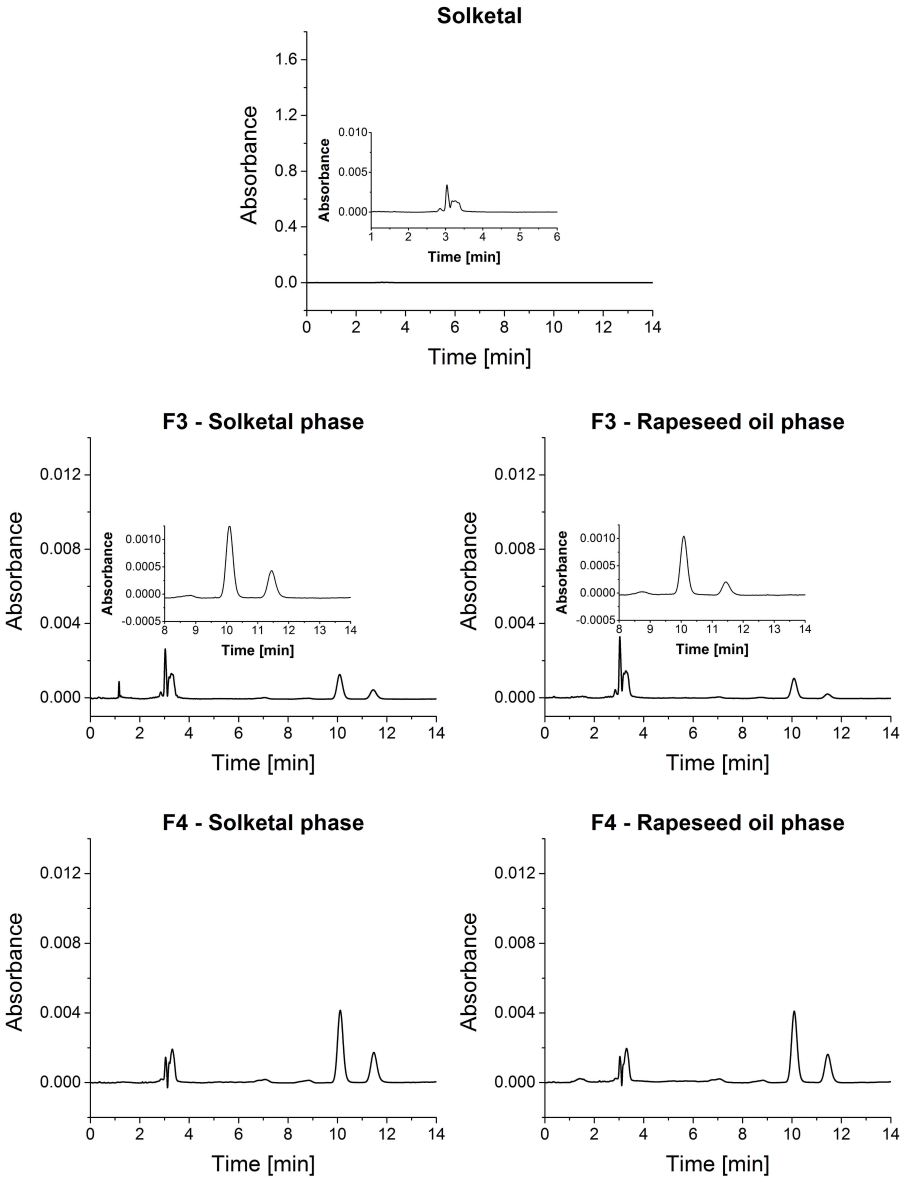

Figure 65: HPLC chromatograms of pure solketal and the separated solketal as well as rapeseed oil phase of the samples F3 and F4.

Fig. 65 shows the HPLC chromatograms of pure solketal as well as of the samples with the best results. Similar to triacetin, solketal does not possess any peaks close to the one of α-tocopherol. Surprisingly, the antioxidant extraction did just work for two completely different compositions. While there is 43 wt% more α-tocopherol in the solketal phase of F3 than in the rapeseed oil, it is 6.5 wt% more α-tocopherol in F4. Based on these results, the influence of every process parameter on the extraction yield was investigated in detail. This included different sampling techniques to avoid contaminations due to the other phase, e.g. usage of different pipettes and syringes, varying temperatures and durations

for the extraction as well as phase separation process and different scales to examine the reproducibility. In general, once the mixture turned monophasic, the duration of this condition does not influence the yield of the antioxidant extraction. The same applies to the phase separation, i.e. cooling process. The examined sampling methods as well as bigger scales led to rather worse than better results. These extractions already indicate that glycerol derivatives could play an important role as alternative extracting agents in the future.

4.2.1.2 Separation of antioxidants from glycerol derivatives

After successfully extracting α-tocopherol from rapeseed oil with glycerol derivatives, in particular solketal, several methods to separate the antioxidant from the extracting agent were examined. This is especially important for use in food industry, as solketal has not been food approved yet. Since the extraction is already as simple as possible, the separation process should also be easily applicable. Therefore, another liquid-liquid extraction step with water as extracting agent was further investigated, as α-tocopherol is not soluble in water. With many different extraction parameters being examined, Table 15 shows just the experiments concerning the influence of the mixing and demixing process on the separation method. After solubilising either 1 wt% (E1-4 and E6) or 10 wt% (E5) of α-tocopherol in solketal, 5 g of water were added to every sample.

Table 15: Compositions of the investigated samples and methods consisting of α-tocopherol (α-Toco), solketal and water within the liquid-liquid extraction process with water.

Sample	$\omega_{\alpha\textbf{-Toco}}$**[wt%]**	$\omega_{\textbf{Solketal}}$**[wt%]**	$\omega_{\textbf{Water}}$**[wt%]**	**Method**
E1	0.17	16.5	83.33	Vortex
E2	0.17	16.5	83.33	1 day at 0 °C
E3	0.17	16.5	83.33	Shaken by hand
E4	0.17	16.5	83.33	Centrifuge
E5	1.7	15	83.33	Centrifuge
E6	0.17	16.5	83.33	Vortex

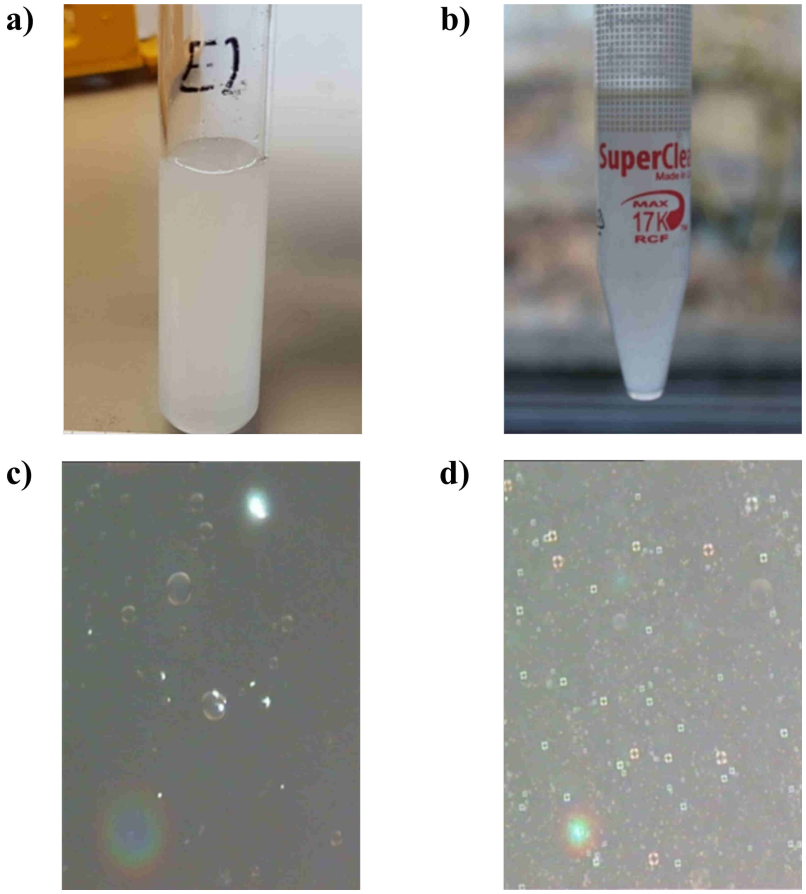

Figure 66: Top: Emulsions E2 (a) and E5 (b) of the separation experiments of antioxidants from glycerol derivatives with water. While E2 illustrates that this liquid-liquid extraction leads to emulsions that are stable for months, E5 shows a pure, yellow α-tocopherol phase on the surface of the mixture after centrifugation. Bottom: Microscopic images of the one week old sample E1 (c) and the freshly prepared mixture E6 (d) at ten times magnification.

Adding water to the α-tocopherol/solketal mixture leads to very stable and turbid emulsions (see Fig. 66a). Even after several months, no phase boundary is observable. Thus, the mixing and demixing methods, given in Table 15, do not influence the extraction process concerning the isolation of α-tocopherol. In reference to the *Ouzo-effect*, this system could have very similar properties, with the amphiphilic solketal stabilising the hydrophobic antioxidant droplets in water [205,287]. With higher amounts of the antioxidant, represented by sample E5, the presence of water causes the formation of a α-tocopherol layer on top of the mixture. After centrifuging the mixture for one minute at 4700 rpm and 20 °C, the α-tocopherol phase is visually observable (see Fig. 66b). To further investigate the stability of these emulsions, sample E1 was examined under the microscope after one week and compared with the freshly prepared mixture E6 with the same composition. The comparison of the microscopic images in Fig. 66c-d shows that E1 possesses less, but distinctly bigger droplets, whereas E6 consists of very small droplets that are rather homogeneously

distributed. These images indicate that there is a very slow phase separation process, driven by Ostwald ripening. In the next step, varying amounts of the antioxidant and water were used. While higher amounts of α-tocopherol lead to an observable antioxidant phase on top of the mixture already before centrifugation, the amount of water does not influence the phase separation before and even after centrifugation. Further parameters like the centrifugation time and temperature as well as the sample volume did not change the phase separation duration and yield. The phase separation can also be influenced by the presence of salts. These so-called *salting-in* and *salting-out* effects were examined with NaCl, $(NH_4)_2SO_4$ and $K_4P_2O_7$. In this system, the *salting-out* effect is important, since the oil phase, i.e. α-tocopherol, should be separated from the water phase. Indeed, the addition of these salts leads to the formation of a clear water phase and an oily phase on top. Therefore, there are several possibilities within the liquid-liquid water extraction to accelerate the isolation of α-tocopherol.

4.2.2 Alternatives to ethanol as freezing point depressant

Since the amphiphilic properties of glycerol derivatives were already examined in detail within this thesis, the research contract of WIGO Chemie GmbH to find sustainable alternatives to ethanol in winter windscreen cleaner formulations was feasible. After a complicated, but eventually successful method development, the freezing points of the aqueous systems could be determined reproducibly. With several potential, alternative substances being investigated, the glycerol derivative solketal, once again, led to the most promising and directly applicable results.

4.2.2.1 Method development

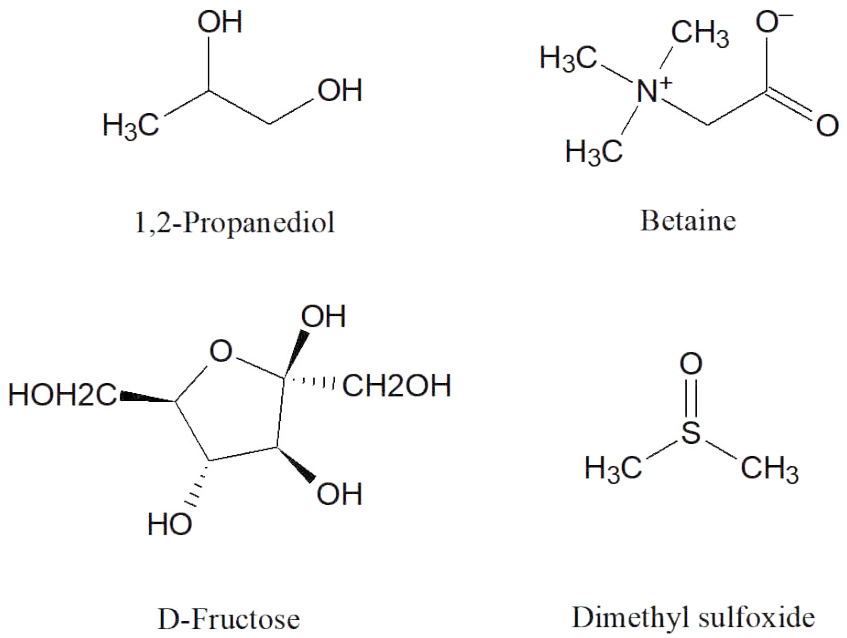

Figure 67: Chemical structures of some of the used substances as potential freezing point depressants. In particular, 1,2-propanediol, betaine, D-fructose, dimethyl sulfoxide (DMSO) and solketal were investigated.

To avoid the same problems as with ethanol as freezing point depressant, the alternative substances need high flash points. Fig. 67 shows the chosen chemicals, except solketal, which either have high flash points or are even solid at room temperature like fructose and betaine. Further, these compounds are non-toxic, cheap, producible via green syntheses and they possess low freezing points, except for the solids. Betaine was chosen as typical hygroscopic osmolyte, whereas the other substances are either hydrogen-bond donors like 1,2-propanediol, solketal and fructose or hydrogen-bond acceptors like DMSO, which are known to induce deep eutectic solvents.

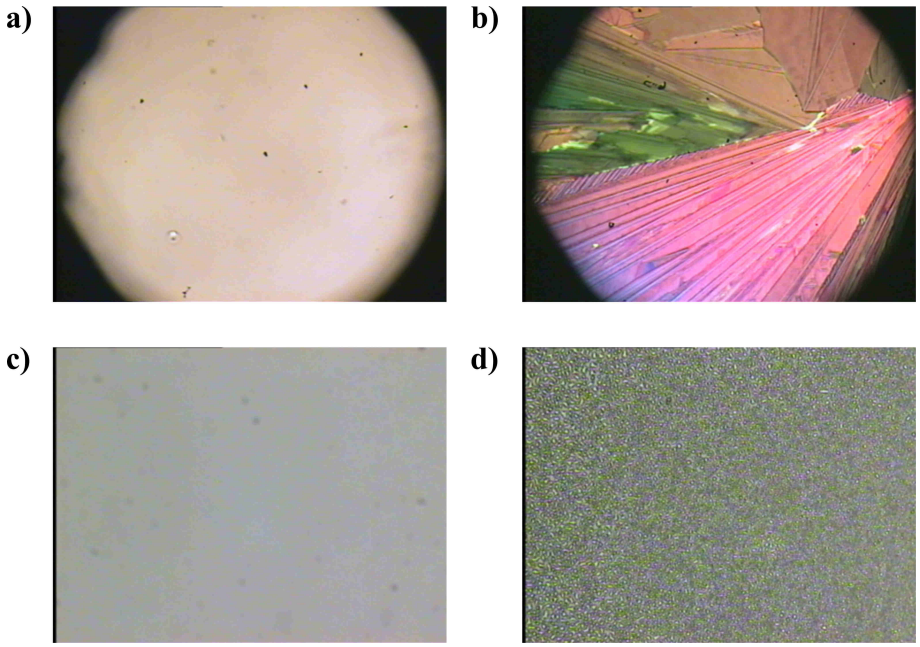

Figure 68: Exemplary microscopic images of the freezing behaviours of binary mixtures of water and a freezing point depressant. Either single crystals were formed during the freezing process (a-b) or the whole mixture froze completely (c-d). The images (b) and (d) are magnifications of (a) and (c), respectively.

At the beginning of these investigations, a polarisation microscope with a cooling system was used to visually observe the formation of crystals during the freezing process. For that, one drop of a sample was just put on an object slide. Fig. 68 shows that either single crystals are formed during the freezing process or the mixture froze completely. As the measured freezing points within these experiments were unexpectedly high and not reproducible, further optimisations were necessary (see Fig. 69). By installing a glove box with a nitrogen flux, the influence of the ambient humidity and thus water condensation around the drop could be prevented. Simultaneously, differential scanning calorimetry (DSC) was used to verify these results. The results of these different microscopic experiments and DSC measurements are summarised in Fig. 69.

Fig. 69a shows that the freezing points of the system 1,2-propanediol/water, obtained by DSC as well as microscopic determination, are rather similar. The same accounts for the microscopic experiments with and without a glovebox in the betaine as well as fructose system, whereby the presence of the glovebox distinctly increases the reproducibility (see Fig. 69c-d). For the solketal mixtures, given in Fig. 69b, both methods were used to investigate its freezing points. The differences between the results of these experiments in this system, however, are too significant to assure a reliable conclusion. Further, concerning every examined system, the freezing points are generally very low. With the freezing point benchmark being $-40\,°C$, every freezing point depressant could be an alternative to ethanol. Nevertheless, considering the results for $0\,wt\%$ of the depressants, i.e. pure

water, the main problem of these experiments becomes obvious: Due to supercooling, pure water freezes at about −18 °C within these measurements. This in turn also queries the reliability of the other freezing points. Therefore, a cryoscopic apparatus according to Beckmann, explained in section 2.2.2.1, was used for the subsequent investigations to avoid supercooling.

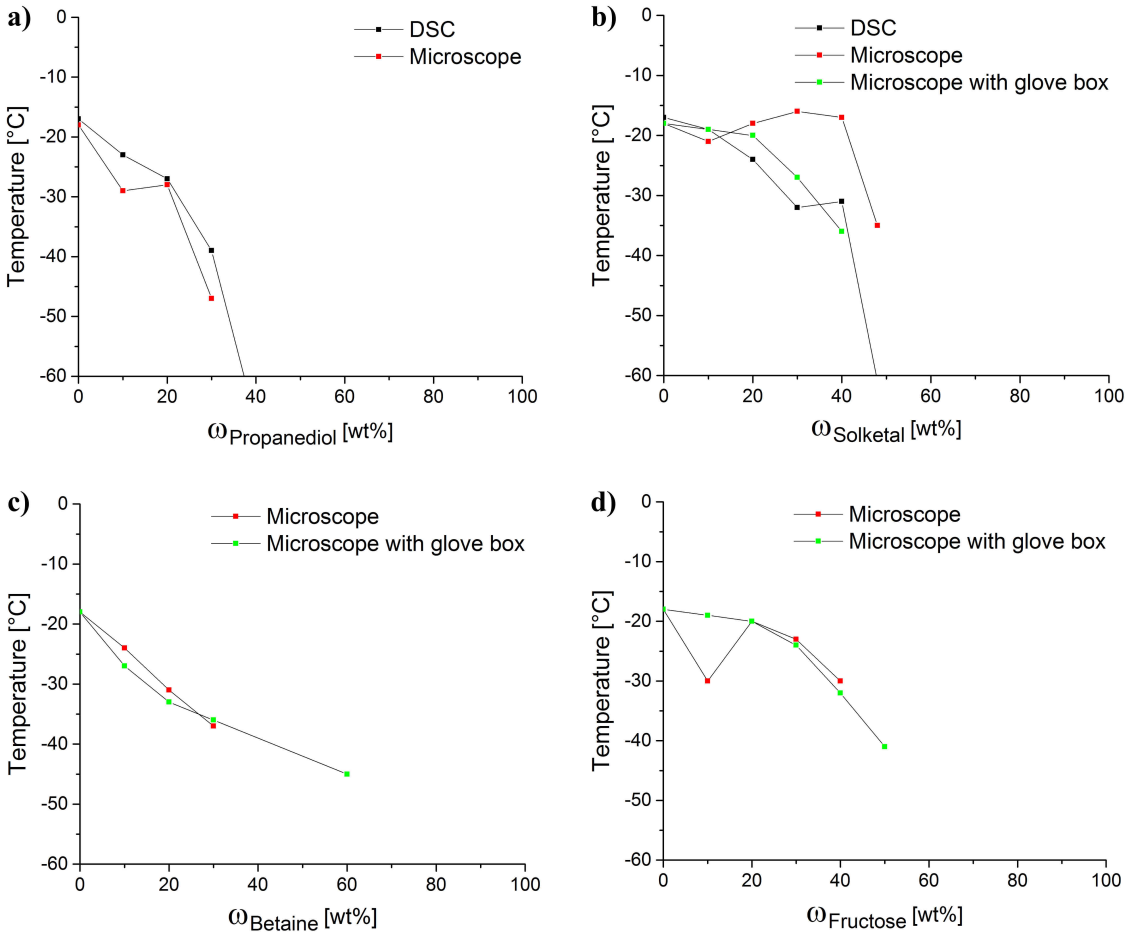

Figure 69: Freezing points of binary systems consisting of water and either 1,2-propanediol (propanediol, a), solketal (b), betaine (c) or fructose (d) obtained by microscopic determination with and without a glove box as well as DSC measurements versus the weight percentage of the freezing point depressant.

4.2.2.2 Cryoscopic measurements with alternative substances

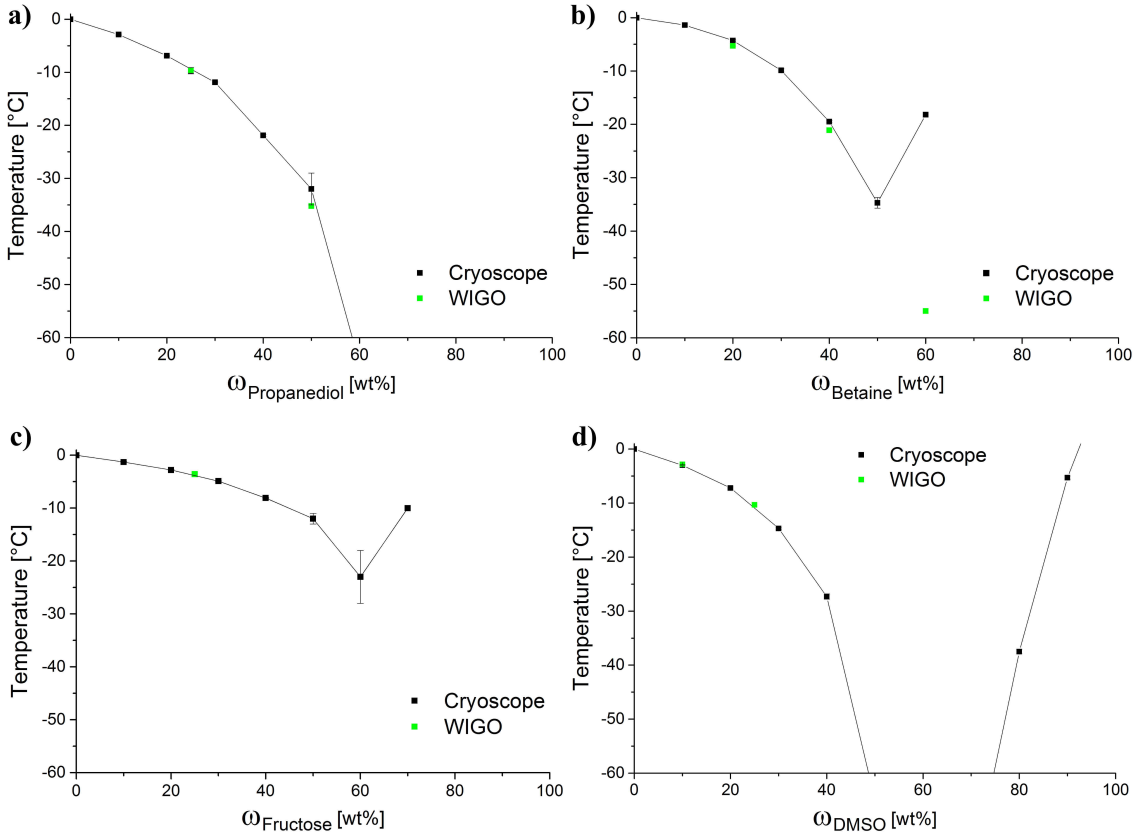

Figure 70: Freezing points of binary systems consisting of water and either 1,2-propanediol (propanediol, a), betaine (b), fructose (c) or dimethyl sulfoxide (DMSO, d) obtained by the cryoscopic experiments as well as the measuring process of WIGO versus the weight percentage of the freezing point depressant.

Fig. 70 shows the freezing points of binary mixtures of water with different freezing point depressants, obtained by the cryoscopic apparatus according to Beckmann and the measuring process of WIGO. Since these measurements were performed at temperatures down to −60 °C, those freezing points are missing that are below this value. In particular, this applies to mixtures with either 60 wt% or more of 1,2-propanediol and between 40 and 80 wt% of DMSO. In general, the comparison of the results obtained by the cryoscopic apparatus with the reference values determined with WIGO's setup makes clear that the developed method leads to reliable results. While the freezing points of the water/fructose system do not decrease sufficiently enough with an increasing amount of fructose, the other systems are more promising. The presence of betaine reduces the freezing point of water below −30 °C. Once more than 50 wt% of betaine are used, the freezing points increase due to the limited solubility of betaine in water. As this problem does not occur in the systems with the liquids 1,2-propanediol and DMSO, the freezing points are distinctly

decreased even at higher amounts of the depressants. Concerning the mixtures with more than 70 wt% of DMSO, however, the freezing points increase, but are still very low. Besides the fact that the industrial synthesis of DMSO is not green, it could be an alternative to ethanol in these formulations. When using 1,2-propanediol in high amounts, the viscosity is increased, which in turn makes the application as windscreen cleaner more difficult, since a layer of the mixture could possibly remain on the surface.

The same experiments were performed with solketal as freezing point depressant (see Fig. 71). Even though the presence of solketal reduces the freezing point of water, another effect occurred: Samples that were at least one day old possessed far lower freezing points than freshly prepared mixtures. This observation was also verified during the measurements in WIGO's head office. With these reduced freezing points, solketal turned out to be the most promising alternative to ethanol as freezing point depressant within these investigations. An explanation for this effect could be the degradation of solketal into acetone and glycerol, which would in turn further reduce the freezing point of the mixture. This degradation, however, can be excluded, since solketal is stable at pH-values above 5. As WIGO was already satisfied with these results, no further experiments were performed to obtain more information on this unexpected behaviour.

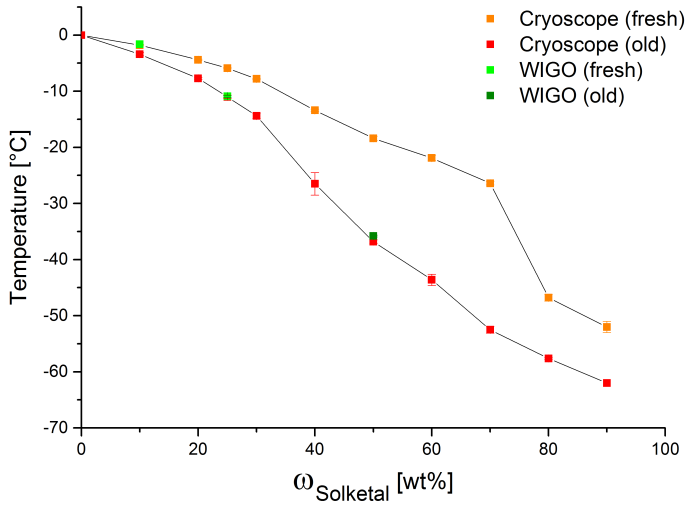

Figure 71: Freezing points of the binary system consisting of water and solketal obtained by the cryoscopic experiments as well as the measuring process of WIGO versus the weight percentage of solketal. These measurements were performed with freshly prepared (fresh) as well as at least one day old (old) mixtures.

5 Conclusion and outlook

Within the scope of this thesis, a new concept of biofuels was developed, which enables the usage of high amounts of vegetable oils and glycerol derivatives simultaneously in mixtures with FAME. These biofuels are directly applicable in unmodified, up-to-date diesel engines. This concept significantly enhances the profitability of FAME production and thus strongly contributes to the sustainability of future biofuels. This work also shows that the presence of glycerol derivatives even leads to several advantages concerning the fuel's properties and the possible implementation of further components. In particular, the amphiphilic character of solketal and tributyrin enables the usage of natural, hydrophilic antioxidants in vegetable oil-containing biofuels. After optimising the composition of the antioxidants in these formulations, they were even more effective than the commonly used, highly toxic hydroquinones. Regarding the concept of hydrofuels, the complete miscibility of solketal with water led to further progress in this research topic. In combination with currently promising biofuel compounds like butanol, water can be implemented into FAME-containing biofuels due to the presence of solketal without any surfactants. This new class of biofuels enables adapted compositions depending on the application and also the usage as possible drop-in fuel without any or just a few further additives. Additionally, the presence of nanostructures in ethanol-containing biofuels could finally be indisputably verified. Due to the precise specification of the structured areas in an exemplary ethanol-containing biofuel, the influence of these structures on relevant physicochemical parameters and thus on their fuel properties could be shown.

The applicability of these amphiphilic glycerol derivatives in completely different, industrial processes, in particular as extracting agents for antioxidants from vegetable oils and as alternatives to ethanol as freezing point depressants was also investigated. For the first possible application, a simple extraction and detection as well as isolation method was developed. While the food approved triacetin could possibly only be used in combination with tributyrin to extract small amounts of antioxidants from vegetable oils, the first extractions with solketal as extracting agent were successful. Due to a subsequent liquid-liquid extraction with water or the addition of salt, the extracted α-tocopherol could be isolated. With regard to the biofuel concept, the extraction of this antioxidant with solketal could be realised within the same facilities before the biofuel formulation, as solketal is added to the vegetable oil anyway. Nevertheless, a lot more optimisations are necessary to ensure reproducible results and higher extraction yields. For another application, several different, possible alternatives to ethanol as freezing point depressants were investigated. Once again, solketal led to the best results and thus, the research contract of WIGO Chemie GmbH could be successfully fulfilled, since the glycerol derivative reduced the freezing point of water sufficiently enough.

Due to several publications, national as well as international presentations and the patent about the developed biofuel concept, there are currently many further projects and collaborations with different research groups and companies. Especially the Handelshaus Runkel, which will start selling its own biofuel in Austria this year, is interested in several aspects of this concept. On the one hand, it still needs the synthetic and highly toxic hydroquinones as antioxidants in its product and on the other hand, Handelshaus Runkel is highly interested in the implementation of water into its biofuel. From its point of view, possible higher costs due to the usage of natural, more expensive antioxidants are negligible, as the consumer is already willing to pay more for completely green products. Further, Volkswagen AG will perform some emission and combustion tests with our biofuels under the supervision of Prof. Dr. Thomas Garbe, who is one of the leading fuel developer of Volkswagen. According to him, biofuels should not be treated as potential transition solutions. If they possess ecologically acceptable properties, there is no reason to completely switch to electric mobility. Additionally, a sample of the optimised antioxidant mixture, solubilised in solketal, was sent to the University of Applied Sciences Coburg to be further examined by the research group of Dr. Olaf Schröder.

This work is also continued within the master thesis of Florian Kerkel. Besides changing the components of the developed biofuel concept, e.g. the less viscous palm oil instead of rapeseed oil, further glycerol derivatives will be investigated. In particular, the main producer of solketal, GLACONCHEMIE GmbH, is currently building a factory in the Netherlands to produce glycerol formal on a high scale. Since this glycerol derivative should be more hydrophilic than solketal, its properties as biofuel component could be

completely different. In contrast to glycerol formal, the characterisation of the product of the addition reaction of 2-butanone, which is currently highly praised as future E-fuel, with glycerol will also be examined in this thesis. With this product being more hydrophobic than solketal, there are many possibilities for further optimisations of the whole concept.

List of Figures

List of Tables

Literature

[1] Gerhard Knothe and Luis F. Razon. Biodiesel fuels. *Progress in Energy and Combustion Science*, 58:36–59, 2017.

[2] Sarah Deutz, Dominik Bongartz, Benedikt Heuser, Arne Kätelhön, Luisa Schulze Langenhorst, Ahmad Omari, Marius Walters, Jürgen Klankermayer, Walter Leitner, Alexander Mitsos, Stefan Pischinger, and Bardow, André. Cleaner production of cleaner fuels: Wind-to-wheel – environmental assessment of CO2 -based oxymethylene ether as a drop-in fuel. *Energy & Environmental Science*, 11(2):331–343, 2018.

[3] John H. Seinfeld. Insights on global warming. *AIChE Journal*, 57(12):3259–3284, 2011.

[4] Andrew A. Lacis, Gavin A. Schmidt, David Rind, and Ruedy, Reto A. Atmospheric CO2: principal control knob governing Earth's temperature. *Science (New York, N.Y.)*, 330(6002):356–359, 2010.

[5] Paul T. Anastas and John C. Warner. *Green chemistry: Theory and practice*. Oxford Univ. Press, Oxford, 1. paperback edition, 2000.

[6] Shiv P. Singh and Dipti Singh. Biodiesel production through the use of different sources and characterization of oils and their esters as the substitute of diesel: A review. *Renewable and Sustainable Energy Reviews*, 14(1):200–216, 2010.

[7] Anjana Srivastava and Ram Prasad. Triglycerides-based diesel fuels. *Renewable and Sustainable Energy Reviews*, 4(2):111–133, 2000.

[8] Silvio. de Almeida. Performance of a diesel generator fuelled with palm oil. *Fuel*, 81(16):2097–2102, 2002.

[9] da Silva, Nívea de Lima, Carlos M. García Santander, Sandra M. Gómez Rueda, Maria R. Wolf Maciel, and Rubens M. Filho. Characterization of blend properties of castor biodiesel and bioethanol. *Industrial & Engineering Chemistry Research*, 52(44):15504–15508, 2013.

[10] Bundesministerium für Umwelt, Naturschutz und nukleare Sicherheit. E10 - Mehr Bio im Benzin. 2011. www.bmu.de/themen/luft-laerm-verkehr/verkehr/kraftstoffe/e10-kraftstoffe/, accessed on 17.04.2018.

[11] Welt. Super E10. 2017. www.welt.de/motor/news/article164278915/Super-E10.html, accessed on 17.04.2018.

[12] Presseportal. Sechs Jahre E10: Autofahrer zapfen immer seltener Biokraftstoff. 2017. www.presseportal.de/pm/29451/3553611, accessed on 17.04.2018.

[13] Andreas J. Janssen, Florian W. Kremer, Jan H. Baron, Martin Muether, Stefan Pischinger, and Juergen Klankermayer. Tailor-made fuels from biomass for homogeneous low-temperature diesel combustion. *Energy & Fuels*, 25(10):4734–4744, 2011.

[14] Raymond E. Paggi. Diesel fuel combustion enhancing additive. Patent WO2012021640 A1, 2012.

[15] Núbia M. Ribeiro, Angelo C. Pinto, Cristina M. Quintella, Gisele O. da Rocha, Leonardo S. G. Teixeira, Lílian L. N. Guarieiro, Maria do Carmo Rangel, Márcia C. C. Veloso, Michelle J. C. Rezende, Rosenira Serpa da Cruz, Ana Maria de Oliveira, Ednildo A. Torres, and Jailson B. de Andrade. The role of additives for diesel and diesel blended (ethanol or biodiesel) fuels: A review. *Energy & Fuels*, 21(4):2433–2445, 2007.

[16] Anthony P. DeCaprio. The toxicology of hydroquinone–relevance to occupational and environmental exposure. *Critical reviews in toxicology*, 29(3):283–330, 1999.

[17] Peter McKendry. Energy production from biomass (part 1): Overview of biomass. *Bioresource Technology*, 83(1):37–46, 2002.

[18] Alan C. Hansen, Qin Zhang, and Peter W. L. Lyne. Ethanol-diesel fuel blends – a review. *Bioresource Technology*, 96(3):277–285, 2005.

[19] Robert L. McCormick and Richard Parish. Milestone report: Technical barriers to the use of ethanol in diesel fuel. national renewable energy laboratory. co. u.s. 2001.

[20] Robin H. Stokes and Marion Adamson. Thermodynamics of dilute solutions of ethanol (1) in p-xylene (2) from freezing-point and enthalpy of dilution measurements. *Journal of the Chemical Society, Faraday Transactions 1: Physical Chemistry in Condensed Phases*, 71(0):1707, 1975.

[21] Farid Chemat and Maryline Abert Vian, editors. *Alternative Solvents for Natural Products Extraction*. Green Chemistry and Sustainable Technology. Springer Berlin Heidelberg, Berlin, Heidelberg and s.l., 2014.

[22] Markus Balser, Thomas Fromm and Klaus Ott. Der Abgasskandal - ein Debakel für die gesamte Autoindustrie. *Süddeutsche Zeitung*, 22.04.2016.

[23] Markus Balser and Joachim Becker. Der Stern sinkt. *Süddeutsche Zeitung*, 12.06.2018.

[24] Diana Dittmer. Von Clean Diesel zu #Dieselgate - Möge die Macht mit VW sein. n-tv Wirtschaft. https://www.n-tv.de/wirtschaft/Moege-die-Macht-mit-VW-sein-article16001236.html, accessed on 18.09.2018.

[25] Bündnis 90/Die Grünen. Abgasskandal - wir kämpfen für die Aufklärung des Abgasskandals. https://www.gruene-bundestag.de/abgasskandal.html, accessed on 25.09.2018.

[26] Jan E. Jonson, Jens Borken-Kleefeld, David Simpson, Agnes Nyíri, Max Posch, and Heyes, Chris. Impact of excess NOx emissions from diesel cars on air quality, public health and eutrophication in Europe. *Environmental Research Letters*, 12(9):94017, 2017.

[27] Guillaume P. Chossière, Robert Malina, Akshay Ashok, Irene C. Dedoussi, Sebastian D. Eastham, Raymond L. Speth, and Steven R. H. Barrett. Public health impacts of excess no x emissions from volkswagen diesel passenger vehicles in germany. *Environmental Research Letters*, 12(3):34014, 2017.

[28] Cristina Guerreiro, Frank de Leeuw, Valentin Foltescu, Alberto González Ortiz, and Jan Horálek. *Air quality in Europe: 2015 report*. EEA report. Publications Office, Luxembourg, 2015.

[29] Gregory J. Thompson, Daniel K. Carder, Marc C. Besch, Thiruvengadam Arvind and Hemanth Kappanna. In-Use Emissions Testing in Light-Duty Diesel Vehicles in the United States. West Virginia University. 2014.

[30] U.S. Environmental Protection Agency. Notice of Violation sent by EPA to Volkswagen. 2015.

[31] Denis Notheis, Olaf Toedter and Thomas Koch. Der Einfluss des Dieselmotors auf die Luftqualität. *Erdöl, Erdgas, Kohle*, (133):188–195, 2017.

[32] Susan C. Anenberg, Joshua Miller, Ray Minjares, Li Du, Daven K. Henze, Forrest Lacey, Christopher S. Malley, Lisa Emberson, Vicente Franco, Zbigniew Klimont, and Heyes, Chris. Impacts and mitigation of excess diesel-related NOx emissions in 11 major vehicle markets. *Nature*, 545(7655):467–471, 2017.

[33] Andrea Minkos, Ute Dauert, Stefan Feigenspan, Susan Kessinger, Stephan Nordmann, and Himpel, Thomas. Air Quality 2017: Preliminary Evaluation. German Environment Agency. 2018.

[34] Rik Oldenkamp, Rosalie van Zelm, and Huijbregts, Mark A. J. Valuing the human health damage caused by the fraud of Volkswagen. *Environmental pollution (Barking, Essex : 1987)*, 212:121–127, 2016.

[35] Norbert Ligterink, Gerrit Kadijk, and van Mensch, Pim. TNO 2012 R11099 Report: Determination of Dutch NOx emission factors for Euro-5 diesel passenger cars. *TNO report*, 2012.

[36] Volker Diegmann. Grenzwertüberschreitungen von NO2 in Hotspots und deren Umgebung. DECHEMA-Sonderkolloquium: Ist der Diesel noch zu retten? Frankfurt am Main, 05.12.2017.

[37] Olaf Opitz. Diesel-Panik: Politik ignoriert Zweifel am Grenzwert 40 Mikrogramm. Focus Online. https://www.focus.de/finanzen/karriere/berufsleben/dieselpanik-wegen-grenzwertluege-politik-ignoriert-zweifel-am-grenzwert-40-mikrogramm-id-7378545.html, accessed on 21.09.2018.

[38] Helmut Greim. Zweierlei Maß: Grenzwerte und Kontrollen für Stickoxide variieren. 3Sat. https://www.3sat.de/page/?source=/nano/umwelt/194620/index.html, accessed on 21.09.2018.

[39] Mikhail Sofiev, James J. Winebrake, Lasse Johansson, Edward W. Carr, Marje Prank, Joana Soares, Julius Vira, Rostislav Kouznetsov, Jukka-Pekka Jalkanen, and James J. Corbett. Cleaner fuels for ships provide public health benefits with climate tradeoffs. *Nature communications*, 9(1):406, 2018.

[40] Liesbeth Schrooten, Ina de Vlieger, Luc Int Panis, Cosimo Chiffi, and Pastori, Enrico. Emissions of maritime transport: a European reference system. *The Science of the total environment*, 408(2):318–323, 2009.

[41] Peter Braun, Jürgen Gebhard, Frank-Michael Matysik, and Rabl, Hans-Peter. Potential Technical Approaches for Improving Low-Temperature NOx Conversion of Exhaust Aftertreatment Systems. *Chemie Ingenieur Technik*, 90(6):762–773, 2018.

[42] Andreas M. Bernhard, Daniel Peitz, Martin Elsener, Tilman Schildhauer, and Kröcher, Oliver. Catalytic urea hydrolysis in the selective catalytic reduction of NOx. Catalyst screening and kinetics on anatase TiO2 and ZrO2. *Catal. Sci. Technol.*, 3(4):942–951, 2013.

[43] Denis Pöhler and Tim Adler. Bestimmung von realen LKW NOx Emissionen (Real Driving Emissions) auf deutschen Autobahnen. *Im Auftrag von Camino Pro e.V. Deutschland & Zweites Deutsches Fernsehen (ZDF)*, 2016.

[44] Pierre Ehrburger, Jean-Francois Brilhac, Yacoub Drouillot, Veronique Logie, and Patrick Gilot. Reactivity of soot with nitrogen oxides in exhaust stream. *SAE Technical Papers Series*, 2002.

[45] Zhihua Liu, Yunshan Ge, Jianwei Tan, Chao He, Asad Naeem Shah, Yan Ding, Linxiao Yu, and Zhao, Wei. Impacts of continuously regenerating trap and particle oxidation catalyst on the NO2 and particulate matter emissions emitted from diesel engine. *Journal of Environmental Sciences*, 24(4):624–631, 2012.

[46] Norbert, Heeb. Der lange Weg zu sauberem Diesel. *Nachrichten aus der Chemie*, (65):1079, 2017.

[47] Bob Dudley and Dale Spencer. BP Statistical Review of World Energy. 2017.

[48] U.S. Energy Information Administration. World crude oil production. 2011.

[49] Gerhard Knothe, Robert O. Dunn, and Marvin O. Bagby. Biodiesel: The use of vegetable oils and their derivatives as alternative diesel fuels. In Badal C. Saha and Jonathan Woodward, editors, *Fuels and Chemicals from Biomass*, volume 666 of *ACS Symposium Series*, pages 172–208. American Chemical Society, Washington, DC, 1997.

[50] Agency for Toxic Substances & Disease Registry. Toxicological profile for fuel oils. US Department of Health and Human Services. Atlanta. 1995.

[51] Kesong Zhang, Jingnan Hu, Shuzheng Gao, Yungang Liu, Xianjiang Huang, and Bao, Xiaofeng. Sulfur content of gasoline and diesel fuels in northern China. *Energy Policy*, 38(6):2934–2940, 2010.

[52] İbrahim Aslan Reşitoğlu, Kemal Altinişik, and Ali Keskin. The pollutant emissions from diesel-engine vehicles and exhaust aftertreatment systems. *Clean Technologies and Environmental Policy*, 17(1):15–27, 2015.

[53] Thomas Koch. Der Beitrag des Dieselmotors zur Immissionssituation. DECHEMA-Sonderkolloquium: Ist der Diesel noch zu retten? Frankfurt am Main, 05.12.2017.

[54] Robert W. Nitske, Wilson C. Morrow. *Rudolf Diesel: Pioneer in the Age of Power*. University of Oklahoma Press, 1965.

[55] Frank Rosillo-Calle, Luc Pelkmans, and Walter, Arnaldo. A Global Overview of Vegetable Oils, with Reference to Biodiesel. A Report for the IEA Bioenergy Task 40. *IEA Bioenergy*, 2009.

[56] Wolfgang Vogel. Supply report 2016/2017. European and world demand for biomass for the purpose of biofuel production in relation to supply in the food and feedstuff markets. Union zur Förderung von Öl- und Proteinpflanzen e.V.. 2017.

[57] Bernat Esteban, Jordi-Roger Riba, Grau Baquero, Antoni Rius, and Rita Puig. Temperature dependence of density and viscosity of vegetable oils. *Biomass and Bioenergy*, 42:164–171, 2012.

[58] Asli IŞigigür, Filiz Karaosmanoglu, Hawa A. Aksoy, Feridun Hamdullahpur, and Ömer L. Gülder. Performance and emission characteristics of a diesel engine operating on safflower seed oil methyl ester. *Applied Biochemistry and Biotechnology*, 45-46(1):93–102, 1994.

[59] Joel Blin, Christel Brunschwig, Arnaud Chapuis, Odilon Changotade, Sayon S. Sidibe, Eric S. Noumi, and Girard, Philippe. Characteristics of vegetable oils for use as fuel in stationary diesel engines—Towards specifications for a standard in West Africa. *Renewable and Sustainable Energy Reviews*, 22:580–597, 2013.

[60] Recep Altın, Selim Çetinkaya, and Hüseyin Serdar Yücesu. The potential of using vegetable oil fuels as fuel for diesel engines. *Energy Conversion and Management*, 42(5):529–538, 2001.

[61] Ernst Schrimpff. Treibstoff der Zukunft - Wasserstoff oder Pflanzenöl? Humane Wirtschaft. 2005.

[62] Gerhard Herres. Rettung des Weltklimas durch Ölpflanzenanbau in der Wüste - Wie Autofahrer dazu beitragen können, den Klimawandel aufzuhalten. Humane Wirtschaft. 2007.

[63] David J. Tenenbaum. Food vs. fuel: diversion of crops could cause more hunger. *Environmental health perspectives*, 116(6):A254–7, 2008.

[64] Max Roser and Ritchie Hannah. Yields and Land Use in Agriculture. Our World in Data. https://ourworldindata.org/yields-and-land-use-in-agriculture, accessed on 29.01.2019.

[65] Kess, Volker. Palm oil: Productive and versatile. World Wildlife Fund. 2004.

[66] John Wiley & Sons, editor. *The CRB Commodity Yearbook 2008*. Hoboken, N.J., U.S., 1st edition, 2008.

[67] Rahul D. Misra and Meena S. Murthy. Straight vegetable oils usage in a compression ignition engine—a review. *Renewable and Sustainable Energy Reviews*, 14(9):3005–3013, 2010.

[68] Hanbey Hazar and Aydin, Hüseyin. Performance and emission evaluation of a CI engine fueled with preheated raw rapeseed oil (RRO)–diesel blends. *Applied Energy*, 87(3):786–790, 2010.

[69] Noulkamol Arpornpong, Chodchanok Attaphong, Ampira Charoensaeng, David A. Sabatini, and Sutha Khaodhiar. Ethanol-in-palm oil/diesel microemulsion-based biofuel: Phase behavior, viscosity, and droplet size. *Fuel*, 132:101–106, 2014.

[70] Brian L. Bettis, Christian L. Peterson, Daniel L. Auld, Daniel J. Driscoll, and Peterson, Eric D.. Fuel Characteristics of Vegetable Oil from Oilseed Crops in the Pacific Northwest. *Agronomy Journal*, 74(2):335, 1982.

[71] Gerhard Knothe, Steven C. Cermak, and Roque L. Evangelista. Cuphea oil as source of biodiesel with improved fuel properties caused by high content of methyl decanoate †. *Energy & Fuels*, 23(3):1743–1747, 2009.

[72] Laura Lomba, Isabel Aznar, Ignacio Gascón, Carlos Lafuente, and Beatriz Giner. Thermophysical study of the furan family. *Thermochimica Acta*, 617:54–64, 2015.

[73] Mario Pagliaro and Michele Rossi. *The Future of Glycerol*. Royal Society of Chemistry, Cambridge, 2010.

[74] Technisches Komitee CEN/TC 19. Kraftstoffe für Kraftfahrzeuge - Dieselkraftstoff - Anforderungen und Prüfverfahren. DIN EN 590. 2014.

[75] Madison L. sheely. Glycerol viscosity tables. *Industrial & Engineering Chemistry*, 24(9):1060–1064, 1932.

[76] Abraham Casas, José Ramón Ruiz, María Jesús Ramos, and Ángel Pérez. Effects of triacetin on biodiesel quality. *Energy & Fuels*, 24(8):4481–4489, 2010.

[77] Mark A. Eiteman and John W. Goodrum. Density and viscosity of low-molecular weight triglycerides and their mixtures. *Journal of the American Oil Chemists' Society*, 71(11):1261–1265, 1994.

[78] Benjamin M. Wood, Kerry Kirwan, Steven Maggs, James Meredith, and Stuart R. Coles. Study of combustion performance of biodiesel for potential application in motorsport. *Journal of Cleaner Production*, 93:167–173, 2015.

[79] Claudio J. A. Mota, da Silva, Carolina X. A., Nilton Rosenbach, Jair Costa, and Flávia da Silva. Glycerin derivatives as fuel additives: The addition of glycerol/acetone ketal (solketal) in gasolines. *Energy & Fuels*, 24(4):2733–2736, 2010.

[80] Scott J. Eaton, George N. Harakas, Richard W. Kimball, Jennifer A. Smith, Kira A. Pilot, Mitch T. Kuflik, and Jeremy M. Bullard. Formulation and combustion of glycerol–diesel fuel emulsions. *Energy & Fuels*, 28(6):3940–3947, 2014.

[81] Travis Kessler, Eric R. Sacia, Alexis T. Bell, and J. Hunter Mack. Predicting the cetane number of furanic biofuel candidates using an improved artificial neural network based on molecular structure. In *ASME 2016 Internal Combustion Engine Fall Technical Conference*, page V001T02A010, Sunday 9 October 2016.

[82] Gerhard Geiseler and James D. Cox and Geoffrey Pilcher. *Thermochemistry of organic and organometallic compounds*, volume 74. Academic Press, London and New York, 1970.

[83] Karrer, Paul. Polysaccharide (XVI. Mitteilung). *Berichte der deutschen chemischen Gesellschaft (A and B Series)*, 55(8):2854–2863, 1922.

[84] Lü Xing-cai, Yang Jian-guang, Zhang Wu-gao, and Huang Zhen. Effect of cetane number improver on heat release rate and emissions of high speed diesel engine fueled with ethanol–diesel blend fuel. *Fuel*, 83(14-15):2013–2020, 2004.

[85] Michael J. Murphy, Joshua D. Taylor and Robert L. McCormick. Compendium of experimental cetane number data.

[86] Ya Ren, Ze-Hang Huang, Dai-Ming Jiang, Wu. Li, Bitang. Liu, and Xao-Bo Wang. Effects of the addition of ethanol and cetane number improver on the combustion and emission characteristics of a compression ignition engine. *Proceedings of the Institution of Mechanical Engineers, Part D: Journal of Automobile Engineering*, 222(6):1077–1087, 2008.

[87] Mustafa Balat. Production of bioethanol from lignocellulosic materials via the biochemical pathway: A review. *Energy Conversion and Management*, 52(2):858–875, 2011.

[88] Barry. Freedman, Everett H. Pryde, and Timothy L. Mounts. Variables affecting the yields of fatty esters from transesterified vegetable oils. *Journal of the American Oil Chemists Society*, 61(10):1638–1643, 1984.

[89] Fangrui Ma and Milford A. Hanna. Biodiesel production: a review. *Bioresource Technology*, 70(1):1–15, 1999.

[90] Jia Luo, Zhen Fang, and Richard L. Smith. Ultrasound-enhanced conversion of biomass to biofuels. *Progress in Energy and Combustion Science*, 41:56–93, 2014.

[91] Vitthal L. Gole and Parag R. Gogate. A review on intensification of synthesis of biodiesel from sustainable feed stock using sonochemical reactors. *Chemical Engineering and Processing: Process Intensification*, 53:1–9, 2012.

[92] Camila da Silva and Vladimir J. Oliveira. Biodiesel production through non-catalytic supercritical transesterification: Current state and perspectives. *Brazilian Journal of Chemical Engineering*, 31(2):271–285, 2014.

[93] David G. B. Boocock, Samir K. Konar, V. Mao, C. Lee, and Sonia Buligan. Fast formation of high-purity methyl esters from vegetable oils. *Journal of the American Oil Chemists' Society*, 75(9):1167–1172, 1998.

[94] Promode Kant and Shuirong Wu. The extraordinary collapse of jatropha as a global biofuel. *Environmental science & technology*, 45(17):7114–7115, 2011.

[95] Giorgos Markou and Elias Nerantzis. Microalgae for high-value compounds and biofuels production: a review with focus on cultivation under stress conditions. *Biotechnology advances*, 31(8):1532–1542, 2013.

[96] Gerhard Knothe. A technical evaluation of biodiesel from vegetable oils vs. algae. will algae-derived biodiesel perform? *Green Chemistry*, 13(11):3048, 2011.

[97] Man Kee Lam and Keat Teong Lee. Microalgae biofuels: A critical review of issues, problems and the way forward. *Biotechnology advances*, 30(3):673–690, 2012.

[98] Ayhan Demirbas. Progress and recent trends in biodiesel fuels. *Energy Conversion and Management*, 50(1):14–34, 2009.

[99] Griffin E. Shay. Diesel fuel from vegetable oils: Status and opportunities. *Biomass and Bioenergy*, 4(4):227–242, 1993.

[100] U.S. Environmental Protection Agency. A comprehensive analysis of biodiesel impacts on exhaust emissions. National Service Center for Environmental Publications, OH., U.S., 2002.

[101] Rhodri W. Jenkins, Martin Munro, Sarah Nash, and Christopher J. Chuck. Potential renewable oxygenated biofuels for the aviation and road transport sectors. *Fuel*, 103:593–599, 2013.

[102] Thomas A. Foglia, Lloyd A. Nelson, Robert O. Dunn, and William N. Marmer. Low-temperature properties of alkyl esters of tallow and grease. *Journal of the American Oil Chemists' Society*, 74(8):951–955, 1997.

[103] Inmok Lee, Lawrence A. Johnson, and Earl G. Hammond. Use of branched-chain esters to reduce the crystallization temperature of biodiesel. *Journal of the American Oil Chemists' Society*, 72(10):1155–1160, 1995.

[104] Inmok Lee, Lawrence A. Johnson, and Earl G. Hammond. Reducing the crystallization temperature of biodiesel by winterizing methyl soyate. *Journal of the American Oil Chemists' Society*, 73(5):631–636, 1996.

[105] Robert O. Dunn, Michael W. Shockley and Marvin O. Bagby. Winterized methyl esters from soybean oil: an alternative diesel fuel with improved low-temperature flow properties. *SAE Transactions*, (106):640–649, 1997.

[106] Gina M. Chupka, Lewis Fouts, James A. Lennon, Teresa L. Alleman, David A. Daniels, and Robert L. McCormick. Saturated monoglyceride effects on low-temperature performance of biodiesel blends. *Fuel Processing Technology*, 118:302–309, 2014.

[107] Terry A. Isbell. Current progress in the development of cuphea. *Lipid Technology*, (14):77–80, 2002.

[108] D02 Committee. Specification for Biodiesel Fuel Blend Stock (B100) for Middle Distillate Fuels. ASTM International, PA, U.S., 2015.

[109] Konstantinos Kalogeras, Stella Bezergianni, Vasiliki Kazantzi, and Petros A. Pilavachi. On the prediction of properties for diesel / biodiesel mixtures featuring new environmental considerations. In *20th European Symposium on Computer Aided Process Engineering*, volume 28 of *Computer Aided Chemical Engineering*, pages 973–978. Elsevier, 2010.

[110] The office of the revisor of statutes, Minnesota Statutes. Biodiesel content mandate: 239.77, 2017.

[111] Bockey, Dieter. Biodiesel 2011/2012. Sachstandbericht und Perspektive - Auszug aus dem UFOP-Jahresbericht. Union zur Förderung von Öl- und Proteinpflanzen e.V.. Berlin. 2012.

[112] Amandeep K. Purewal. Policy fuels uncertainty for biodiesel: Current situation. AHDB Cereals & Oilseeds. https://cereals.ahdb.org.uk/markets/market-news/2017/march/09/prospects-policy-fuels-uncertainty-for-biodiesel-current-situation.aspx, accessed on 21.09.2018.

[113] Neumann, Hinrich. Biodiesel: Produktion könnte auf 2.3 Mio. t sinken. topagrar online. https://www.topagrar.com/news/Energie-Energienews-Biodiesel-Produktion-koennte-auf-2-3-Mio-t-sinken-9196223, accessed on 21.09.2018.

[114] Giacomo M. Lari, Giorgio Pastore, Moritz Haus, Yiyu Ding, Stavros Papadokonstantakis, Cecilia Mondelli, and Javier Pérez-Ramírez. Environmental and economical perspectives of a glycerol biorefinery. *Energy & Environmental Science*, 11(5):1012–1029, 2018.

[115] OECD-FAO Agricultural Outlook 2016-2025. Special Focus: Sub-Saharan Africa. Food and Agriculture Organization of the United Nations. OECD Publishing. Paris. 2016.

[116] Eva García, Miriam Laca, Elena Pérez, Angel Garrido, and Julián Peinado. New class of acetal derived from glycerin as a biodiesel fuel component. *Energy & Fuels*, 22(6):4274–4280, 2008.

[117] Malaya R. Nanda, Zhongshun Yuan, Wensheng Qin, Hassan S. Ghaziaskar, Marc-Andre Poirier, and Chunbao Charles Xu. Thermodynamic and kinetic studies of a catalytic process to convert glycerol into solketal as an oxygenated fuel additive. *Fuel*, 117:470–477, 2014.

[118] Anne Jaecker-Voirol, Isabelle Durand, Gerard Hillion, Bruno Delfort, and Xavier Montagne. Glycerin for new biodiesel formulation. *Oil & Gas Science and Technology - Revue de l'IFP*, 63(4):395–404, 2008.

[119] Adi Wolfson, Alex Snezhko, Tal Meyouhas, and Dorith Tavor. Glycerol derivatives as green reaction mediums. *Green Chemistry Letters and Reviews*, 5(1):7–12, 2012.

[120] Klaus Gottlieb, Horst Neitsch, and Wessendorf, Richard. Glycerin - ein nachwachsender Rohstoff. *Chemie Ingenieur Technik*, 66(1):64–66, 1994.

[121] Hannu Aatola, Martti Larmi, Teemu Sarjovaara, and Mikkonen, Seppo. Hydrotreated Vegetable Oil (HVO) as a Renewable Diesel Fuel: Trade-off between NOx, Particulate Emission, and Fuel Consumption of a Heavy Duty Engine. *SAE International Journal of Engines*, 1(1):1251–1262, 2009.

[122] Martin Mittelbach. Fuels from oils and fats: Recent developments and perspectives. *European Journal of Lipid Science and Technology*, 117(11):1832–1846, 2015.

[123] Heiko Pflaum, Peter Hofmann, Bernhard Geringer, and Weissel, Werner. Potential of Hydrogenated Vegetable Oil (HVO) in a Modern Diesel Engine. In *Small Engine Technology Conference & Exposition*, SAE Technical Paper Series. SAE International400 Commonwealth Drive, Warrendale, PA, United States, 2010.

[124] Junya Yano, Tatsuki Aoki, Kazuo Nakamura, Kazuo Yamada, and Shin-ichi Sakai. Life cycle assessment of hydrogenated biodiesel production from waste cooking oil using the catalytic cracking and hydrogenation method. *Waste management (New York, N.Y.)*, 38:409–423, 2015.

[125] Viktor Wesselak. *Handbuch Regenerative Energietechnik*. Springer Verlag, Berlin, Heidelberg, 3rd ed. edition, 2017.

[126] Alexis M. Bazzanella and Florian Ausfelder. Low carbon energy and feedstock for the European chemical industry. DECHEMA - Technology study. 2017.

[127] Kurt Wagemann and Florian Ausfelder. E-Fuels - Mehr als eine Option. DECHEMA - White Paper. 2017.

[128] Mustafa Balat. Potential importance of hydrogen as a future solution to environmental and transportation problems. *International Journal of Hydrogen Energy*, 33(15):4013–4029, 2008.

[129] Mingyong Wang, Zhi Wang, Xuzhong Gong, and Zhancheng Guo. The intensification technologies to water electrolysis for hydrogen production – a review. *Renewable and Sustainable Energy Reviews*, 29:573–588, 2014.

[130] Reinhard Otten. The first industrial PtG plant - Audi e-gas as driver for the energy turnaround. CEDEC Gas Day, Verona, 27.05.2014.

[131] Dragica Lj. Stojić, Milica P. Marčeta, Sofija P. Sovilj, and Šćepan S. Miljanić. Hydrogen generation from water electrolysis—possibilities of energy saving. *Journal of Power Sources*, 118(1-2):315–319, 2003.

[132] Vladimir M. Nikolic, Gvozden S. Tasic, Aleksandar D. Maksic, Djordje P. Saponjic, Snezana M. Miulovic, and Milica P. Marceta Kaninski. Raising efficiency of hydrogen generation from alkaline water electrolysis – energy saving. *International Journal of Hydrogen Energy*, 35(22):12369–12373, 2010.

[133] Gvozden S. Tasic, Sladjana P. Maslovara, Dragana L. Zugic, Aleksandar D. Maksic, and Milica P. Marceta Kaninski. Characterization of the ni–mo catalyst formed in situ during hydrogen generation from alkaline water electrolysis. *International Journal of Hydrogen Energy*, 36(18):11588–11595, 2011.

[134] Martin Wietschel. Welchem Motor gehört die Zukunft? DECHEMA-Sonderkolloquium: Ist der Diesel noch zu retten? Frankfurt am Main, 05.12.2017.

[135] Karsten Büker. Nutzung von CO2 in fossilen Energieumwandlungskreisläufen. 13. Brandenburger Energietag. Cottbus, 15.09.2011.

[136] Florian Ausfelder, Christian Beilmann, Martin Bertau, Sigmar Bräuninger, Angelika Heinzel, Renate Hoer, Wolfram Koch, Falko Mahlendorf, Anja Metzelthin, Marcell Peuckert, Ludolf Plass, Konstantin Räuchle, Martin Reuter, Georg Schaub, Sebastian Schiebahn, Ekkehard Schwab, Ferdi Schüth, Detlef Stolten, Gisa Teßmer, Kurt Wagemann, and Ziegahn, Karl-Friedrich. Energiespeicherung als Element einer sicheren Energieversorgung. *Chemie Ingenieur Technik*, 87(1-2):17–89, 2015.

[137] Friedrich Asinger. *Methanol - Chemie- und Energierohstoff: D. Mobilisation d. Kohle*. Akademie-Verl., Berlin, 1987.

[138] Ahmad Omari, Benedikt Heuser, and Stefan Pischinger. Potential of oxymethylenether-diesel blends for ultra-low emission engines. *Fuel*, 209:232–237, 2017.

[139] Niklas Schmitz, Jakob Burger, Eckhard Ströfer, and Hans Hasse. From methanol to the oxygenated diesel fuel poly(oxymethylene) dimethyl ether: An assessment of the production costs. *Fuel*, 185:67–72, 2016.

[140] Martin Härtl, Philipp Seidenspinner, Eberhard Jacob, and Georg Wachtmeister. Oxygenate screening on a heavy-duty diesel engine and emission characteristics of highly oxygenated oxymethylene ether fuel ome1. *Fuel*, 153:328–335, 2015.

[141] Ayhan Demirbas and Selami Karslioglu. Biodiesel production facilities from vegetable oils and animal fats. *Energy Sources, Part A: Recovery, Utilization, and Environmental Effects*, 29(2):133–141, 2007.

[142] Badal C. Saha, Nancy N. Nichols, Nasib Qureshi, Gregory J. Kennedy, Loren B. Iten, and Michael A. Cotta. Pilot scale conversion of wheat straw to ethanol via simultaneous saccharification and fermentation. *Bioresource Technology*, 175:17–22, 2015.

[143] Sadr A. Shahir, Haji H. Masjuki, Mohammad A. Kalam, Ali Imran, Rizwanul I. M. Fattah, and Ahmed Sanjid. Feasibility of diesel–biodiesel–ethanol/bioethanol blend as existing ci engine fuel: An assessment of properties, material compatibility, safety and combustion. *Renewable and Sustainable Energy Reviews*, 32:379–395, 2014.

[144] Magín Lapuerta, Octavio Armas, and Reyes García-Contreras. Stability of diesel–bioethanol blends for use in diesel engines. *Fuel*, 86(10-11):1351–1357, 2007.

[145] Jie Liu, Guangle Li, and Shenghua Liu. Influence of ethanol and cetane number (cn) improver on the ignition delay of a direct-injection diesel engine. *Energy & Fuels*, 25(1):103–107, 2011.

[146] Pascale Satgé de Caro. Interest of combining an additive with diesel–ethanol blends for use in diesel engines. *Fuel*, 80(4):565–574, 2001.

[147] European Commission. A European Strategy on Clean and Energy Efficient Vehicles: Communication from The Comission to The European Parliament, The Council and The European Economic and Social Committee. Brussels, 2011.

[148] Mehmet Efe Biresselioglu, Melike Demirbag Kaplan, and Barbara Katharina Yilmaz. Electric mobility in europe: A comprehensive review of motivators and barriers in decision making processes. *Transportation Research Part A: Policy and Practice*, 109:1–13, 2018.

[149] William Sierzchula, Sjoerd Bakker, Kees Maat, and Bert van Wee. The influence of financial incentives and other socio-economic factors on electric vehicle adoption. *Energy Policy*, 68:183–194, 2014.

[150] Martina Wikström, Lisa Hansson, and Per Alvfors. An end has a start – investigating the usage of electric vehicles in commercial fleets. *Energy Procedia*, 75:1932–1937, 2015.

[151] Adnan Nadia, Nordin Shahrina M, Rahman Imran, and Muhammad A Noor. An Integrative Approach to Study on Consumer Behavior towards Plug-In Hybrid Electric Vehicles Revolution: Consumer Behavior towards Plug-In Hybrid Electric Vehicles. Applied Behavioral Economics Research and Trends. 183-213, 2017.

[152] Han Hao, Zhexuan Mu, Shuhua Jiang, Zongwei Liu, and Fuquan Zhao. Ghg emissions from the production of lithium-ion batteries for electric vehicles in china. *Sustainability*, 9(4):504, 2017.

[153] Arno Kwade, Wolfgang Haselrieder, Ruben Leithoff, Armin Modlinger, Franz Dietrich, and Klaus Droeder. Current status and challenges for automotive battery production technologies. *Nature Energy*, 3(4):290–300, 2018.

[154] Naoki Nitta, Feixiang Wu, Jung Tae Lee, and Gleb Yushin. Li-ion battery materials: Present and future. *Materials Today*, 18(5):252–264, 2015.

[155] Pilar Swart, Jo Dewulf, and Alexis Biernaux. Resource demand for the production of different cathode materials for lithium ion batteries. *Journal of Cleaner Production*, 84:391–399, 2014.

[156] Deutsche Energie-Agentur. Ungeliebt, aber unentbehrlich - Bedarf und Produktion von Mineralöl im künftigen Energiemix. Studie. Berlin, 2011.

[157] Bundesministerium für Bildung und Forschung. Power-to-X. Kopernikus-Projekt. https://www.kopernikus-projekte.de/projekte/power-to-x, accessed on 31.10.2018.

[158] Christof Maul. Viskosimetrie. Apparatives Praktikum Physikalische Chemie. TU Braunschweig. 2009.

[159] Viskosimetrische Bestimmung der Molekülmasse von Polyvenylalkohol. Praktikum Physikalische Chemie I für Studierende der Chemie (B.Sc. 3. Semester) an der Universität Regensburg. 2012.

[160] Anton-Paar. Viskosimeter: Die erfolgreichsten Viskosimeter der Welt. https://www.anton-paar.com/corp-de/produkte/gruppe/viskosimeter/, accessed on 25.09.2018.

[161] Gvidonas Labeckas and Stasys Slavinskas. The effect of ethanol, petrol and rapeseed oil blends on direct injection diesel engine performance and exhaust emissions. *Transport*, 25(2):116–128, 2010.

[162] Xing-Cai Lü, Wu-Gao Zhang, Xin-Qi Qiao, and Zhen Huang. Fuel design concept for improving the spray characteristics and emissions of diesel engines. *Proceedings of the Institution of Mechanical Engineers, Part D: Journal of Automobile Engineering*, 219(4):547–557, 2005.

[163] Hyun Kyu Suh, Hyun Gu Roh, and Chang Sik Lee. Spray and combustion characteristics of biodieseldiesel blended fuel in a direct injection common-rail diesel engine. *Journal of Engineering for Gas Turbines and Power*, 130(3):32807, 2008.

[164] Kraftstoffe für pflanzenöltaugliche Motoren - Rapsölkraftstoff - Anforderungen und Prüfverfahren. DIN 51605. 2016.

[165] Gangadharan Ajithkumar, Narakathra H. Jayadas, and Marath Bhasi. Analysis of the pour point of coconut oil as a lubricant base stock using differential scanning calorimetry. *Lubrication Science*, 21(1):13–26, 2009.

[166] Svajus Asadauskas and Sevim Z. Erhan. Depression of pour points of vegetable oils by blending with diluents used for biodegradable lubricants. *Journal of the American Oil Chemists' Society*, 76(3):313–316, 1999.

[167] Francisco A. M. Silva, Fernanda Borges, and Margarida A. Ferreira. Effects of phenolic propyl esters on the oxidative stability of refined sunflower oil. *Journal of Agricultural and Food Chemistry*, 49(8):3936–3941, 2001.

[168] Eunok Choe and David B. Min. Mechanisms and factors for edible oil oxidation. *Comprehensive Reviews in Food Science and Food Safety*, 5(4):169–186, 2006.

[169] Maria D. Guillén and Nerea Cabo. Fourier transform infrared spectra data versus peroxide and anisidine values to determine oxidative stability of edible oils. *Food chemistry*, 77(4):503–510, 2002.

[170] Lawrence B. Harding and William A. Goddard. The mechanism of the ene reaction of singlet oxygen with olefins. *Journal of the American Chemical Society*, 102(2):439–449, 1980.

[171] Metrohm AG. Oxidation stability of oils and fats - Rancimat method. Application Bulletin 204/2 e. 2010.

[172] Ferdinand Bär and Jürgen Krahl, Schaffung eines biodieselbasierten Kraftstoffs mit geringem NO2-Ausstoß und hoher Oxidationsstabilität. Abschlussbericht. Union zur Förderung von Öl- und Proteinpflanzen e.V.. Technologietransferzentrum Automotive der Hochschule Coburg. 2014.

[173] Andrea Neumann, Thomas Jebens and Volkmar Wierzbicki. A Method for Determining Oxidation Stability of Petrodiesel, Biodiesel, and Blended Fuels. American Laboratory. https://www.americanlaboratory.com/914-Application-Notes/34716-A-Method-for-Determining-Oxidation-Stability-of-Petrodiesel-Biodiesel-and-Blended-Fuels/, accessed on 26.09.2018.

[174] Lucía Botella, Fernando Bimbela, Lorena Martín, Jesús Arauzo, and José L. Sánchez. Oxidation stability of biodiesel fuels and blends using the rancimat and petrooxy methods. effect of 4-allyl-2,6-dimethoxyphenol and catechol as biodiesel additives on oxidation stability. *Frontiers in chemistry*, 2:43, 2014.

[175] Anton Paar GmbH. Oxidationsstabilitätsprüfer: RapidOxy 100. https://www.anton-paar.com/de-de/produkte/details/oxidationsstabilitaetspruefer-rapidoxy-100/, accessed on 26.09.2018.

[176] Maria L. Medeiros, Cordeiro, Angela M. M. T., Neide Queiroz, Luiz E. B. Soledade, Antonia L. Souza, and Antonio G. Souza. Efficient antioxidant formulations for use in biodiesel. *Energy & Fuels*, 28(2):1074–1080, 2014.

[177] Cristiane D. Alexandrino, Selene M. Morais, Micheline S. C. Oliveira, Lyeghyna K. A. Machado, Clécio G. Martins, Afrânio A. Craveiro, Naele C. Rocha, Camila P. Valle, Jackson Q. Malveira, and Fernando A. S. Jorge. Influence of hydrogenation and antioxidants on the stability of soybean oil biodiesels. *European Journal of Lipid Science and Technology*, 115(6):709–715, 2013.

[178] Abdul Monyem and Jon van H. Gerpen. The effect of biodiesel oxidation on engine performance and emissions. *Biomass and Bioenergy*, 20(4):317–325, 2001.

[179] Casimir C. Akoh and David B. Min. *Food Lipids: Chemistry, Nutrition and Biotechnology*. Food Science and Technology. Marcel Dekker Inc, Hoboken, 2002.

[180] Fereidoon Shahidi and Ying Zhong. Revisiting the polar paradox theory: a critical overview. *Journal of agricultural and food chemistry*, 59(8):3499–3504, 2011.

[181] Robert O. Dunn. Effect of antioxidants on the oxidative stability of methyl soyate (biodiesel). *Fuel Processing Technology*, 86(10):1071–1085, 2005.

[182] Axel Ingendoh. Storage-stable compositions of antioxidants containing ascorbic acid. Patent WO/2017/054921, 2017.

[183] Dong-Ping Xu, Ya Li, Xiao Meng, Tong Zhou, Yue Zhou, Jie Zheng, Jiao-Jiao Zhang, and Hua-Bin Li. Natural antioxidants in foods and medicinal plants: Extraction, assessment and resources. *International journal of molecular sciences*, 18(1), 2017.

[184] Sarah S. Damasceno, Nataly A. Santos, Ieda M.G. Santos, Antônia L. Souza, Antônio G. Souza, and Neide Queiroz. Caffeic and ferulic acids: An investigation of the effect of antioxidants on the stability of soybean biodiesel during storage. *Fuel*, 107:641–646, 2013.

[185] Raphaël Lebeuf, Véronique Nardello-Rataj, and Jean-Marie Aubry. Dramatic synergistic effects between hydroquinone and resorcinol derivatives for the organocatalyzed reduction of dioxygen by diethylhydroxylamine. *Chemical communications (Cambridge, England)*, 50(7):866–868, 2014.

[186] Tsutao Kurechi and Tetsuta Kato. Studies on the antioxidants: Xi. oxidation products of concomitantly used butylated hydroxyanisole and butylated hydroxytoluene. *Journal of the American Oil Chemists' Society*, 57(7):220–223, 1980.

[187] Kazuo Mukai, Shingo Itoh, and Hitoshi Morimoto. Stopped-flow kinetic study of vitamin e regeneration reaction with biological hydroquinones (reduced forms of ubiquinone, vitamin k, and tocopherolquinone) in solution. *The Journal of biological chemistry*, 267(31):22277–22281, 1992.

[188] Bryan M. Jenkins, Larry L. Baxter, and Thomas R. Miles. Combustion properties of biomass. *Fuel Processing Technology*, 54(1-3):17–46, 1998.

[189] Changdong Sheng and Joao L. T. Azevedo. Estimating the higher heating value of biomass fuels from basic analysis data. *Biomass and Bioenergy*, 28(5):499–507, 2005.

[190] IKA-Werke GmbH & Co. KG. IKA Kalorimeter C 200. https://www.ika.com/de/Produkte-Lab-Eq/Kalorimeter-Verbrennungskalorimeter-Bombenkalorimeter-Brennwertbestimmung-csp-330/C-200-cpdt-8802500/, accessed on 26.09.2018.

[191] Kai Borgeest. Elektronik in der Fahrzeugtechnik: Hardware, Software, Systeme und Projektmanagement and mit 28 Tabellen. ATZ/MTZ-Fachbuch. Springer Vieweg Verlag, Wiesbaden, 3, 2014.

[192] Cedinox - Acero inoxidable. EGR systems. https://www.cedinox.es/en/actividades/highlighted/detail-highlighted/EGR-Systems/, accessed on 23.09.2018.

[193] European Committee for Standardization. Automotive Fuels. Fatty Acid Methyl Esters (FAME) for Diesel Engines. Requirements and test methods. EN 14214. Beuth Verlag. Berlin. 2014.

[194] Prasenjeet Ghosh. Predicting the effect of cetane improvers on diesel fuels. *Energy & Fuels*, 22(2):1073–1079, 2008.

[195] Stefan Pischinger. Verbrennungsmotoren: Vorlesungsumdruck. Band 2. RWTH Aachen. 2004.

[196] Günter P. Merker and Gunnar Stiesch. *Technische Verbrennung - motorische Verbrennung*. Teubner Verlag, Stuttgart, 1999.

[197] Jakow B. Zeldovich. Oxidation of nitrogen in combustion and explosions. *European Physical Journal A. Hadrons and Nuclei*, (21):577–628, 1946.

[198] Kurt Kosswig and Adam Wolfgang. Die Tenside. Hanser Verlag, München. 1993.

[199] Fennell D. Evans and Håkan Wennerström. *The colloidal domain: Where physics, chemistry, biology, and technology meet*. Advances in interfacial engineering series. Wiley-VCH, New York, NY, 2. edition, 1999.

[200] Hans F. Eicke. Surfactants in nonpolar solvents - aggregation and micellization. *Topics in current chemistry*, 87:85–145, 1980.

[201] Björn Lindman and Håkan Wennerström. Miceles - amphiphile aggregation in aqueous solution. *Topics in current chemistry*, 87:1–87, 1980.

[202] Garland D. Smith, Barry B. Garrett, Smith L. Holt, and Roland E. Barden. The interaction of copper and n-alpha.-acyl-l-histidinol at the interface of an oil-continuous microemulsion. *The Journal of Physical Chemistry*, 80(15):1708–1713, 1976.

[203] Garland D. Smith, Colleen E. Donelan, and Roland E. Barden. Oil-continuous microemulsions composed of hexane, water, and 2-propanol. *Journal of Colloid and Interface Science*, (60):488–496, 1977.

[204] Werner Kunz, Krister Holmberg, and Thomas Zemb. Hydrotropes. *Current Opinion in Colloid & Interface Science*, 22:99–107, 2016.

[205] Thomas N. Zemb, Michael Klossek, Tobias Lopian, Julien Marcus, Sebastian Schöettl, Dominik Horinek, Sylvain F. Prevost, Didier Touraud, Olivier Diat, Stjepan Marčelja, and Werner Kunz. How to explain microemulsions formed by solvent mixtures without conventional surfactants. *Proceedings of the National Academy of Sciences of the United States of America*, 113(16):4260–4265, 2016.

[206] Chirravuri V. Subbarao, Ichapurapu P. K. Chakravarthy, Sai A. V. S. L. Bharadwaj, and Kommuri M. M. K. Prasad. Functions of hydrotropes in solutions. *Chemical Engineering & Technology*, 35(2):225–237, 2012.

[207] Clifford A. Moses, Thomas W. Ryan, and William E. Likos. Experiments with alcohol/diesel fuel blends in compression-ignition engines. VI International Symposium on Alcohol Fuels Technology, Guaruja, Brazil, 1980.

[208] Evandro J. Silva, Elisabete M. D. Zaniquelli, and Watson Loh. Light-scattering investigation on microemulsion formation in mixtures of diesel oil (or hydrocarbons) + ethanol + additives. *Energy & Fuels*, 21(1):222–226, 2007.

[209] Ibrahim Kayali, Chemboli K. Jyothi, Khawla Qamhieh, and Ulf Olsson. Surfactant-free alternative fuel: Phase behavior and diffusion properties. *Journal of Colloid and Interface Science*, 463:173–179, 2016.

[210] Lada Bemert, Sandra Engelskirchen, Christof Simon, and Reinhard Strey. Low emissions with microemulsion-fuels. *Prepr. Pap.-Am. Chem. Soc., Div. Fuel Chem.*, (54(1)):290, 2009.

[211] Lada Bemert and Reinhard Strey. Diesel-Mikroemulsionen als alternativer Kraftstoff. Universität zu Köln. 2009.

[212] Peter Dittmann, Heinrich Dörksen, Dirk Steiding, and Florian Kremer. Einfluss von Mikroemulsionen auf die dieselmotorische Verbrennung. *MTZ - Motortechnische Zeitschrift*, (76):60–67, 2015.

[213] Jae W. Park, Kang Y. Huh, and Kweon H. Park. Experimental study on the combustion characteristics of emulsified diesel in a rapid compression and expansion machine. *Proceedings of the Institution of Mechanical Engineers, Part D: Journal of Automobile Engineering*, 214(5):579–586, 2005.

[214] Reinhard Strey, Lada Bemert, Christof Simon, and Heinrich Dörksen. Verfahren zur in-situ-Herstellung von Treibstoff-Wasser-Gemischen in Verbrennungsmotoren. Patent WO2011042432 A1. 2011.

[215] Bruce J. Berne and Robert Pecora. *Dynamic Light Scattering: With Applications to Chemistry, Biology, and Physics*. Dover Books on Physics. Dover Publications, Newburyport, 2013.

[216] Robert Pecora. *Dynamic Light Scattering: Applications of Photon Correlation Spectroscopy*. Springer US, Boston, MA, 1985.

[217] Harald Preu, Christine Schirmer, Matija Tomšič, Marija Bešter Rogač, Andrej Jamnik, Luc Belloni, and Werner Kunz. Light, neutron, x-ray scattering, and conductivity measurements on aqueous dodecyltrimethylammonium bromide/1-hexanol solutions. *The Journal of Physical Chemistry B*, 107(50):13862–13870, 2003.

[218] Julien Marcus, Michael L. Klossek, Didier Touraud, and Werner Kunz. Nano-droplet formation in fragrance tinctures. *Flavour and Fragrance Journal*, 28(5):294–299, 2013.

[219] Bappaditya Naskar, Olivier Diat, Véronique Nardello-Rataj, and Pierre Bauduin. Nanometer-size polyoxometalate anions adsorb strongly on neutral soft surfaces. *The Journal of Physical Chemistry C*, 119(36):20985–20992, 2015.

[220] Devinderjit S. Sivia. *Elementary scattering theory: For X-ray and neutron users*. Oxford Univ. Press, Oxford, 2011.

[221] Peter Lindner and Thomas Zemb. *Neutrons, X-rays and light: Scattering methods applied to soft condensed matter*. North-Holland delta series. North-Holland Elsevier, Amsterdam, 1. edition, 2002.

[222] Bernard Lagourette, Jean Peyrelasse, Christian Boned, and Marc Clausse. Percolative conduction in microemulsion type systems. *Nature*, 281(5726):60–62, 1979.

[223] Marc Clausse, Jean Peyrelasse, Jeremy Heil, Christian Boned, and Bernard Lagourette. Bicontinuous structure zones in microemulsions. *Nature*, 293(5834):636–638, 1981.

[224] Yuri Feldman, Nikolay Kozlovich, Ido Nir, and Nissim Garti. Dielectric relaxation in sodium bis(2-ethylhexyl)sulfosuccinate–water–decane microemulsions near the percolation temperature threshold. *Physical Review E*, 51(1):478–491, 1995.

[225] Michel Lagues and Claude Sauterey. Percolation transition in water in oil microemulsions. electrical conductivity measurements. *The Journal of Physical Chemistry*, 84(26):3503–3508, 1980.

[226] Michael L. Klossek, Julien Marcus, Didier Touraud, and Werner Kunz. The extension of microemulsion regions by combining ethanol with other cosurfactants. *Colloids and Surfaces A: Physicochemical and Engineering Aspects*, 427:95–100, 2013.

[227] Gary Grest, Itzhak Webman, Samuel Safran, and Amy Bug. Dynamic percolation in microemulsions. *Physical review. A, General physics*, 33(4):2842–2845, 1986.

[228] Damian Brock, Alexander Koder, Hans-Peter Rabl, Didier Touraud, and Werner Kunz. New completely renewable biofuels: Formulations and engine tests on an unmodified up-to-date diesel engine. *Green Chemistry*, 20(14):3308–3317, 2018.

[229] George E. W. Huber. Breaking the chemical and engineering barriers to lignocellulosic biofuels: Next generation hydrocarbon biorefineries. *National Science Foundation*, 2008.

[230] Yuriy Román-Leshkov, Christopher J. Barrett, Zhen Y. Liu, and James A. Dumesic. Production of dimethylfuran for liquid fuels from biomass-derived carbohydrates. *Nature*, 447(7147):982–985, 2007.

[231] Heather A. Meylemans, Roxanne L. Quintana, and Benjamin G. Harvey. Efficient conversion of pure and mixed terpene feedstocks to high density fuels. *Fuel*, 97:560–568, 2012.

[232] Alexander Wollinger, Élodie Perrin, Jamal Chahboun, Valérie Jeannot, Didier Touraud, and Werner Kunz. Antioxidant activity of hydro distillation water residues from rosmarinus officinalis l. leaves determined by dpph assays. *Comptes Rendus Chimie*, 19(6):754–765, 2016.

[233] Sebastian Krickl, Lucija Jurko, Karolina Wolos, Didier Touraud, and Werner Kunz. Surfactant-free microemulsions with cleavable constituents. *Journal of Molecular Liquids*, 271:112–117, 2018.

[234] Theresa Höß. Alternative Green Extraction Methods for Natural Products, Dissertation, University of Regensburg, 2018.

[235] Jeanne I. Rader, Carol M. Weaver, Lucia Patrascu, Laila H. Ali, and Gerald Angyal. α-Tocopherol, total vitamin A and total fat in margarines and margarine-like products. *Food chemistry*, 58(4):373–379, 1997.

[236] Marina Cvjetko, Zika Lepojevic, Zoran Zekovic, Senka Vidovic, and Svetlana Milosevic. Antioxidant properties of rapeseed. *Zbornik radova Tehnoloskog fakulteta Leskovac*, pages 27–33, 2009.

[237] Eva Gimeno, Ana I. Castellote, Rosa M. Lamuela-Raventós, De la Torre, Maria C, and Maria C. López-Sabater. Rapid determination of vitamin E in vegetable oils by reversed-phase high-performance liquid chromatography. *Journal of Chromatography A*, 881(1-2):251–254, 2000.

[238] Leonardo P. Ozorio, Rafael Pianzolli, Maria Beatriz S. Mota, and Claudio J. A. Mota. Reactivity of glycerol/acetone ketal (solketal) and glycerol/formaldehyde acetals toward acid-catalyzed hydrolysis. *Journal of the Brazilian Chemical Society*, 23(5):931–937, 2012.

[239] Evellyn Câmara Grilo, Priscila Nunes Costa, Cristiane Santos Sânzio Gurgel, Beserra, Andressa Fernanda de Lima, Almeida, Fernanda Niéce de Souza, and Roberto Dimenstein. Alpha-tocopherol and gamma-tocopherol concentration in vegetable oils. *Food Science and Technology*, 34(2):379–385, 2014.

[240] Cristina M. Sabliov, Claudia Fronczek, Carlos E. Astete, Margarita Khachaturyan, Lavrent Khachatryan, and Claudia Leonardi. Effects of Temperature and UV Light on Degradation of α-Tocopherol in Free and Dissolved Form. *Journal of the American Oil Chemists' Society*, 86(9):895–902, 2009.

[241] Jin Dai and Russell J. Mumper. Plant phenolics: extraction, analysis and their antioxidant and anticancer properties. *Molecules (Basel, Switzerland)*, 15(10):7313–7352, 2010.

[242] Linh D. Do and David A. Sabatini. Aqueous extended-surfactant based method for vegetable oil extraction: Proof of concept. *Journal of the American Oil Chemists' Society*, 87(10):1211–1220, 2010.

[243] John Shi, Haseeb Nawaz, Joseph Pohorly, Gauri Mittal, Yukio Kakuda, and Yueming Jiang. Extraction of polyphenolics from plant material for functional foods—engineering and technology. *Food Reviews International*, 21(1):139–166, 2005.

[244] Xu, Zhimin. Comparison of extraction methods for quantifying vitamin E from animal tissues. *Bioresource Technology*, 99(18):8705–8709, 2008.

[245] Aleksandra Szydłowska-Czerniak and Agnieszka Tułodziecka. Antioxidant capacity of rapeseed extracts obtained by conventional and ultrasound-assisted extraction. *Journal of the American Oil Chemists' Society*, 91(12):2011–2019, 2014.

[246] Mariassyova Magda. Antioxidant activity of some herbal extracts in rapeseed and sunflower oils. *J Food Nutr Res*, (45):104–109, 2006.

[247] Suk-Nam Kang, Young-Min Goo, Mi-Ra Yang, Rashid Ismael Hag Ibrahim, Jae-Hyeon Cho, Il-Suk Kim, and Ok-Hwan Lee. Antioxidant and antimicrobial activities of ethanol extract from the stem and leaf of impatiens balsamina l. (balsaminaceae) at different harvest times. *Molecules (Basel, Switzerland)*, 18(6):6356–6365, 2013.

[248] Aleksandra Szydłowska-Czerniak, Ryszard Amarowicz, and Edward Szłyk. Antioxidant capacity of rapeseed meal and rapeseed oils enriched with meal extract. *European Journal of Lipid Science and Technology*, 112(7):750–760, 2010.

[249] Jennifer Komaiko and David Julian McClements. Low-energy formation of edible nanoemulsions by spontaneous emulsification: Factors influencing particle size. *Journal of Food Engineering*, 146:122–128, 2015.

[250] Iva Kralova and Johan Sjöblom. Surfactants used in food industry: A review. *Journal of Dispersion Science and Technology*, 30(9):1363–1383, 2009.

[251] Jennifer S. Komaiko and David Julian McClements. Formation of food-grade nanoemulsions using low-energy preparation methods: A review of available methods. *Comprehensive Reviews in Food Science and Food Safety*, 15(2):331–352, 2016.

[252] Stauffer, Daniel. Das Chromatogramm. Chromatogramme richtig integrieren und bewerten. Wiley-VCH, Weinheim, Germany, 1-53, 2008.

[253] Matthias Otto. *Analytische Chemie*. Wiley-VCH, Weinheim, Germany, 4th edition, 2014.

[254] Lander Viktor and Heinz, Boos. Bestimmung von Vitamin E in kosmetischen Mitteln. SÖFW-Journal, 120, 444-449, 1994.

[255] Bruno P. Kremer and Horst Bannwarth. *Einführung in die Laborpraxis*. Springer Verlag, Berlin, 2014.

[256] Gordon W. Monier-Williams. The determination of the true freezing point of milk. *The Analyst*, 58(686):254, 1933.

[257] Julius Hortvet. The cryoscopy of milk. *Journal of Industrial & Engineering Chemistry*, 13(3):198–208, 1921.

[258] WIGO Chemie GmbH. Winterscheibenreinigerkonzentrat. Patent DE202005004452. 2005.

[259] Daniel Stöhr. Fast Facts About Ethanol and the Hazardous Material Regulations of the PHMSA. 2014. https://danielstraining.com/fast-facts-about-ethanol-and-the-hazardous-material-regulations-of-the-phmsa/, accessed on 12.11.2018.

[260] Standard Test Method for Freezing Point of Aqueous Engine Coolants. ASTM International D1177-12, PA, U.S., 2012.

[261] Julien Cambedouzou and Olivier Diat. Quantitative small-angle scattering on mesoporous silica powders: From morphological features to specific surface estimation. *Journal of Applied Crystallography*, 45(4):662–673, 2012.

[262] Damian Brock, Tobias Lopian, Ali Khoshsima, Pierre Bauduin, Olivier Diat, Didier Touraud, and Werner Kunz. Nanostructuring in ethanol/“ethanolotrope”/rapeseed oil automotive biofuels. *Colloid and Interface Science Communications*, 14:1–3, 2016.

[263] Ali Khoshsima, Damian Brock, Didier Touraud, and Werner Kunz. Pre-formulation of biofuels: Kinematic viscosities, low-temperature phase behaviour and nanostructuring of ethanol/“ethanolotrope”/rapeseed oil mixtures. *Fuel*, 191:212–220, 2017.

[264] Ali Khoshsima, Mohammad Reza Dehghani, Didier Touraud, Julien Marcus, Olivier Diat, and Werner Kunz. Nanostructures in clear and homogeneous mixtures of rapeseed oil and ethanol in the presence of green additives. *Colloid and Polymer Science*, 293(11):3225–3235, 2015.

[265] Christopher M. Sorensen and Genmiao Wang. Size distribution effect on the power law regime of the structure factor of fractal aggregates. *Physical Review E*, 60(6):7143–7148, 1999.

[266] Olivier Diat, Michael L. Klossek, Didier Touraud, Bruno Deme, Isabelle Grillo, Werner Kunz, and Thomas Zemb. Octanol-rich and water-rich domains in dynamic equilibrium in the pre-ouzo region of ternary systems containing a hydrotrope. *Journal of Applied Crystallography*, 46(6):1665–1669, 2013.

[267] Ying Li, Anne Sylvie Fabiano-Tixier, Karine Ruiz, Anne Rossignol Castera, Pierre Bauduin, Olivier Diat, and Farid Chemat. Comprehension of direct extraction of hydrophilic antioxidants using vegetable oils by polar paradox theory and small angle x-ray scattering analysis. *Food chemistry*, 173:873–880, 2015.

[268] Yuriy Alexandrov, Nick Kozlovich, Yuri Feldman, and John Texter. Dielectric spectroscopy of cosurfactant facilitated percolation in reverse microemulsions. *The Journal of Chemical Physics*, 111(15):7023–7028, 1999.

[269] Tobias Lopian, Sebastian Schöttl, Sylvain Prévost, Stéphane Pellet-Rostaing, Dominik Horinek, Werner Kunz, and Thomas Zemb. Morphologies observed in ultraflexible microemulsions with and without the presence of a strong acid. *ACS central science*, 2(7):467–475, 2016.

[270] A. A. Al-Farayedhi, A. M. Al-Dawood, and P. Gandhidasan. Experimental investigation of si engine performance using oxygenated fuel. *Journal of Engineering for Gas Turbines and Power*, 126(1):178, 2004.

[271] Krzysztof Górski, Asok K. Sen, Wincenty Lotko, and Marek Swat. Effects of ethyl-tert-butyl ether (etbe) addition on the physicochemical properties of diesel oil and particulate matter and smoke emissions from diesel engines. *Fuel*, 103:1138–1143, 2013.

[272] Georg Huber, Edgar Remmele, Klaus Thuneke, and Peter Emberger. Use of Citric Acid Esters as Alternative Fuel for Diesel Engines. 21st European Biomass Conference and Exhibition. Copenhagen, Denmark.

[273] Luis A. Follegatti-Romero, Marcelo Lanza, da Silva, César A. S., Eduardo A. C. Batista, and Antonio J. A. Meirelles. Mutual solubility of pseudobinary systems containing vegetable oils and anhydrous ethanol from (298.15 to 333.15) k. *Journal of Chemical & Engineering Data*, 55(8):2750–2756, 2010.

[274] Malcolm M. Haring, Samuel Glasstone, Keith J. Laidler, and Henry Eyring. The theory of rate processes. *Journal of Chemical Education*, 19(5):249, 1942.

[275] Shantilal L. Oswal and Harshal. S. Desai. Studies of viscosity and excess molar volume of binary mixtures. *Fluid Phase Equilibria*, 186(1-2):81–102, 2001.

[276] Lorenzo de Lorenzi, Maurizio Fermeglia, and Giovanni Torriano. Density and viscosity of 1-methoxy-2-propanol, 2-methyltetrahydrofuran, α,α,α-trifluorotoluene, and their binary mixtures with 1,1,1-trichloroethane at different temperatures. *Journal of Chemical & Engineering Data*, 41(5):1121–1125, 1996.

[277] Pierre Bauduin, Fabienne Testard, and Thomas Zemb. Solubilization in alkanes by alcohols as reverse hydrotropes or "lipotropes". *The journal of physical chemistry. B*, 112(39):12354–12360, 2008.

[278] Matija Tomsic, Andrej Jamnik, Gerhard Fritz-Popovski, Otto Glatter, and Lukás Vlcek. Structural properties of pure simple alcohols from ethanol, propanol, butanol, pentanol, to hexanol: comparing monte carlo simulations with experimental saxs data. *The journal of physical chemistry. B*, 111(7):1738–1751, 2007.

[279] Damian Brock, Didier Touraud and Werner Kunz. Fuel derived from renewable resources. EP17184759.3, 2017.

[280] Damian Brock, Alexander Koder, Hans-Peter Rabl, Didier Touraud and Werner Kunz. Optimising the biodiesel production process: Implementation of glycerol derivatives into biofuel formulations and their potential to form hydrofuels. Fuel. 2019. Submitted.

[281] Godwin Kafui Ayetor, Albert Sunnu, and Joseph Parbey. Effect of biodiesel production parameters on viscosity and yield of methyl esters: Jatropha curcas, elaeis guineensis and cocos nucifera. *Alexandria Engineering Journal*, 54(4):1285–1290, 2015.

[282] Oguzhan Ilgen, Senol Yerlikaya, and Funda Oguzkaya Akyurek. Synthesis of solketal from glycerol and acetone over amberlyst-46 to produce an oxygenated fuel additive. *Periodica Polytechnica Chemical Engineering*, 2016.

[283] Ertan Alptekin and Mustafa Canakci. Performance and emission characteristics of solketal-gasoline fuel blend in a vehicle with spark ignition engine. *Applied Thermal Engineering*, 124:504–509, 2017.

[284] Earl Christensen, Janet Yanowitz, Matthew Ratcliff, and Robert L. McCormick. Renewable oxygenate blending effects on gasoline properties. *Energy & Fuels*, 25(10):4723–4733, 2011.

[285] Riccardo Amorati, Stefano Menichetti, Elisabetta Mileo, Gian Franco Pedulli, and Caterina Viglianisi. Hydrogen-atom transfer reactions from ortho-alkoxy-substituted phenols: an experimental approach. *Chemistry (Weinheim an der Bergstrasse, Germany)*, 15(17):4402–4410, 2009.

[286] Chao Jin, Mingfa Yao, Haifeng Liu, Chia-fon F. Lee, and Jing Ji. Progress in the production and application of n-butanol as a biofuel. *Renewable and Sustainable Energy Reviews*, 15(8):4080–4106, 2011.

[287] Steven A. Vitale and Joseph L. Katz. Liquid droplet dispersions formed by homogeneous liquid−liquid nucleation: “the ouzo effect”. *Langmuir*, 19(10):4105–4110, 2003.

Eidesstattliche Erklärung

Ich erkläre hiermit an Eides statt, dass ich die vorliegende Arbeit ohne Hilfe Dritter und ohne Benutzung anderer als der angegebenen Hilfsmittel angefertigt habe. Die aus anderen Quellen direkt oder indirekt übernommenen Daten und Konzepte sind unter Angabe des Literaturzitats gekennzeichnet. Weitere Personen waren an der inhaltlich-materiellen Herstellung der vorliegenden Arbeit nicht beteiligt. Insbesondere habe ich hierfür nicht die entgeltliche Hilfe eines Promotionsberaters oder anderer Personen in Anspruch genommen. Niemand hat von mir weder unmittelbar noch mittelbar geldwerte Leistungen für Arbeiten erhalten, die im Zusammenhang mit dem Inhalt der vorgelegten Dissertation stehen.
Die Arbeit wurde bisher weder im In- noch im Ausland in gleicher oder ähnlicher Form einer anderen Prüfungsbehörde vorgelegt.

Regensburg, den 21. Februar 2019

(Damian Brock)